DOCTOR OF PHILOSOPHY

Advanced materials for organic solar cells: influence of generation and pH on PAMAM-Based devices

Alshahrani, Thamraa

Award date:
2016

Awarding institution:
Bangor University

PRIFYSGOL
BANGOR
UNIVERSITY

Advanced Materials for Organic Solar Cells: Influence of Generation and pH on PAMAM-Based Devices

By

Thamraa Mohammed Alshahrani

A thesis submitted in partial fulfillment for the

degree of Doctor of Philosophy

in the

College of Physical and Applied Sciences

School of Electronic Engineering

February 2016

Declaration and Consent

Details of the Work

I hereby agree to deposit the following item in the digital repository maintained by Bangor University and/or in any other repository authorized for use by Bangor University.

Author Name: **Thamraa Mohammed Alshahrani** Title: **Advanced Materials for Organic Solar Cells: Influence of Generation and pH on PAMAM-Based Devices**

Supervisor/Department: **Dr. Mohammed Mabrook /Electronic Engineering**

Qualification/Degree obtained**: PhD**

This item is a product of my own research endeavours and is covered by the agreement below in which the item is referred to as "the Work". It is identical in content to that deposited in the Library, subject to point 2 below.

Non-exclusive Rights

Rights granted to the digital repository through this agreement are entirely nonexclusive. I am free to publish the Work in its present version or future versions elsewhere.

I agree that Bangor University may electronically store, copy or translate the Work to any approved medium or format for the purpose of future preservation and accessibility. Bangor University is not under any obligation to reproduce or display the Work in the same formats or resolutions in which it was originally deposited.

Bangor University Digital Repository

I understand that work deposited in the digital repository will be accessible to a wide variety of people and institutions, including automated agents and search engines via the World Wide Web.

I understand that once the Work is deposited, the item and its metadata may be incorporated into public access catalogues or services, national databases of electronic theses and dissertations such as the British Library's EThOS or any service provided by the National Library of Wales.

I understand that the Work may be made available via the National Library of Wales Online Electronic Theses Service under the declared terms and conditions of use (http://www.llgc.org.uk/index.php?id=4676). I agree that as part of this service the National Library of Wales may electronically store, copy or convert the Work to any approved medium or format for the purpose of future preservation and accessibility. The National Library of Wales is not under any obligation to reproduce or display the Work in the same formats or resolutions in which it was originally deposited.

Statement 1:

This thesis is the result of my own investigations, except the preparation of PAMAM dendrimers materials were performed in collaboration with the School of chemistry, Bangor University, UK.

Signed …… (Candidate) Date ……

Statement 2:

I agree to deposit an electronic copy of my thesis (the Work) in the Bangor University (BU) Institutional Digital Repository, the British Library ETHOS system, and/or in any other repository authorized for use by Bangor University and where necessary have gained the required permissions for the use of third party material.

In addition to the above I also agree to the following:

1. That I am the author or have the authority of the author(s) to make this agreement and do hereby give Bangor University the right to make available the Work in the way described above.

2. That the electronic copy of the Work deposited in the digital repository and covered by this agreement, is identical in content to the paper copy of the Work deposited in the Bangor University Library, subject to point 4 below.

3. That I have exercised reasonable care to ensure that the Work is original and, to the best of my knowledge, does not breach any laws – including those relating to defamation, libel and copyright.

4. That I have, in instances where the intellectual property of other authors or copyright holders is included in the Work, and where appropriate, gained explicit permission for the inclusion of that material in the Work, and in the electronic form of the Work as accessed through the open access digital
5. Repository, or that I have identified and removed that material for which adequate and appropriate permission has not been obtained and which will be inaccessible via the digital repository.

6. That Bangor University does not hold any obligation to take legal action on behalf of the Depositor, or other rights holders, in the event of a breach of intellectual property rights, or any other right, in the material deposited.

7. That I will indemnify and keep indemnified Bangor University and the National Library of Wales from and against any loss, liability, claim or damage, including without limitation any related legal fees and court costs (on a full indemnity bases), related to any breach by myself of any term of this agreement.

Signature: …… Date: …….....

Contents

Abstract

A systematic approach has been used to investigate the application of new PAMAM dendrimers materials as acceptors in the fabrication of different organic photovoltaic (OPV) structures. In the first part of this work, a new PAMAM cores (FC0, FC1 and FC2) as well as different PAMAM generations (G0, G0.5, G1 and G2) were used as acceptors in the fabrication of organic bulk heterojunction (OBHJ) structures. The devices exhibited electronic properties dependent on morphology and optical absorption as well as the surface group in the PAMAM generations. Power conversion efficiency (*PCE*) of 0.2%, under AM1.5G illumination (100 mW/cm^2), was found for PAMAM-FC2 based OBHJ devices. Based on this result, different generations (G0, G0.5, G1 and G2) were synthesis from PAMAM FC2 core to improve the efficiency. Devices based on PAMAM G0.5 (half generation with ester terminated group in the surface group) with condense branching units and good connections in the composition active layer film resulted in a *PCE* of 1.8 %. For comparison, devices based on IC70BA were also investigated in OBHJ structures. The results show that devices, with the polymer to IC70BA ratio of 1:1 and annealed at 150^{0}C for 10 min, exhibited the best device performance (J_{SC} = 23. 33 mA/cm^2, V_{OC} = 0.53 V, *FF* 0.44, and *PCE* = 5.8 %).
The second part of this work aimed to investigate the effect of generation and pH of the new acceptor PAMAM dendritic materials on the performance of organic bilayer heterojunction (OBiHJ) structures. Increasing PAMAM dendritic generation from G0.5 to G2.5 influences significantly the bilayer OHJ solar cells efficiency performance. PCE of 7 % were achieved at the natural PAMAM G2.5 pH 6.85. Atomic force microscopy shows that PAMAM morphology changes with their generation and pH values. The improved performance seen with PAMAM G2.5 at natural pH was due to the number of surface groups and tertiary amines in the dendrimer are increases with generation size and at different pH values. The protonation of dendrimers varies with the generation size. The PAMAM G0 copolymerised with a thienopyrrolodione (TPD) accepting moiety as A-A copolymer structures in order to enhance their charge transport properties was also investigated. PAMAMG0-TPD was used as electron acceptor component coupled with P3HT as donor in OHJ solar cell structures. The devices yield a *PCE* of about 4.5 %. This result demonstrated the potential to use PAMAM-TPD based conjugated copolymers as acceptor component for organic solar cells.
The third part of this work is based on the moderate performance of part two.Three different organic tandem solar cells were fabricated and characterised. They have the same active layer (P3HT:IC70BA) as bulk-heterojunction structure in the bottom cells where the top cell is a bilayer heterojunction structure. The differences between the three structures is the acceptor layer of the top cells. From results in part two PAMAM-G1.5 (pH= 7.03), PAMAM-G2.5 (pH= 6.85) and PAMAM-G0-TPD were chosen as they have the highest efficiency to be applied in the top cells of organic tandem structures. The results from the three tandem structures displayed reasonably high PCE due to the enhanced V_{OC}.

Publications

1. **T Alshahrani**, M F Mabrook , A El-Betany , H Tai, I Alrougy and N McKeown (2014) "The Effect of pH of the New Acceptor PAMAM Dendritic Material on the Organic Bilayer Solar Cells Performance" International Conference of Solution Processed Semiconductor Solar Cells, 10-12 September, Oxford, UK.
2. A El-Betany, **T Alshahrani**, M F Mabrook, N B McKeown and H Tai (2013) "Benzimidazol Naphthalic Anhydride Derivatives -Based Solar Cells: Structure, Morphology and Electronic Properties Relationships", APME, 18-22 August, Durham, UK.
3. **T Alshahrani**, A El-Betany, M F Mabrook, H Tai, I Alrougy, A Sleiman and N McKeown (2012) "The effect of pH of a new PAMAM dendritic material on the performance of organic bilayer solar cells" EMRS Spring Meeting, 26-30 May, Congress Centre - Lille, France.
4. A. Sleiman, M. Kreyenborg-Nichols, **T. Alshahrani**, D. Ashall, P. W. Sayers and M. F. Mabrook, "Enhanced holes mobility in AlO and pentacene-based OTFTs due to the passivation of the oxide surface using PVP," E-MRS, Lille, France, 26-30 May, 2014.
5. **T Alshahrani**, A El-Betany, M Mabrook, H Tai, I Alrougy, A Sleiman and N McKeown (2014) " The effect of pH of a new PAMAM dendritic material on the performance of organic bilayer solar cells" 4th International Conference on Nanotek & Expo, December 01-03, San Francisco, USA.
6. T Alshahrani, A EL-Betany, M Mabrook, H Tai and N B McKeown (2013) "High open-circuit voltage bulk-heterojunction solar cells by using new dendritic acceptor material", Nanotech 2013, 3, 572-575.
7. **T Alshahrani**, A EL-Betany, M Mabrook, H Tai and N B McKeown, " Highly efficient organic bilayer heterojunction solar cells using new dendritic acceptor materials" [to be submitted].
8. **T Alshahrani**, A EL-Betany, M Mabrook, H Tai and N B McKeown, "The effect of generation and pH of the new acceptor PAMAM dendritic materials on the organic bilayer solar cells performance " [to be submitted].
9. **T Alshahrani**, A EL-Betany, M Mabrook, H Tai and N B McKeown, "Influence of thermal annealing on the morphology of the P3HT: IC70BA blend film and the performance of organic bulk Heterojunction solar cells" [to be submitted].
10. **T Alshahrani**, A EL-Betany, M Mabrook, H Tai and N B McKeown, "new A-A copolymers material to enhance charge transport properties in organic solar cells" [to be submitted].

Dedicated to my Mum and my husband, my daughter and my sister and brothers

Acknowledgements

Alhamdulillah, all praises to Allah for his blessing and the strengths in completing this thesis. I would like to express my appreciations and thanks to my supervisor, Dr. Mohammed Mabrook for his support, advice, guidance, and encouragement throughout my work. I would like to thank him for the valuable information that he provided me in order to bring this dissertation to fruition.

Many thanks to Dr. Paul Sayers for the help, and advice in our cleanroom facility at Bangor University. I would also like to thank all members of Plastic Electronics Research group. Thank you to Colin, Dan, Eifion, Adam and Sundes for their discussions and encouragement.

I would like to thank the School of Chemistry at Bangor University, particularly Dr. Hongyun Tai and Alaa El-Betany For preparation of PAMAM dendrimers materials that we used in our study.

I would like to thank princess Noura University in Riyadh for the provision of a studentship and to Saudi cultural attaché in UK for help and support.

Last but not least, many thanks to all my family, especially my mother, my husband (Khalid), my daughter (Sarah) and my sister and brothers. Thanks you for standing beside me, giving me the love and strength to overcome my obstacles and achieve my goals.

Chapter 1

Introduction

1.1Introduction

There has been increased search of renewable sources of energy due to the current increase in demand for energy supply such as oil, coal and uranium. Oil prices are anticipated to increase to meet the increased demand for energy, according to financial research in the last few years. It is worth noting that, non-renewable sources of energy have high impacts to the environment as they cause a lot of pollution leading to the depletion of the ozone layer. Curb such effects requires quite a lot of time and resources [1, 2]. The major current source of energy is fossil fuel, which is the major contributor to global warming leading to increased temperatures and raise in sea levels [3]. Below is a graph showing global energy consumption.

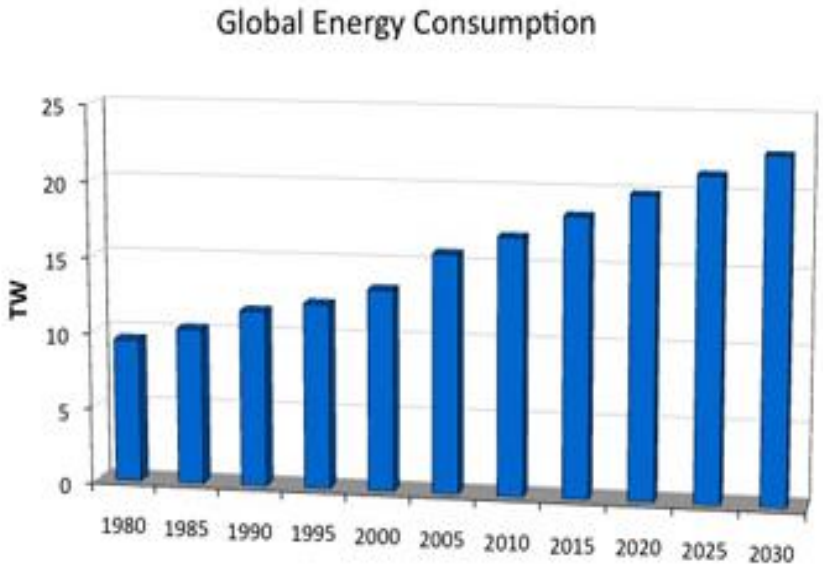

Figure 1.1: Global energy demand for the period 1980-2030[4].

Today, there is a need for a better energy policy. This involves coming up with a cheaper source of energy, and more so, renewable sources. This is due to the fact that the government and different companies are not in the position to renew fossil fuels. Due to this, there is a lot of research on the design of more cost effective sources of energy, and more so, a renewable one. The main sources for renewable energy are from sun and wind, which are low cost and environmentally friendly. Research from different academic and industry places revealed that the amount of sun rays that hit the ground in one hour is equivalent to the amount that the whole world utilizes in one year [5]. However, the drawback for this kind of technology is the big gap between the costs of energy produced from fossil fuel in comparison with renewable energy. Consequently, finding low–cost procedures for producing renewable energy has attracted the interest of researchers worldwide.

One of the ways through which the sun's energy can be converted into electricity is through photovoltaic devices. These devices were discovered in the 1839 by Edmund Becquerel. He came up with this idea after a thorough study on the generation of current through the action of light from a silver covered platinum electrode dipped in an electrolyte [6]. In 1883, Charles Fritts developed the first photovoltaic gadget, which was a continuation of the work of Edmund development of the photovoltaic effect. He produced a cell with efficiency rated at 1%. In this discovery, Charles Fritts used semiconductor selenium, which was covered with a thin film of gold forming a junction. Thereafter, this photovoltaic cell was demonstrated by the use the theory of metal-semiconductor contacts [7].

Later in 1954, Chapin developed a photovoltaic cell with a power efficiency of 6%. This was the first Silicon solar cell which was further enhanced to an efficiency of 44.7% in 2013 [8, 9]. Compared to previous structures and devices, this was a major achievement. Despite its increased efficiency, these devices require a lot of resources for its development, and therefore, are more expensive. Consequently, there has been significant research conducted in the last few years in an effort to improve cell efficiency and reduce production cost. One of these low cost and high efficiency approaches is the use of organic semiconductors material [10, 11].

The use of organic semiconductor materials has proved to be very successful as in organic light emitting diodes (OLEDs). This has been highly advocated for due to their low manufacturing cost and high efficiency. Despite this advancement, there is still a room for improvement through the use of technology to come up with major sources of

power generation systems [12, 13]. Through chemical alteration, the properties of different polymers and small molecule materials can be changed, making it possible to alter the electronic and chemical properties of organic semiconductor materials. This is one of the major advantages of the use of organic semiconductor materials [10, 14, and 15]. Additionally, through the use of different morphology contained in the thin film of the organic semiconductor materials gives a room for control through the use of chemical alterations. A good example is the energy band gap in materials used in OLEDs, which can be altered into a given wavelength of light [11-16]. Through different research, different organic materials, classified in terms of class, have been made, which show promising characteristics for application in photovoltaic cells. Examples of such materials are conjugated polymers and dendrimers [17-20]. Such materials attracted research in the energy sector due to the fact that they can be developed at low temperatures, lowering the use of resources which in turn lowers material costs. The productions of these kinds of materials are very adaptable and therefore give room for electronic constraint and solubility to be changed. This technology has further been enhanced by the introduction of plastic substrates making the structure more flexible [21, 22].

1.2 History of solar cells

The history of photovoltaic effect is dated back in the year 1839 with the first discovery by Edmund Becquerel. He discovered that some materials produce very small electric current when exposed to light. This process of using light to generate an electric current is known as the photovoltaic (PV) effect. At that time the process was explained by the Schottky effect as the photovoltaic effect in these devices was dependent on the barrier between the metal and the oxide. The current semiconductor junction to make solar cell was developed in 1946 by Russel Ohl [23]. Through this discovery the first experiment was carried out by the Bell Laboratories coming up with the first cell with a diffused silicon p-n junction. The fact that the cost of producing the cell was very high; there was low production and use of such cells. The only suitable use at that time was for use as power sources for satellites. In fact, they had much longer life times than using normal batteries.

The efficiency of single junction mono-crystalline silicon has been developed to over 25% [24]. However, such cells are very costly due to its manufacturing costs. In the

manufacture of a flaw free crystal cell, high temperatures are required and more so such processing should be conducted under vacuum. This makes large scale production of such cells more expensive. To reduce the costs, amorphous silicon was then used but the efficiency of the cells was highly affected, leading to reducing the efficiency by approximately 10% [25]. Such silicon cells are also referred to as first generation cells. Through technological advancement, solar cell fabrication was enhanced giving rise to second generation solar cells. This involved the use of diverse inorganic materials in thin films so as to cut costs of materials in the cell manufacture in comparison with the first generation cells. The use of different mixture such as gallium arsenide (GaAs) or cadmium telluride (CdTe) lead to the development of inorganic thin films where their band gap is tuneable [26, 27]. This allows tailoring the preparation of different parts of the solar cell. It is through this that the first set of multi-junction devices were developed and referred to as the third generation solar cells in which different junction absorbed different spectrums. This was a huge step in solar cells developments that reduced the loss of energy through thermalisation of hot-carriers [7]. With the use of solar concentrators, these cells have a very high power conversion efficiency of about 41% [28]. Despite its increased efficiency, solar cell is still very expensive due to the increased cost of production and more so limited materials for its development. Additional limitation to these kinds of cells is the emission of environmental hazard gases during production.

According to the National Renewable Energy Laboratory, the emergent photovoltaics are the most recent generation of solar cells, which involve new development and a shift in material choice. This has been made possible by the development of organic semiconductors used in different applications such as OLEDs [25]. Such kinds of cell put into practice the organic semiconductor junctions or organic /inorganic hybrid junction in the generation of organic-photovoltaic's (OPV). These cells utilize dye or chromophore to collect sunlight. Hybrid cells utilize some high absorbers of organic semiconductors to give a room for thin and low cost absorbing layers while on the other hand utilizing an inorganic acceptor due to their high strength and conductivity [29].

Organic compounds are made up of elements such as carbon, nitrogen, oxygen and hydrogen. The major advantage of these elements is that they all exist in abundance and therefore can be altered easily at very low temperatures, hence cheaper than the inorganic materials. However, their efficiencies are much lower compared to that of inorganic materials [30]. Figure 1.2 shows the advancement of technologies related to

solar cell development [31]. It is clear from Fig. 1.2 that efficiencies of about 3% for OPV recorded in 2001 by the University of Linz. The efficiency increased steadily to over 11% in 2012, as seen in Fig. 1.2.

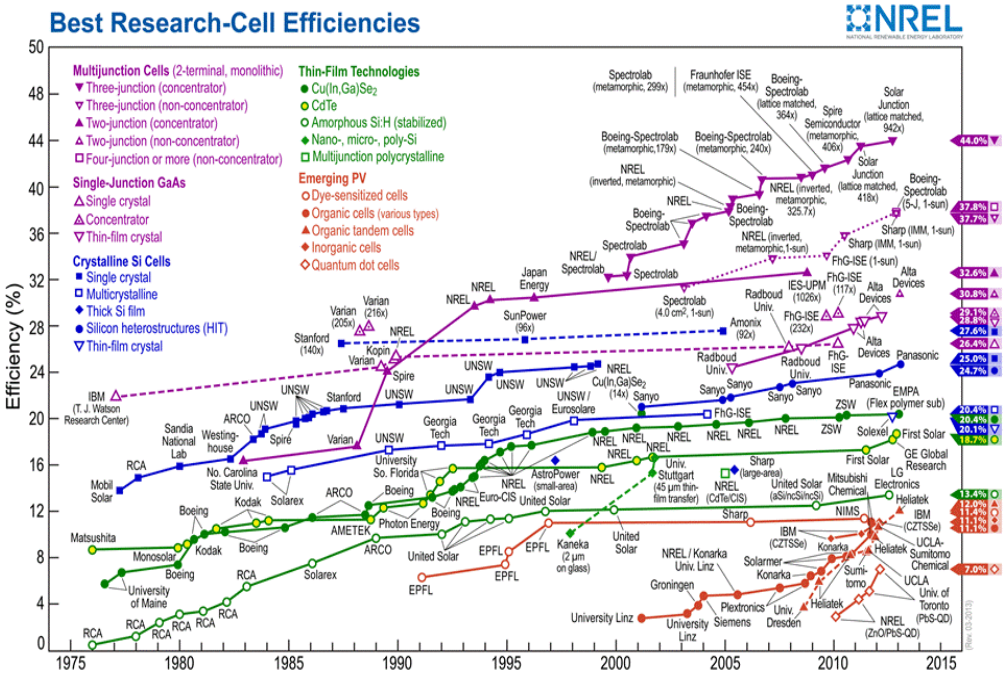

Figure1. 2: *Research cells efficiencies from 1975 to 2015 from US National Renewable Energy Laboratory (NREL)* [31].

1.3 The photovoltaic effect

When a material absorbs light, electrons are excited as such electrons gain energy equivalent to the energy absorbed by the photon. Photovoltaic effect is a process in which a contact junction (metal-semiconductor or a pn junction) produce electrical voltage when exposed to light. These exited electrons cross the contact junction between the two materials more easily in one direction giving one side of the junction a negative charge with respect to the other side. An example of solar cell is made by joining a p-type semiconductor and an n-type semiconductor as shown in Fig. 1.3. The p-n junction form a depletion region with ionised dopant due to the diffusion of electrons from the n-side of the junction to the p-side of the junction, and holes from the p-side of the junction to the n-side of the junction. This will result in an electric field between the two materials which only allows electrons to flow from the p-type semiconductor to the n-type semiconductor. When photons with sufficient energy hit

the cell, they create electron-hole pairs (excitons) and cause electrons to move from the n-side to the p-side of the junction producing excess electrons in the n-side and fewer electrons in the p-side. The voltage difference between the n-side and the p-side pushes the flow of electrons to the contacts at the front and back of the cell creating electrical current (photocurrent) in the reverse direction as shown in Fig.1.3. The creation of photocurrent will results in a clear shift in the current-voltage characteristics where two important parameters, namely short circuit current (I_{SC}) and open circuit voltage (V_{OC}), are clearly identified. When the load resistance is zero ($V = 0$) the cell current is called the short circuit current (I_{SC}), whereas when the load resistance is ∞ (open circuit), the cell voltage is called open circuit voltage (V_{OC}).

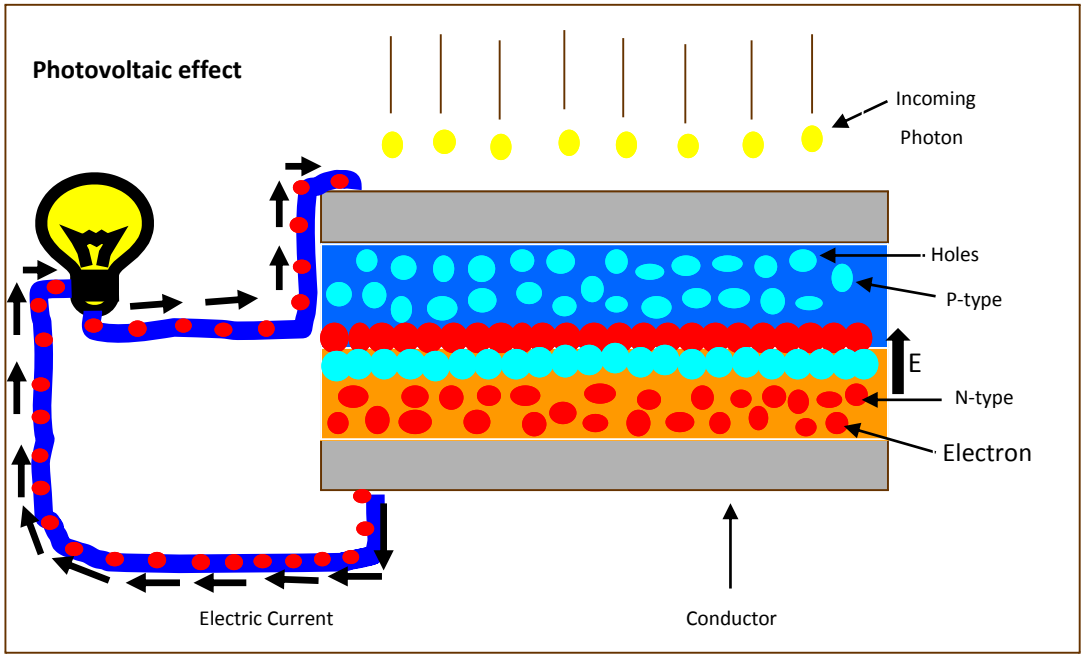

Figure 1.3: *Semiconductor photoelectric effect*

1.4 Organic solar cells developments

Organic solar cells (or some time called organic photovoltaic, OPV) are divided into three categories, dye-sensitized solar cells (DSSCs), small molecule solar cells and polymer solar cells. Also, a hybrid solar cell is a cell that combines both organic and inorganic materials where in the organic materials act as the donor layer and the inorganic one act as the acceptors. The main advantages of OPVs are the low-cost fabrication, low fabrication temperatures during fabrication.

DSSCs came into attention in 1991 after O'Regan and Gratzel developed the first DSSC with an efficiency of about 7.4% [32]. Through technological development the efficiency of DSSCs had increased about 10% in 1994 and in 2001 there was a dramatic increase in efficiency to 10.4% and in 2005 it reached 11.1% [33, 34]. Cell development is related to the redox reaction by utilization of a dye in electrolyte and a solid electron acceptor such as titanium dioxide (TiO_2). The dye takes in light leading to electron gaining kinetic energy which in turn transfers the charge to the titanium dioxide. By using the electrolyte, the dye neutralizes itself through oxidation. The oxidized electrolyte diffuses to the other electrode where it is reduced, thereby completing the circuit.

On the other hand, the polymer and small molecule cells were developed on almost the same technology. It is worth noting that polymer layers are normally solution processed while the small molecules are spin-coated, spray paint or deposited under vacuum using organic molecular beam deposition taking into consideration their features. At the start of organic solar cell development, thin films of one coating of small molecules such as porphyrins or phthalocyanines were used as the active layer [35]. Such devices were deemed to be very inefficient due to the defects in the material compared to inorganic semiconductors. The large concentration of impurities and defects resulted in interference with the electrical properties of the solar cells reducing the power efficiency. The other important setback in the early stages of the development of OPVs is the exciton separation. However, researchers developed a double layer donor/acceptor heterojunction design to improve charges dissociation. With such heterojunction structures between materials, excitons can easily dissociate into free charges and move efficiently as compared to Schottky cells [36]. The earliest cell made use of copper Phthalocyanine (CuPc) and perylenetetracarboxylic to generate a power of about 1% [36]. The developments of new low-bandgap organic materials in the last

few years have led to dramatic improvement in the power conversion efficiency. The main organic materials used in OPVs are based on C60 as the acceptor due to high mobility and the ability to absorb shorter wavelengths. These materials possess enough energy levels for excitons dissociation and can be used with a large number of organic donors. Recently, similar structure with oligothiophene derivative: C60 junction reported much improved 4.9% power efficiency [37]. On the other hand, there was further development of the heterojunction cells with the creation of bulk heterojunction. This structure was achieved by spin coating of poly (2-methoxy-5-(2'-ethyly-hexyloxy)-1, 4phenylene vinylene) (MEH-PPV) with dissolvable fullerene. The coating of the active layer of this structure was performed at the same time rather than creating junction between layers. In this regard, the polymer and the fullerene dissociated into two domains such that from one molecule to the next molecules is a very short distance. This process has highly helped to increase the current cells to an efficiency of about 7.4% [38]. However, due to the formation of different domains, there is a limitation in charge transport to access the paths hence reducing efficiency. In the last 10 years, there has been a great effort to improve the process of charge transport in the bulk heterojunction structures using materials such as polystyrene sphere to produce a better arrangement of these charges by arranging 3D structures of the donor and the acceptor materials. In these spheres all round vacuum and void spaces are filled with donors and acceptors to enable a continuous transport of charges [39].

Another advanced structure was introduced later, that is tandem cells, which can be produces by stacking more layers to create another cell on top of the first cell. This structure increases the absorption levels while at the same time allowing the cell to be thin, giving room for the electron excitement and movement. This involves the use of different materials in the front and back cells to increase absorption level, thereby increasing the efficiency of the cell. The first tandem cell was reported by Hiramoto et al in 1990 [40]. It was made of two metal-free phthalocyanine: perylenetetracarboxylic derive sub cells seperated by gold. The separation layer was very vital in that it prevented the build-up of charges between the sub cells preventing recombination centres of all charges from both sides. In 2013, organic tandem solar cells using solution-processed polymers reached efficiency of 10.6 % [40].

Despite the steady increase in OPVs efficiencies, fullerene acceptors have so many disadvantages such as no light absorption in the close visible IR region, low

photochemical and chemical stability, limited photo-voltage (low V_{OC}), limited fullerene synthesis derivatives and lastly the recycling process of fullerene is expensive [41-44]. Therefore, to improve efficiency, there is a need to develop a new n-type organic semiconductors to replace fullerene acceptors in organic solar cells.

1.5 Thesis outlines

The main aim of this thesis is to design and test new acceptor materials for organic solar cell devices. During this work, three different structures of organic solar cells are fabricated and characterised. These structures are based on organic bilayer solar cells, organic bulk-heterojunction solar cells (OBHJ) and organic tandem solar cells. Different materials have been used in this thesis such as Poly(3-hexylthiophene-2,5-diyl) (P3HT) as the donor, indene-C60 bisadduct (ICBA) and Poly(amido amine) (PAMAM) dendrimers (with different generation size and pH conditions) as the acceptors of the active layer. Poly(3,4ethylenedioxythiophene):poly(styrenesulfonate) (PEDOT:PSS) was used as the hole transport layer while titanium dioxide (TiOx) as the electron transport layer. Indium Tin Oxide (ITO) used as the anode (hole injection layer) and aluminium (Al) used as the cathode. In addition, the effects of different pH conditions and thermal annealing on the active layer morphology and device performance also have been investigated.

In Chapter 1, a general introduction to energy demand and resources is reviewed. The historical background of solar cells and photovoltaic effects are briefly given. A brief background of the organic solar cells development is reviewed.

An introduction to organic solar cells and organic conjugated materials is given in Chapter 2. This chapter illustrated the organic solar cells structures and the essential elements in the operation of organic solar cells: coupling of photons, light absorption and exciton generation, exciton migration, exciton dissociation, charge transport and collection at the electrode. Also present the characterization of solar cell devices.

Chapter 3 provides information about the materials, experimental details and the vacuum system setup and equipment used for studying electronic properties and morphology of the active layers.

Chapter 4 is the first result chapter, which presents the fabrication and characterisation of organic bulk heterojunction (OBHJ) solar cells based on new PAMAM dendrimer materials with different cores and different generations (G0, G0.5, G1, G2) as acceptors

focused on the effect of surface morphology on device characteristics. This chapter also shows the results for OBHJ solar cells based on IC70BA as an acceptor with different concentration ratios and annealing temperatures.

In Chapter 5, the results are split into two parts. The first part presents the result of organic bilayer heterojunction solar cells based on new PAMAM dendrimer salt material as acceptor with different generation (G0.5, G1.5, and G2.5). The influence of pH conditions and annealing temperatures on device operation and active layer morphology is also presented in this part of the chapter. The second part presents the result of organic block copolymer solar cells based on new PAMAM dendrimer G0-TPD acceptor -acceptor material as active layer then OHJ was fabricated with P3HT as donor and PAMAMG0-TPD (A-A materials) as an acceptor to compare the results.

Chapter 6 presents the fabrication and characterisation organic tandem solar cells combined between two cells with different acceptors (IC70BA, PAMAM dendrimers).

Finally, Chapter 7 provides the main conclusions derived from this work, together with possible further work.

References

[1] Annual Energy Outlook 2008 with Projections to 2030. http://www.globalbioenergy.org/uploads/media/0806_EIA__Annual_Energy_Outlook_2008.pdf.

[2] The Environment. http://www.utm.edu/staff/jfieser/class/160/10-environment.htm.

[3] M. Venkataramanan and S. "Causes and effects of global warming", *Indian Journal of Science and Technology*, Vol. 4 (3), pp. 226-229, **2011.**

[4] Solar Energy Systems: *Why study solar energy.*US Department of Energy. http://web.anl.gov/pse/solar/primer/primer1.html.

[5] J. Radosavljević and A. Đorđević. "Deffering Of The Intensity Of Solar Radiation On Horizontal and Oblique Surfaces On Earth", *Facta Universitatis, Series: Working and Living Environmental Protection,* Vol.2(1), pp.77-86, **2001.**

[6] A. E. Becquerel, Comptes Rendus, Vol. 9, pp. 561, **1983.**

[7] J. Nelson, The Physics of Solar Cells, Imperial College Press, London, p. 363, **2003.**

[8] D. Chapin, C. Fuller, &G. Pearson, "A New Silicon P-N Junction Photocell for Converting Solar Radiation into Electrical Power", *Journal of Applied Physics*, Vol. 25 (5), pp. 676-677, **1954.**

[9] The Fraunhofer Institute for Solar Energy Systems ISE, Soitec, CEA-Leti and the Helmholtz Center Berlin. 2013. http://www.ise.fraunhofer.de/en/press-and-media/press-releases/presseinformationen-2013/world-record-solar-cell-with-44.7-efficiency.

[10] A. Murat, K. Tolga and A. Saracb. "Conducting Polymers and their Applications", *Current Physical Chemistry*, Vol. 2, pp. 224-240, **2012.**

[11] L. Dai, B. Winkler, L. Dong, L. Tong, and A. Mau, "Conjugated Polymers for Light-Emitting Applications", *Advanced Materials*. Vol. 13(12), pp. 915-925, **2001.**

[12] Y. Karzazi, "Organic Light Emitting Diodes: Devices and applications*", Journal of Materials and Environmental Science,* Vol. 5(1), pp.1-12, **2013.**

[13] T. Xu and L.Yu., "How to design low bandgap polymers for highly efficient organic solar cells", *Materials Today*, Vol. 17(1), pp. 11-15, **2014.**

[14] A. Pron and P. Rannou., "processible conjugated polymers: from organic semiconductor to organic metal and superconductor", *Processing in polymer science*, Vol. 27, pp. 135-190, **2002.**

[15] T. Hasegawa and J. Takeya., "Organic field-effect transistors using single crystals*", Science and technology of advance materials,* Vol.10, pp. 1-16, **2009.**

[16] S. Eliseevaab and J. Bu¨nzli., "Rare earths: jewels for functional materials of the future", *New Journal of Chemistry*, Vol.35, pp. 1165–1176, **2011.**

[17] J. Wang, C. Zhong, Z. Tang, H. Wu, Y. Ma, Y. Cao and J. Pei., "Solution-Processed Bulk Heterojunction Photovoltaic Cells from Gradient π- Conjugated Thienylene Vinylene Dendrimers", *Chemistry – An Asian Journal*, Vol.5, pp. 105-113, **2010.**

[18] A. Bagher., "Introduction to Organic Solar Cells", *Sustainable Energy*, Vol. 2(3), pp. 85-90, **2014.**

[19] M. Waltera, A. Rudineb and C.Wamser, "Porphyrins and phthalocyanines in solar photovoltaic cells", *Journal of Porphyrins and Phthalocyanines*, Vol. 14, pp 759–792, **2010.**

[20] F. Lincker, B. Heinrich, R. Bettignies, P. Rannou, J. Pecaut, B. Grevin, A Pron, B. Donnio and R. Demadrille., "Fluorenone core donor–acceptor–donor p-conjugated molecules end-capped with dendritic oligo(thiophene)s: synthesis, liquid crystalline behaviour, and photovoltaic applications", *Journal of Materials Chemistry*, Vol.21, pp. 5238-5247, **2011.**

[21] P. Pudasaini and A. Ayon, "Low-cost, high-efficiency organic/inorganic hetero-junction hybrid solar cells for next generation photovoltaic device", *Power MEMS, Journal of Physics: Conference Series 476*, **2013.**

[22] O. Wiedenmann, A. Abdellah, G. Scarpa and P. Lugli., "Design and fabrication of organic solar cells structured via nanoimprint lithography", *EDISON 16, Journal of Physics: Conference Series 193,* **2009.**

[23] R. Ohl, "light-sensitive electric devices", Vol. 2402662 (Ed. U. S. P. Office), United States, **1946**.

[24] J. Zhao, A. Wang, M. Green, and F. Ferrazza, "19.8% efficient "honeycomb" textured multicrystalline and 24.4% monocrystalline silicon solar cells", *Applied Physics Letters*, Vol.73 (14), pp. 1991-1993, **1998.**

[25] M. Green, K. Emery, Y. Hishikawa and W. Warta., "Solar cell efficiency tables (version 37)", *Progress in Photovoltaics: Research and Applications*, Vol.19(1), pp. 84–92,**2011.**

[26] S. Naseem and T. Coutts., "Indium tin oxide/gallium arsenide solar cells", *Journal of Applied Physics*, Vol.58 (11), pp. 4463-4464, **1985.**

[27] R. Bube, A. Fahrenbruch, R. Sinclair, T. Anthony, C. Fortmann, W. Huber, C. Lee, T. Thorpe and T. Yamashita, "Cadmium telluride films and solar cells", *IEEE Transactions on Electron Devices*, Vol.31, pp. 528-538, **1984.**

[28] S. Wojtczuk , P. Chiu , X. Zhang, D. Derkacs , C. Harris , D. Pulver , and M. Timmons., "InGaP/GaAs/lnGaAs 41% concentrator cells using bi-facial Epigrowth", *Photovoltaic Specialists Conference (PVSC)*, 35th IEEE, pp. 001259 – 001264, **2010.**

[29] S. Schumann, R. Campo, B. Illy, A.Cruickshank, M. McLachlan, M. Ryan, D. Riley, D. McComb and T. Jones., "Inverted organic photovoltaic devices with high efficiency and stability based on metal oxide charge extraction layers*"*, *Journal of Materials Chemistry*, Vol.21, pp. 2381-2386, **2011.**

[30] Z. Alparslan, A. Kösemen, O. Örnek, Y. Yerli, and S. San, "TiO_2-Based Organic Hybrid Solar Cells with Mn^{+2} Doping*"*, *International Journal of Photoenergy*, Vol.2011,pp.1-6,**2011.**

[31] N. Carpenter., Chemistry of Sustainable Energy, CRC press, pp. 216, 2014.

[32] B. O'Regan and M. Gratzel, "A low-cost, high-efficiency solar cell based on dye-sensitized colloidal TiO2 films*"*, *Nature*, Vol.353, pp. 737-740, **1991.**

[33] M. Gratzel and K. Kalyanasundaram., "Artificial photosynthesis- efficient dye-sensitized photochemical cells for direct conversion of visible-light to electricity*"*, *Current Science,* Vol. 66, pp.706-714, **1994.**

[34] M. Nazeeruddin, F. Angelis, S. Fantacci, A. Selloni, G. Viscardi, P. Liska, S. Ito, T. Bessho and M. Gratzel., "Combined Experimental and DFT-TDDFT Computational Study of Photoelectrochemical Cell Ruthenium Sensitizers*"*, *Journal of the American Chemical Society*, Vol.127(48), pp. 16835–16847, **2005.**

[35] G. Chamberlain, "Organic solar cells: A review", Solar *Cells*, Vol.8, pp. 47-83, **1983.**

[36] C. Tang, "Two-layer organic photovoltaic cell", *Applied Physics Letters*, Vol. 48, pp. 183-185, **1986.**

[37] D. Wynands, M. Levichkova, K. Leo, C. Uhrich, G. Schwartz, D. Hildebrandt,M. Pfeiffer and M. Riede., "Increase in internal quantum efficiency in small molecular oligothiophene: C60 mixed heterojunction solar cells by substrate heating", *Applied Physics Letters*, Vol. 97(3), **2010.**

[38] Y. Liang, Z. Xu, J. Xia, S.-T. Tsai, Y. Wu, G. Li, C. Ray and L. Yu., "For the Bright Future—Bulk Heterojunction Polymer Solar Cells with Power Conversion Efficiency of 7.4%", *Advanced Materials*, Vol. 22(20), pp. E135–E138, **2010.**

[39] S. Schumann, S. Bon, R. Hatton and T. Jones, "Open-cellular organic semiconductor thin films by vertical co-deposition using sub-100 nm nanosphere templates", *Chemical Communications*, pp. 6478-6480, **2009.**

[40] J. You, L. Dou, K. Yoshimura, T. Kato, K. Ohya, T. Moriarty, K. Emery, C. Chen, J. Gao1, G. Li and Y. Yang., "A polymer tandem solar cell with 10.6% power conversion efficiency", *Nature Communications*, Vol. 4, pp. 1-10, **2013.**

[41] G. Li, R. Zhu and Y. Yang, "polymer solar cells", *nature photonics*, Vol.6(3), pp. 153-161,**2012.**

[42] Z. He, C. Zhong, X. Huang, W. Wong, H. Wu, L. Chen, S. Su and Y. Cao., "Simultaneous Enhancement of Open-Circuit Voltage, Short-Circuit Current Density, and Fill Factor in Polymer Solar Cells", *Advanced Materials*, Vol. 23(40), pp. 4636–4643, **2011.**

[43] Y. Liang, D. Feng , Y. Wu , S. Tsai , G. Li , C. Ray and L. Yu., "Highly Efficient Solar Cell Polymers Developed via Fine-Tuning of Structural and Electronic Properties", *Journal of the chemical society*, Vol. 131(22), pp. 7792–7799,**2009.**

[44] E. Ahmed, G. Ren, F. Kim, E. Hollenbeck, and S. Jenekhe., "Design of New Electron Acceptor Materials for Organic Photovoltaics: Synthesis, Electron Transport, Photophysics, and Photovoltaic Properties of Oligothiophene-Functionalized Naphthalene Diimides", *Chemistry of materials*, Vol. 23, 4563–4577, **2011.**

Chapter 2

Review of organic solar cells

2.1 Introduction

Over the years, quite a number of developments have been made leading to the exploration of new materials for solar cells. The advancement in research in this sector have now been able to come up with a mechanism whereby organic polymers and small molecular materials are used in solar cells. A lot of attention in terms of research is being channelled towards organic photovoltaic cells and their capability to convert power has been shown to grow remarkably. This has been made possible by the use of new polymer materials, inorganic molecules, and methods of fabrication that are more advanced and sophisticated. Organic cells have a number of areas in which they can be applied including: power supplies for mobile devices, sensor networks, radio frequency tags, laptops and iPods. In fact organic solar cells have characteristics of low cost, mechanical flexibility, large scale production, fast production and their properties can be easily modified hence making them suitable for use in a wide range of environments. In this chapter, we are going to be reviewing the theoretical background, the behavioural characteristics and concepts that are related to organic solar cells so that can create a basis on which the results that will be presented in subsequent chapters 4, 5 and 6 will be discussed. An introduction to the main component of organic solar cells, organic semiconductors is provided in Sections 2.2. Organic solar cells device structures are discussed in Section 2.6, followed by the process of generating power from a photovoltaic device in section 2.7. Finally the equivalent circuit model of an organic solar cell and current-voltage properties of solar cell devices under both illumination and in the dark are discussed under electrical characterisation of organic solar cells title in Section 2.8.

2.2 Organic semiconductors

Organic materials are promising materials to fabricate low cost solar cell devices. The interest in organic materials for electronic application (light emitting diode, transistors and solar cells) was started when the conducting polymers were discovered in 1980s [1, 2]. Organic semiconductor materials considered to be good conductive materials than other semiconductor materials due to their chemical structures. It can gain a lot of features from chemical synthesis of organic semiconductors such as solubility, flexibility and conductivity. Organic semiconductor materials based on carbon atoms, and the electron structures for the carbon atom in the ground state is: $1s^2 2s^2 2p_x^1 2p_y^1$ which means that orbital 1s has two electrons, orbital 2s has two electrons and orbital 2p has also two electrons. It can be noted that orbital s extremely filled and orbital p has two unpaired electrons, one electron in $2p_x$, one electron in $2p_y$ and $2p_z$ has no electrons. That means 1s contained the core electrons, and the valence electrons are in the $2s^2\ 2p^2$ orbitals [3-5]. Figure 2.1 shows the orbital shapes for s orbital, p orbitals (p_x, p_y and p_z) and their combination.

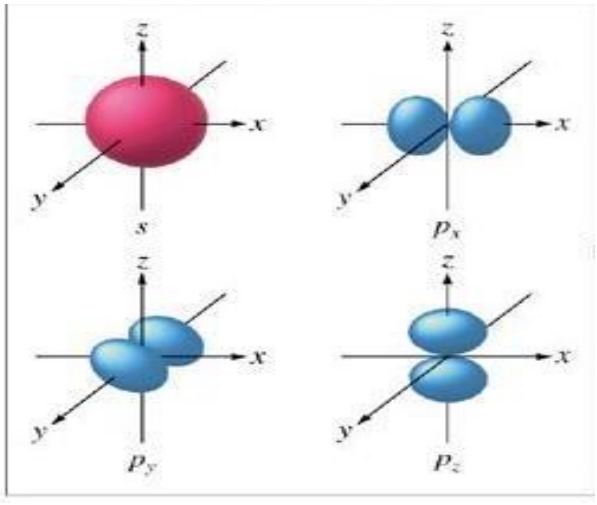

Figure 2.1: O*rbital shapes for s orbital, p orbitals (p_x, p_y and p_z) and their combination.*

However, the hybridisation between (2s and $2p_{(x,y)}$) orbitals leave $2p_{(z)}$ unchanged as can be seen in Fig. 2.2:

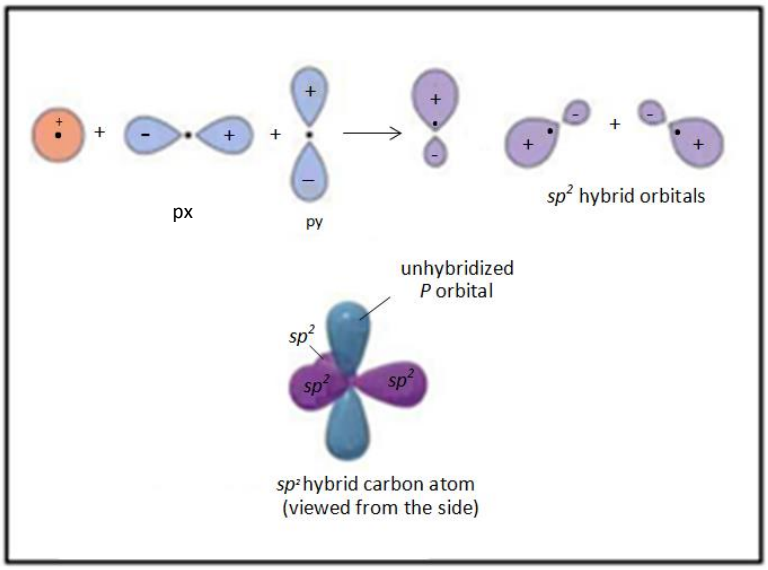

Figure 2.2: *Hybridization between (2s and $2p_{(x,y)}$) orbitals.*

As a result of the hybridisation, two types of bonds are formed; σ bonds are single bonds between carbon-carbon and carbon-hydrogen atoms, for localised electrons, and π bonds possess delocalised electrons. It can be observed from the sp^2 hybridisations in Fig. 2.2 that three carbon electrons form σ bonds where these electrons are localized. These hybrid orbitals lied at 120^0 to each other. This configuration leaves the forth (not hybridised) electron, which is delocalized to give the π bond as shown in Fig. 2.3. Moreover, electrons in conjugated polymers, for example , sp^2 hybridized carbon atoms, can move along of the polymer chain easily. Thus, electrons in these bonds are responsible for the electrical conductivity of organic semiconductors [3,5,6]. Also, molecular orbitals which form σ and π bonds represent the energy levels for organic semiconductor materials [6]. The denoted bonding molecular orbitals (σ and π) form the lowest molecular orbital (lowest energy levels) where the denoted anti-bonding molecular orbitals (σ* and π*) form the highest molecular orbitals (highest energy levels). These molecular orbitals are similar to energy bands levels in inorganic

materials. Figure 2.4 shows the method of creating energy gap levels in organic semiconductor.

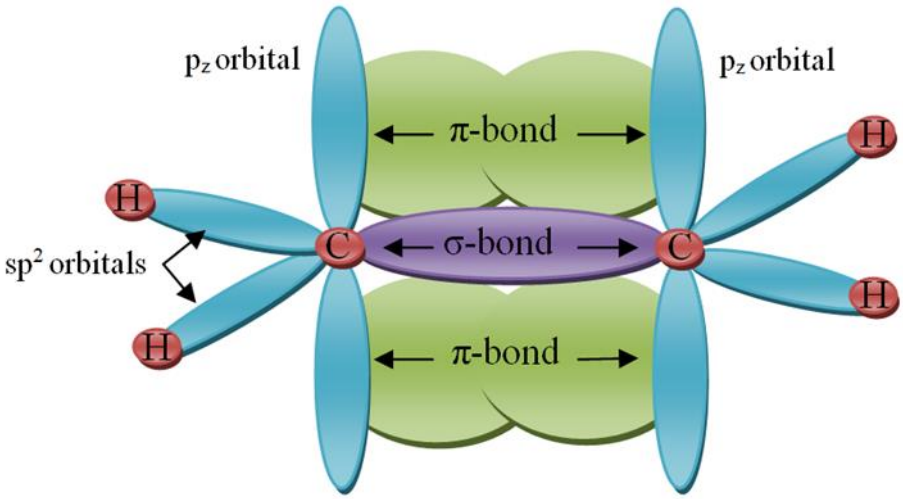

Figure 2.3: *Schematic diagram of the bond and orbitals for two ap2 hybridised carbon atoms*

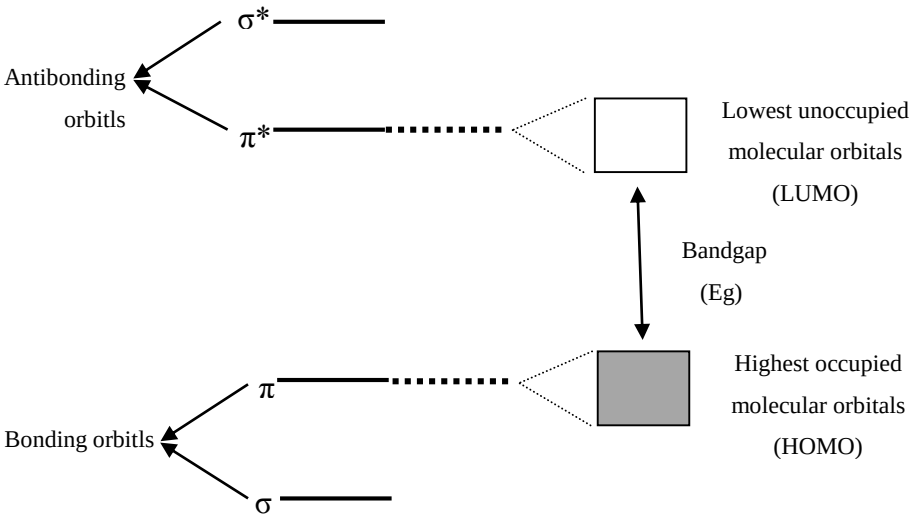

Figure 2. 4: *The energy levels in organic semiconductors.*

The anti-bonding π* molecular orbitals (conduction band) joined the π bonding molecular orbitals (valance band) to create the Lowest Unoccupied Molecular Orbital (LUMO) and High Occupied Molecular Orbital (HOMO). The gap between the LUMO and HUMO is the energy gap which the conductivity in organic semiconductor depends on. Thus, from Fig. 2.4 it is clear that σ bonds are extremely filled with electrons where π bonds are empty. On the other hand, if the energy band gap becomes as small as possible the tolerance of electrons to move from the HUMO to LUMO increases. Some organic semiconductors have a very small band gap of < 2 eV, which mean that it is good materials compared to some inorganic semiconductors, which haves a large energy band gap [3, 5, 6].

Organic semiconductors can be divided into small-molecule and polymer semiconductors. The discovery of the electrical conductivity of doped polyacetylene 30 years ago made the conjugated polymers an interesting areas of research in electronic applications. Organic semiconductor polymers properties including electrical conductivity, optoelectronic, colour (absorption and emission) and photoinduced charge transfer lead them to be used in many electronic and optical applications such as organic light-emitting diodes, organic field-effect transistors, organic photovoltaic cells, and sensors [7-9]. The main advantage in conjugated polymer materials is the ability to tune the band gap by changes in the synthesis materials and it can be used to cover large surfaces. They combine between mechanical properties of polymers and electronic properties of metals and semiconductors. Conjugated polymers in fact are potential materials in the development of new organic solar cells. Researchers developed conjugated polymer synthesises and deposition process methods to achieve unique electrical properties [10]. The highest reported efficiency organic solar cells based in these materials reached 7% [11, 12].

However, the small molecular materials, including oligomers, dendrimers, pigments, dyes, liquid crystal, and organo-mineral hybrid materials also based on π conjugated electron [13]. π-conjagted electrons mean that it can be produced from the rotation between the single and double bonds. It was reported that the long conjugation in the backbone for these materials gives small band gab which is one of the main advantages for these materials in the application of organic solar cell. Furthermore, these materials have better chemical purity than polymer materials due to the small size. Many types of these materials cannot be produced from solution [14, 15]. However, dendritic materials are a type of small molecules combine between the high chemical purity and

the ability to be produced from solution. Dendrimers are composed of highly branched, well-defined and nature monodisperse macromolecules, which can support charge transport and film morphology [16, 17]. Due to their unique properties over conventional polymers such as low viscosity, good solubility, nano-scaled size, low-disparity and multi-functionality, dendritic materials became interesting materials in many application areas including organic solar cells [18, 19]. Dendrimers are perfect monodisperse macromolecular (tree-like structures) with highly branched three dimensional structures: core, branches, and end groups [20-22]. Figure 2.5 shows the general structures of dendrimers.

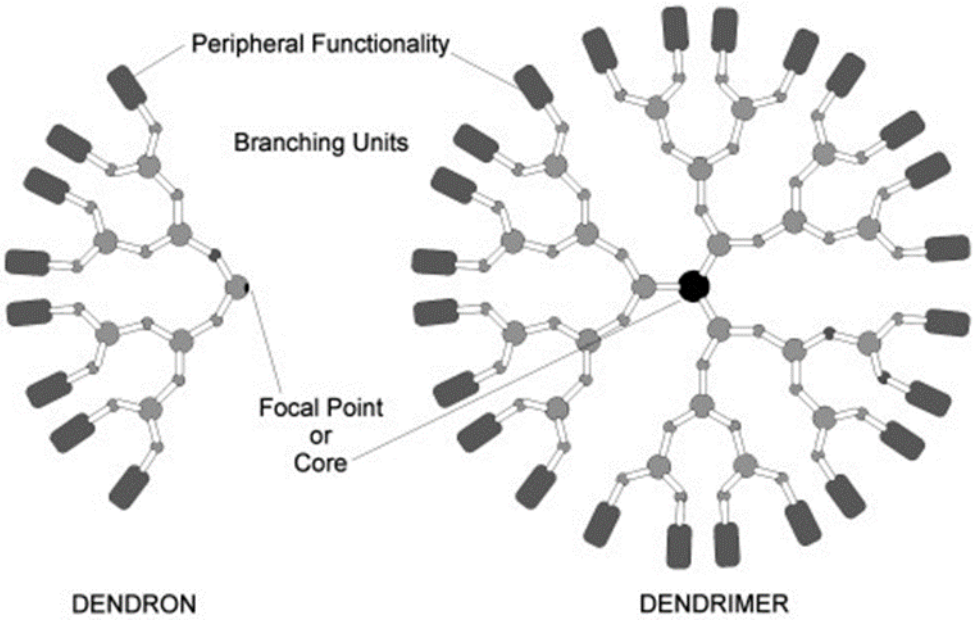

Figure 2.5: *Schematic diagram of the general structures of dendrimers [22].*

The core responsibility is to control the absorption of light where the charge transport and molecules separation take place within the dendrones. The end groups determine the solubility of the dendrimers. One advantage of these structures is the ability to tune each component separately. This means that to absorb a wide range of solar spectrum within organic solar cell devices the change must occur in the core. The branching number of dendrimers which is equal to the generation number of dendrimers affects the charge mobility in organic solar cells. Thus, hole mobility and optical properties of dendrimers can be tuned by changing generation number and attachment point of the dendron to the core [23]. However, when going from the centre towards the dendrimer

periphery the number of focal points is called the generation number. For example, if the dendrimer having three focal points when going from the core to the dendrimers surface is denoted as the 3rd generation dendrimer (G3) as shown in Fig. 2.6 [24]. Intermediates during the dendrimer synthesis are sometimes denoted half-generations. Carboxylic acid-terminated PAMAM dendrimers are a well-known example of half generation dendrimers. These half generation some time have properties better than the amino-terminated dendrimers in the application of biological and electronic systems [25, 26]. Furthermore, their small size and monodisperse nature leads to a high degree of ordering in organic solar cell devices and thus high carrier mobilities [27].

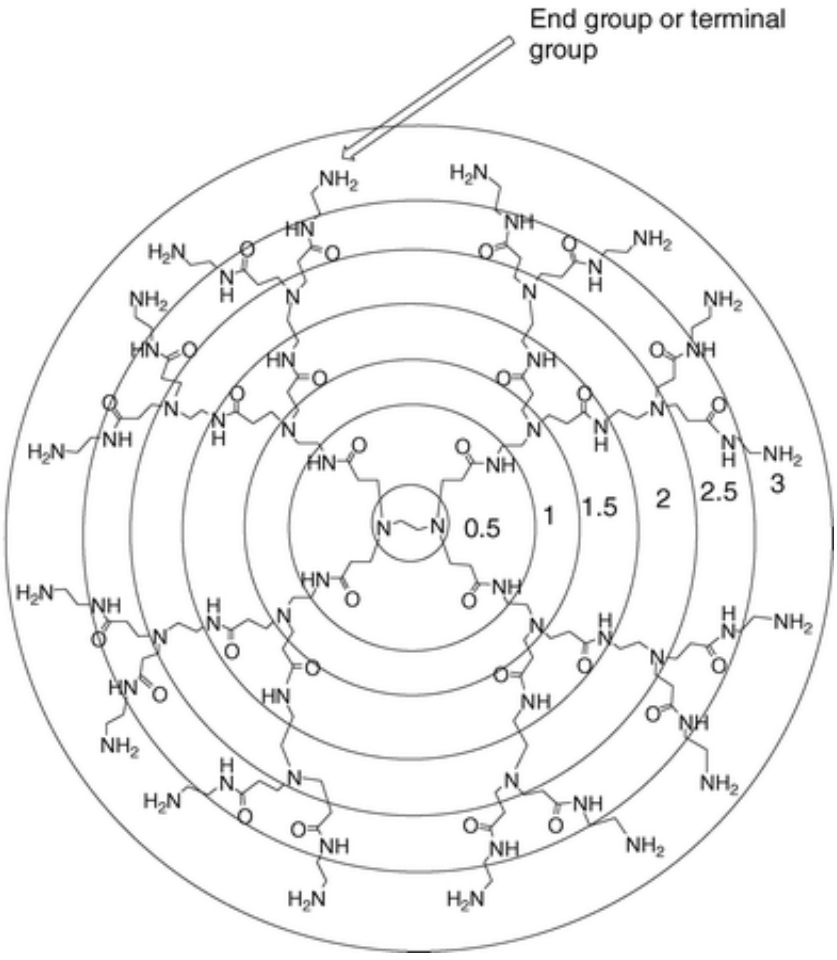

Figure 2.6: *PAMAM dendrimers G3 [24]*.

However, the functional group in light harvesting dendrimers mechanism (chromospheres) positioned on the periphery, branching point and focal point (core) where the periphery combine the energy and transfer it to the core. In light harvesting dendrimer applications, due to the small band gap core and big band gap periphery, the short wavelength absorb by periphery and the long wavelength absorb by the core [28]. In the application of organic solar cells the absorbing of red light in the solar spectrum is desirable as much more photons exiting in the red wavelength. The advantage of using dendrimers materials in the applications of organic solar cells is the ability to mix different cores together without any separation occurred. This arise the ability to access more solar spectrum of light absorption. Mixing several dendrimers with different cores leads to absorb a wide range of wavelengths of light. Another advantage in using dendrimers materials in the application of organic solar cells is the ability to blend without any phase separation. This blend would be covering the whole solar spectrum which leads to harvest much more light and enhance the photovoltaic device performance [29, 30].

2.3 Electron transport materials

This section gives an overview of the developments of some of the electron transport material that have occurred lately for the application as electron acceptor in organic solar cells. It is expected that an ideal acceptor should have a number of behavioural properties which are then combined to create a more efficient component. Some of these properties include: good light harvesting, high electron mobility, stability under processing and operational conditions, and ease and cost of synthesis. N-type materials are typically characteristic of low electron deficiency and their energy LUMO is quite low and they are easily reduced. Molecules that are electron deficient and have already been reduced are more stable towards water and oxygen [31].

Since 1985 when clusters that consist of 60 carbon atoms and high degree of stability, Buckminsterfullerene they received a great deal of attention as an electro active material. C60 (see Fig. 2.7) is readily available in the market and it acts as an electron acceptor having electrons that add up to over six in the solution. This is an indication of a high electron mobility [32-33]. C60 has a limited solubility and this made it possible to employ the vacuum deposition technique as the main technique for

deposition. This technique has been applied in heterojunction solar cells and have efficiencies of about 3.6% [34]. In 1995 Hummellen and his research group identified a soluble version of C60 namely methano-fullerene derivative Phenyl-C61-butyric acid methyl ester (PC61BM) [35]. They were able to demonstrate separation of charges that was more efficient and this in return resulted in a photoinduced electron transfer that was fast. It was these findings that excited more research into the development of organic solar cells (or organic photovoltaics (OPVs). PC61BM has been in use as an acceptor in most of the OPV devices. It has a spherical shape that gives it an advantage over t other planar semiconductors enabling the transport of electrons in three dimensions. The disadvantage of PC61BM is the absorption inability in the visible light. This has led to the development of PC71BM, C70 analogue and PC61BM that given rise to higher photocurrent and power conversion efficiency (PCE) in OPV cells due to the ability to absorb very strongly in the blue region of the solar spectrum [36]. Today there are a solar cells that are highly optimized with either PC61BM or PC71BM and are thus able to reach over 8% PCE if the most suitable low band gap polymers are provided [37,38]. In order to create more improvements on open circuit voltages (V_{OC}) materials, it can best be achieved through the use of materials with low levels of LUMO. HOMO and LUMO energy levels can be tuned by attaching groups to be used in solubilisation to the fullerene core enablling processing of the solution. There has been a number of substituents that have been surveyed and developed and the resulting C60 component shows less delocalized π-electrons reduces its affinity to electrons by about 50-100 mV for every substituent [31]. The knowledge of the resulting changes in LUMO energy levels has led to the synthesis of a variety of mono-bi- and tri adducts (as shown in Fig. 2.7). This has helped researchers achieve a higher V_{OC} in solar cells. For instance, Indene-C60 bisadduct (IC60BA) that has a LUMO level at 3.74 eV (0.17 eV up-shifted than that of PCBM) shows superior photovoltaic performance at 0.84 V V_{OC} and 6.48% PCE when used in P3HT-based OPVs as acceptor [39]. Indene-C70 bisadduct (IC70BA) has also been synthesized at a higher LUMO level of 3.72 eV (0.19 eV higher than that of PCBM). IC70BA possesses good solubility in common organic solvents and stronger visible absorption. P3HT/IC70BA OPVs with methyl-thiophene additives have been shown to have higher PCEs of up to 6.69% with a 0.86 V V_{OC} upon using pre-thermal annealing for 10 minutes at 150^0C [40]. Fig. 2.7 show the chemical structures of relevant fullerene derivatives used as electron transport material in OPVs.

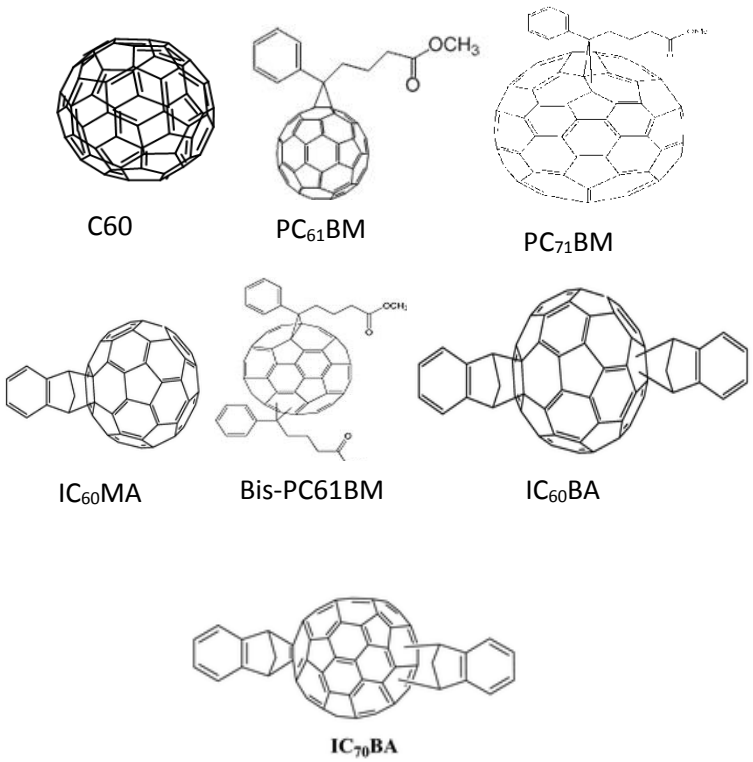

Figure 2. 7: *Chemical structures of relevant fullerene derivatives used as electron transport material in OPV.*

On the other hand, many researchers developed non-fullerene acceptor materials due to some limitations of fullerene acceptors [41]. The polyamidoamines (PAMAM) are first recognised class of commercial dendrimers. New systems with high efficiency of energy could be approaches through the use of the flexible aliphatic PAMAM bone as a scaffold for light-harvesting antennae. 1,8-naphthalimide fluorophores could beneficial for PAMAM light-harvesting antennae due to the strong fluorescence and good photostability [42]. The 1,8-naphthalimide derivatives were applied in a number of various areas including organic solar cells[43]. PAMAM dendrimers was first developed by Tomalia in 1979. PAMAM dendrimers have an ethylene diamine core, amido amine branching structure and available as cationic (full) generation (G1, G2,..etc) with amine-terminated branches and anionic (half) generations (G0.5, G1.5….etc) with carboxylic acid-terminated branches [44]. PAMAM dendrimers functionalized groups could be amine, carboxylic acid, and hydroxyl moieties with high

generation of G. PAMAM dendrimers have been used in various areas including: light harvesting, chemical sensor, catalysis, cross link agent, gene transfer, imaging contrast agents, and polymer-based drug delivery. 11^{th} generation is the highest generation can PAMAM dendrimers reach due to the steric hindrance caused by the growing number of branches which does not allow enough room for further branches to grow. The dendrimer structure becomes mores spherical and less flexible with every increase in generation [45]. PAMAM structure and rigidity was found to depend on the pH of the media. At low pH primary and tertiary amine are positively charged, which makes the dendrimer less flexible due to the intermolecular electrostatic interactions. At neutral pH, dendrimer become more flexible as only the primary amine are positively charged. At higher pH none of primary or tertiary amine are charged, thus the dendrimer becomes highly flexible. It was reported that PAMAM properties such as the shape and size of the dendrimers as a function of generation, solvent accessible surface area, monomer distribution, and distribution of terminal groups are all crucial for several applications of dendrimers [46-48]. PAMAM-G2 (Fig. 2.8) was used as the electron-collection interlayer material between the active layer and ITO of inverted OPVs [49]. C60–PAMAM G0.0 also used to modify the nanocrystalline TiO_2 silanized electrodes which resulted in a novel photoelectrochemical sensitization film that showed particularly high photocurrent and global photo- conversion efficiencies. This makes them (fullerene–dendrimer modified electrodes) attractive for solar cell technology development [50].

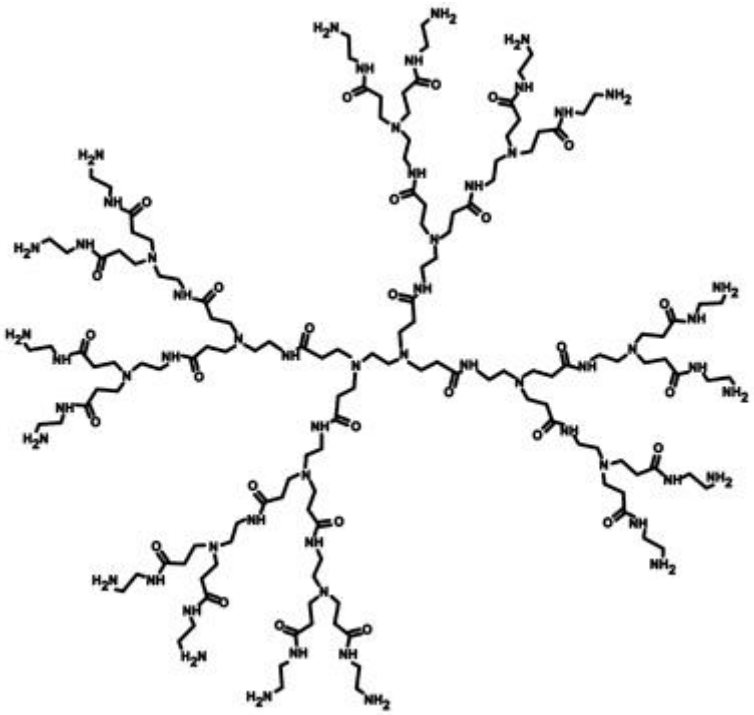

Figure 2.8*: Chemical structure of PAMAM-G2*

On the other hand, majority of the research studies have emphasised on a thienopyrrolodione (TPD) as the electron acceptor moiety in the synthesis of donor-acceptor (D-A) polymers. It provided reasonable optoelectronic properties, thus the field-effect mobility enhanced to 0.6 $cm^2V^{-1}s^{-1}$ in organic field-effect transistors (OFETs). Also, TPD and power conversion efficiency of over 7% in organic bulk heterojunction organic solar cells (BHJ OSCs) was achieved [51]. TPD acceptor moiety is simple, compact, symmetric, and planar structure could be useful for electron delocalization when it is integrated into various conjugated polymers [52]. Based on that, it appeared probable that TPD enhance intra chain and interchain interactions along and between coplanar polymer chains. Its strong electron-withdrawing effect lead to low HOMO and LUMO energy levels in order to maximize the OBHJ V_{OC} and then improve the PCE [53]. Furthermore, introduce different alkyl side chains on the pyrrolering result in good solubility and processability of the copolymers. Finally, coplanar structure of TPD and its highly fused allows high crystallinity morphology of the active layers which is support charge transport to the corresponding polymer and reduces recombination of charge carriers in BHJ films [52].

2.4 Hole transport materials

Conjugated donor polymers can be the most promising p-type materials (hole transport) for application in OPV devices. This is due to the fact that they have the potential to combine their good films forming properties, intensive light absorption, suitable HOMO and LUMO levels and high hole mobilities to achieve better electronic characteristics that make them much more efficient. There has also been a significant rise in the number of publications regarding new polymers over the last few year and several review articles have been written in regard to this new development [54-56]. The first bulk-heterojunction (BHJ) structures that were based on poly(phenylenevinylene) (PPV) were built in 1995 including : poly[2-methoxy-5(2'ethylhexyloxy)-1,4-phenylenevinylene] (MEH-PPV) and (poly[2-methoxy-5-(3,7-dimethyloctyloxy)]-1,4-phenylenevinylene (MDMO-PPV) as donor materials [55,57]. When these poly-components were combined with fullerene acceptors, the resulting components had high PCEs of up to 3.3% [58, 59].

However, 550 nm is the absorption edges for MEH-PPV and MDMO-PPV which corresponding to a band gap of ca. 2.3 eV. Organic solar cells based on these materials produced low output current density due to the big mismatch between their absorption spectra and the solar irradiation spectrum [60]. Through the progression in research, p-type polymer poly(3-hexylthiophene) (P3HT) was synthesis and achieved approximately 5% PCE in the process of optimisation in the application of organic solar cells. The performance of the device based on P3HT as donor was affected by number of factors including processing conditions, regioregularity and molecular weight [61, 62]. Due to the low band gap (1.9 eV), broader absorption band and also high hole mobility for P3HT exhibited much better photovoltaic properties. By using P3HT as donor material blending with PCBM as acceptor, PCE of over 4% has been reported by different researcher. Thus, P3HT has attracted much attention in the OPV filed. The absorption band of P3HT/PCBM covers the range from 380 to 670 nm, which means that photons with energy between 2.0 and 3.3 eV can be absorbed by the active layer, to generate excitons [63].

2.5 Electrodes and buffer layers:

2.5.1 Transparent conducting electrode:

Conducting films that are transparent and have thin conducting films form a class of materials that are able to achieve a large value of conductivity while at the same time trying to maintain a transmission that is high within the visible range of the electromagnetic spectrum [64]. There has a great deal of research that has been directed towards making the thin film coatings commercial. Today, the current commercial products are usually based on the n-doped metal oxide films that are normally referred to as transparent conducting oxides. These transparent films are applied in a wide range of areas including: heat-mirror window-coatings which are used to controll the transmission of infrared energy into and out of buildings, use as transparent electrode materials in photovoltaic cells, touch-screen technology and flat panel displays e.g. liquid crystal displays (LCD), organic light emitting displays (OLED) and plasma screen displays [65].

Indium tin oxide (ITO) was discovered in 1954 by Rupperecht and is identified as the first modern transparent conducting oxide (TCO) materials [66]. It is an n-type transparent semi-conductor and usually has a wide band gap of approximately 4 eV. With the technology today that is growing very rapidly, these properties have made ITO to play a very important role in the optical and electronic industries [67]

2.5.2 Top electrode

The cathode works are achieved through extraction of electrons through a strong electric field. Cathode materials is supposed to be a metal of low work function so that it can be deeper in energy as compared to the LUMOs of the material that acts as the acceptor as well as a suitable material for the extraction of electrons. Many of the OPV devices made use of metals of low work function like calcium, magnesium or aluminium as the cathode material. Among all the metals, aluminium is the most commonly used cathode material because of its stability in air. However, V_{OC} does not depend on the working of the cathode which is able to support pinning of Fermi level that are formed between the cathode and the active layer [68]. The electrons in organic molecules are usually highly localized and it is most likely that the Fermi level pinning

will form an interfacial dipole which results from the contact between the cathode and the active layer hence, which resulting in an equilibrium layer. The formation of dipoles results in reduction of the energy barriers that exist between the Fermi levels and the acceptors of the LUMO level and this helps in transfer of electrons [69]. Fig. 2.9 show the energy diagram for metal/semiconductor contact after interfacial dipole formed.

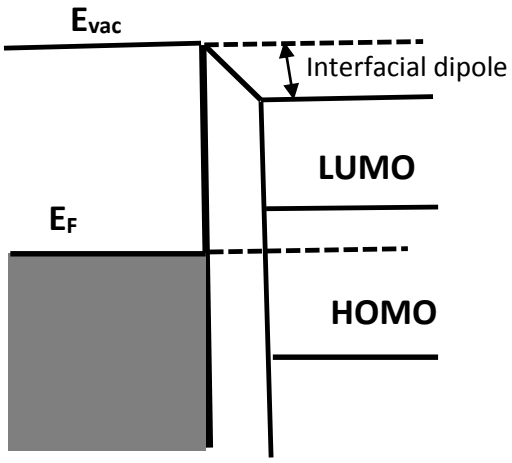

Figure 2.9: *Energy diagram for metal/semiconductor contact after interfacial dipole is formed.*

2.5.3 Buffer layers

One major problem that faces organic solar cells is that it has both the donor polymer and the acceptor molecule touching the two electrodes. This results into the formation of acceptor electrons at an interface that is located very close to the anode. Therefore, if any of the electrons were transferred to the anode, they are likely to recombine very easily, resulting in the reduction of the working voltage of the device [70]. It also provides an electronic blocking layer between the active layer blend and the anode and therefore serves to prevent the transfer of electrons in the acceptor to the anode. The same effect also occurs at the cathode in situations where holes may be produced in the HOMO of the polymer at a point very close to the aluminium and the barrier between the Fermi level of the metal and the organic semiconductor LUMO is reduced. The design however plays a very crucial role in organic tandem solar cells in order to achieve a device with a high performance capability. Therefore, for tandem devices that

are conventionally built with sub cells connected in series, the layers at the level should enable an efficient recombination of charge in order to prevent the sub cells from charging again. There is an Ohmic contact that exists between both the intermediate layer and the photoactive layer which is very important in reducing the energy loss when the charges are entering the intermediate layers as they exit the photoactive layer. Analysis conducted in many studies has shown that TiOx, which is an electron transport layer, can be inserted together with poly(3,4-ethylenedioxythiophene), poly(styrenesulfonate) (PEDOT:PSS), which act as the hole transport layer, to achieve the buffer layer [71,72].

2.6 Organic solar cells structure

2.6.1 Single layer organic solar cell

The first photovoltaic solar cells contains two electrodes with a semiconductor layer between them and these two electrodes have different work functions. ITO was used normally due to the high transparency and it has also high work function. However, the second electrode which has a low work function can be aluminium, gold, silver, calcium with a layer of aluminium on top of it or lithium fluoride capped by aluminium [73, 74]. Figure 2.10(a) show a typical solar cell structure and Fig.2.10 (b) shows schematic energy-band diagram of an organic single layer solar cell. The difference in the work function between the electrodes creates an electric current through the active layer to separate the exciton (electron-hole pairs formed when a photon is absorbed by a semiconductor and are attracted to each other by Coulomb's electrostatic attraction) [73]. However, the efficiency for this device is very low due to low charge mobility through the organic semiconductor layer, which has short exciton diffusion length about 10 nm where the light absorption length is 100 nm. The electric current which flows through the semiconductor layer is not sufficient to separate the exition effectively. Furthermore, the possibility for the charges to recombine with holes is high rather than to reach the interface between the semiconductor layer and cathode. The best recorded efficiency for this type of structures was 0.3% from doped conjugated materials [73]. To overcome this limitation bilayer heterojunction structures were introduced [74-76].

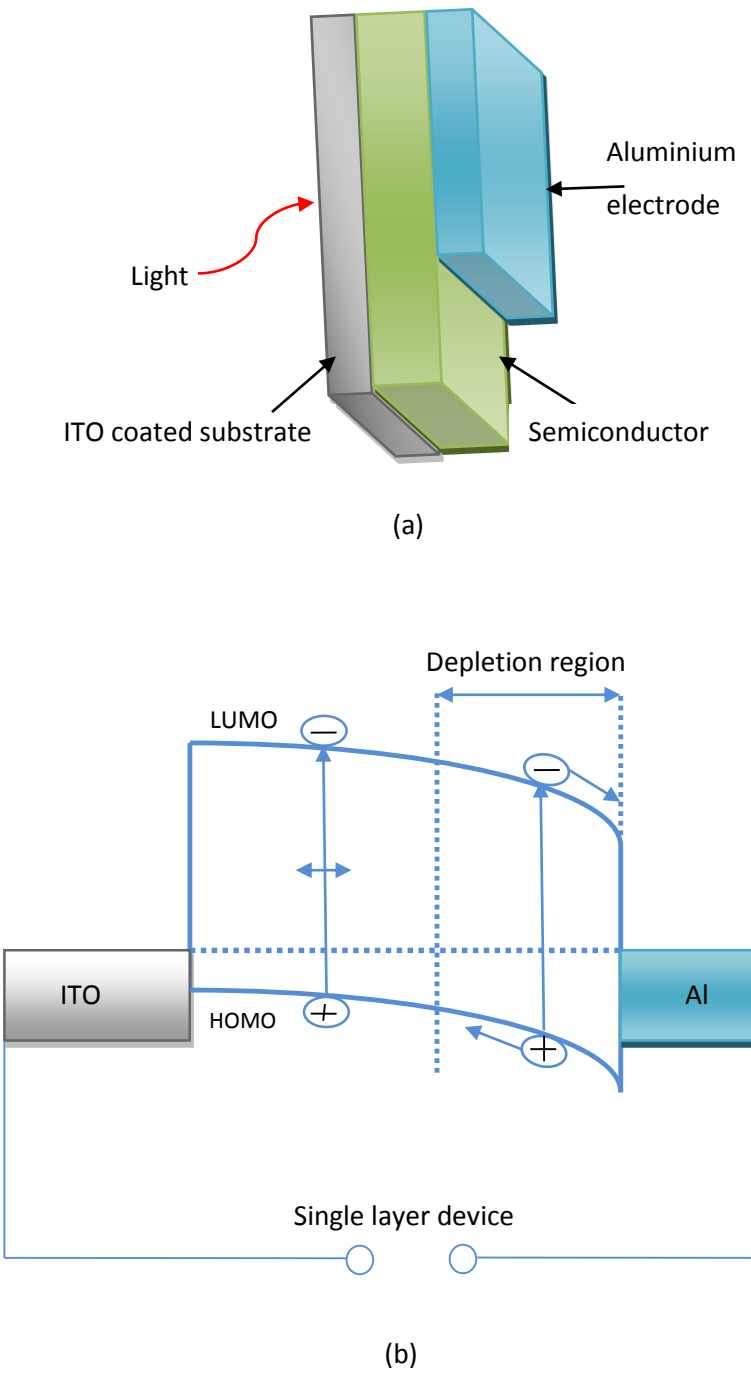

Figure 2.10: *a) structure of a single layer solar cell b) energy band diagram of a single layer solar cell.*

2.6.2 Bilayer organic solar cell

With the introduction of the bilayer heterojuction solar cells, charge separation and PCEs became more efficient. In this case, p-type (hole transport material) and n-type (electron transport material) are put together in a stack and result in an interface that is planar in nature. In 1986 Tang reported a bilayer heterojuction solar cell and it was shown to have a remarkably improved efficiency of about 1% for a photovoltaic cell that is two layered and consists of copper phtalocyanine which acts as the donor and perylene which plays the role of an acceptor [77]. In another case whereby the possibility of band bending at the interface between the semiconductor and the metal being neglected and this calls for a suitable offset for the energy between the LUMO that is contained in the donor and that of the acceptor and also the HOMO of the donor as well as that of the acceptor. This results in creation of a potential drop and the formation of a heterojuction when the two materials come into contact. In a case where an excitation is created in the donor, the electron is left to exist in the LUMO of the excited state of the donor and it can therefore be transferred to the acceptors' LUMO. For this type of photoinduced electron transfer to happen, there must be a bigger energy offset than the excitation energy that binds the coulomb and thus it is possible to overcome coulomb interaction and then separate the excitation into free charges [78]. The same case can be applied for all the reverse hole transfers from an acceptor excited state. The excitation must be created at a point that is close to the interface of the donor and the acceptor in order to be able to reach the heterojunction within the diffusion length of the excitation. After the excitation has been separated, it is then possible to transport the free charges to the electrodes whereby the holes are able to travel within the donor and the electrons within the acceptor [79]. This concept is advantageous as recombination is minimized and therefore the holes and electrons are separated. For the extraction of the charges to be conducted efficiently, the electrodes are supposed to match the donor HOMO and the acceptor LUMO [80]. To prove this argument, the vacuum deposited copper pthalocyanine/C60 film was proved to give out approximately 3.6% PCE within the architecture of this device [40]. However, the main disadvantage of this concept is that it makes it possible for exclusive excitations to be able to contribute to the charge generation which in return hampers the performance of the device. It also requires orthogonal solvents for the purpose of solution processing of the two organic layers and this limits its capability. Therefore it is important that

understand that most of the bilayered devices are usually fabricated by thermal evaporation process which is normally more expensive and much more complicated to carry out as compared to the process of solution processing. The bilayer concept has however been expanded and developed extensively by Chang et al using halogen-free solvents and devices with PCE exceeded 7% were reported [81]. In order to improve the exciton diffusion length at the interface bulk heterojunction structures were introduced. Figure 2.11 show the structure of an organic bilayer heterojunction solar cell and the energy band diagram of bilayer heterojunction cell.

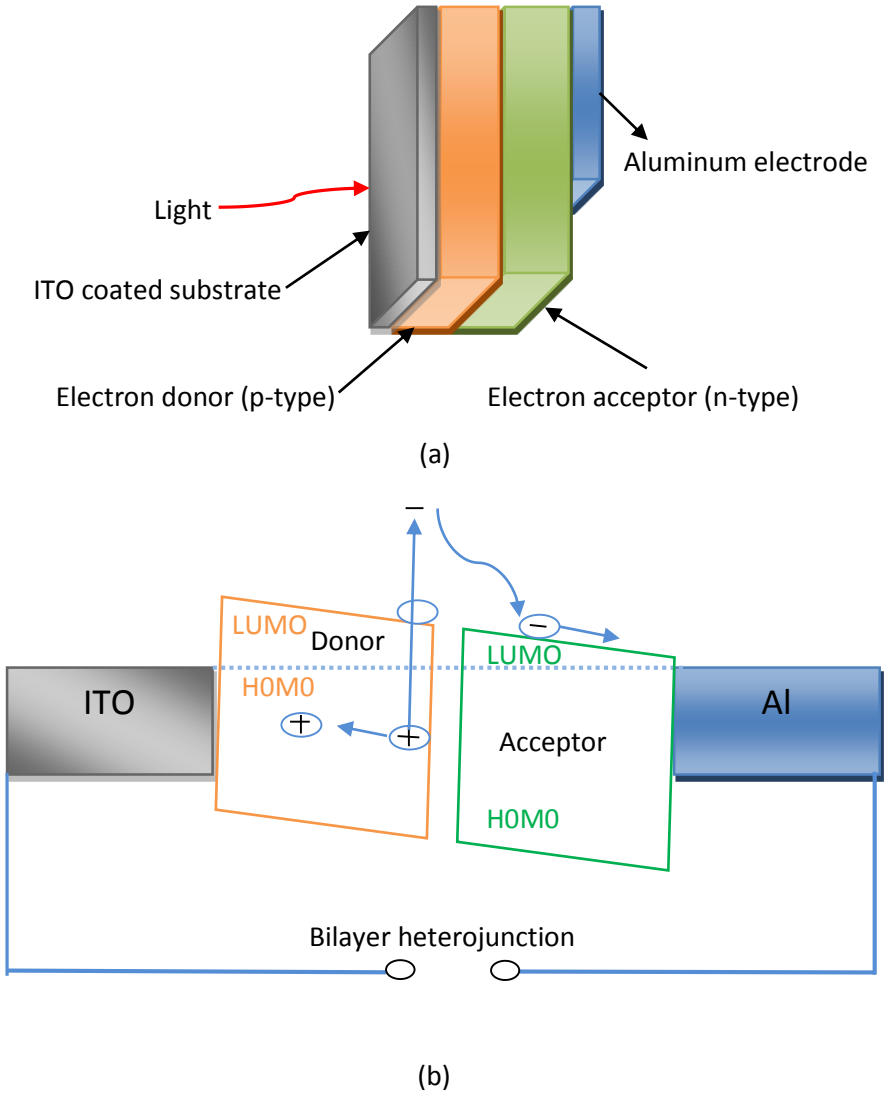

Figure 2.11: *a) Device structure of an organic bilayer heterojunction solar cell b) the energy band diagram of a bilayer heterojunction cell.*

2.6.3 Bulk Heterojunction (BHJ) organic solar cells

The invention of the concept of bulk heterojunction (BHJ) created a major breakthrough in OPVs. This was put into reality by Heeger and Friend in 1995 [57,82]. The donating and the accepting materials are mixed in an intimate way so that they form an interpenetrating network that is three dimensional. Most of the BHJ devices usually comprise of a number of components but at least one of them is a polymer semiconductor and this is usually a conjugated polymer. They have a bicontinous network that is usually organized on a nanometer and this result into a large interface area and thus every excitation that is created is able to reach the interface that is acceptable to the donor within its diffusion length. Thus, the possibility of recombination reduces resulting in higher J_{SC}. To compare this with the bilayer device, the interface area is massively increased and this ensures that a very efficient photoinduced charge transfer exists. Durrant and co-workers recently carried out insightful review into the photogeneration of charge in the organic BHJ solar cells [83]. An excitation that has been created in the polymer phase is capable of undergoing an electron transfer from the polymer to the acceptor and this results in the formation of an interfacial charge transfer state which then relaxes thermally with an electron hole separation distance (thermalization length). The state of charge transfer is then able to undergo germinate recombination either back to the zero ground state or a triplet excitation. Otherwise, free charge carriers can form and migrate towards the respective electrodes. According to Onsager theory, the probability of the desired dissociation into free charges is usually dependent on the ratio of the separation distance (a) and the coulomb capture radius (r_c). If a bigger domain exists, this may favour the dissociation of the charge transfer state and also less efficient excitation diffusion to the interface [84]. The charge transfer is capable of raising its energy level hence decreasing the barrier that exists between the charges separation but this is dependent on the size and bulkiness of the solubilizing components of the polymer backbone. These results therefore show that the molecular design of a device impact both the morphology and the charge photogeneration directly. In order to avoid any form of bimolecular recombination losses, a high interface area must be present and sufficient percolation pathways must be created. The morphology has a substantial influence on the performance of the devices and this point out the process of controlling and tuning the morphology as its plays a very crucial role [85, 86]. The interfaces of both the organic

materials and the electrodes are also decisive as well. Buffer layer introduced to avoid situations where the charge carriers reach the opposite electrodes and also so as to maximise the V_{OC} [87]. In order to be able to realize highly efficient OPV cells we need to have a comprehensive understanding of the complex interplay of the design of materials, the processing conditions and the morphology. Another key benefit of BHJ cells in comparison to bilayer devices is that they have an easier processing capability from solution where bilayers solution processed require orthogonal solvent systems, in order to avoid dissolve the underlying layer through processing and this limits the choice of materials which can be used. In the BHJ devices, it is possible for the active layer to be deposited from one solution using several film deposition techniques which include: spin coating and doctor blading methods. The process of films drying has a great influence on the morphology of the bulk heterojuntion. The heterojunctions are often influenced by the poor morphological stability due to an increase in the phase segregation of any two compounds in question and this usually results in degradation of the device [80, 82, 88-93]. The most widely used is the thermal annealing and it normally functions to alter the morphology. Applying thermal annealing has also been shown to enhance phase separation which somehow improves the performance of the device [94-96]. In order to be able to have a better understanding on how to blend the morphology and its influence on the solar cell characteristics, several techniques can be use for the characterization of BHJ including: Atomic force microscopy (AFM) and Scanning electron microscopy (SEM) and Transmission electron microscopy (TEM). AFM can gain High resolution information about surface topography and the surface distribution of donor and acceptor [80]. Figure 2.12 shows the structure of an organic bulk heterojunction (BHJ) solar cell as well as the energy band diagram of the cell.

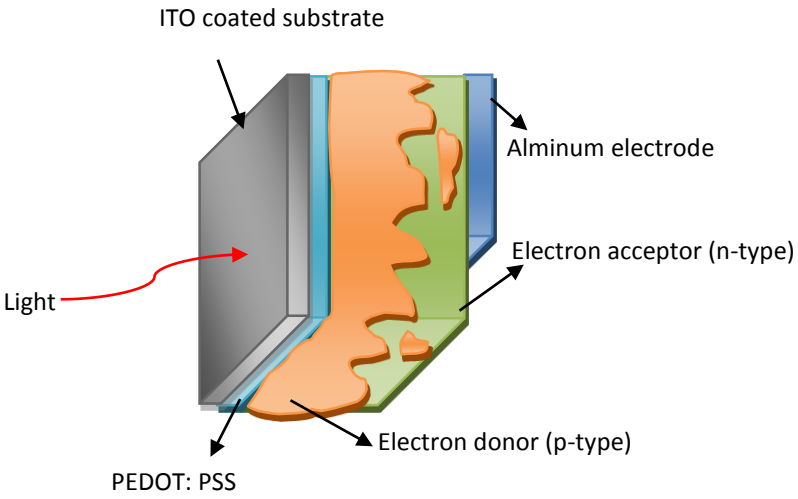

(a)

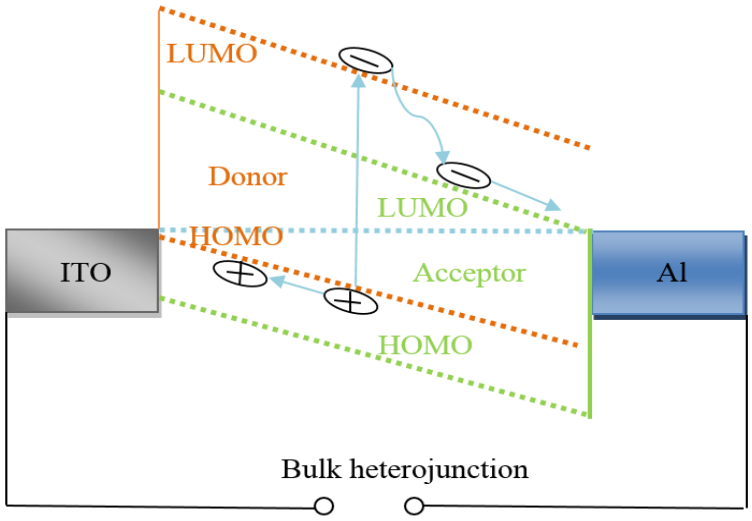

(b)

Figure 2.12: *a) Device structure of an organic bulk heterojunction (BHJ) solar cell; b) energy band diagram of a BHJ cell.*

2.6.4 Tandem (multijunction) organic solar cells

Tandem solar cell structures can be used to overcome the thermalisation losses mechanism in single junction device where organic tandem solar cells structure is a combine of two (or more) single heterojunction organic solar cells in one structure called multi-junction solar cells (tandem solar cells) as shown in Fig. 2. 13. This structure contains different active layers in each single heterojunction organic solar cells where each active layer formed from two materials: donor material and acceptor material [97, 98]. In most cases, two sub cells are connected in series through a recombination layer where holes from one sub cell meet electrons from the other. The open-circuit voltage is the summation of each sub cell, and the overall current is limited by the sub cell that has the smallest photocurrent. In an ideal situation both sub cells should generate the same photocurrent in order to minimize losses. Three-terminal (3T) tandem devices are an alternative option that eliminates the need of current matching, while potential losses in terms of unbalanced photovoltages would be less dramatic for the performance of the cell. However, the parallel-connection is more difficult to adapt and optimize [99]. From this discussion, it was noted that the multi junction solar cells have a structure that makes them effective solutions to be used for thermalization losses during the process of conversion of photons to electrons. The combination of both the wide and small band gap polymers in the configuration of a tandem to enable the coverage of both the invisible and infrared ranges of the solar spectrum. Referring to Kirchhoff's law, the equal current are able to flow through the sub cells and therefore the total voltage becomes the summation of the voltages of the sub cells. The active layers are usually separated by an intermediate contact in serial connection. This contact usually is composed of an electron transport layer that collects electron from one sub cell to the other and also a hole transporting layer that is tasked with the collection of holes from the other sub cells. In order to avoid loss of voltage at the interfaces, the opposite charges must therefore meet at a point where the energy levels are the same. Transparency is also required in the intermediate contact, when dealing with solution processing, it is very crucial that these layers are used to prevent the impairment of the first active layer when the second active layer is being deposited. The energy levels of the electron transport (ET) and hole transport (HT) layers are aligned to both the LUMO acceptor and the HOMO donor respectively. Also at the ET/HT interface, the layers are aligned so that the voltage loss is minimized. A modification of the thickness of the two

layers causes a redistribution of the optical electric field that is inside the solar cell and this enables an extra tool that is used for optimization of the tandem solar cells [100-102]. At the ET/HT interface, the electrons are then extracted from the front cell and are then recombined with the holes that have been collected from the back cell. Thus, PEDOT: PSS and metal oxide (NiO, MoO3, V2O5, WO3 and ITO) based HT layers are commonly used in single junction and polymer tandem solar cells, while ZnO, TiOx and Cs2CO are widely applied as ET layer [103-111]. The power conversion was shown to reach approximately 40% in the inorganic tandem cells while the organic structures reached about 11.1% [112-113]. Figure 2.13 shows the schematic structure of organic tandem solar cell and the energy band diagram of organic tandem solar cell.

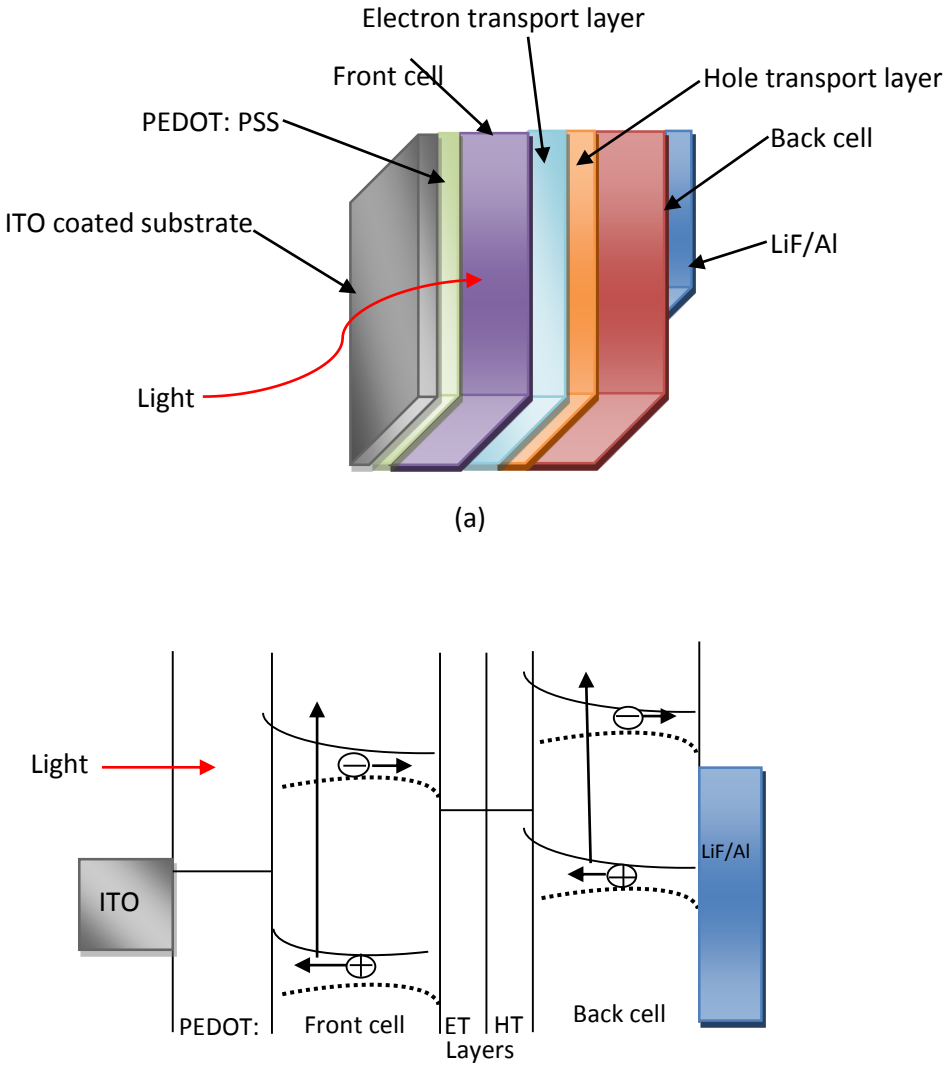

Figure 2.13: a) *Device of an organic tandem solar cell; b) energy band diagram of organic tandem solar cell.*

2.7 Basic operation principles of Organic solar cells

The difference between solar cells based on the inorganic semiconductors and organic semiconductors is that in solar cells that have been created from inorganic semiconductors, the photons are converted directly into carriers of direct charge and the carriers are then collected at the appropriate electrodes. In organic photovoltaic devices, a molecule that is photo excited leads to formation of pair's holes and electrons that are referred to as excitons which are composed of charge carriers and they usually have energies that bind them from 0.05 to over 1 e.V [114]. They are capable of undergoing diffusion over a length of about 5-15 nm and then decay either in a radiative way or non-radiative way. The process of generation of power from organic photovoltaic devices can be broken down into several stages. First, the light is absorbed and this leads to the generation of excitons which then diffuse and dissociate when they reach the interface. The holes and electrons that result from this dissociation process are then transported to appropriate electrodes so that a photovoltage can be generated and in cases where an external circuit is present, current is driven around it. Figure 2.14 shows these stages and further illustrated in the relevant sections.

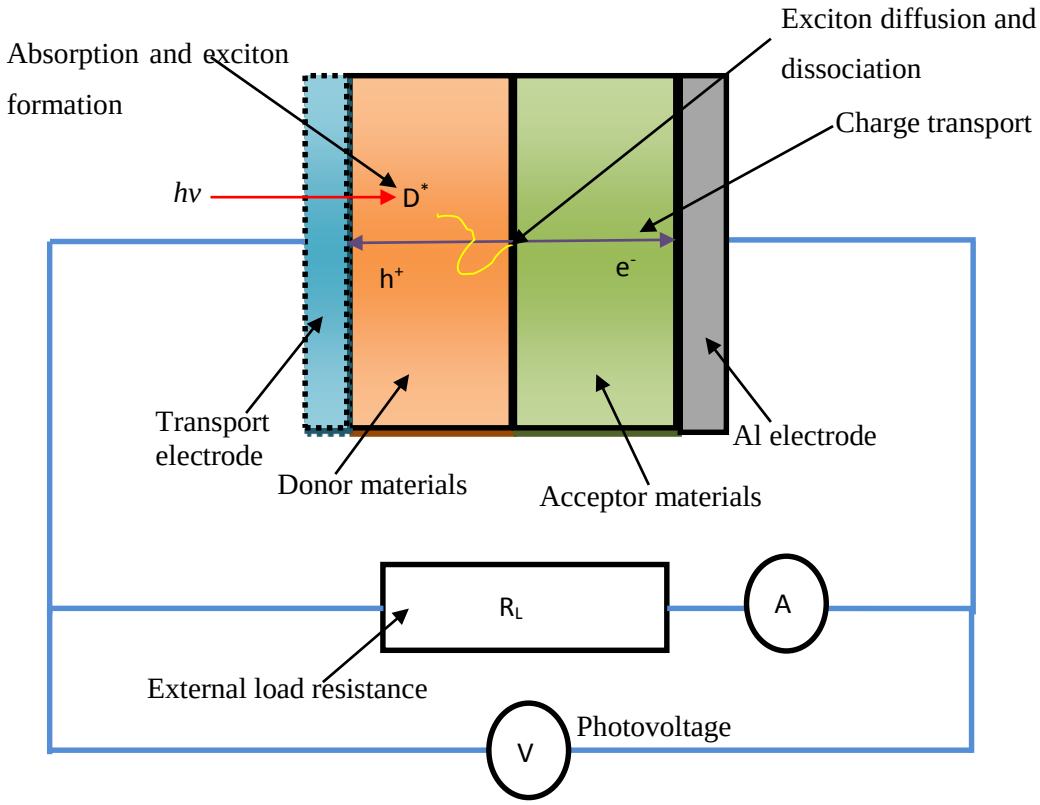

Figure 2.14: *diagram illustrate the power generation in an organic solar cell.*

2.7.1 Light absorption and exciton generation

The process of absorption in semiconductors usually occurs when a photon that have an energy equal to or greater than the bandgap of the semiconductor material absorbed. This photon is able to promote an electron from the HOMO to the LUMO leaving behind a vacant space in the previous level, referred to as a hole. The hole is capable of forming a coulombic attraction together with the electron which is referred to as an exciton state [115,116]. Figure 2.15 shows exciton binding energy.

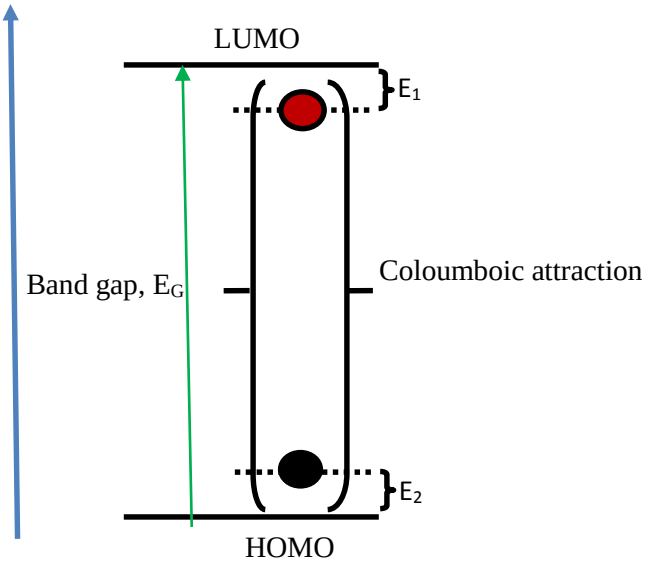

Figure 2.15: *Excition binding energy*

2.7.2 Exiton migration and dissociation

The possibility of dissociating an exciton is normally made available by the creation of a heterojunction between two organic semiconductors whereby the second semiconductor can be selected such that the electron that results from the exciton can be able to drop into it. This releases the energy difference that exists between the LUMO and the HOMO therefore, breaking the bound states. Dissociation only occurs when the excitons from the donor where $\Delta LUMO > E_B$ (donor) and for the excitons from the acceptor, $\Delta HOMO > E_B$ (acceptor). This method of carrying out dissociation requires that the excitation reaches the interface that exists between the two semiconductors. Since an excitation has no charge at all, an external electric field cannot therefore be used to either make sure that dissociation is accomplished or it is driven towards an interface. However for excitons to reach the interface this can only be accomplished through transfer of energy to adjacent molecules (hopping process) [117]. The mobility of excitons in the range of 10 nm, which is called the exciton diffusion length. The exciton have very small lifetime of few picoseconds if not seperated the excitons will recombine. Thus, exciton diffusion length (and lifetime) plays a critical role in performance of organic solar cells [118].

2.7.3 Charges transport and collection

After free charges have been generated at the interface, it is required that they reach the external circuit in an OPV device, the holes can be transported through the material that acts as the electron donor while the electrons can be transported though the material that acts as the electron acceptor. There have been some recent developments in the modification of the electrodes using ultra-thin internal layers such as metal oxides like TiOx and ZnOx to give a perfect match to the energy levels of the organic semiconductors [118-119]. This can be done by using an electron transporter layer (ETL) on the acceptor side with a work function less than the LUMO level of the acceptor to facilitate the collection of the electron from the acceptor. On the other hand, a hole transporter layer (HTL) can be used on the donor side with a work function higher than the HOMO level of the donor to facilitate the collection of the electron from the donor [120].

2.8 Electrical Characterisation of organic solar cells

2.8.1 Equivalent circuit diagram of organic solar cells

It is important to understand the electrical model of a solar cell before the discussion of the electrical properties of organic solar cells. It can be modelled by a diode parallel with a current source in an ideal case but practically a series and a shunt resistance is supposed to be included in the model in a way that; the shunt resistor R_{sh} is availed to recombination of charge carriers around the dissociation area and the series resistor R_s considers free migration or movement of charge carriers in the transport medium. Figure 2. 16 shows the typical equivalent circuit for solar cell, ideally $R_s = 0$ and $R_{sh} = \infty$ [121].

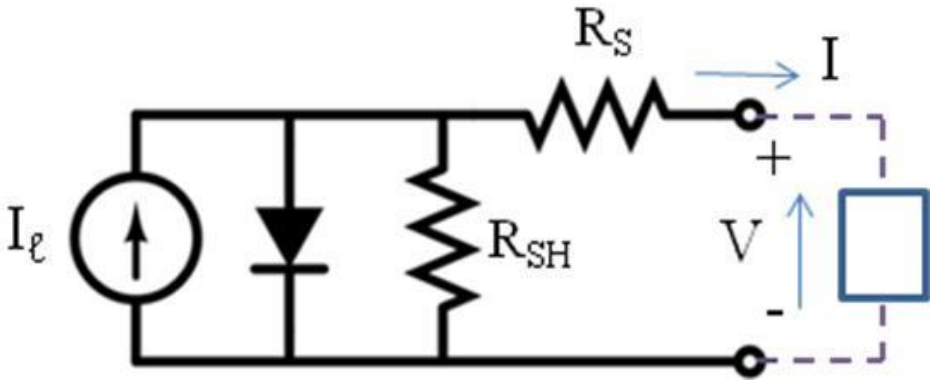

Figure 2.16*: Equivalent circuit diagram of organic solar cells.*

The current source (I_1) represents the produced current from the incident light and the diode explains the nonlinearity of the *I-V* curve. It is only when the series resistor drops down to zero that the circuit`s *I-V* characteristic equals the ideal diode and the shunt resistor moves to infinity. The material conductivity, thickness of the proactive layer and impurity concentrations are usually responsible for series resistor in solar cells as it comes from the charge carrier recombination mostly at the surface of the donor-acceptor junction. The shunt resistance (R_{sh}) can be calculated from the reverse bias of the illuminated *I-V* where the current change linearly with bias voltage. However, the serial resistance (R_s) can be calculated from the slop of the illuminated *I-V* under high forwarded bias voltage ($V > V_{OC}$). Increasing the R_s lower the short circuit current (I_{SC}) and decrease the fill factor of the solar cells while decreasing R_{sh} affect the V_{OC} and then the FF [122].

2.8.2 Current-voltage characterisation

After having done a review of the major technologies of the solar, shall then look at the fundamental electrical characteristics that are similar to all solar cells. For most workable inorganic and organic solar cells, characteristics of the current-density to voltage (*J-V*) take after the exponential response of a diode with low current in reverse bias and high current in forward bias when carried out in a dark place. A photocurrent in the cell builds up when light is directed on a device besides the diode characteristic,

and the superposition of the dark characteristic and the photocurrent are basically the *J-V* characteristic under lighting. Shockley equation perfectly describes the *J-V* characteristics of the device and also the photocurrent term, J_{ph}:

$$J = J_0 [exp (eV/ nkT) -1]-J_{ph}$$

Where *J* is the current density, J_0 is the reverse saturation current density of the diode,*e* the elementary charge, *V* is the applied voltage, *n* is the ideality factor, k is the Boltzmann constant and T is temperature [118]. In fact, the photocurrent will be dependent on the applied voltage and similarly the lighting affects the diode's characteristics.

Figure 2.17 shows the *J-V* plot for a typical solar cell in the dark; under illumination. The consider performance parameters from the *J-V* curve of a solar cell under a known illumination source are open-circuit voltage (V_{OC}), short-circuit current density (J_{SC}), fill factor (FF), and power conversion efficiency (PCE).

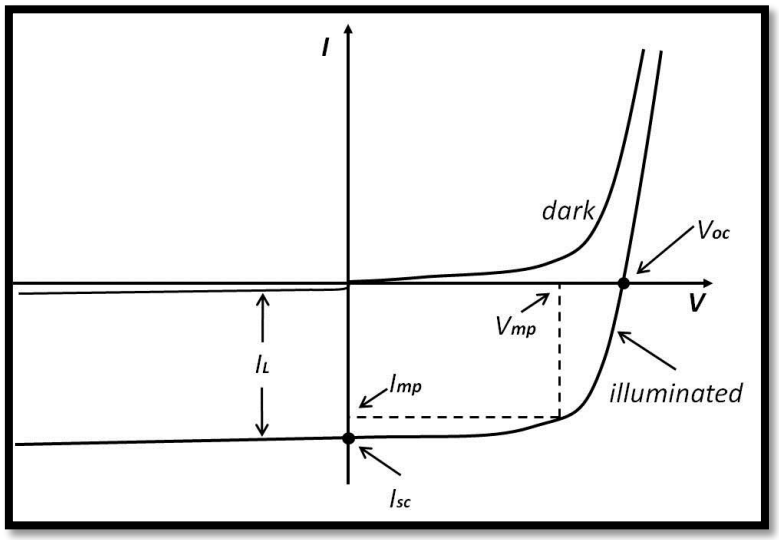

Figure 2.17: *shows the J-V plot for a typical solar cell in the dark and under illumination.*

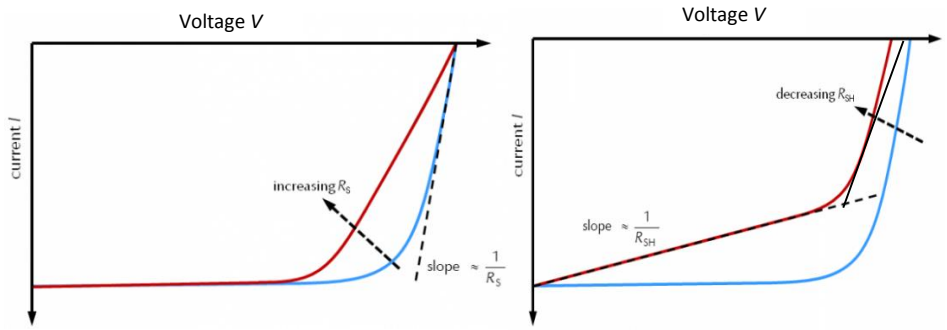

Figure 2.18: *Effect of the series resistance R_S and the shunt resistance R_{SH} on the shape of an I-V curve*

2.8.2.1 Open-circuit voltage

When J= 0, V_{OC} is the open circuit voltage across the cell at that point similar to the same device open-circuited. No power is generated at the voltage cause power = current*voltage and J = 0. Nonetheless, the voltage boundaries within which power can be generate are defined by the V_{OC}. The point at which the processes of production of photocurrent and dark current compensate one another is the open-circuit voltage [124].

2.8.2.2 Short-circuit current

When V=0, the current density is the short-circuit current density J_{SC}, same to V_{OC}, which are in similar conditions as the two cell's electrodes being short-circuited. Here too, no power is generated but the start of power generation is marked by the J_{SC}. In practical devices, the photocurrent density will be equal to the J_{SC}. J_{SC} is technically negative with the conventions signs used here but reviews of varying J_{SC} values will be majorly on its magnitude and treat it as a positive integer. For instance a higher J_{SC} is correspondent to a high J_{ph} [125].

2.8.2.3 Fill-factor

The ultimate power density generated P_{max} happens at the voltage V_{max} and current density J_{max} where the resultant product of J and V is at a minimum or highest in absolute value. This is so while J_{SC} and V_{OC} define the power production boundaries in a solar cells. Due to the diode characteristic and increased resistance and recombination losses, J_{max} and V_{max} are less than J_{SC} and V_{OC}, respectively. FF can be defining as:

$$\text{FF} = \frac{J_{max} \, X \, V_{max}}{J_{SC} \, X \, V_{OC}}$$

FF to the power generation demarcations of J_{SC} and V_{OC} and also indicates the acute bend in the exponentiated *J-V* curve linking J_{SC} and V_{OC}. High FF is desired because it is related to higher maximum power; nevertheless, the diode-like characteristic of solar cells results in FF always being less than one. Something must be done to enhance device quality because devices with high $|J_{SC}|$ and V_{OC} can still have low FF [126].

2.8.2.4 Power conversion efficiency

The power conversion efficiency defined as the percentage irradiance I_L (light power per unit area) which is transformed into output power (P_{light}) is the most discussed performance parameter of a solar cell. Having the point where the cell operates on the *J-V* curve varying depending on the load, the highest output power is used to calculate efficiency to enhance consistency. The efficiency can be written as following:

$$\text{PCE} = \frac{J_{max} X \, V_{max}}{P_{light}} \text{ x } 100\ \% = \frac{FF \; X \; J_{SC} X \; Voc}{P_{light}} \text{ x}100\ \%$$

This equation give evidence that FF, J_{SC} and V_{OC} all affect PCE directly. Moreover, the area used in calculation of *J* affects PCE and it is obligatory to include inactive areas vital to the solar cells for example grids and interconnects when probably working out efficiency value for large area devices or modules. How effective the space occupied by a cell is put into use is determined by the power conversion efficiency. Higher PCE

is often desirable because vast areas require more resources to cover with solar cells. The trade-offs between PCE and cost per solar cell must be balanced. The power and spectrum of the light source are core factors are determining power conversion efficiency because solar cells do not absorb and convert photons to electrons at all wavelengths with same efficiency. A standard spectrum is picked for working out PCE so as to effectively draw comparisons between different solar cells. The AM1.5 G spectrum is the most widely used standard spectrum for calculating and comparing the performance of photovoltaic that are intended for outdoor use despite the fact that the spectrum of the sunlight at the earth's surface varies with location, cloud coverage plus other factors [127].

In this work, thin films of PAMAM (see Section 2.2) with different generations are used as the acceptor for different solar cell structures as explained in Section 2.6. The photovoltaic behaviours were explained with reference to the theoretical background in Section 2.8.

References

[1] M. AlSalhi, J. Alam , L. Dass and M. Raja, "Recent Advances in Conjugated Polymers for Light Emitting Devices". *International Journal of Molecular Sciences*. Vol. 12, pp.2036-2054, **2011.**

[2] N. Belghiti, M. Bennani, M. Hamidi, S. M. Bouzzine, M. Bouachrine, "New compounds based on anthracene for organic solar cells applications", *Journal of Materials and Environmental Science*, Vol. 5, pp. 2191-2197, **2014.**

[2] A. Janotti and C. Walle, "Fundamentals of zinc oxide as a semiconductor", *Reports on Progress in Physics*, Vol. 72, pp. 126501-29, **2009.**

[3] V. Coropceanu, J. Cornil, D. Filho, Y. Olivier, R. Silbey, and J. Bredas., "Charge Transport in Organic Semiconductors", *Chemical Reviews*, Vol. 107, pp. 926−952, **2007.**

[4] E. Orgiu, J. George, J. Hutchison, E. Devaux, J. Dayen, B. Doudin, F. Stellacci,C. Genet, J. Schachenmayer, C. Genes, G. Pupillo, P. Samorì, and T. Ebbesen., "Conductivity in organic semiconductors hybridized with the vacuum field", *Nature Materials,* Vol. 14, pp. 1123–1129, **2015.**

[5] M. Terrones, "science and technology of the twenty-first century: Synthesis, Properties,and Applications of Carbon Nanotubes", *Annual review of materials research*, Vol. 33, pp. 419-501, **2003.**

[6] A. Alias, Z. Zabidi, A. Ali, and M. Harun, "Optical characterization and properties of polymeric materials for optoelectronic and photonic applications", *International journal of applied science and technology*, Vol. 3, pp. 11-38, **2013.**

[7] S. Cataldo and B. Pignataro, "Polymeric thin films for organic electronics: properties and adaptive Structures", *Materials,* Vol. 6, pp. 1159-1190, **2013.**

[8] S. Nasir, M. Sulaiman, N. Ludin, M. Ibrahim, K. Sopian, and M. Teridi " review of polymer, dye-sensitized, and hybrid solar cells", *International journal of photoenergy*, Vol. 2014, pp. 1-12, **2014.**

[9] M. Harun, E. Saion, A. Kassim, N. Yahya and E. Mahmud. "Conjugated Conducting Polymers: A Brief Overview". Journal for the advancement of science and art. Vol.2, pp. 63-68, **2007.**

[10] M. Scharber, N. Sariciftci, "Efficiency of bulk-heterojunction organic solar cells", *Progress in polymer science*, Vol. 38, pp. 1929-1940, **2013.**

[11] Etxebarria, J. Ajuria and R. Pacios, "Polymer:fullerene solar cells: materials, processing issues, and cell layouts to reach power conversion efficiency over 10%, a review", *Journal of Photonics for Energy*, Vol. 5, pp. 057214-25, **2015.**

[12] Nunzi. "Organic photovoltaic materials and devices". *Comptes Rendus Physique*, Vol. 3(4), pp. 523-542, **2002.**

[13] Dou, Y. Liu, Z. Hong, G. Li, and Y. Yan, "Low-bandgap near-IR conjugated polymers/molecules for organic electronics", *Chemical reviews*, Vol. 115(23), pp. 12633–12665, **2015.**

[14] E. Wang , W. Mammo , and M. Andersson, " 25th Anniversary Article: Isoindigo-Based Polymers and Small Molecules for Bulk Heterojunction Solar Cells and Field Effect Transistors", *Advanced materials*, Vol. 26(12), pp. 1801-1826, **2014.**

[15] B. Klajnert, M. Bryszewska. "Dendrimers: properties and applications".*Acta Biochimica Polonica*. Vol.48 (1), pp.199-208, **2001.**

[16] S. Lo and P. Burn, "Development of dendrimers: macromolecules for use in organic Light-Emitting diodes and solar cells", *Chemical reviews*, Vol. 107(4), pp. 1097–1116, **2007.**

[17] V. Sujitha, B. Sayani and P. Kalyani., "Dendrimers and its applications", International research journal of pharmacy, Vol. 2(9), pp. 25-32, **2011.**

[18] Z. Petrović and J. Ferguson, "Polyurethane elastomers", *Progress in Polymer Science*, Vol. 16, pp. 695-836, **1991.**

[19] T. Zhong, P. Ai and J. Zhou, "Structures and properties of PAMAM dendrimer: A multi-scale simulation study", *Fluid Phase Equilibria*, Vol. 302, pp. 43-47, **2015.**

[20] K. Inoue. "Functional dendrimers, hyperbranched and star polymers". *Progress in polymer science*. Vol.25, pp. 453-571, **2000**.

[21] J. Wang, Y. Cheng and T. Xu. "Current Patents of Dendrimers and Hyperbranched Polymers in Membranes". *Recent Patents on Chemical Engineering*. Vol. 1, pp. 41-51. **2008.**

[22] A. Adronov and J. Fréchet. "Light-harvesting dendrimers". *Chemical Communications*. Vol.1 (18), pp.1701-1710, **2000.**

[23] T. Anthopoulos , J. Markham, E. Namdas , J. Lawrence , I. Samuel , S. Lo and P. Burn. "Influence of molecular structure on the properties of dendrimer light-emitting diodes". *Organic electronics*. Vol.4, pp.71-76, **2003.**

[24] R. Gor, B. Sonvane and V. Saha, "Dendrimer -an emerging approach for drug delivery", *International Journal of Pharmaceutical Sciences Review*, Vol. 26(1), pp. 264-270, **2014.**

[25] J. Bharti, S. Prajapati, M. Jaiswal and R. Yadav, "Dendrimers multifunctionality nano-device: a review", *International journal of pharma sciences and research*, Vol. 2(8), pp. 1947-1960, **2011.**

[26] S. Tripathy, and M. Das, "Dendrimers and their applications as novel drug delivery carrier", *Journal of Applied Pharmaceutical Science*, Vol. 3(9), pp. 142-149, **2013.**

[27] M. Kose, W. Mitchell, N. Kopidakis, C. Chang, S. Shaheen, K. Kim, and G. Rumbles. "Theoretical studies on conjugated phenyl-cored thiophene dendrimers for photovoltaic applications". *Journal of American chemical society*. Vol. 129(46), pp. 14257–14270. **2007.**

[28] Y. Zeng, Y. Li, J. Chen, J. Yang and Y. Li, "dendrimers: a mimic natural light-harvesting system", *Chemistry an Asian journal*, Vol. 5, pp. 992–1005, **2010.**

[29] D. Bradshaw and D. Andrews, "Mechanisms of light energy harvesting in dendrimers and hyperbranched polymers", *Polymers*, Vol. 3, pp. 2053-2077, **2011.**

[30] A. Nantalaksakul, D. Reddy, C. Bardeen and S. Thayumanavan, "Light harvesting dendrimers", *Photosynthesis Research*, Vol.87, pp. 33–150, **2006.**

[31] J. Anthony, A. Facchetti, M. Heeney, S. Marder and X. Zhan. "n-Type Organic Semiconductors in Organic Electronics", Advanced Materials, Vol.22 (34), pp. 3876–3892, **2010.**

[32] H. Kroto , J. Heath, S. O'Brien, R. Curl and R. Smalley, "C60: Buckminsterfullerene", Nature, Vol. 318(6042), pp.162-163,**1985.**

[33] J. Haddock, X. Zhang, B. Domercq and B. Kippelen. "Fullerene based n-type organic thin-film transistors", Organic Electronics, Vol. 6, pp. 182–187, **2005.**

[34] P. Peumans and S. Forrest. "Very-high-efficiency double-heterostructure copper phthalocyanine/C60photovoltaic cells", Applied physics letters, Vol. 79(1), pp.126-128, **2001.**

[35] J. Hummelen, B. Knight, F. LePeq, F. Wudl, J. Yao and C. Wilkins. "Preparation and characterization of fulleroid and methanofullerene derivatives", Journal of Organic Chemistry, Vol. 60(3). pp. 532–538, **1995.**

[36] M. Wienk, J. Kroon, W. Verhees, J. Knol, J. Hummelen, P. Hal and R. Janssen. "Efficient Methano[70]fullerene/MDMO-PPV Bulk Heterojunction Photovoltaic Cells", Angewandte Chemie International Edition, Vol. 42(29), pp. 3371–3375, **2003.**

[37] G. Li, R. Zhu and Y. Yang. "Polymer solar cells", Nature Photonics, Vol. 6, pp. 153–161, **2012.**

[38] Z. He, C. Zhong, X. Huang, W. Wong, H. Wu, L. Chen, S. Su and Y.Cao. "Simultaneous Enhancement of Open-Circuit Voltage, Short-Circuit Current Density, and Fill Factor in Polymer Solar Cells", Advanced Materials, Vol. 23(40), pp. 4636–4643, **2011.**

[39] M. Helgesen, R. Søndergaard, F. Krebs. "Advanced materials and processes for polymer solar cell devices", Journal of Materials Chemistry, Vol.20 (1), pp. 36-60, **2010.**

[40] G. Yu, J. Gao, J. Hummelen, F. Wudi, A. Heeger. "Polymer Photovoltaic Cells: Enhanced Efficiencies via a Network of Internal Donor-Acceptor Heterojunctions", Science, Vol. 270 (5243), pp. 1789-1791, **1995.**

[41] D. Sun, D. Meng, Y. Cai, B. Fan, Y. Li, W. Jiang, L. Huo, Y. Sun, and Z. Wang, "Non-Fullerene-Acceptor-Based Bulk-Heterojunction Organic Solar Cells with Efficiency over 7%", *Journal of the American Chemical Society*, Vol. 137(34), pp. 11156–11162, **2015.**

[42] N. Georgiev and V. Bojinov, "Design, Synthesis and Photostability of Novel 1,8-naphthalimide PAMAM Light-harvesting Dendrons", *Journal of Fluorescence*, Vol. 21(1), pp. 51-63, **2011.**

[43] D. Gudeika, A. Michaleviciute, J. Grazulevicius, R. Lygaitis, S. Grigalevicius, V. Jankauskas, A. Miasojedovas, S. Jursenas, and G. Sini. "Structure Properties Relationship of Donor–Acceptor Derivatives of Triphenylamine and 1,8-Naphthalimide", *The Journal of Physical Chemistry C*, Vol. 116(28), pp. 14811–14819, **2012.**

[44] T. Baig, J. Nayak, V. Dwivedi, A. Singh, A. Srivastava ,and P. Tripathi, "A review about dendrimers: synthesis, types, characterization and applications", *International Journal of advances in Pharmacy, Biology and Chemistry*, Vol. 4(1), pp. 44-59, **2015.**

[45] K. Inoue, "Functional dendrimers, hyperbranched and star polymers", *Progress in Polymer Science*, Vol. 25, pp. 453-571, **2000.**

[46] M. Kleinman, J. Flory, D. Tomalia, and N. Turro, "Effect of protonation and PAMAM dendrimer size on the complexation and dynamic mobility of 2-naphthol", *The Journal of Physical Chemistry B*, Vol. 104, pp.11472–11479, **2000.**

[47] P. Maiti ,T. Çağın , S. Lin , and W. Goddard, "Effect of Solvent and pH on the Structure of PAMAM Dendrimers" *Macromolecules*, Vol. 38(3), pp. 979–991, **2005.**

[48] D. Ouyang, H. Zhang, H. Parekh, S. Smith, "The effect of pH on PAMAM dendrimer–siRNA complexation — Endosomal considerations as determined by molecular dynamics simulation", *Biophysical Chemistry*, Vol. 158, pp. 126–133, 2011.

[49] V. Murugesan, K. Sun and J. Ouyang, "Highly efficient inverted polymer solar cells with a solution-processable dendrimer as the electron-collection interlayer", *Applied Physics Letters*, Vol. 102, pp. 083302-4, **2013.**

[50] E. Bustos, J. quez, L. Echegoyen and L. Godinez, "preparation, characterization and photoelectrochemical study of mixed C60–Starburst PAMAMG0.0 dendrimer films anchored on the surface of nanocrystalline TiO2 semiconductor electrodes", *Chemical Communications*, Vol. 12, pp. 1613–1615,**2005.**

[51] A. Pron, P. Berrouard andM. Leclerc, "Thieno[3,4-c]pyrrole-4,6-dione-Based Polymers for Optoelectronic Applications", *Macromolecular Chemistry and Physics*, Vol. 214, pp. 7-16, **2013.**

[52] Y. Zou, A. Najari, P. Berrouard, S. Beaupre´ , B. Aıch,, Y. Tao,and M. Leclerc, "A Thieno[3,4-c]pyrrole-4,6-dione-Based Copolymer for Efficient Solar Cells", *Journal of the American Chemical Society*, Vol. 123,pp. 5330-5331. **2010.**

[53] J. Jiang, M. Yuan, K. Dinakaran, A. Hariharan and K. Wei, "Crystalline donor–acceptor conjugated polymers for bulk heterojunction photovoltaics", *Journal of Materials Chemistry A*, Vol. 1,pp. 4415-4422, **2013.**

[54] R. Uy, S. Price and W. You. "Structure-Property Optimizations in Donor Polymers via Electronics, Substituents, and Side Chains toward High Efficiency Solar Cells", *Macromolecular Rapid Communications*, Vol. 33, pp. 1162–1177, **2012.**

[55] C. Chochos and S. Choulis. “How the structural deviations on the backbone of conjugated polymers influence their optoelectronic properties and photovoltaic performance”, *Progress in Polymer Science*, Vol. 36(10), pp. 1326–1414, **2011.**

[56] H. Son, F. He, B. Carsten and L. Yu. “Are we there yet? Design of better conjugated polymers for polymer solar cells”, *Journal of Materials Chemistry*, Vol. 21(47), pp. 18934-18945, **2011.**

[57] J. Halls, C. Walsh, N. Greenham, E. Marseglia, R. Friend, S. Moratti and A. Holmes. “Efficient photodiodes from interpenetrating polymer networks”, Nature, Vol. 376, pp. 498-500, **1995.**

[58] S. Shaheen, C. Brabec, N. Sariciftci, F. Padinger, T. Fromherz, J. Hummelen. “2.5% efficient organic plastic solar cells”, Vol. 78(6), pp. 841-843, **2001.**

[59] C. Brabec, S. Shaheen, C. Winder, N. Sariciftci, P. Denk. “Effect of LiF/metal electrodes on the performance of plastic solar cells”, Applied Physics Letters, Vol. 80(7), pp. 1288-1290, **2002.**

[60] G. Li, V. Shrotriya, Y. Yao, J. Huanga and Y. Yang, “Manipulating regioregular poly(3-hexylthiophene) : [6,6]-phenyl-C61-butyric acid methyl ester blends—route towards high efficiency polymer solar cells”, *Journal of Materials Chemistry*, Vol. 17, pp. 3126–3140, **2007.**

[61] P. Khlyabich, B. Burkhart, A. Rudenko, and B. Thompson, “Optimization and simplification of polymer–fullerene solar cells through polymer and active layer design”, *Polymer*, Vol. 54, pp. 5267–5298,**2013.**

[62] S. Bavel, M. Bärenklau, G. With, H. Hoppe, J. Loos, “P3HT/PCBM Bulk Heterojunction Solar Cells: Impact of blend composition and 3D morphology on device performance”, *Advanced functional materials*, Vol. 20. pp. 1458-1463, **2010.**

[63] M. Dang, L. Hirsch, G. Wantz, and J. Wuest, “Controlling the Morphology and Performance of Bulk Heterojunctions in Solar Cells. Lessons Learned from the Benchmark Poly(3-hexylthiophene):[6,6]-Phenyl-C61-butyric Acid Methyl Ester System”, *Chemical Reviews*, Vol. 113(5), pp. 3734–3765, **2013.**

[64] P. Edwards, A. Porch, M. Jones, D. Morgan and R. M. Perks. “Basic materials physics of transparent conducting oxides”, Dalton Transactions, Vol. 2004(19), pp. 2995-3002, **2004.**

[65] D. Ginley and C. Bright, Guest Editors. “Transparent Conducting Oxides”, MRS Bulletin, Vol. 25 (8), pp.15-18, **2000.**

[66] G. Rupprecht. “Investigations of the electrical and non-electrical conductivity of thin indium oxide layers”, Journal of Physics, Vol. 139(5), pp. 504-517, **1954.**

[67] D. Hecht , L. Hu , and G. Irvin, “Emerging transparent electrodes based on thin films of carbon nanotubes, graphene, and metallic nanostructures”, *Advanced materials,* Vol. 23, pp. 1482-1513, **2011.**

[68] L. Chen, Z. Xu, Z. Honga and Y. Yang, “Interface investigation and engineering – achieving high performance polymer photovoltaic devices”, *Journal of Materials Chemistry*, Vol. 20, pp. 2575–2598, **2010.**

[69] B. Qi, Z. Zhang and J. Wang, “Uncovering the role of cathode buffer layer in organic solar cells”, *Scientific report,* Vol. 5 (7803), pp. 1-8, **2015.**

[70] R. Po, C. Carbonera, A. Bernardi and N. Camaioni. “The role of buffer layers in polymer solar cells”, Energy & Environmental Science, Vol. 4. pp. 285-310, **2010.**

[71] Y, Yuan, J. Huang and G. Li. “Intermediate layers in tandem organic solar cells: review”, Green, Vol. 1, pp. 65–80, **2011.**

[72] K. Akito and F. Katsuhiko. “Intermediate layers for tandem structure of bulk heterojunction photovoltaic cells”, Organic Photovoltaics, Proc.SPIE, Vol. 8477, **2012.**

[73] C. Deibel , and V. Dyakonov, “Polymer–Fullerene Bulk Heterojunction Solar Cells: review article”, *Reports on Progress in Physics*, Vol. 73(9). pp. 1-68, **2010.**

[74] S. Lattante, “electron and hole transport layers: their use in inverted bulk Heterojunction polymer solar cells”, *Electronics*, Vol. 3, pp. 132-164, **2014.**

[75] P. Kumar and S. Chand, “Recent progress and future aspects of organic solar cells”, *Progress in photovoltics: research and application,* Vol. 20, pp. 377-415, **2011.**

[76] T. Kietzke, “Recent advances in organic solar cells”, *Advances in optoelectronics*, Vol.2007, pp. 1-15. **2007.**

[77] C. Tang, “Two- layer organic photovoltaic cell”, Applied physics letters, Vol. 48(2), pp. 183-185, **1986.**

[78] E. Bittner, J. Ramon and S. Karabunarliev. “Exciton dissociation dynamics in model donor-acceptor polymer heterojunctions. I. Energetics and spectra”, Journal of Chemical Physics, Vol. 122(21), pp. 214719-214719-9, **2005.**

[79] P. Peumans, A. Yakimov, and S. Forrest. " Small molecular weight organic thin-film photodetectors and solar cells". Journal of Applied Physics, Vol. 93, pp.3693–3723, **2003.**

[80] H. Hoppe and N. Sariciftci, "Organic solar cells: an overview," Journal of Materials Research, vol. 19(7), pp. 1924–1945, **2004.**

[81] J. Chang, H. Wang, W. Lin, K. Chiang, K. Chen, W. Huang, Z. Huang, H. Meng, R. Hob and H. Lin. "Efficient inverted quasi-bilayer organic solar cells fabricated by using non-halogenated solvent processes", Journal of Materials Chemistry A, Vol. 2(33), pp. 13398-13406, **2014.**

[82] G. Yu, J. Gao, J. Hummelen, F. Wudl, A. Heeger. "Polymer Photovoltaic Cells: Enhanced Efficiencies via a Network of Internal Donor-Acceptor Heterojunctions", Science, New Series, Vol. 270(5243), pp. 1789-1791, **1995.**

[83] T.Clarke, J. Durrant. "Charge Photogeneration in Organic Solar Cells", Chemical Reviews, Vol. 110(2665), pp. 6736-6767, **2010.**

[84] T. Holcombe, J. Norton, J. Rivnay, C. Woo, L. Goris , C. Piliego, G, Griffini , A. Sellinger , J. Brédas , A. Salleo and J. Fréchet. "Steric Control of the Donor/Acceptor Interface: Implications in Organic Photovoltaic Charge Generation", Journal of the American Chemical Society, Vol. 133(31), pp. 12106-12114, **2011.**

[85] G. Li, V. Shrotriya, J. Huang, Y. Yao, T. Moriarty, K. Emery and Y. Yang. "High-efficiency solution processable polymer photovoltaic cells by self-organization of polymer blends", Nature Materials, Vol.4, pp. 864 – 868, **2005.**

[86] W. Ma, C. Yang, X. Gong, K. Lee and A. Heeger. "Thermally Stable, Efficient Polymer Solar Cells with Nanoscale Control of the Interpenetrating Network Morphology", Vol. 15(10), pp. 1617–1622, **2005.**

[87] W. Cai, X. Gong and Y. Cao. "Polymer solar cells: recent development and possible routes for improvement in the performance", Solar Energy Materials and Solar Cells, Vol. 94(2), pp. 114-127, **2010.**

[88] H. Hoppe, M. Niggemann, C. Winder, J. Kraut, R. Hiesgen, A. Hinsch, D. Meissner, N. Sariciftci. "Nanoscale Morphology of Conjugated Polymer/Fullerene-Based Bulk-Heterojunction Solar Cells", Advanced Functional Materials, Vol. 14(10), pp. 1005-1011, **2004.**

[89] C. Chochos, S. Choulis, "How the structural deviations on the backbone of conjugated polymers influence their optoelectronic properties and photovoltaic performance", Progress in Polymer Science, Vol. 36(10), pp. 1326-1414, **2011.**

[90] V. Kamm, G. Battagliarin, I. Howard, W. Pisula, A. Mavrinskiy, C. Li, K. Müllen andF. Laquai. "Polythiophene:Perylene Diimide Solar Cells – the Impact of Alkyl-Substitution on the Photovoltaic Performance", Advanced Energy Materials, Vol.1(2), pp. 297–302, **2011.**

[91] N. Miller , E. Cho , R. Gyse , C. Risko , V. Coropceanu , C. Miller , S. Sweetnam , A. Sellinger , M. Heeney , I. McCulloch , J. Brédas , M. Toney and M. McGehee. "Factors Governing Intercalation of Fullerenes and Other Small Molecules Between the Side Chains of Semiconducting Polymers Used in Solar Cells", Advanced Energy Materials, Vol. 2 (10), pp. 1208-1217, **2012.**

[92] X. Yang , J. Loos , S. Veenstra , W. Verhees , M. Wienk , J. Kroon , M. Michels and R. Janssen. "Nanoscale Morphology of High-Performance Polymer Solar Cells", Nano letters, Vol.5 (4), pp. 579–583, **2005.**

[93] M. Campoy-Quiles , T. Ferenczi , T. Agostinelli , P. Etchegoin , Y. Kim , T. Anthopoulos , P. Stavrinou , D. Bradley , J. Nelson . "Morphology evolution via self-organization and lateral and vertical diffusion in polymer:fullerene solar cell blends", Nature Materials, Vol. 7(2), pp. 158-164, **2008.**

[94] Y. Kim, S. Choulis, J. Nelson, D. Bradley, S. Cook and J. Durrant. "Device annealing effect in organic solar cells with blends of regioregular poly(3-hexylthiophene) and soluble fullerene", Applied physics letters, Vol. 86(6), pp. 063502-3, **2005.**

[95] L. Nguyen, H. Hoppe, T. Erb, S. Günes, G. Gobsch and N. Sariciftci. "Effects of Annealing on the Nanomorphology and Performance of Poly(alkylthiophene):Fullerene Bulk-Heterojunction Solar Cells", Advance functional materials, Vol. 17(7), pp. 1071-1078, **2007.**

[96] G. Li, Y. Yao, H. Yang, V. Shrotriya, G. Yang and Y. Yang. "Solvent Annealing Effect in Polymer Solar Cells Based on Poly(3-hexylthiophene) and Methanofullerenes", Advanced Functional Materials, Vol.17(10), pp. 1636–1644, **2007.**

[97] M. Riede , C. Uhrich , J. Widmer , R. Timmreck , D. Wynands , G. Schwartz , W. Gnehr , D. Hildebrandt , A. Weiss , J. Hwang , S. Sundarraj , P. Erk , M.

Pfeiffer and K. Leo. “Efficient Organic Tandem Solar Cells based on Small Molecules”. Advanced Functional materials. Vol.21, pp. 3019–3028, **2011.**

[98] D. Cheyns, J. Poortmans, H. Gommans, J. Genoe, and P. Heremans, "Stacked organic solar cells increase efficiency", SPIE Newsroom, May 11, **2007.**

[99] I. Etxebarria, A. Furlan, J. Ajuria, F. Fecherd, M. Voigt, C. Brabec, M. Wienk, L. Slooff, S. Veenstra, J. Gilot, and R. Pacios, "Series vs parallel connected organic tandem solar cells: Cell performance and impact on the design and operation of functional modules", *Solar Energy Materials and Solar Cells*, Vol. 130, pp. 495–504, **2014.**

[100] J. Drechsel, B. Männig, F. Kozlowski, M. Pfeiffer, K. Leo and H. Hoppe. "Efficient organic solar cells based on a double p-i-n architecture using doped wide-gap transport layers", Applied physics letters, Vol. 86, pp. 244102-3, **2005.**

[101] A. Hadipour, B. Boer and P. Blom. "Solution-processed Organic Tandem Solar Cells with embedded Optical Spacers", Journal of applied physics, Vol. 102 (7), pp. 074506, **2007.**

[102] R. Schueppe, R. Timmreck, N. Allinger, T. Mueller, M. Furno, C. Uhrich, K. Leo and M. Riede. "Controlled current matching in small molecule organic tandem solar cells using doped spacer layers", Journal of Applied Physics, Vol. 107(4), pp. 044503, **2010.**

[103] J. Gilot, M. Wienk and R. Janssen. " Double and triple junction polymer solar cells processed from solution", Applied physics letters, Vol. 90, pp. 143512, **2007.**

[104] M. Irwin, D. Buchholz, A. Hains,R. Chang, T. Marks. "P-Type semiconducting nickel oxide as an efficiency-enhancing anode interfacial layer in polymer bulk-heterojunction solar cells". PNAS , Vol.105, pp.2783-2787, **2008.**

[105] F. Chen and C. Lin. "Construction and characteristics of tandem organic solar cells featuring small molecule-based films on polymer-based subcells", Journal of Physics D: Applied Physics, Vol. 43(2), pp. 025104, **2010.**

[106] G. Li, C. Chu, V. Shrotriya, J. Huang and Y. Yang. "Efficient inverted polymer solar cells", Applied physics letters, Vol. 88, pp. 253503, **2006.**

[107] A. Janssen, T. Riedl, S. Hamwi, H. Johannes and W. Kowalsky. " Highly efficient organic tandem solar cells using an improved connecting architecture", Applied physics letters, Vol. 91, pp. 073519, **2007.**

[108] K. Kenji, I. Norihiro,T. Nishimori and J. Sakai, "Open circuit voltage of stacked bulk heterojunction organic solar cells", Applied physics letters, Vol. 88(7), pp. 073514, **2006.**

[109] J. Gilot, I. Barbu, M. Wienk and R. Janssen. "The use of ZnO as optical spacer in polymer solar cells: Theoretical and experimental study", Applied physics letters, Vol. 91(11), pp. 113520, **2007.**

[110] J. Kim, S. Kim, H. Lee, K. Lee, W. Ma, X. Gong and A. J. Heeger. "New Architecture for High-Efficiency Polymer Photovoltaic Cells Using Solution-Based Titanium Oxide as an Optical Spacer", Advanced Materials, Vol. 18(5), pp. 572–576, **2006.**

[111] B. Lee, H. Kim, W. Jeong and J. Kim. "A transparent conducting oxide as an efficient middle electrode for exible organic tandem solar cells", Solar Energy Materials and Solar Cells, Vol. 94,pp. 542-546, **2010.**

[112] S. Sista, Z. Hong, L. Chenx and Y. Yang. "Tandem polymer photovoltaic cells—current status, challenges and future outlook", *Energy & Environmental Science*, Vol. 4, pp. 1606–1620, **2011.**

[113] J. You, L. Dou, K. Yoshimura, T. Kato, K. Ohya, T. Moriarty, K. Emery,C. Chen, J. Gao, G. Li and Y. Yang. "A polymer tandem solar cell with 10.6% power conversion efficiency", *Nature communications*, Vol. 4(1446), pp. 1-10, **2013.**

[114] B. Gregg: "Excitonic solar cells". *Journal of physical chemistry B,* Vol. 107, pp. 4688, **2003.**

[115] B. Gregg and M. Hanna. "Comparing organic to inorganic photovoltaic cells: Theory, experiment, and simulation", *Journal of Applied Physics*, Vol. 93 (6), pp. 3605-3614, **2003.**

[116] A. Hains, Z. Liang, M. Woodhouse, and B. Gregg, "Molecular Semiconductors in Organic Photovoltaic Cells", *Chemical reviews*, Vol. 110(11), pp.6689–6735, **2010.**

[117] T. Stubinger and W. Brutting, "Exciton diffusion and optical interference in organic donor–acceptor", Journal of Applied Physics, Vol.90, pp. 3632-3641, **2001**.

[118] P. Sullivan, G. Collis, L. Rochford, J. Arantes, P. Kemppinen, T. Jones and K. Winzenberg, "An N-ethylated barbituric acid end-capped bithiophene as an

electron-acceptor material in fullerene-free organic photovoltaics", *Chemical Communications*, Vol. 51, pp. 6222—6225, **2015.**

[119] I. Hancox, K. V. Chauhan, P. Sullivan, R. A. Hatton, A. Moshar, C. P. A. Mulcahy and T. S. Jones. "Increased efficiency of small molecule photovoltaic cells by insertion of a MoO3 hole-extracting layer", Energy & Environmental Science, Vol.3, pp. 107-110, **2010.**

[120] M. Pfeiffer, K. Leo, X. Zhou, J. Huang, M. Hofmann, A. Werner, J. Blochwitz-Nimoth. "Doped organic semiconductors: Physics and application in light emitting diodes", Organic Electronics, Vol. 4(2-3), pp. 89–103, **2003.**

[121] A. Cheknane, H. Hilal, F. Djeffal, B. Benyoucef, and J. Charles, "An equivalent circuit approach to organic solar cell modelling", *Microelectronics Journal*, Vol. 39, pp. 1173–1180, **2008.**

[122] J. Zhang, S. Lee, and B. Sun, "Effect of Series and Shunt Resistance on Organic-Inorganic Hybrid Solar Cells Performance", *Electrochimica Acta*, Vol. 146, pp. 845-849, **2014.**

[123] R. Pierret, Semiconductor Device Fundamentals. New York: Addison-Wesley Publishing Company, Inc., **1996.**

[124] J. Blakesley and D. Neher, "Relationship between energetic disorder and open-circuit voltage in bulk heterojunction organic solar cells", *Physical review B*, Vol. 84, pp. 075210-12, **2011.**

[125] N. Nehaoua, , Y. Chergui, and D. Mekki, "Determination of organic solar cell parameters based on single or multiple pin structures", *Vacuum*, Vol. 84(2), pp. 326-329, **2009.**

[126] B. Qiab and J. Wang, "Fill factor in organic solar cells", *Physical Chemistry Chemical Physics*, Vol. 15, pp. 8972-8982, **2013.**

[127] U. Würfel, D. Neher, A. Spie and S. Albrecht, "Impact of charge transport on current–voltage characteristics and power-conversion efficiency of organic solar cells", *Nature communications*, Vol. 6, pp. 1-9, **2014.**

Chapter 3

Materials and Experimental Techniques

3.1 Introduction

In this chapter various experimental methods and techniques used during this work are described. The choice of process used in this work is determined by the nature of the material and the required properties of the device. Materials and techniques employed to fabricate organic solar cell are described in the first part of this chapter. The fabrication process was carried out in a class 1000 clean room to minimize atmospheric contamination. The second part outlines the equipment used for studying the electrical properties and morphology of organic solar cell devices.

The research in this thesis includes the fabrication of different types of devices with different materials, i.e. organic bilayer heterojunction solar cells (OHJ), organic bulk heterojunction solar cells and organic tandem solar cells, while most of the experimental techniques were similar. Section 3.2 describes all the materials used in this research. Section 3.3 explained the main techniques of film deposition that have been used in this work. The description of the general experimental details for the fabrication of devices can be found in Section 3.4. However, the detailed experimental procedures for fabrication of any device will be described in the main section of that device. In Section 3.4.3 atomic force microscopy (AFM) used to study the surface morphology of films is briefly explained. The UV-visible absorption spectra of the various materials used in the construction of organic solar cells were obtained using a Hitachi Model U-2000 Double Beam Ultra-Violet/Visible (UV/VIS) spectrophotometer as described in section 3.4.4.3. Finally, the design of vacuum system setup and the electrical characteristics measurements setups are summarised in Section 3.4.4.1 and 3.4.4.2.

3.2 Materials

Poly(3-hexylthiophene-2,5-diyl) (P3HT) was purchased from Sigma-Aldrich. Titanium oxide (TiOx) and Poly(amidoamine) (PAMAM) dendritic wedges were synthesized in the School of Chemistry, Bangor University. Poly(3,4-ethylenedioxythiophene)-poly(styrenesulfonate) (PEDOT: PSS) solutions (CLEVIOS AL 4083) and pH500 were purchased from Heraeus. IC70BA was purchased from Solaris Chem Inc.

3.2.1 Poly(3-hexylthiophene-2,5-diyl) (P3HT)

Regio-regular poly (3-hexylthiophene) (P3HT) is used as an electron donor/hole transporter and light absorber. Regio-regular implies that each 3- hexylthiophene unit in the chain in this polymer is oriented in such a way that the C_6H_{13} residue group is either head to tail or head to head [1, 2]. Due to this property the polymer has the qualities of better ordering and self-organisation during deposition, meaning that the device mobility is increased substantially [3, 4]. The chemical structure of the material is shown in Fig. 3.1.

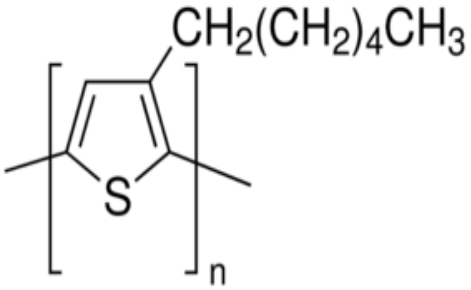

Figure 3.1: *Poly(3-hexylthiophene-2,5-diyl) chemical structure*

The optical and electrical properties of the P3HT have been used to estimate the HOMO level at 5.1 eV, LUMO level 3.2 eV and the bandgap 1.9 eV [1, 5]. P3HT can be used as a hole transporting polymer for improving PCE or blend OPV cells [6]. A blend of OPV cell was fabricated by Gang Li *et al.* (2005) using fullerene derivative [6,6]-phenyl-C61-butyric acid methyl ester (PCBM) and P3HT soluble C60 derivative. After PCBM blend solutions were casted on PEDOT: PSS/ITO, evaporation rates were varied to control the morphology of the blend film.

A well-mixed blend film was then formed by PCBM and P3HT during solvent annealing, as P3HT formed a crystalline fibril-like morphology embedded with PCBM aggregates [7, 8]. The hole mobility of the blend PCBM-P3HT conjugated polymer is reported to increase because of the blended layers' phase separated morphology. The absorption efficiency of the conjugated polymer is also improved as the p3HT aggregates and forms fibril-like crystalline morphology [6]. In general, P3HT thin film serves as an electron donor during photoexcitation and has a high hole mobility, approximately 10^{-3} cm^2 V^{-1} s^{-1} in thin poorly organized films and approximately 2×10^{-1} cm^2 V^{-1} s^{-1} in well crystallized films. The P3HT has a 550 nm wavelength optical absorption peak and a broad absorption spectrum of 400 to 650 nm, rich region energy regarding to the solar spectrum at 1.5 AM [9-11].

3.2.2 Poly(amidoamine) (PAMAM) dendritic wedges

Dendrimers and dendritic polymers found great applications in the last few years due to their unique structures as well as biological and physical properties that can be precisely controlled [12-13]. For this reason the material is used to develop multifunctional nano-scale devices. Dendrimers are regularly hyperbranched, nanometer-sized (2-10 nm diameter), flexible, monodispersed macromolecules that have many peripheral functional groups [14, 15].

Their high degree of branching facilitates facile multifunctionalisation as it is possible to conjugate multiple biological and chemical moieties at their surfaces [12, 16]. Dendrimers have two functional domains (core and branches) in addition to the peripheral domains that enable their tuning in order to alter their properties such as surface charge, molecular size and weight, and functionality. They have garnered a great deal of interest in the last few decades because of their applicability as molecular scaffolds, which can be used in the development of catalytic nanoreactors, liquid crystals, light harvesting systems and drug delivery systems [17,18]. Light harvesting assemblies made of dendrimers have also been greatly explored because of their unique properties and structures. Their globular shape offers a large surface area which can be modified using chromophores that results in an efficient photon capture and large absorption cross-section [18-20]. The structure of dendrimers is characterized by layers between generations (G) or focal points [21]. PAMAM (polyamidoamines) are a

popular class of commercially used dendrimers and the use of their flexible aliphatic bone as a scaffold in developing light harvesting antennae could help the development of new high efficiency energy transfer systems [22]. Fluorophores like 1, 8-naphthalimide derivatives are some of the PAMAM light harvesting antennae that are particularly useful. These derivatives have good photostability and strong fluorescence because of which they are used in various applications such as anticancer agents, laser active media, coloration of polymers, analgesics in medicine, fluorescent markers in biology, potential photosensitive biological units, fluorescence switchers, liquid crystal displays and electroluminescent materials [23-25].

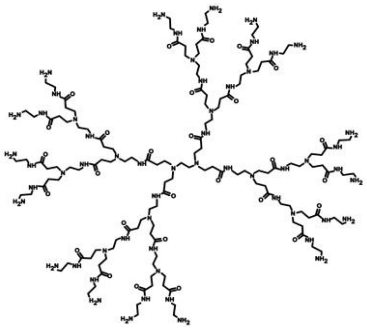

Figure 3.2: *PAMAM Dendrimer generation 2.*

PAMAM generation 2 poly(amidoamine) (Fig. 3.2) has been reportedly used as an electron-collection interlayer material placed between the ITO and active layer of inverted organic solar cells (OSCs). Under AM1.5G illumination, these OSCs were found to have a power conversion efficiency of 3.53%, a figure greater than that of control inverted OSCs blank ITO. It is also comparable with that of control OSCs having normal architecture [26]. PAMAM dendrimers were originally developed in 1979 by Donald Tomalia and have primary amine groups and tertiary amine groups at each brand end and at each branching point, respectively. They also possess an amido amine branching structure and an ethylene diamine core. Those with amine-terminated branches are commercially available as cationic "full" generations (G1, G2, etc.) and those with carboxylic acid terminated branches are available as anionic "half" generations (G1.5, G2.5, etc.) [27-32]. Tomalia's first dendrimer was a result of the reaction of an ammonia core with three methylacrylate molecules followed by three ethylenediamine molecules addition that resulted in the formation of G0 amidoamine.

These two steps were continued to produce successive amidoamine generations through which the terminal amine groups were doubled each time [33].

PAMAM dendrimers have been employed in chemical sensors, light harvesting devices, gene transfer, cross link agent, polymer based drug delivery and imaging contrast agent technology [34-36]. Lower generation PAMAM dendrimers have an elliptical or planar shape while the higher generation ones are spherical because of the densely packed branches as shown in Fig. 3.3. They can be prepared through two routes, one is the convergent approach and the other is the divergent approach. The convergent approach involves synthesis at the periphery and proceeds inwards while the divergent approach is vice versa [37-39]. The structure and properties of Poly(amidoamine) (PAMAM) dendrimers have been of particular interest to scientists as the physical properties of their solutes and their adaptability to studies of droplet evaporation are unique. Their molecular structure is highly controllable and they can be easily synthesised in large amounts [40-44].

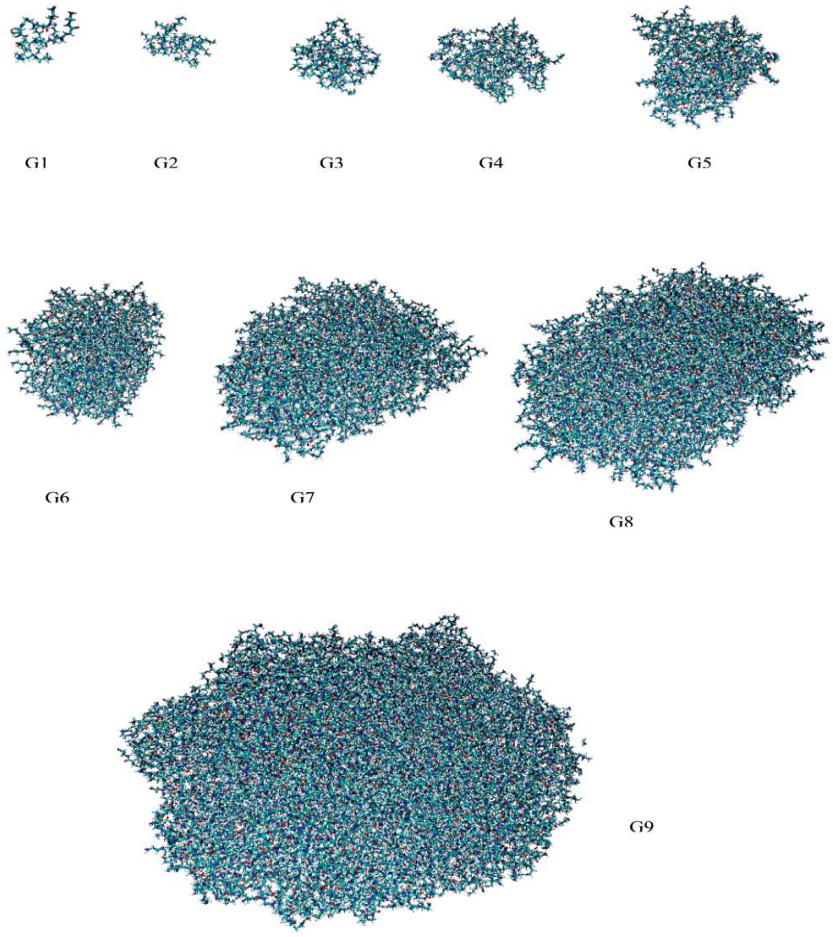

Figure 3.3: *PAMAM dendrimers shapes from G1 to G9* [45].

3.2.3 Indene-C70 bisadduct (IC70BA)

Buckminsterfullerenes are aromatic, stable, spherical shaped clusters discovered in 1985, consisting of 60 carbon atoms (C60) [46]. Because of their electroactive properties, they have gained significant attention. C60 is readily available and acts as electron acceptor that has high electron mobility and accepts up to six electrons when in solution [47]. It has limited solubility and therefore, its deposition is primarily achieved through vacuum deposition. It is widely applied in bilayer heterojunction (BHJ) solar cells that have high efficiencies of up to 3.6% with a copper phtalocyanine donor [48]. In 1995, Hummelen and co-workers had reported Phenyl-C61-butyric acid methyl ester (PC61BM), a methano-fullerene derivative as a soluble C60 version [49]. Efficient charge separation in BHJ solar cells resulting due to ultrafast photoinduced electron transfer to PCBM from a p-type polymer was also reported that year [50].

These two discoveries propelled organic solar cell development further. PCBM is the most widely used acceptor in OPV. Its spherical shape offers it advantage over other planar semiconductors because 3D electron transport is possible in it. However, the main drawback is the weak absorption of visible light. In order to address this, a C70 analogue of it, called the PC71BM was developed to have a higher photocurrent in OPV devices as it had a stronger absorption in the solar spectrum's blue region [51]. Currently, solar cells are highly optimized and those incorporating the C60 and C70 analogues reach more than 8% PCE in conjunction with suitable low-band gap polymers [52, 53]. Materials with lower LUMO have been implemented for bringing about further improvements. Solubilising groups are also being attached to the fullerene core in order to enable the tuning of their LUMO and HOMO levels and also to allow the organic electronic devices (OED's) solution processing. Various mono, bis and tris adducts have also been developed to take advantage of the changes in LUMO levels and also to achieve higher open circuit voltage (V_{OC}). For instance, Indene-C60 bisadduct (IC60BA) that has a LUMO level at 3.74 eV (0.17 eV up-shifted than that of PCBM) shows superior photovoltaic performance at 0.84 V V_{OC} and 6.48% PCE when used P3HT-based OSCs as acceptor [54]. Indene-C70 bisadduct (IC70BA) has also been synthesized at a higher LUMO level of 3.72 eV (0.19 eV higher than that of PCBM). P3HT/IC70BA PSCs with methyl-thiophene additives have been shown to have higher PCEs of up to 6.69% with a 0.86 V V_{OC} upon using pre-thermal annealing for 10 minutes at 150^0C [55]. Figure 3.4 shows the chemical structure for different C60-based fullerene derivatives.

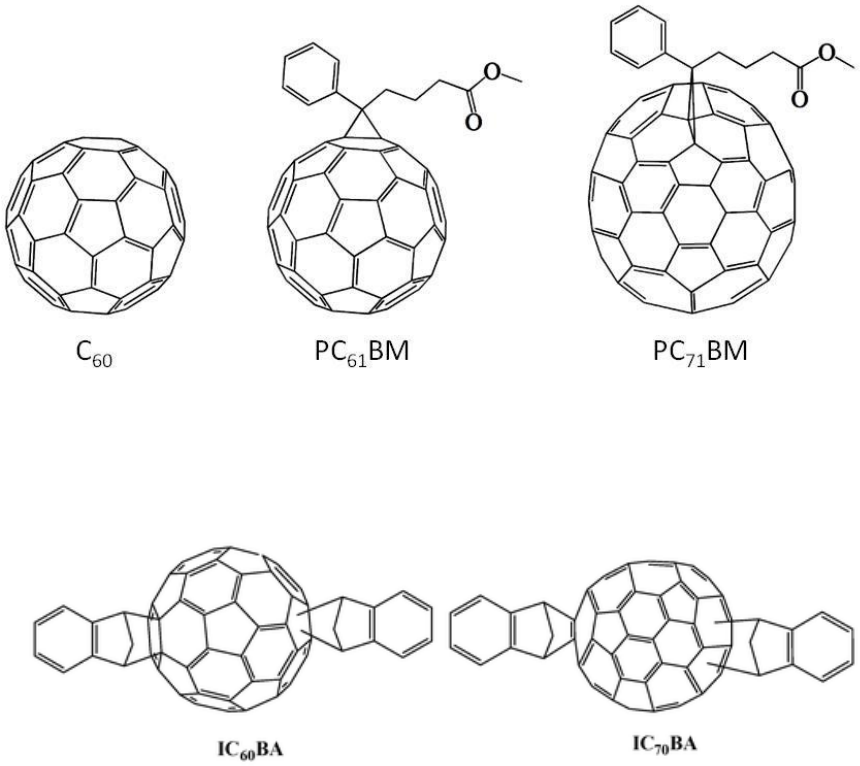

Figure 3.4: *Chemical structures of fullerene derivatives used in OPV devices.*

3.2.4 Poly(3,4-ethylenedioxythiophene) poly (styrenesulfonate) (PEDOT: PSS)

Poly (3, 4-ethylenedioxythiophene) poly (styrenesulfonate) (PEDOT: PSS) is used in organic electronics because of its hole conducting properties. It was earlier used as active layer in transistors, buffers or electrode material between dielectric material and the gate electrode [56-58]. It has a number of advantages such as good thermal stability, high transparency, and mechanical flexibility. Because of these properties, it has been used in OSCs as an anode buffer layer [48, 59]. It is one of the best hole-conducting buffers as it has a high ionization potential that is almost equal to ITO work function, while its electron affinity is 2.2 eV, which is adequately low for blocking electrons [60]. It is a single component polymer with two ionomers. The first component (PEDOT) is

a polythiophene polymer carrying positive charge while the other component (PSS) is a sodium polystyrene sulfonate polymer carrying negative charge. The mixture PEDOT: PSS is used for improving the ITO-anode contact [61, 62]. Figure 3.5 shows the chemical structure of PEDOT-PSS.

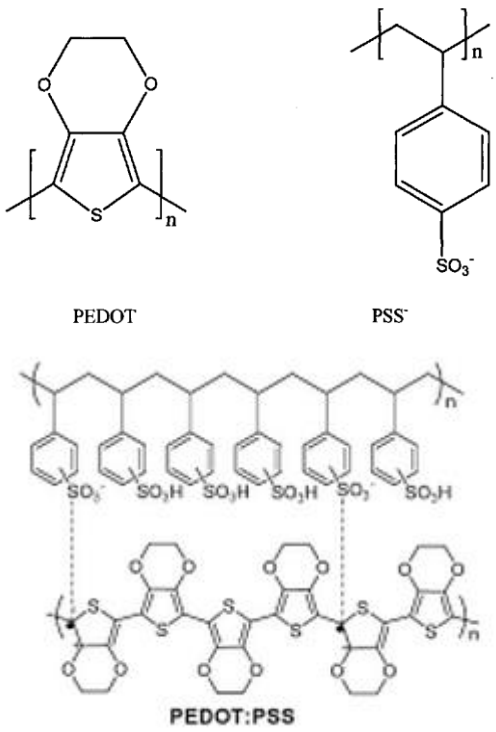

Figure 3.5: *PEDOT, PSS and PEDOT: PSS structures.*

3.2.5 Titaniom oxide (TiOx)

Titaniom oxide (TiOx) in its amorphous form is an equally good electron transfer layer (ETL) as crystalline TiO_2 after optimization. It is also as good as zinc oxide as an electron transfer layer because it is characterized with high transparency in the visible range and high electron mobility [63-65]. Studies have shown that it is possible to create a TiOx electron transfer layer from a solution at room temperature without the need for an annealing process after deposition [66]. It has been demonstrated that such a layer

was equally good to calcium in extracting electrons from a heterojunction device, leading to the confirmation that TiOx has the right energy level for being an efficient electron transfer layer in combination with active blends. It has also been reported that the TiOx properties are the same when deposition occurs in a glove box or in air, an important requirement for their application in roll-to-roll manufacturing [66]. TiOx has been used in a variety of electronic devices such as in solar cells as an ETL, thin film transistors (TFTs) as channel material and as energy harvesting device possessing piezoelectric properties. Electron mobility of TiOx films is found to be 1.7 x 10^{-4} cm^2 V^{-1} s^{-1}, with 4.4 eV LUMO level close to Al work function, making it an efficient in electron transport. Its large band gap blocks excitons and holes efficiently [67].

A device enhancement was reported by Hayakawa *et al.* for a TiOx layer over the active layer but with a small rise in short circuit current density (J_{SC}). Because of its superior hole blocking properties, increase in rectification ratio and shunt resistance (R_{sh}) have contributed to improvements in full factor (*FF*) as well as (V_{OC}), while the layer also acts as a barrier against chemical degradation and physical damage [68]. The TiOx layer also acts as an optical spacer that optimizes efficiency by redistributing the intensity of light. It has also been demonstrated that TiOx layer improves air stability by almost two orders of magnitude. It acts as an electron transport layer and as a hole blocking layer as the top of the TiOx valence band is electronegative, 8.1 eV below vacuum. The layer acts as a charge selective collection layer and also breaks the symmetry, because of which it results in open circuit voltage [63].

3.3 Experimental techniques

3.3.1 Spin coating

Spin coating technique has been used for deposition of thin films for several decades [68]. It can be used for all types of solutions (generally polymers) on flat areas, e.g. glass or plastic. The process starts by applying a small amount of solution (coating materials) into the centre of the flat substrate, which is held by a vacuum chuck during the coating process as shown in Fig. 3.6. Then the substrate starts to rotate at a fixed speed, typically about several thousand rpm. The applied solution spreads outwards as the substrate is rotating. Organic materials thin films can be produced with thicknesses ranging from nanometers to micrometers using spin coating.

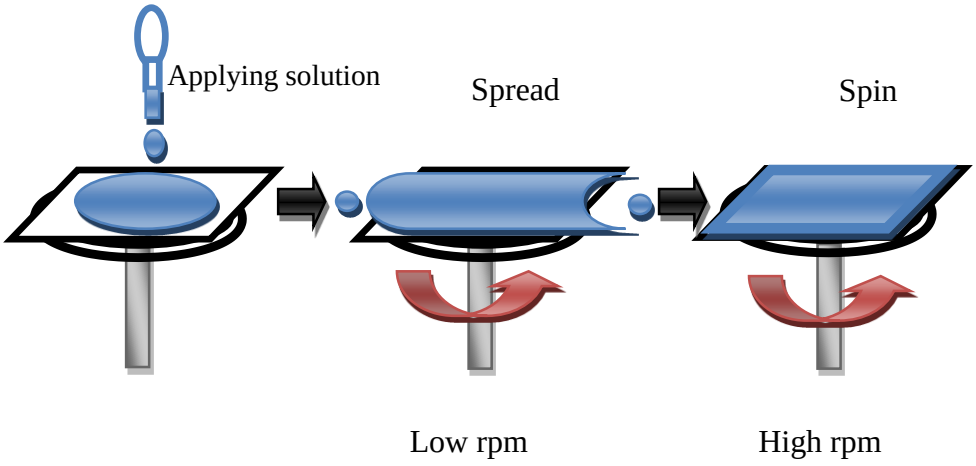

Figure 3.6: *Stages of the spin coating process.*

The theoretical model for the spin coating process that predicts the relationship between the thickness of the spun film d, viscosity coefficient of the solution η, material density ρ, the angular velocity of the spinning ω, and the spinning time t is [69]:

$$d = (\eta / (4\pi \rho \omega^2)^{1/2} t^{-1/2} \qquad (3.1)$$

The final film thickness also rely on other factors, such as the drying rate (temperature per minute), viscosity, surface tension, concentration of solids, etc. However, the spin speed is the most important factor of the spin process to determine the final film thickness.

3.3.2 Thermal evaporation

The physical vapour deposition of metal (Al cathode) were carried out by thermal evaporation using a Kurt. J. Lesker mini-spectros system as shown in Fig. 3.7. The electrical energy was used to heat a filament which led to heat the deposition material to evaporation point. A shadow mask was used to create a pattern of the thin film where the vapour material form a thin film on the cold substrate surface at this pattern. This process performed at very high levels of vacuum about 10^{-4} Torr, allowing for a long

mean free path to reduce film impurities. Low pressures of about 1 x 10^{-7} Torr was used to prevent reaction between the vaporized materials and the atmosphere. Quartz crystal sensor (QCS) was used to monitor the film thickness and the Sigma software used to control the processes of film deposition.

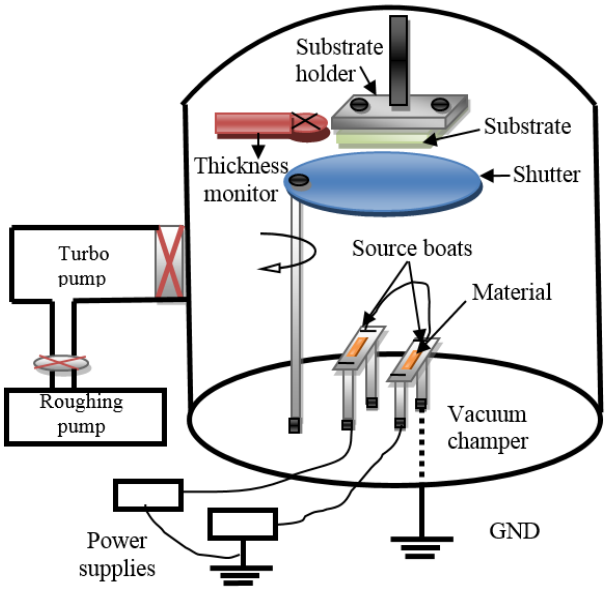

Figure 3.7: *Kurt Lesker mini-spectros system diagram.*

3.4 Experimental details

3.4.1 Substrate preparation

ITO glass substrates were cut into small pieces with dimensions of 2.5 cm x 2 cm. Each of these substrate slides produces four devices through a shadow mask. The substrates were cleaned with soap, warm water and deionised water, then were placed on a cleanroom wipe inside the fume hood. A few drops of acetone were dispensed from the acetone bottle onto the substrates to remove the photo resist. The substrates were wiped gently with a cleanroom wipe to remove the solvent and any remaining photoresists and were placed on a clean tissue. Glass substrates were arranged in a specially designed substrates holder, then the holder was placed in acetone beaker so that the acetone level is above the substrates. The beaker was covered with a piece of foil then was placed in

the ultrasonic bath for 10 minutes. After that, the beaker was removed from the ultrasonic bath, the substrates were removed from the holder with a clean tweezers and blow-dried with compressed nitrogen. Previous steps were repeated but this time using isopropanol instead of acetone. Followed with UV-ozone treatment for 20 minutes.

3.4.2 Film deposition

3.4.2.1 Spin coating of the hole transport layer

The EMS spin coater model 4000 was used in this process. Conducting poly (3, 4-ethylenedioxylenethiophene)-polystylene sulfonic acid (PEDOT:PSS,Baytron P) was spin-cast (5000 rpm) from aqueous solution (after passing a 0.45 μm filter) for 40 second with approximate thickness of ~40 nm. The substrate was subjected to drying for 10 minutes at 140°C in air. For spin-casting of the photoactive layer, the glass substrates were moved into a glove box for nitrogen environment**.**

3.4.2.2 Spin coating of active layer

In the bilayer heterojunction solar cells the donor (P3HT) was spin coated first then the acceptor was deposited. A solution of the Poly (3-hexylthiophene) (P3HT) was prepared by dissolving 0.03g of P3HT in 2 ml of chloroform (Sigma Aldrich) in a 20ml glass vial yielding a concentration of 1% w/w. The vial was placed inside ultrasonic bath at a temperature of 50^{o}C for 30 minutes to increase the solubility of P3HT. Finally, the solution was syringed through a 0.2μm PTFE filter into a second clean vial to remove any un-dissolved particles. Then, the P3HT was spin-cast at 800 rpm for 60 second with expected thickness ~100 nm on top of the PEDOT layer. The second charge separation layer (PAMAM dendrimers) spin-cast at 500 rpm for 30 second on top of the P3HT with the thickness ~70 nm.

3.4.2.3 Spin coating of electron transport layer

Titanium(IV) isopropoxide (Ti[OCH(CH_3)$_2$]4, Aldrich, 99.999%, 10mL) was prepared as a precursor, and mixed with 2-methoxyethanol ($CH_3OCH_2CH_2OH$, Aldrich, 99.9+%, 50mL) and ethanolamine ($H_2NCH_2CH_2OH$, Aldrich, 99+%, 5mL) in a three necked flask connected with a condenser, thermometer, and argon gas inlet/outlet. Then, the mixed solution was heated to 80°C for 2 hours in silicon oil bath under magnetic stirring, followed by heating to 120°C for 1 hour. The two-step heating (80 and 120°C) was then repeated. The resulted TiOx precursor solution was then prepared in isopropyl alcohol (the TiOx gels were diluted in isopropyl alcohol (IPA) to be utilized in the solution processes).

TiOx precursor solution in methanol was spin-cast at 5000 rpm for 20 second with thickness ~20 nm in air on top of the active layer. After 10 minutes in air at 80°C, the precursor is converted to TiOx by hydrolysis.

3.4.2.4 Evaporation of top electrodes

Aluminium electrodes were deposited on top of the electron transport layer through a shadow mask. The deposition thickness of the aluminium electrodes was 100 nm, with evaporation rate of 0.1 nm s^{-1} using the Kurt. J. Lesker deposition system. Figure 3.8 represents schematic images of the fabrication process.

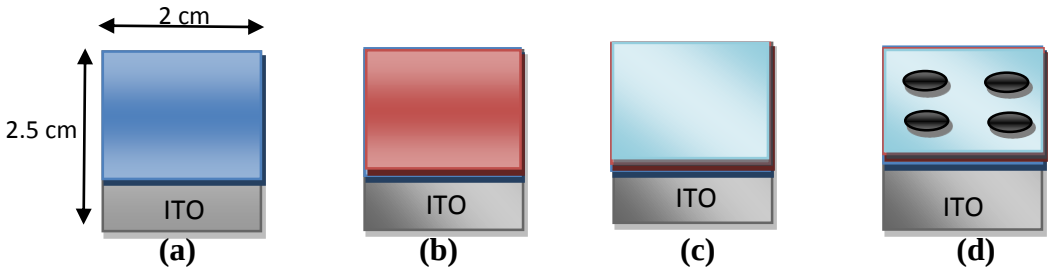

Figure 3.8: *device preparation process: a) ITO glass with PEDOT:PSS deposited b) active layer deposited on top of the PEDOT:PSS c) TiOx deposited on top of active layer d) Al deposited through shadow mask on top of the TiOx.*

3.4.3 Thin film characterization

Atomic Force Microscopy (AFM)

Atomic force microscopy (AFM) is a high-resolution scanning probe microscopic technique that helps researchers study surface morphology of thin films. The AFM technique was developed by Binnig, Quate and Gerber in 1985 so they could study materials and take high resolution images of sample surfaces [70]. The technique is employed in analysing van der Waals forces, magnetic forces, repulsive forces and lateral friction forces. In this study, digital instrument nanoscope AFM was used to analyse the surface properties of active layer thin films [71].

Images in the AFM technique are obtained by using a sharp probe to scan the sample surface while analysing the interactions of the sample with the tip. The scanning process involves the placement of a sharp microscope cantilever tip close to the sample's surface [71]. Distance between the tip and the surface is adjusted in order to keep the cantilever deflection constant and small deflections will cause it to bend upwards [72]. Measurement of the bending is carried out using a laser spot reflected to sensor following which an image of the surface can be obtained at atomic level resolution. Depending on the interaction between tip and sample surface, AFM measurement is of two types, one is the contact mode and the other is the non-contact mode. In the contact mode, the tip touches the sample surface while in the non-contact mode, the tip only stays near the surface without contact. Vibrations are induced on the tip and these are monitored using a laser [71, 73].

3.4.4 Electrical characterisation

3.4.4.1 Vacuum system setup

A vacuum system used in organic solar cells electric characterisation was designed with low Vacuum system (10^{-2} torr) contained a steel chamber connected to a rotary pump. Inside the chamber, the substrate holder mounted in copper stage opposite to the light window where the substrate holder dimensions is 2.5 cm x 2cm and the light source is a tungsten halogen lamp (50W) focused through a window onto the substrate (anode). Researchers have mostly used the tungsten lamp in the solar cell field although it has a slight difference with the AM 1.5 solar simulator, thus providing a reasonable

light for comparison. [74, 75]. The intensity of the light falling on the device could be varied from ~1 to 200 mW/cm^2 by moving the light source toward or away from the test sample. The light intensity was measured using a light intensity meter. A light intensity equivalent to AM1.5 radiation from the halogen lamp was set using an AM1.5 calibrated Si photodiode (Thorlabs SM1PD2A). Figure 3.9 shows the schematic design of the measurement setup and a picture of the system.

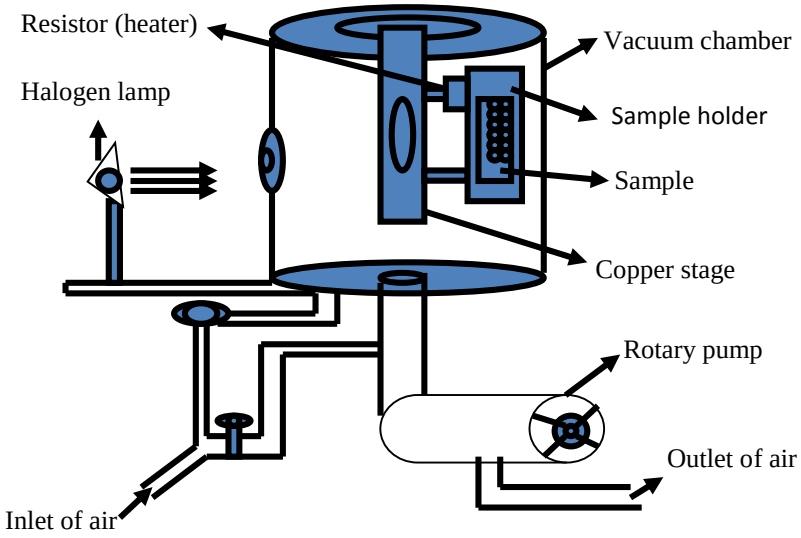

Figure 3.9: *Schematic diagram of the designed vacuum system and a picture of the system.*

3.4.4.2 DC measurements

The current density-voltage (J-V) measurements were performed under dark and light by applying voltage to the Al electrode while the ITO electrode was grounded using computer driven LCR meter HP 4284A controlled through a custom-made analysis program by MATLAB. The software measures J-V curves where *FF*, *Voc*, *Jsc*, and *PCE* are calculated using applicable equations.

For electrical measurements, contacts were made to the solar cells in the sample holder using fine gold wire and silver paste. The gold wire was connected to sockets in the lid of the chamber. The sample holder were designed to contain four devices. The Schematic diagram and optical picture of the substrate holder shown in figure 3.10.

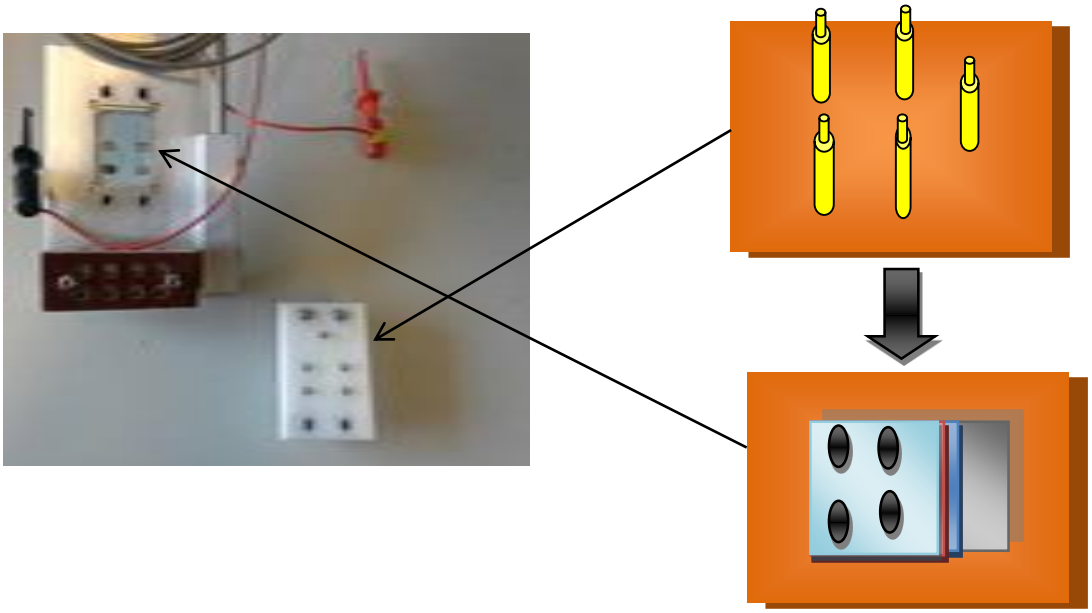

Figure 3.10: *The sample holder used for device measurements and the top view of the sample with optical picture.*

3.4.4.3 Ultra-violet/visible Spectroscopy

Hitachi Model U-2000 Double Beam Ultra-Violet/Visible (UV/VIS) spectrophotometer used to obtain the UV-visible absorption spectra of the various materials in the construction of the solar cells. A deuterium discharge lamp emits the primary light beam. The beam pass through a half-silvered mirror beam splitter with one beam passing through the sample while the other used as a reference. The wavelength range was ~190 nm to 1100 nm with a wavelength resolution of 1nm.

UV/Vis spectroscopy is a widely used technique for the quantitative determination of solutions of highly conjugated organic compounds, biological macromolecules and transition metal ions [76]. Organic compounds, particularly those that are highly conjugated, absorb light in the visible or UV regions of the electromagnetic spectrum. Solvents used for this technique are usually water or ethanol. However, not all solvents are suitable for UV spectrophotometry. The pH and polarity of solvent can also influence the absorption spectrum of the compound under study. For instance, the molar extinction coefficient and absorption maxima of Tyrosine increase with an increase in pH from 6 to 13 or with a decrease in the polarity [77].

References

[1] D. Chirvasea, Z. Chiguvarea, M. Knippera, J. Parisia, V. Dyakonova and J.Hummelenb. 'Electrical and optical design and characterisation of regioregular poly(3-hexylthiophene-2,5diyl)/fullerene-based heterojunction polymer solar cells', *Synthetic Metals*, Vol. 138, pp. 299–304, **2003.**

[2] G. Li, V. Shrotriya, Y. Yao, J. Huanga and Y. Yang. 'Manipulating regioregular poly(3-hexylthiophene) : [6,6]-phenyl-C61-butyric acid methyl ester blends—route towards high efficiency polymer solar cells', *Journal of Materials Chemistry*, Vol. 17, pp. 3126–3140, **2007.**

[3] D. Chirvase, J. Parisi, J. Hummelen and V. Dyakonov. 'Influence of nanomorphology on the photovoltaic action of polymer–fullerene composites', *Nanotechnology*, Vol. 15, pp. 1317–1323, **2004.**

[4] D. Chirvase, Z. Chiguvare, M. Knipper, J. Parisi, V. Dyakonov, and J. Hummelen. 'Temperature dependent characteristics of poly„3 hexylthiophen-fullerene based heterojunction organic solar cells', *Journal of applied physics*, Vol. 93 (6), pp. 3376- 3383, **2003.**

[5] J. Youa, L. Doua, Z. Hongc, G. Li and Y. Yang. 'Recent trends in polymer tandem solar cells research', *Progress in Polymer Science*, Vol. 38, pp. 1909–1928, **2013.**

[6] G. Li, R. Zhu and Y. Yang. 'Polymer solar cells', *Nature photonics*, Vol. 6, pp. 153–161, **2012.**

[7] G. Li, V. Shrotriya, J. Huang, Y. Yao, T. Moriarty, K. Emery and Y. Yang. 'High-efficiency solution processable polymer photovoltaic cells by self-organization of polymer blends', *Nature Materials*, Vol. 4, pp. 864 – 868, **2005.**

[8] X. Yang , J. Loos , S. Veenstra ,W. Verhees , M. Wienk , J. Kroon , M. Michels , and R. Janssen. 'Nanoscale Morphology of High-Performance Polymer Solar Cells', *Nano letters*, Vol.5 (4), pp. 579–583, **2005.**

[9] G. Kalonga, G. Chinyama, M. Munyati and M. Maaza. 'Characterization and optimization of poly (3-hexylthiophene-2, 5- diyl) (P3HT) and [6, 6] phenyl-C61-butyric acid methyl ester (PCBM) blends for optical absorption', *Journal of chemical engineering and materials science*, Vol. 4(7), pp. 93 – 102, **2013.**

[10] J. Huang, T. Goh, X. Li, M. Sfeir, E. Bielinski, S. Tomasulo,M. Lee, N. Hazari and A. Taylor. 'Polymer bulk heterojunction solar cells employing Förster resonance energy transfer', *Nature Photonics*, Vol. 7, pp. 479–485, **2013.**

[11] B. Moon, S. Cho, K. Lee, S. Bae, S. Lee1, J. Hwang, B. Angadi, Y. Yi, M. Park and D. Son. 'Enhanced Photovoltaic Performance of Inverted Polymer Solar Cells Utilizing Multifunctional Quantum-Dot Monolayers', *Advanced Energy Materials*, Vol. 4(12), pp. 519–423, **2014.**

[12] R. Pearson, S. Sunoqrot, H. Hsu, J. Bae and S. Hong. 'Dendritic nanoparticles: the next generation of nanocarriers? ', *Therapeutic delivery*, vol. 3(8), pp. 941-959, **2012.**

[13] B. Kumar, I. Chandiran, B. Bhavya, U. Sravanthi and M. Sindhuri. 'Dendrimer: a complete drug delivery', International *Journal of Pharmacy Review & Research*, Vol. 1(1), pp. 25-39, **2011.**

[14] D. Tomaliaa. 'The dendritic state', *Materials today*, Vol.8 (3), pp. 34-46, **2005.**

[15] V. Babu, V. Mallikarjun, S. Nikhat and G. Srikanth. Dendrimers: 'A new carrier system for drug delivery', *International Journal of Pharmaceutical and Applied Sciences*, Vol. 1(1), pp. 1-10, **2010.**

[16] C. Bonduelle and E. Gillies. 'Dendritic Guanidines as Efficient Analogues of Cell Penetrating Peptides', *Pharmaceuticals (Basel)*, Vol. 3(3), pp. 636–666, **2010.**

[17] N. Georgiev, V. Bojinov and P. Nikolov. 'Design and synthesis of a novel pH sensitive core and peripherally 1, 8-naphthalimide-labeled PAMAM dendron as light harvesting antenna', *Dyes and Pigments*, Vol. 81(1), pp. 18–26, **2009.**

[18] N. Georgiev, V. Bojinov and N. Marinova. 'Novel PAMAM light-harvesting antennae based on 1, 8-naphthalimide: Synthesis, energy transfer, photophysical and pH sensing properties', *Sensors and Actuators B: Chemical*, Vol. 150(2), 655–666, **2010.**

[19] O. Bozdemir, M. Yilmaz, O. Buyukcakir, A. Siemiarczuk, M. Tutasd and E. Akkaya. 'Convergent synthesis and light harvesting properties of dendritic boradiazaindacene (BODIPY) appended perylenediimide dyes', *New Journal of Chemistry*, Vol. 34(1), pp. 151-155, **2010.**

[20] S. Schlundt, G. Kuzmanich, F. Spänig, G. Rojas, C. Kovacs, M. Garcia-Garibay, D. Guldi and A. Hirsch. 'Dendritic porphyrin-fullerene conjugates: efficient light-

harvesting and charge-transfer events', *Chemistry*, Vol. 15(45), pp. 12223–12233, **2009.**

[21] D. Landge, S. Shyale, S. Kadam, Darshan, V. Katare, and J. Pawar. 'Dendrimer: an innovative acceptable approach in novel drug delivery system', *Pharmacophore*, Vol. 5(1), pp. 24-34, **2014.**

[22] K. Alamry, N. Georgiev, S. El-Daly, L. Taib and V. Bojinov. 'A highly selective ratiometric fluorescent pH probe based on a PAMAM wavelength-shifting bichromophoric system', Spectrochimica acta part a: molecular and biomolecular spectroscopy, vol. 135(25), pp. 792–800, **2015.**

[23] N. Georgiev and V. Bojinov. 'Design, Synthesis and Photostability of Novel 1,8-naphthalimide PAMAM Light-harvesting Dendrons', *Journal of Fluorescence*, Vol. 21(1), pp. 51-63, **2010.**

[24] N. Georgiev, V. Bojinov and A. Venkova. 'Design, Synthesis and pH Sensing Properties of Novel PAMAM Light-Harvesting Dendrons Based on Rhodamine

[25] 6G and 1,8-naphthalimide', *Journal of Fluorescence*, Vol. 23(3), pp. 459-471, **2013.**

[26] N. Georgiev, V. Bojinov and P. Nikolov. 'Design and synthesis of a novel pH sensitive core and peripherally1,8-naphthalimide-labeled PAMAM dendron as light harvesting antenna', *Dyes and Pigments*, Vol.81,pp. 18-26, **2009.**

[27] V. Murugesan, K. Sun and J. Ouyang. 'Highly efficient inverted polymer solar cells with a solution-processable dendrimer as the electron-collection interlayer', *Applied physics letters*, Vol. 102, pp. 083302- 4, **2013.**

[28] K. Kitchens, R. Kolhatkar, P. Swaan, N. Eddington and H. Ghandehari. 'Transport of poly (amidoamine) dendrimers across Caco-2 cell monolayers: Influence of size, charge and fluorescent labeling', *Pharmaceutical Research*, Vol. 23(12), pp. 2818-2826, **2006.**

[29] K. Kitchens, M. El-Sayed, H. Ghandehari. 'Transepithelial and endothelial transport of poly (amidoamine) dendrimers', *Advanced Drug Delivery Reviews*, Vol. 57(15), pp. 2163–2176, **2005.**

[30] R. Jevprasesphant, J. Penny, D. Attwood, N. McKeown and A. D'Emanuele. 'Engineering of dendrimer surfaces to enhance transepithelial transport and reduce cytotoxicity', *Pharmaceutical research*, Vol. 20(10), pp. 1543-1550, **2003.**

[31] K. Kitchens, A. Foraker, R. Kolhatkar, P. Swaan, H. Ghandehari. 'Endocytosis and interaction of poly (amidoamine) dendrimers with Caco-2 cells', *Pharmaceutical research*, Vol. 24(11), pp. 2138-2145, **2007.**

[32] R. Jevprasesphant, J. Penny, D. Attwood, A. D'Emanuele. 'Transport of dendrimer nanocarriers through epithelial cells via the transcellular route', *Journal of Controlled Release*, Vol. 97(2), pp. 259–267, **2004.**

[33] M. Najlah, S. Freeman, D. Attwood, A. D'Emanuele. 'In vitro evaluation of dendrimer prodrugs for oral drug delivery', *International Journal of Pharmaceutics*, Vol. 336(1), pp. 183–190, **2007.**

[34] D. Tomalia, 'Dendrimer Molecules', *Scientific American*, Vol. 272(5), pp. 62-66, **1995.**

[35] M. Saboktakin, A. Maharramov and M. Ramazanov. 'Poly(amidoamine)(PAMAM) /CMS Dendritic nanocomposite for controlled drug delivery', *The Journal of American Science*, Vol. 4(1), pp. 48-52, **2008.**

[36] K. Madaan, S. Kumar, N. Poonia, V. Lather and D. Pandita. 'Dendrimers in drug delivery and targeting: Drug-dendrimer interactions and toxicity issues', *Journal of pharmacy and bioallied sciences*, Vol. 6(3), pp. 139-150, **2014.**

[37] B. Hari, K.Kalaimagal, R.Porkodi, P. Gajula and J.Ajay. 'Dendrimer: Globular nanostructured materials for drug delivery', *International Journal of PharmTech Research*, Vol. 4(1), pp. 432-451, **2012.**

[38] J. Eichman, A. Bielinska, J. Kukowska-Latallo and J. Baker. 'The use of PAMAM dendrimers in the efficient transfer of genetic material into cells', *Pharmaceutical science and technology today*, Vol. 3(7), pp. 232–245, **2000.**

[39] N. Azar, P. Mutlu, R. Khodadust and U. Gunduz. 'Poly(amidoamine) (PAMAM) Nanoparticles: Synthesis and Biomedical Applications', *Hacettepe Journal of Biology and Chemistry*, Vol. 41(3), pp. 289-299, **2013.**

[40] B. Ostrovskii, S. Sulyanov, N. Boiko, V. Shibaev, S. Astaf'ev, L. Yanusova and W. Jeu. 'Order and frustration in liquid-crystalline dendrimers', The European physical journal E, Vol. 36(134), pp. 1-11, **2013.**

[41] D. Tomalia, A. Naylor and W. Goddard. 'Starburst Dendrimers: Molecular-Level Control of Size, Shape, Surface Chemistry, Topology, and Flexibility from Atoms to Macroscopic Matter', *Angewandte Chemie*, Vol. 29(2), pp. 138–175, **1990.**

[42] D. Tomalia, H. Baker, J. Dewald, M. Hall, G. Kallos, S. Martin, J. Roeck, J. Ryder and P. Smith. 'A New Class of Polymers: Starburst-Dendritic Macromolecules', *Polymer journal,* Vol. 17, pp. 117-132, **1985.**

[43] D. Tomalia, V. Berry, M. Hall and D. Hedstrand. 'Starburst dendrimers. 4. Covalently fixed unimolecular assemblages reiminiscent of spheroidal micelles', *Macromolecules,* Vol. 20(5), pp. 1164–1167, **1987.**

[44] G. Caminati, N. Turro and D. Tomalia. 'Photophysical investigation of starburst dendrimers and their interactions with anionic and cationic surfactants', *Journal of American chemical society,* Vol. 112(23), pp. 8515–8522, **1990.**

[45] K. Copidas, A. Leheny, G. Caminati, N. Turro and D. Tomalia. 'Photophysical investigation of similarities between starburst dendrimers and anionic micelles', *Journal of American chemical society,* Vol. 113, pp. 1335-1342, **1991.**

[46] P. Maiti, T. Cagin, G. Wang and W. Goddard. 'Structure of PAMAM Dendrimers: Generations 1 through 11', *Macromolecules,* Vol. 37, pp. 6236-6254, **2004.**

[47] H. Kroto, J. Heath, S. O'Brien, R. Curl and R. Smalley, 'C60: Buckminsterfullerene', *Nature,* Vol. 318(6042), pp. 162-163, **1985.**

[48] J. Haddock, X. Zhang, B. Domercq and B. Kippelen. 'Fullerene based n-type organic thin-film transistors', *Organic electronics,* Vol. 6(4), pp. 182-187, 2005.

[49] P. Peumans and S. Forrest. 'Very-high-efficiency double-heterostructure copper phthalocyanine/C60 photovoltaic cells', *Applied Physics Letters,* Vol. 79(1), pp. 126-128, **2001.**

[50] J. Hummelen, B. Knight, F. LePeq, F. Wudl, J. Yao and C. Wilkins. 'Preparation and characterization of fulleroid and methanofullerene derivatives', *The Journal of Organic Chemistry,* Vol. 60(3), pp. 532-538, **1995.**

[51] G. Yu, J. Gao, J. Hummelen, F. Wudl and A. Heeger. 'Polymer photovoltaic cells: enhanced efficiencies via a network of internal donor-acceptor heterojunctions', *Science,* Vol. 270 (5243), pp. 1789-1791, **1995.**

[52] [50] M. Wienk, J. Kroon, W. Verhees, J. Knol, J. Hummelen, P. Hal and R. Janssen. 'Efficient Methano[70]fullerene/MDMO-PPV Bulk Heterojunction Photovoltaic Cells', *Angewandte Chemie,* Vol. 42(29), pp. 3371–3375, **2003.**

[53] G. Li, R. Zhu and Y. Yang. 'Polymer solar cells', *Nature Photonics,* Vol. 6, pp. 153–161, **2012.**

[54] Z. He, C. Zhong, X. Huang, W. Wong, H. Wu, L. Chen, S. Su and Y. Cao. 'Simultaneous enhancement of open-circuit voltage, short-circuit current density, and fill factor in polymer solar cells', *Advanced Materials*, Vol. 23(40), pp. 4636-4643, **2011.**

[55] G. Zhao,Y. He and Y. Li. '6.5% Efficiency of polymer solar cells based on poly(3-hexylthiophene) and Indene-C60 Bisadduct by device optimization', *Advanced Materials*, Vol. 22(39), pp. 4355–4358, **2010.**

[56] A. Guerrero, L. Marchesi, P. Boix, S. Ruiz-Raga, T. Ripolles-Sanchis, G. Garcia-Belmonte and J. Bisquert. 'How the Charge-Neutrality Level of Interface States Controls Energy Level Alignment in Cathode Contacts of Organic Bulk-Heterojunction Solar Cells', *ACS Nano*, Vol. 6(4), pp. 3453–3460, **2012.**

[57] F. Chen, C. Chu, J. He and Y. Yang. 'Organic thin-film transistors with nanocomposite dielectric gate insulator', *Applied physics letters*, Vol. 85(15), pp. 3295- 3297, **2004.**

[58] D. Khodagholy,T. Doublet, P. Quilichini, M. Gurfinkel, P. Leleux, A. Ghestem, E. Ismailova, T. Sanaur, C. Bernard and G. Malliaras. 'In vivo recordings of brain activity using organic transistors', *Nature Communications*, Vol. 4(1575), pp. 1-7, **2013.**

[59] I. Cruz-Cruz, A. Tavares, M. Reyes-Reyes, R. Sandoval and I. Hummelgen. 'Interfacial insertion of a poly(3,4-ethylenedioxythiophene): poly(styrenesulfonate) layer between the poly(3-hexyl thiophene) semiconductor and cross-linked poly(vinyl alcohol) insulator layer in organic field-effect transistors', *Journal of Physics D: Applied Physics*, Vol. 47(7), pp. 1-9, **2014.**

[60] Z. Su, L. Wang, Y. Li, H. Zhao, B. Chu and W. Li. 'Ultraviolet-ozone-treated PEDOT:PSS as anode buffer layer for organic solar cells', *Nanoscale Research Letters*, Vol. 7(465), pp. 2-6, **2012.**

[61] Y. Han, M. Chang, W. Huang, H. Pan, K. Ho, T. Hsieh and S. Pan. 'Improved performance of polymer solar cells featuring one-dimensional PEDOT nanorods in a modified buffer layer', *Journal of The Electrochemical Society*, Vol. 158(3), pp. 88-93, **2011.**

[62] A. Bello, M. Giannetto, G. Mori, R. Seeber, F. Terzi, and C. Zanardi, 'Optimization of the DPV potential waveform for determination of ascorbic acid on PEDOT-modified electrodes', *Sensors and Actuators B: Chemical*, Vol. 121, pp. 430–434, **2007.**

[63] Y. Jun, S. Chenghua, T. Furui, H. Xiujie, Ch. Ping, Q. Shengchun, and Z. Shuyun, 'Electropolymerized poly(3,4-ethylenedioxythiophene): poly(styrene sulfonate) (PEDOT:PSS) film on ITO glass and its application in photovoltaic device', *Solar Energy Materials and Solar Cells*, Vol. 94, pp. 390–394, **2010.**

[64] S. Lattante. 'Electron and hole transport layers: their use in inverted bulk heterojunction polymer solar cells', *Electronics*, Vol. 3, pp. 132-164, **2014.**

[65] T. Kuwabara, H. Sugiyama, T. Yamaguchi and K. Takahashi. 'Inverted type bulk-heterojunction organic solar cell using electrodeposited titanium oxide thin films as electron collector electrode', *Thin Solid Films*, Vol. 517(13), pp. 3766–3769, **2009.**

[66] J. Kim, S. Kim, H. Lee, K. Lee, W. Ma, X. Gong and A. Heeger. 'New architecture for high-efficiency polymer photovoltaic cells using solution-based titanium oxide as an optical spacer', *Advanced Materials*, Vol. 18(5), pp. 572–576, **2006.**

[67] A. Hadipoura, R. Müllera and P. Heremans. 'Room temperature solution-processed electron transport layer for organic solar cells', *Organic Electronics*, Vol. 14(10), pp. 2379–2386, **2013.**

[68] H. Kim, A. Yusoff, H. Kim, H. Lee, G. Seo and J. Jang. 'Inverted organic photovoltaic device with a new electron transport layer', *Nanoscale Research Letters*, Vol. 9(150), pp. 1-9, **2014.**

[69] L. Chen, Z. Xu, Z. Honga and Y. Yang. 'Interface investigation and engineering – achieving high performance polymer photovoltaic devices', *Journal of materials chemistry*, Vol. 20(13), pp. 2575-2598, **2010.**

[70] N. Sahu, B. Parija and S. Panigrahi. 'Fundamental understanding and modeling of spin coating process: A review', *Indian Journal of Physics*, Vol. 83(4), pp. 493-502, **2009.**

[71] I. Brodie and J. J. Muray, 'The Physics of Micro/Nano-Fabrication', Plenum Press, New York, **1992.**

[72] G. Binnig, C. F. Quate, and C. Gerber, 'Atomic Force Microscope', Physics review letter, Vol. 56, pp. 930–933, 1986.

[73] F. Giessibl. 'Atomic force microscopy's path to atomic resolution', *Materials Today*, vol. 8(5), pp. 32–41, **2005.**

[74] M. Pfreundschuh, D. Martinez-Martin, E. Mulvihill, S. Wegmann and D. Muller. 'Multiparametric high-resolution imaging of native proteins by force-distance curve–based AFM', *Nature Protocols*, Vol. 9, pp. 1113–1130, **2014.**

[75] A. Ugural and S. Fenster, 'Advanced Strength and Applied Elasticity,'4th edition, Prentice Hall, 2003.

[76] E. Williams and G. Jabbour. 'Conducting polymer and hydrogenated amorphous silicon hybrid solar cells', *Applied Physics Letters*, Vol. 87, pp. 223504, **2005.**

[77] W. Beek, M. Wienk and R. Janssen, Efficient hybrid solar cells from zinc oxide nanoparticles and a conjugated polymer , *Advanced Materials*, Vol. 16(12), pp. 1009- 1013, **2004.**

[78] G. McMahon, Analytical Instrumentation: A Guide to Laboratory, Portable and Miniaturized Instruments, West Sussex: John Wiley & Sons, 2008.

[79] S. Crouch, D. Skoog, D. West and F. Holler, Fundamentals of Analytical Chemistry, London: Cengage Learning, **2013.**

Chapter 4

Organic Bulk-Heterojunction solar cells

4.1 Introduction

Heterojunction organic solar cells can be fabricated in two different structures: bilayer heterojunction structure and bulk- heterojunction structure. Polymers bulk-hetrojunction solar cell (OBHJ) particularly Solution-processed solar cells have more attention in the last few years due to their advantages of low cost fabrication process, flexibility, light –Weight and possibility of application in large area [1]. The active layer of OBHJ commonly contained mixed of donor polymer and a soluble acceptor to gain a large interface area between donor and acceptor for effective charge separation. However, nanometre scale network structure of OBHJ is the key for high efficiency where the dissociation can occur anywhere in the bulk and transfer to appropriate electrodes. It was reported that the control of OBHJ blend morphology is the key for high OBHJ efficiency [2].This chapter, investigates the fabrication and characterisation of organic bulk-heterojunction solar cells (OBHJ) based on two different acceptor materials: a new polyamidoamine (PAMAM) dendrimers (cores and different generations) and indene-C70 bisadduct (IC70BA). The current density–voltage (*J*-*V*) characteristics for these devices were investigated in the dark and under illumination with a halogen lamp. The experimental details, surface morphology and optical characteristics of each of these seven devices are also presented and discussed in this chapter.

4.2 PAMAM cores based OBHJ solar cells

4.2.1 Fabrication process

Fabrication of OBHJ solar cell devices with the structure of ITO/PEDOT: PSS/P3HT: PAMAM cores /TiO_2/Al (as shown in the Fig. 4.1) was started by spin coating of 40 nm thick layer of PEDOT: PSS with a spin speed of 5000 rpm on cleaned ITO coated glass substrate (anode). The PEDOT-PSS films were then cured at 140°C for 10 minutes in air to represent the hole transfer layer (HTL). 130 nm thick active layer

(P3HT: PAMAM cores) was deposited by spin coating of 1wt%:1wt% chloroform solution of PAMAM cores and P3HT (PAMAM cores and IC70BA solutions prepared in chloroform with equal weight ratio of 30 mg/mL) with spin speed of 2000 rpm on top of the hole transfer layer. Then, 20 nm TiOx electron transfer layer (ETL) was deposited with a spin speed of 5000 rpm on top of the active layer and cured at 80°C for 10 minutes under nitrogen environment. After that, a 100 nm layer of Al was deposited through a shadow mask by thermal evaporation. The deposited Al electrode area defines the active area of the devices as 0.12 cm^2. All films preparation and materials evaporation technique were discussed in Chapter 3. The chemical structures of the PAMAM cores is shown in Fig.4.1. Fluorescent PAMAM core (FC0) is 3,6-diamino-l,8-naphthalic anhydride, fluorescent PAMAM core (FC1) is 2-(l-aminopropan-2-yl)-1H-benzo[de]isoquinoline-l,3(2H)-dione, and fluorescent PAMAM core (FC2) is 3-bromo-7H- benz[de]benzimidazo[2,1-a]isoquinoline-7-one. Figure 4.1 also represents the schematic diagram of PAMAM cores based OBHJ solar cells.

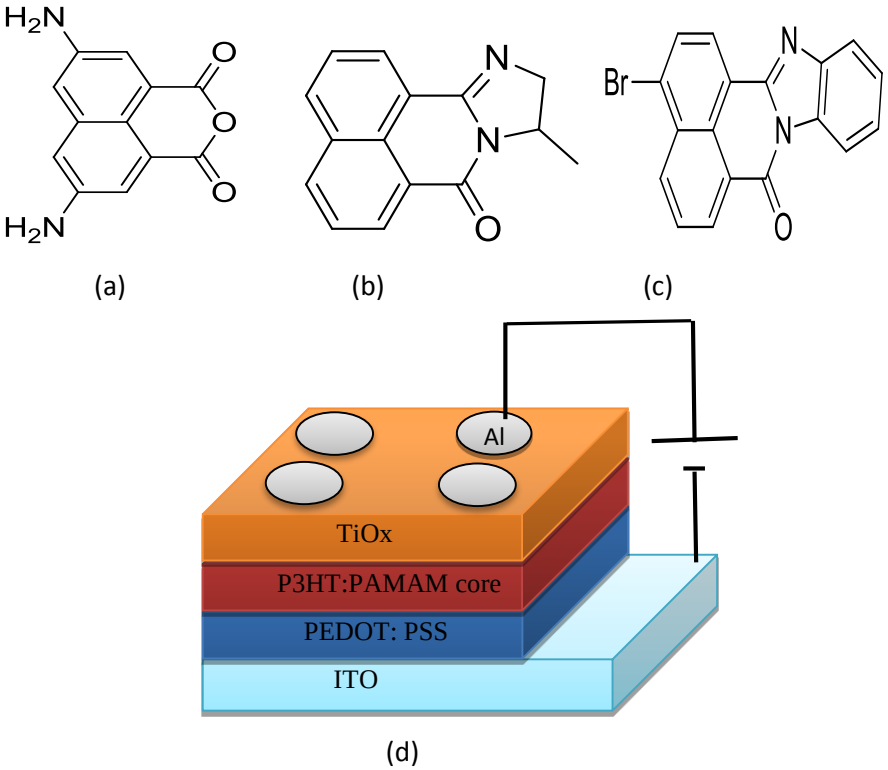

Figure 4.1: *PAMAM cores chemical structure a) PAMAM core FC0,b) PAMAM core FC1, c) PAMAM core FC2, d) Schematic diagram of PAMAM cores based OBHJ solar cell.*

4.2.2 Surface morphology

Studying the surface morphology of the active layer in OBHJ solar cell structures is important in order to understand the effect of the microstructure of the active layer on photovoltaic properties. It was reported that surface morphology play a crucial role in the percolation pathways for transport of both photogenerated excitons and charges. Atomic Force Microscopy (AFM) is used to study donor: acceptor surface structure and how electrical performance characteristics depends on the morphology of the devices [1-3]. Optical image were taken to the fluorescent P3HT and PAMAM-cores (FC0, FC1, FC2) active layer blend on top of ITO/PEDOT:PSS substrate to examine the coating uniformity and quality of the active layer blend. As shown in Fig. 4.2, the optical image of the P3HT and PAMAM-cores active blends spreads smoothly without any substrate-solution incompatibility problems such as pin holes or separated islands in the film. Therefore, Fig. 4.2 shows that the ITO/PEDOT:PSS substrate is a suitable substrate that active blend can be spin coated smoothly.

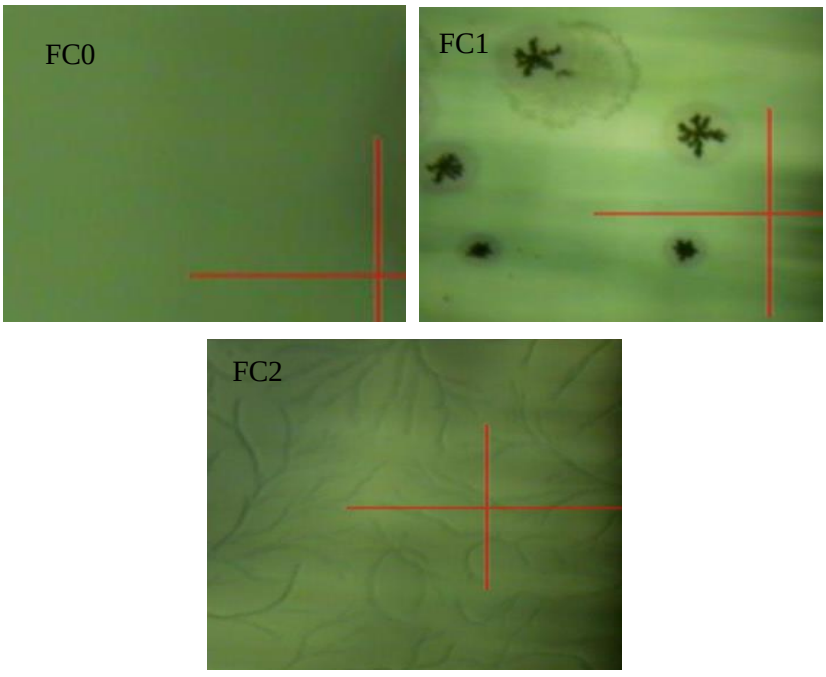

Figure 4.2: *Optical image of the blend of PAMAM-cores and P3HT spin coated on ITO/PEDOT:PSS substrate*

The morphology of the blend exhibits a composition dependent morphology, so it might be useful to study the morphology of, at least, one of the materials as a reference then compare it to the morphology of the blend. In these devices the active blend consists of PAMAM-cores and P3HT. Therefore, P3HT morpology was studied first and then compared with the whole blends morphology.

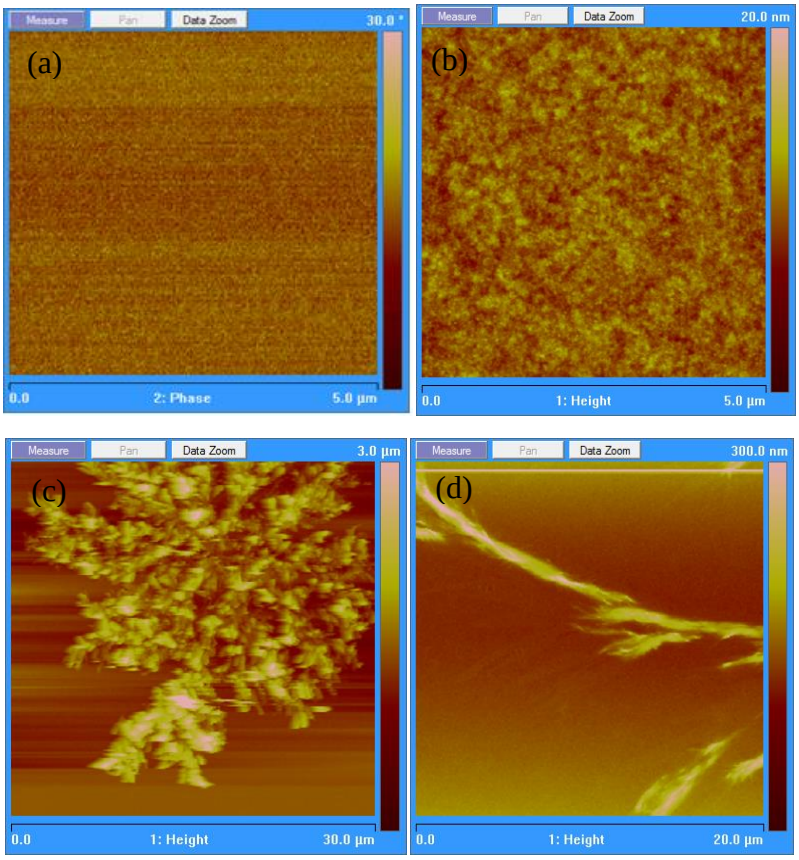

Figure 4.3: *AFM morphology image of: a) P3HT spin coated on ITO/ PEDOT:PSS, and the active blends consisting of P3HT mixed with PAMAM-cores spin coated on ITO/ PEDOT:PSS : b) P3HT:FC0, c)P3HT:FC1and d) P3HT:FC2 .*

Figure 4.3 shows the AFM images of the active blends consisting of P3HT mixed PAMAM-cores with P3HT spin coated onto the ITO/ PEDOT: PSS substrate. A clear difference in the morphology of the active blend can be observed compared to that of the P3HT.

The morphology of the active blend contained P3HT:FC0 a shows phase separation structure with an average roughness of about 1.50 nm. P3HT:FC1 blend shows a few agglomeration of branching spread on the surface forming star-shape branches without

connections with average roughness of about 329 nm. It is evident from Fig. 4.3 that FC1-based films contain aggregated branches with a diameter of about 30 µm. However, P3HT:FC2 show clear branching units similar to a tree spread on the whole surface with weak connections in the deposited film as compared to the others with average roughness of about 21.9 nm . The average length of branches resulted from FC2-based films is about 10 µm.

4.2.3 Electrical characterisation

The current density-voltage (*J-V*) characteristics of P3HT: PAMAM cores are shown in linear and semilog in Fig. 4.4. The *J-V* characteristics of the devices were measured by applying the bias voltage to the aluminium electrode while the ITO electrode was grounded. The solar cells characterization composed of two bias scans: under dark and the same scan under light illumination. Each scan started from -1V and ended at +1V. Under dark condition, the devices displayed good rectifying characteristics as current stayed at almost 0 A from -1V and turned on at 0.6 V, where it started to increase showing clear rectifying behaviour. This indicates that the very low current from -1 V until 0.6 V reflects the lack of carriers in the structure and thus a non-conducting behaviour.

Under illumination with the halogen lamp (100 mW/ cm^2), the *J-V* characteristics did not display any photovoltaic behaviour (no open circuit voltage was detected) for the devices based on P3HT: PAMAM core FC0 and FC1 as active layers due to low conductivity. This is expected as AFM images showed clear disconnected branches of the deposited films, resulted in high film resistance and discontinuity in charge carrier conduction. The results indicate that PAMAM cores FC0 and FC1 are not suitable as acceptor materials of organic solar cells. However, for the device based on P3HT: PAMAM core FC2 a non-zero current is recorded which reflects the existence of the generated carriers due to light absorption and thus the conducting behaviour of the structure. The device produced an open circuit voltage, V_{OC}, of 0.6V, short-circuit current density, J_{SC} of 1.3 mA/ cm^2 with fill factor of 22 % and a maximum power, P_{max}, of 0.2 mW/cm^2 (Fig. 4.5) yielding a power conversion efficiency (PCE) of 0.2%.

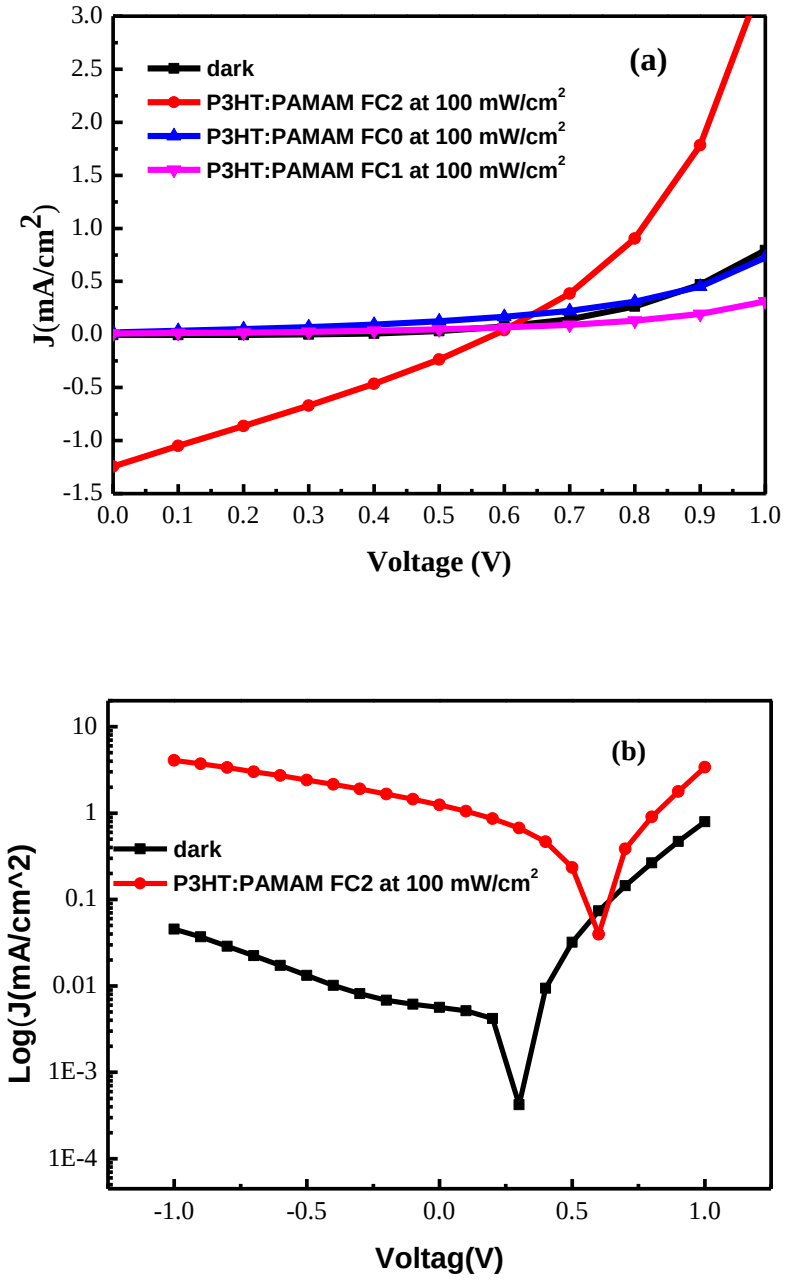

Figure 4.4: *J-V characteristics of the fabricated PAMAM-Cores bulk devices under dark and under a 100 mW/cm^2 (a) linear scale and (b) logarithmic scale.*

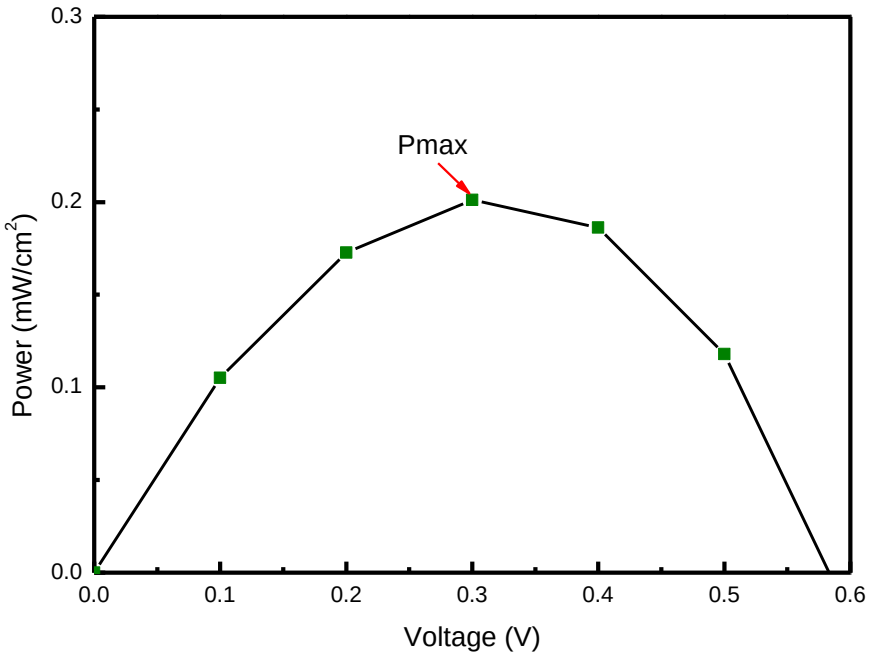

Figure 4.5: *Power curve of PAMAM-FC2 bulk device maximum power of approximately 0.2 mW/cm^2*

At high forward bias, there was a large difference between the dark current and that under illumination, suggesting that photoconductivity is very small. This is attributed to the presence of a high resistance in the bulk semiconductor and the weak connection between branching unites in PAMAM core FC2.

As it was mentioned earlier that the typical solar cells *I-V* curve has series resistance (R_s) equal to zero where the shunt resistant (R_{sh}) should be high. However, Fig. 4.6 shows that the R_s = 500 Ω where the R_{sh} = 2 kΩ which reduce the fill factor as the main impact of the serial resistance is lowering the fill factor. Accordingly, low fill factor (*FF*=22%) will affect the maximum power and then the efficiency. However, it was reported that series resistance arises from individual resistances in the materials used in the device. While shunt resistance results from leakage of current within the device due to poor transport pathways that increase recombination [4]. This confirmed by the morphology of P3HT:FC2 which show clear branching units similar to a tree spread on the whole surface with weak connections. The weak connections may affect the charge transport through the device and lower R_{sh}.

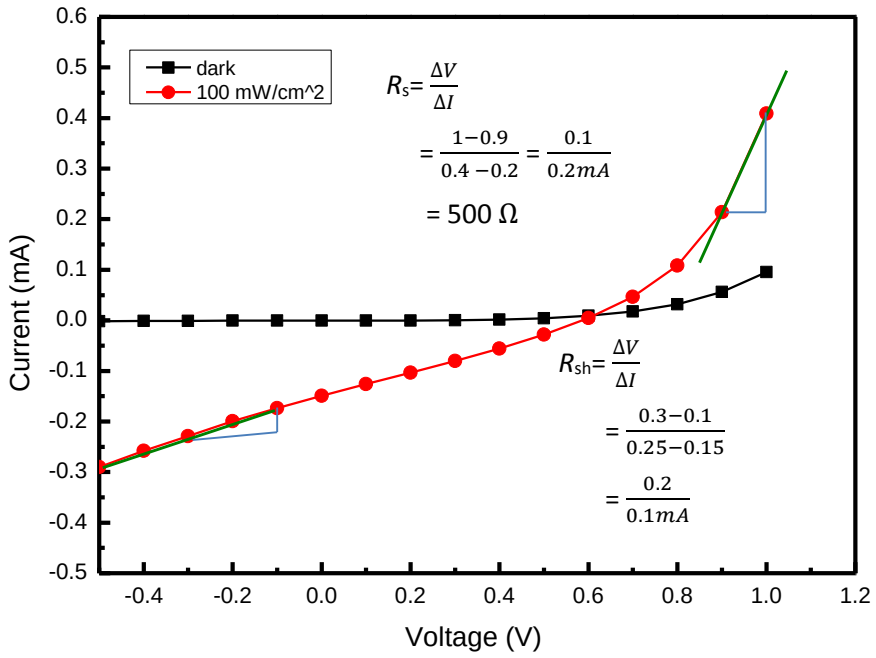

Figure 4.6: *Slops calculation of R_s and R_{sh} from the I-V characteristics of the fabricated PAMAM-FC2 core bulk devices under a 100 mW/cm^2.*

However, the conducting behaviour under light illumination is a result of the generated carriers after photons absorption, then the change in the incident light intensity and consequently photon absorption reflected specifically in the value of $J_{SC.}$ The relationship between the short circuit current density and the light intensity is a positive relationship as shown in equation 4.1 [5].

$$J_{SC} \alpha I_{in} \qquad (4.1)$$

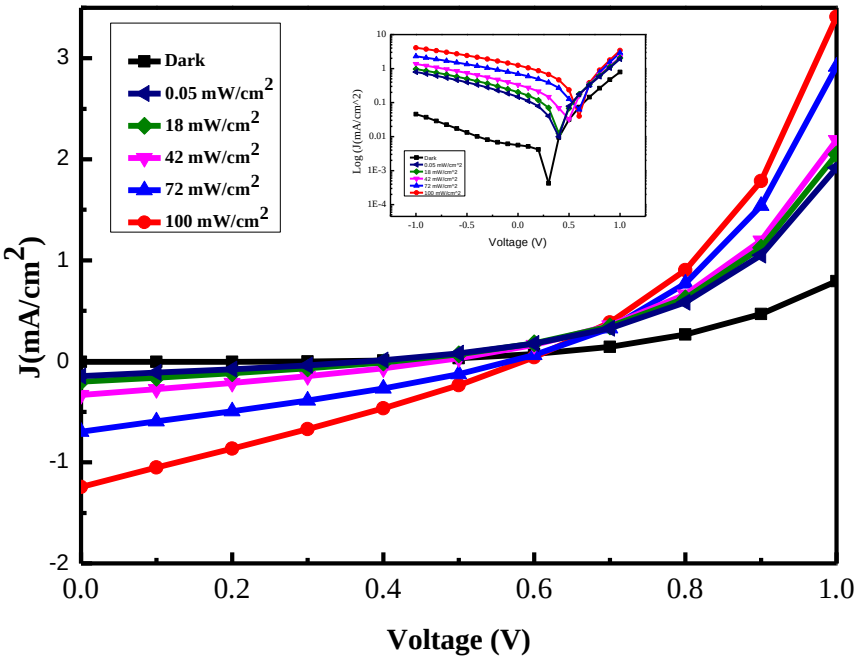

Figure 4.7: *Effect of the light intensity on the I-V characteristics of PAMAM-Core FC2 bulk devices.*

Where I_{in} is the incident light intensity. A lower incident light intensity result in a lower J_{SC} value and higher incident intensity should yield a higher J_{SC} value. Figure 4.7 shows the effect of light intensity on the *J-V* characteristics of the PAMAM-Core FC2 device. The incident light intensity was altered between 0.05 mW/cm^2 and 100 mW/cm^2. Figure 4.8 shows that the J_{sc} is increased with the increasing of the incident light intensity. This is a result of the direct correlation between the incident light intensity and absorption, and accordingly to the amount of charge carriers generated. Similarly a linear correlation was observed between the variation in the light intensity and the V_{OC} (Fig. 4.9), where the V_{OC} increased from 0.45 to 0.6 V as the light intensity increased from 0.05 mW/cm^2 to 100 mW/cm^2, which is again an evidence of the interrelation between the light absorption and the amount of generated carriers.

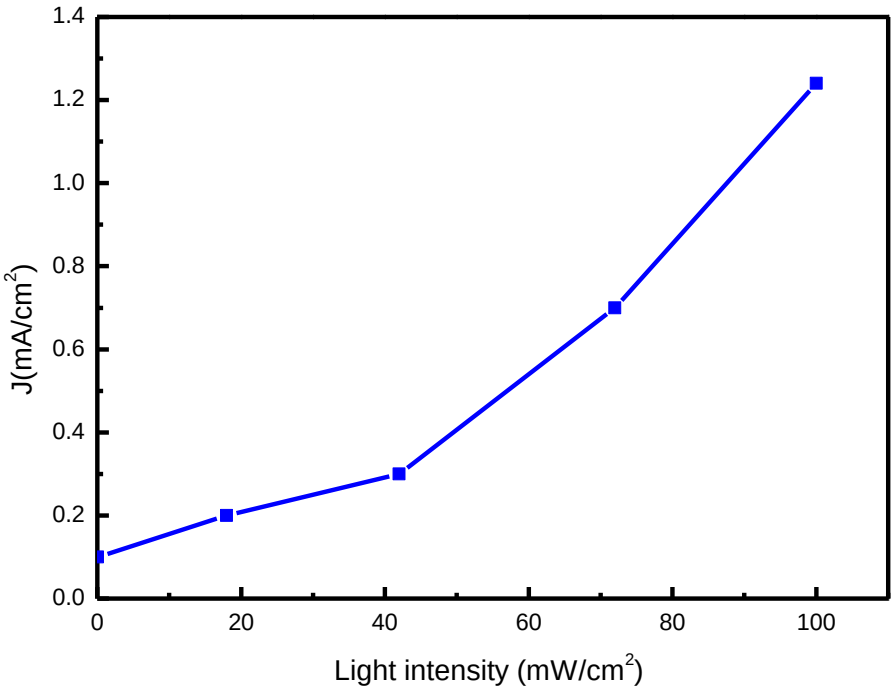

Figure 4.8: *Dependence of J_{sc} on incident light intensity.*

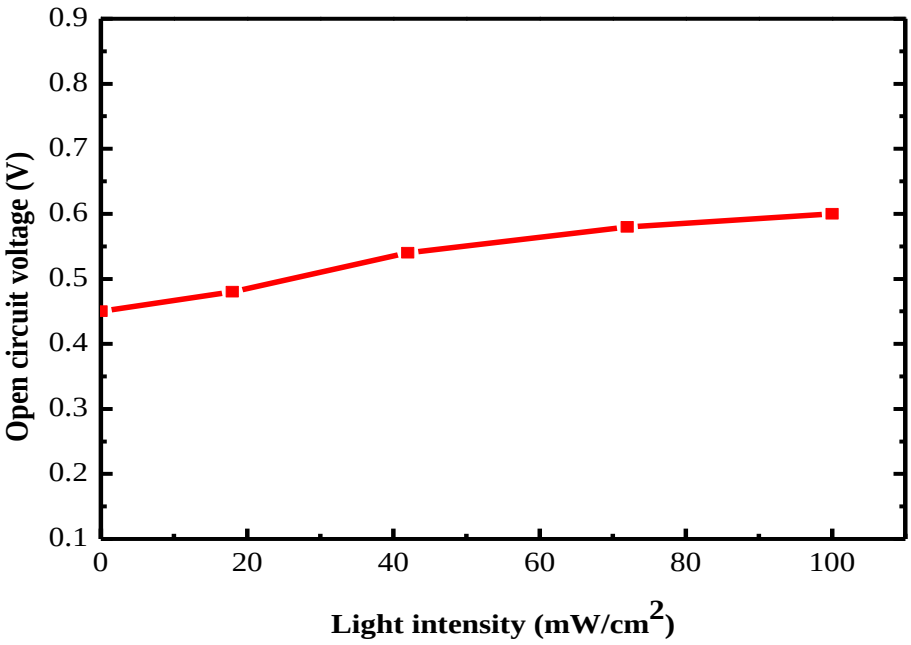

Figure 4.9: *Dependence of V_{OC} on incident light intensity.*

4.2.4 Optical Absorption measurement

The optical bandgap *Eg* is defined as the difference between the lowest unoccupied molecular orbital (LUMO) and the highest occupied molecular orbital (HOMO) of the absorber material [6-8]. The band gap measurement is very important in semiconductor materials as it determines the portion of the spectrum the PV cell absorbs. 4 eV band gap value determines whether the material is a semiconductor (less than 4 eV) or an insulator (more than 4 eV) [9-11]. The Majority of solar radiation reaches the earth with combination wavelengths there energy greater than the band gap of silicon. Solar cell will absorb this energy, but the difference in energy is converted into heat rather than electrical energy [12]. In the visible light spectrum (400 nm to 800 nm), the energy of photons areas from nearly 1.55 eV to 3.1 eV. The corresponding wavelengths of these energies are 750 and 400 nm, respectively. These wavelengths match the red and violet ends of the spectrum of visible light. The absorption property, particularly the absorption in visible region, is very important for the photovoltaic (PV) materials [13, 14]. Low bandgap materials (Eg < 2 eV) are interesting materials in the application of solar cells as their absorption spectra cover from the visible to the near-infrared region. Semiconductors with band gap < 2eV have great chance to form an efficient solar cell [15]. UV-Vis spectrum (absorbance Vs wavelength) of PAMAM FC2 core acceptor is shown in Fig.4.10 and shows absorption edge at 470 nm where the bandgap at this point 2.6 eV. Figure 4.10 also shows absorption peak at 390 nm (equivelant to 3.18 eV). However, Fig.4.11 shows the UV–visible absorption spectra of the materials used for OBHJ solar cells based on PAMAM FC2 core as an acceptor. For OBHJ device with the structure of ITO/PEDOT: PSS/P3HT: PAMAM FC2/TiOx/Al the absorption edge shifts to ~650nm with a peak occurring at 450 nm as a result of absorption in the P3HT. UV-Vis spectrum of PAMAM FC0 and FC1 cores was also measured to compare between them and PAMAM FC2. As shown in Fig. 4.12 the UV-Vis spectrum of PAMAM FC0 is the same as the UV-Vis spectrum of PAMAM FC1, as no change occur. The absorption edge for both films is 350 nm (3.54 eV) with a peak absorption at 330 nm (3.75 eV). It is clear from optical absorption spectra and surface morphology of the active layers why these materials (PAMAM FC0 and FC1) did not show any photovoltaic behaviour when mixed with P3HT in the OBHJs devices. In organic solar cell materials the bandgap should be < 3 eV. 77% of the solar irradiation can be absorbed by a semiconductor materials with a bandgap of 1.1 eV (1100 nm) but

semiconducting polymers have bandgaps higher than 2 eV (620 nm) and can only absorbe about 30% of the solar photons [16, 17].

There is an inverse relation between the energy E, of the photon and the wavelength of light λ as follow:

$$E = \frac{hc}{\lambda} \qquad [4.2]$$

Where h is Planck's constant (h = 6.626 × 10^{-34} J·s) and c is the speed of light (c = 2.998 × 10^{8} m/s).

In terms of wavelength, in nanometers (nm), and energy (E), in electronvolts (eV), equation 4.2 can be expressed for light as:

$$E = \frac{hc}{e\,\lambda} \qquad [4.3]$$

1 electronvolt is the energy gained by an electron moving through a potential difference of 1 V.

1 eV = 1.6x10^{-19} J

$$E = \frac{(6.63X\ 10^{-34})X(3X10^{8})}{(1.6X10^{-19})X\lambda\ (nm)}$$

$$E = \frac{1.240X10^{-6}}{\lambda}$$

If λ in nanometer unit (nm):

$$E = \frac{1.240X10^{-6}}{\lambda\ X\ 10^{-9}}$$

$$E = \frac{1240}{\lambda\ (nm)}$$

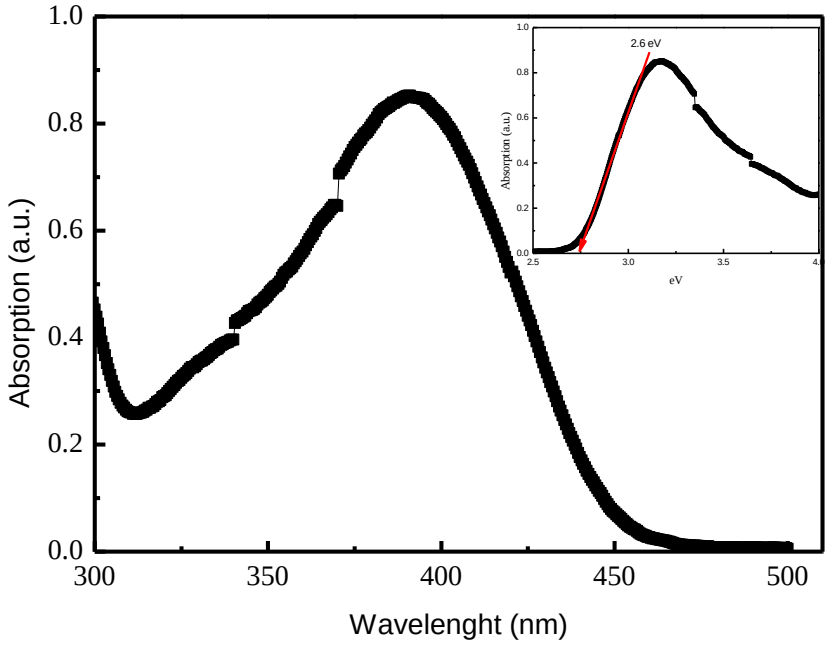

Figure 4.10: *The optical absorption of a PAMAM FC2 film.*

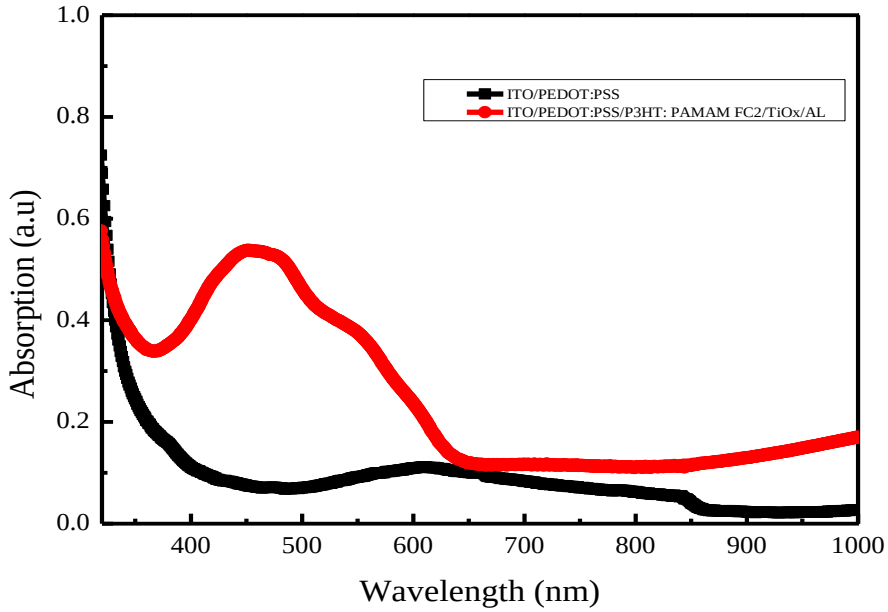

Figure 4.11: *The optical absorption of the PAMAM FC2 based OBHJ solar cells*

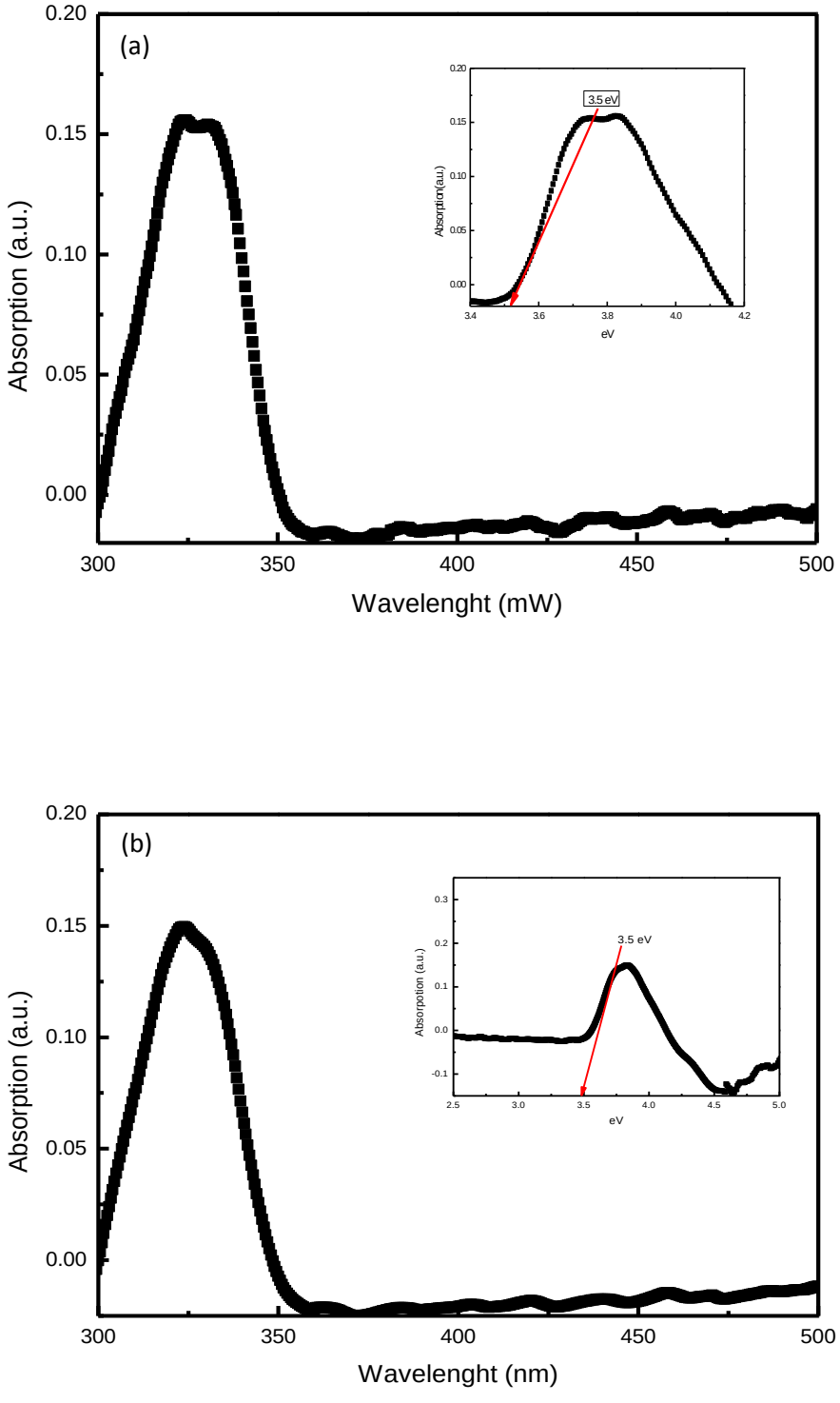

Figure 4.12: *The optical absorption of a) PAMAM FC0 film and b) PAMAM FC1 film.*

4.2.5 Thermal annealing of PAMAM-Core FC2 bulk device

A common method to improve the efficiency of polymer photovoltaic cells is annealing. The purpose of annealing OPV devices is to change the properties of the film from unordered and amorphous to a more homogenous nature structure [18, 19]. Optimum OBHJ morphology through thermal annealing stabilizes the photoactive layer to be more robust to the chemical degradation under prolonged operation and improves the power conversion efficiency of the photovoltaic device [10, 20]. However, it was reported that PAMAM dendrimers show stronger cross-linking ability at room temperature [21].

The thermal annealing was performed for the active layer at different temperatures for 10 min before the TiOx electron transfer layer (ETL) and vacuum deposition of the metal electrode (pre-thermal annealing). Fig. 4.13 shows the current density–voltage (*J–V*) curves of the OBHJ solar cells with different thermal annealing temperatures under the illumination of 100 mW/cm^2 white light.

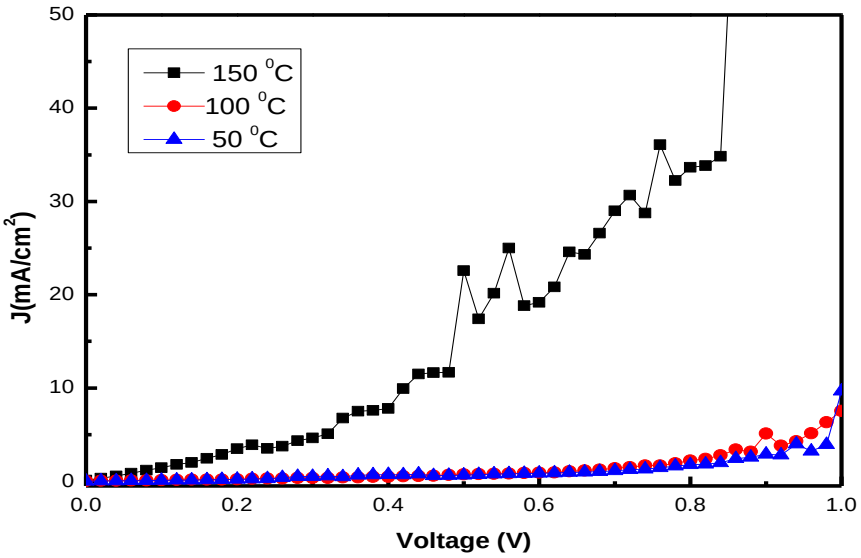

Figure 4.13: *current density–voltage (J–V) curves of the PAMAM FC2 OBHJ solar cells with different pre-thermal annealing temperature under the illumination of 100 mW/cm2 white light.*

After annealing for 50 ^{0}C, 100 ^{0}C and 150 ^{0}C the *J-V* characteristics did not display any photovoltaic behaviour (no open circuit voltage was detected) under illumination with the halogen lamp (100 mW/cm^2).

In order to understand the morphological changes that occur in the polymer layer as a result of thermal annealing, AFM images of the active layer surface were studied. The tapping-mode atomic force microscope (AFM) images in Fig.4.14 shows the variation in OBHJ active layer morphology after annealing at different temperatures. The dimensions in Fig. 4.14 at 150 ^{0}C was kept at 20 µm due to the low contrast at lower dimensions.

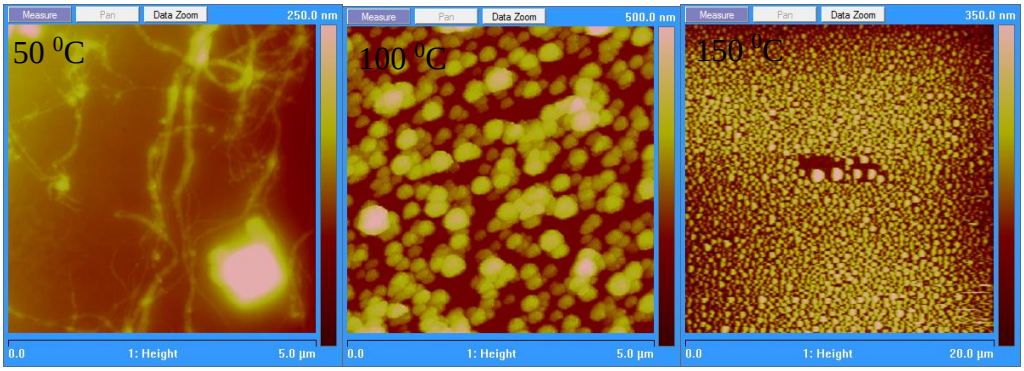

Figure 4.14: *shows the variation in OBHJ active layer morphology after annealing at different temperatures*

Before annealing as seen in Fig. 4.3, PAMAM core FC2 had branches morphology with connections however, after annealing (Fig.4.14) grain growth and agglomeration increased with annealing. It was reported that PAMAM dendrimers undergo some folding, shape and size changes in response to changes in their environment, such as altered solvent type, pH and temperature [22-25]. It can be seen that, the film morphology was changed from branched morphology to globular structures upon temperature increase. This result is in good agreement with other reported results that annealing dendrimers at high temperature retain their globular structure and uniformity at the molecular level [26-28]. On other hand, other researchers reported that thermal annealing enhanced phase separation at micrometre scale and that results in incomplete energy transfer in the dendrimer [29, 230]. These results are in full agreement with the

J-V characterisation results as the branches disappeared from the surface with annealing and the structure of dendrimers become globular structure without any connections. Thus, energy transfers in the dendrimers become difficult.

4.3 PAMAM dendritic based OBHJ solar cells

4.3.1 Fabrication process

The structure of the ITO/PEDOT: PSS/P3HT: PAMAM dendritic /TiO_2/Al is shown in Fig. 4.15. The devices were fabricated by spin coating of 40 nm thick layer of PEDOT: PSS with spin speed of 5000 rpm on cleaned ITO coated glass substrate (anode) and curing at 140°C for 10 minutes in air to represent the HTL. 130 nm thick active layer (P3HT: PAMAM dendritic) was formed by spin coating of 1wt%:1wt% chloroform solution of P3HT and PAMAM dendritic (P3HT and PAMAM in chloroform with equal weight ratio 30 mg/mL) with spin speed of 2000 rpm on top of the hole transfer layer (HTL). Figure 4.15 show the chemical structure of the PAMAM dendritic (G0, G0.5, G1 and G2) and Table 4.1 shows the surface groups, number of primary and tertiary amine in the PAMAM generations used. PAMAM G0, G1 and G2 are full generations where the primary amine is the surface group. PAMAM G0 with one primary amine in the surface group, generation G1 with two primary amine in the surface group and PAMAM G2 with four primary amine in the surface group.

PAMAM G0.5 is half generation with two Ester-terminated groups. The backbone of PAMAM G0.5 and G0, G1 and G2 is the same, the only difference being the terminal groups (–COOCH3 for the half generation (ester group), –NH2 for the full generation (amine group). Then, 20 nm TiOx electron transfer layer (ETL) was deposited with spin speed of 5000 rpm on top of the active layer and cured at 80°C for 10 minutes under nitrogen environment. After that, a100 nm layer of Al was deposited through a shadow mask by thermal evaporation. The deposited Al electrode area defines an active area of the devices as 0.12cm^2.

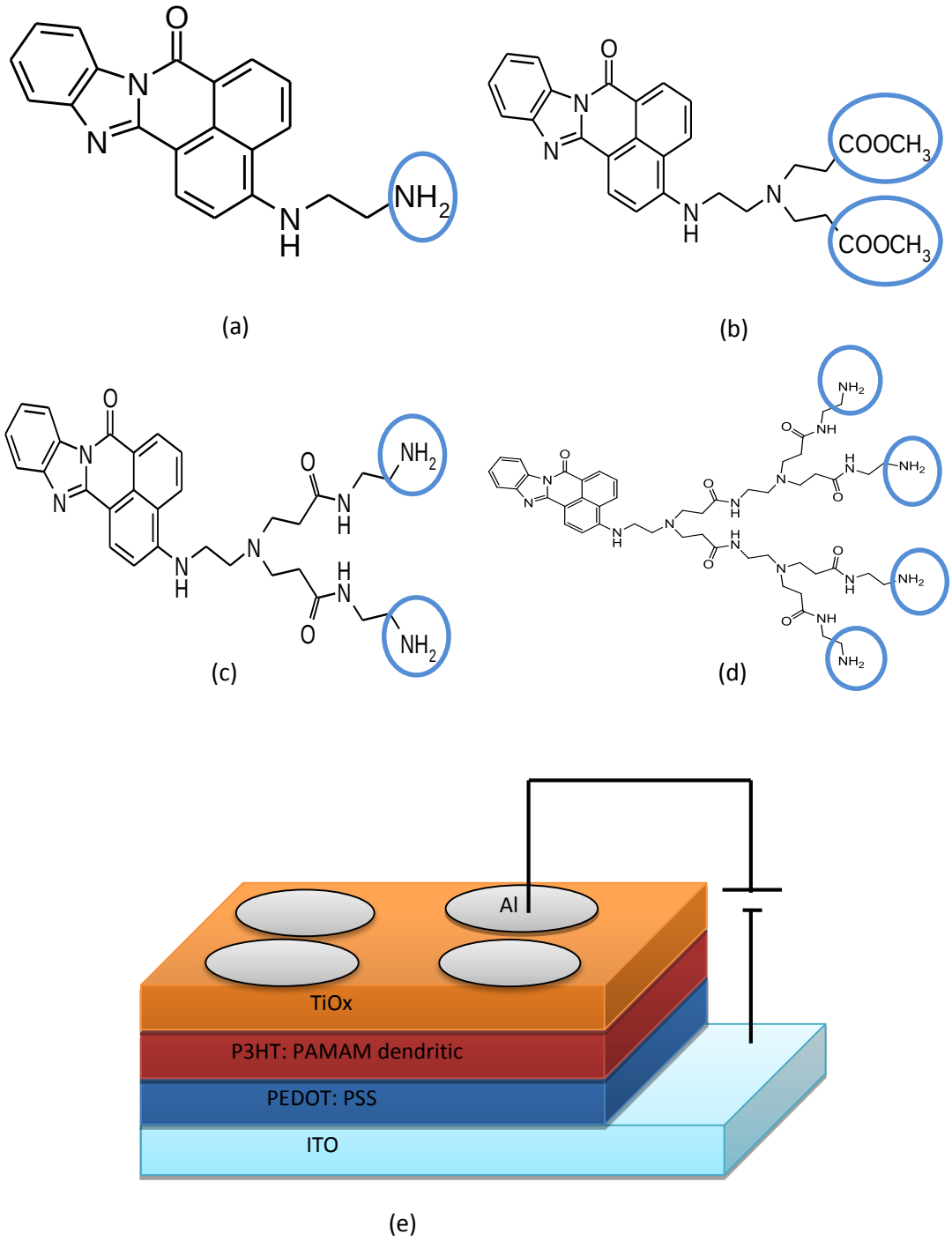

Figure 4.15: *PAMAM dendritic chemical structure a) PAMAM dendritic G0,b) PAMAM dendritic G0.5, c) PAMAM dendritic G1, d) PAMAM dendritic G2, e) Schematic diagram of PAMAM dendritic based OBHJ solar cells.*

PAMAM generations	Primary amine -NH2	Tertiary amine =N-	Surface group
G0	1	0	Amine
G0.5	0	1	Ester
G1	2	1	Amine
G2	4	3	Amine

Table 4.1: *surface groups, number of primary and tertiary amine in different PAMAM generations.*

4.3.2 Surface morphology

The surface morphology for PAMAM dendritic with P3HT and different generations (G0, G0.5, G1 and G2) active blend layer on top of the ITO/PEDOT: PSS substrates are shown in Fig. 4.16. The morphology of the active blend contained P3HT: PAMAM G0 show phase separation with small agglomerations without connection spread on the surface with an average roughness of about 4.78 nm.

However, P3HT: PAMAM G0.5 blend shows condense branching units with good connections as shown in Fig. 4.17. P3HT: PAMAM G1 blend demonstrate a phase separation with average roughness of about 0.48 nm where P3HT: PAMAM G2 blend shows small spots spared in the surface with average roughness of about 13.6 nm.

It is clear from the morphology of the PAMAM G0.5 has optimal surface morphology for energy transfer in dendritic structure. It shows condense branching units with good connections which assist charge transferring between these branches.

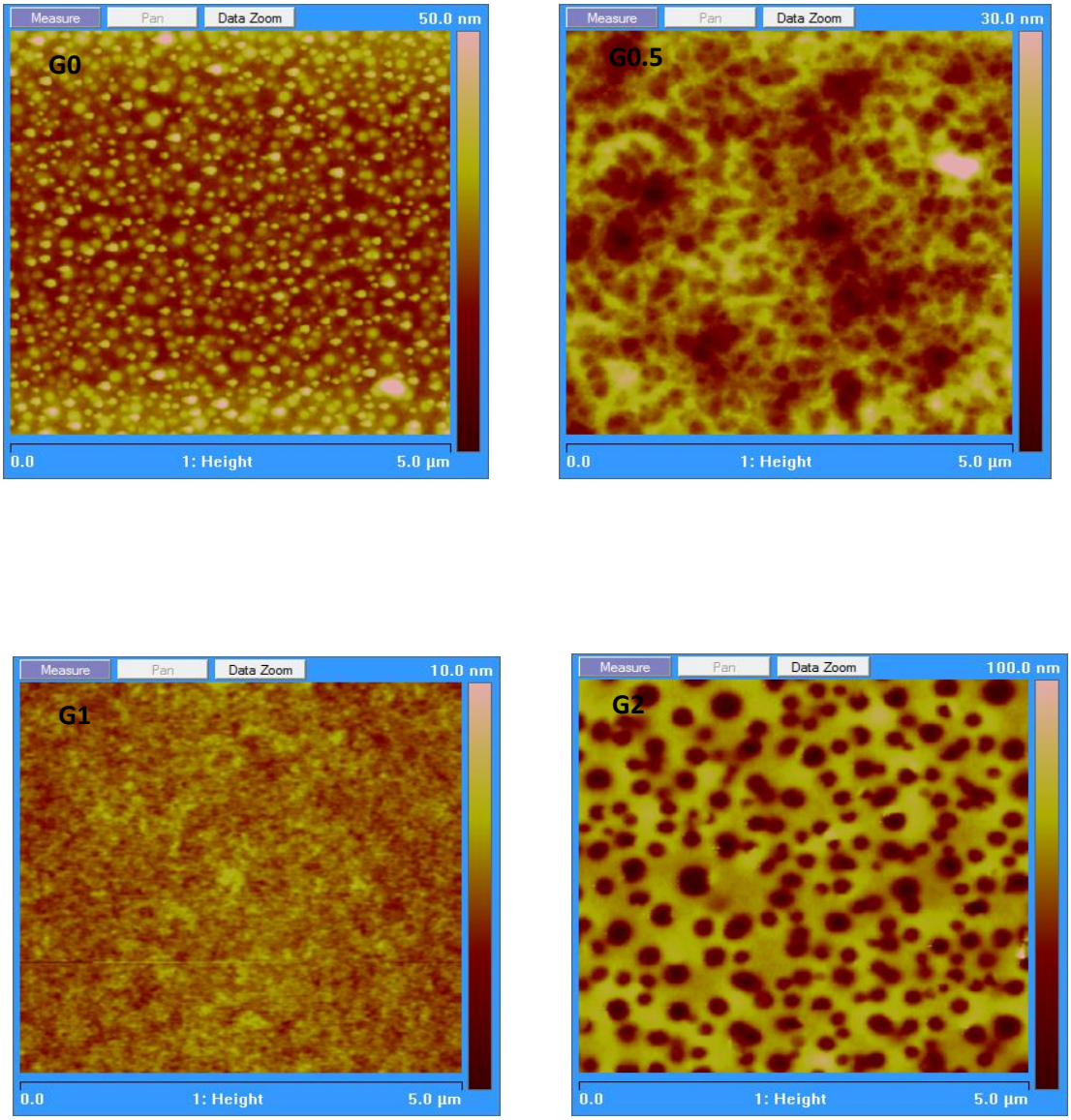

Figure 4.16: *AFM morphology image of the active blends consisting of PAMAM-dendritic mixed with P3HT spin coated on ITO/ PEDOT: PSS with different generations.*

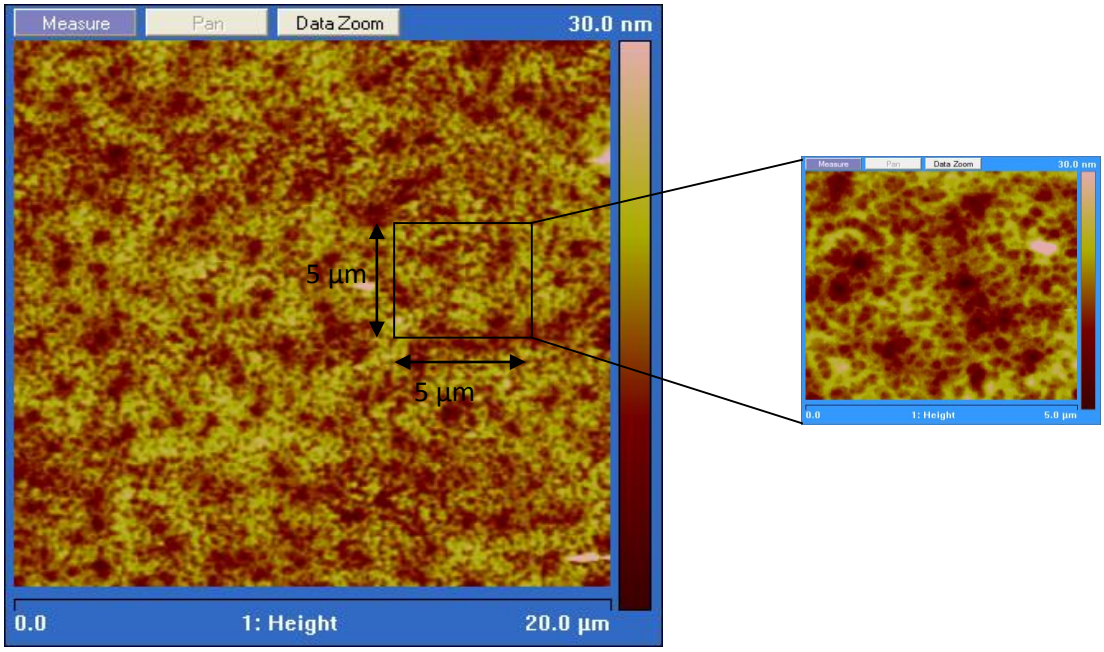

Figure 4.17: *AFM morphology image of P3HT: PAMAM G0.5 blend at different scan scales.*

4.3.3 Electrical characterisation

The *J-V* characteristics of PAMAM dendritic (G0, G0.5, G1 and G2) are shown in Fig. 4.18. In the dark, the turn-on voltage was 0.75V then started to increase showing a rectifying behaviour. Under illumination no open circuit voltage was detected for the PAMAM dendritic G0, G1 and G2 which means the photoconductivity in these devices is very low.

However, the device based on P3HT: PAMAM G0.5 show a non-zero current which reflects the existence of the generated carriers due to light absorption and thus the conducting behaviour of the structure. The device produced an open circuit voltage, *Voc*, ~ 0.85V, short-circuit current density, *Jsc*,~ 6 mA/ cm^2 with fill factor of ~26 % and P_{max} 1.6 mW/cm^2 yielding a power conversion efficiency of 1.6%. The calculated values of R_s and R_{sh} are 83 Ω 800 Ω, respectively.

At high forward bias, there was no difference between the dark current and that under illumination, suggesting that photoconductivity is very high. This is due to low resistance in the bulk semiconductor (small R_s).

As mentioned earlier that the backbone of PAMAM G0.5, G0, G1 and G2 is the same, and the only difference is the terminal groups (–$COOCH_3$ for the half generation (ester group), –NH_2 for the full generation (amine group). From chemical point of view, the full generation amine-termnate PAMAM surface group (G0, G1 and G2) are protonated at physiological pH. Thus there is electrostatic repulsion between the primary amine in the surface preventing the electrostatic interaction with other materials [30-32]. However, ester terminated half-generation dendrimers are less susceptible to protonation compared to the full generation dendrimers and more opening structure for electrostatic interaction with other materials to occur. It was demonstrated that ester-terminated PAMAM interacted more strongly with cationic surfactants than amine-terminated PAMAM. Also, half-generation dendrimers are hydrolyze readily [33, 34]. Recent studies have demonstrated that a change in generation alternatively from amine- to ester-terminated PAMAM changes its interactions with surfactants significantly [35, 36].

Figure 4.19 shows the effect of light intensity on the *J-V* characteristics of the PAMAM-G0.5 ester group device. The incident light intensity was altered between 18 mW/cm^2 and 100 mW/cm^2. The *J*sc and *V*oc are linearly increased with the increasing of the incident light intensity. This is a result of the direct correlation between the incident light intensity and absorption, and accordingly to the amount of charge carriers generated.

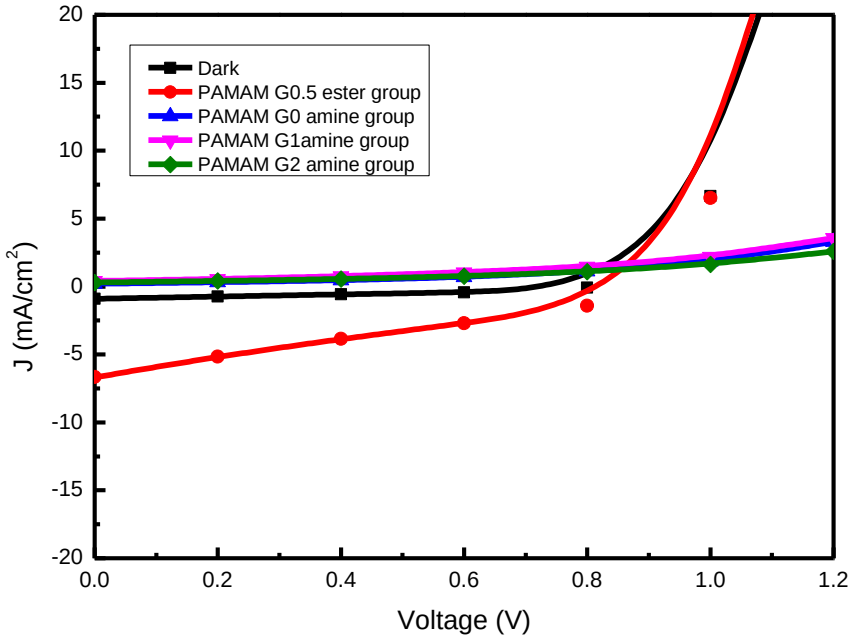

(a)

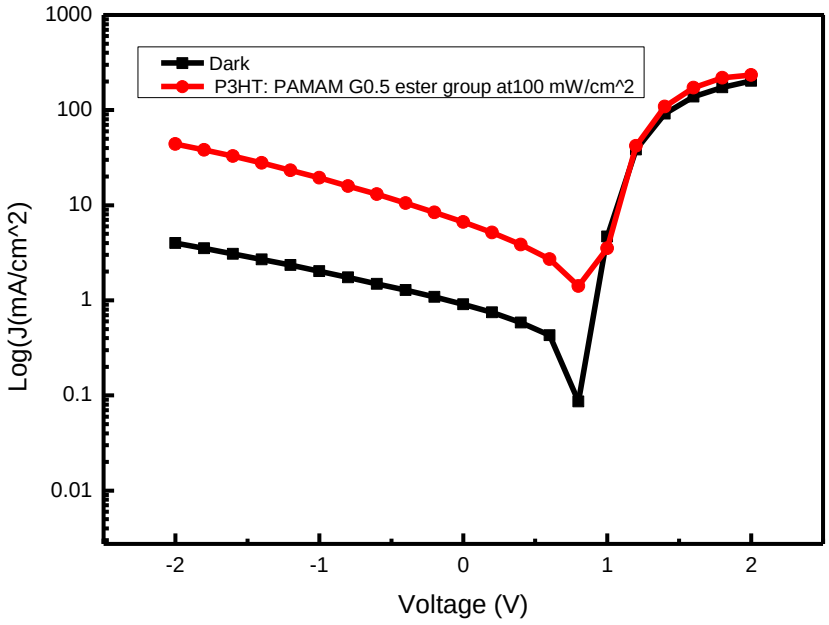

(b)

Figure 4.18: *J-V characteristics of the fabricated PAMAM generations bulk devices under dark and under a 100 mW/cm2 (a) linear scale and (b) logarithmic scale.*

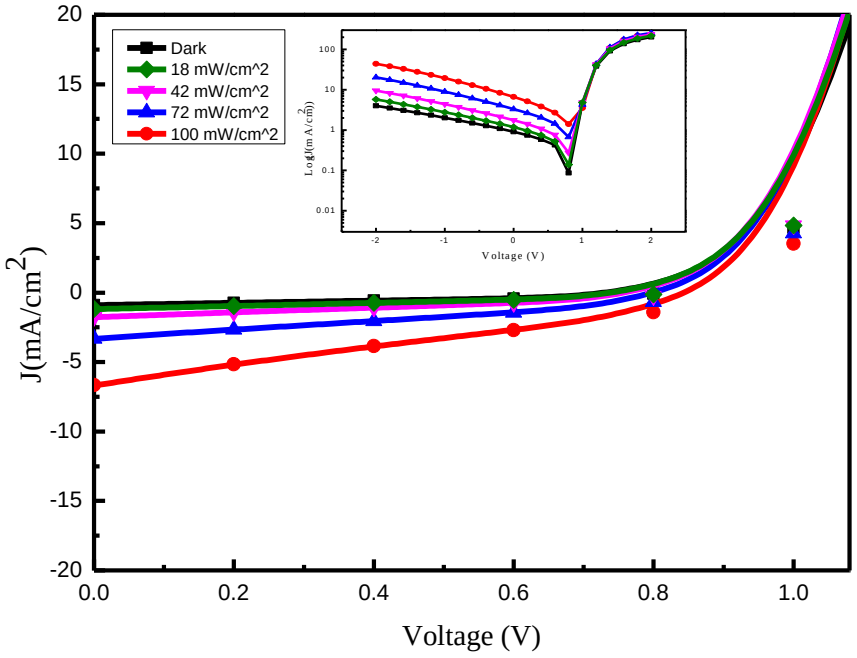

Figure 4.19: *Effect of the light intensity on the I-V characteristics of PAMAM G0.5ester group bulk devices.*

4.3.4 Optical Absorption measurement

UV-Vis spectra of PAMAM generations (G0, G0.5, G1 and G2) are shown in Fig.4.20. PAMAM G0 absorption edge at 500 nm where the bandgap at this point is about 2.5 eV, with peak absorption at 440 nm (2.8 eV). However, PAMAM G0.5 absorption edge at 530 nm where the bandgap at this point 2.3 eV, with peak absorption at 450 nm (2.7 eV). The other two PAMAM generations (G1 and G2) demonstrated the same UV-Vis spectrum of PAMAM G0 with same absorption edge and peak values.

Figure 4.21 shows the UV–Vis absorption spectra of the materials used for OBHJ solar cells based on PAMAM G0.5 as an acceptor. For OBHJ device with the structure of ITO/PEDOT: PSS/P3HT: PAMAM G0.5 /TiOx/Al the absorption edge shifts to ~650 nm for a bandgap of 1.9 eV as a result of absorption in the P3HT. Although the absorption spectra is almost the same for these structures, the surface morphology shows difficulties in conduction due to the disconnected branches in G0, G1 and G2-based films as well as condense and connected branches for G0.5-based films.

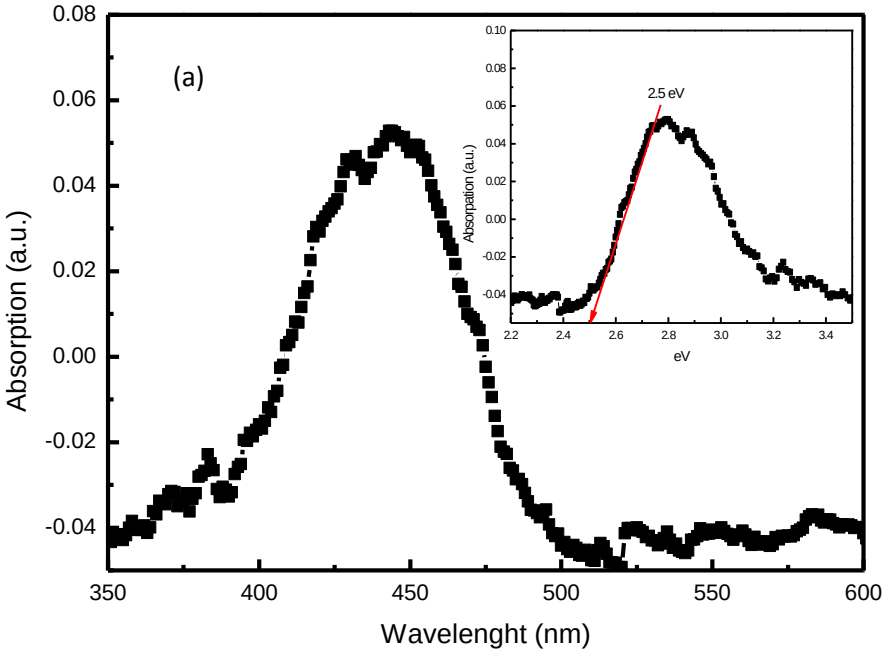
(a)
Absorption (a.u.)
Wavelenght (nm)
2.5 eV
eV
Absorpation (a.u.)

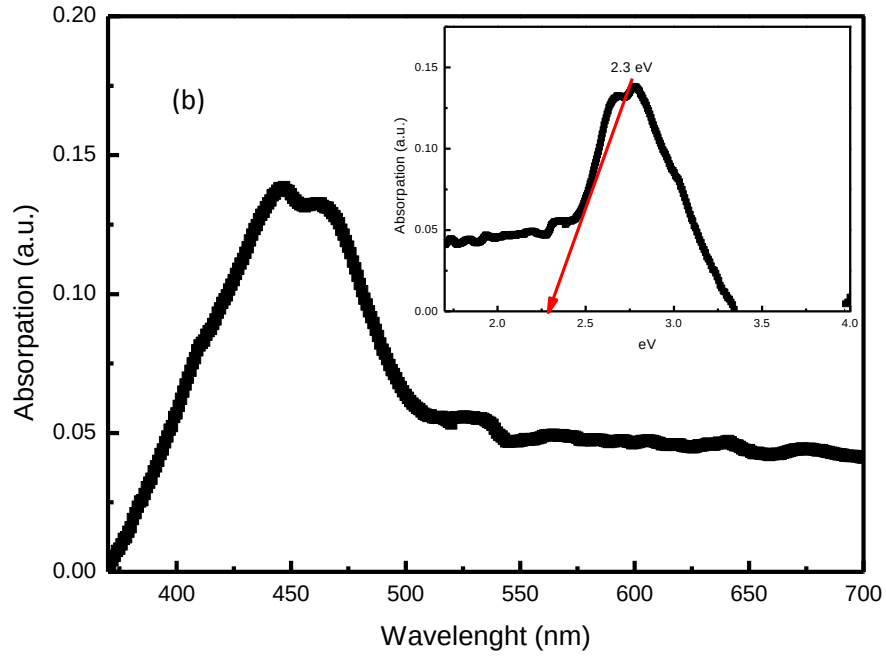
(b)
Absorpation (a.u.)
Wavelenght (nm)
2.3 eV
eV
Absorpation (a.u.)

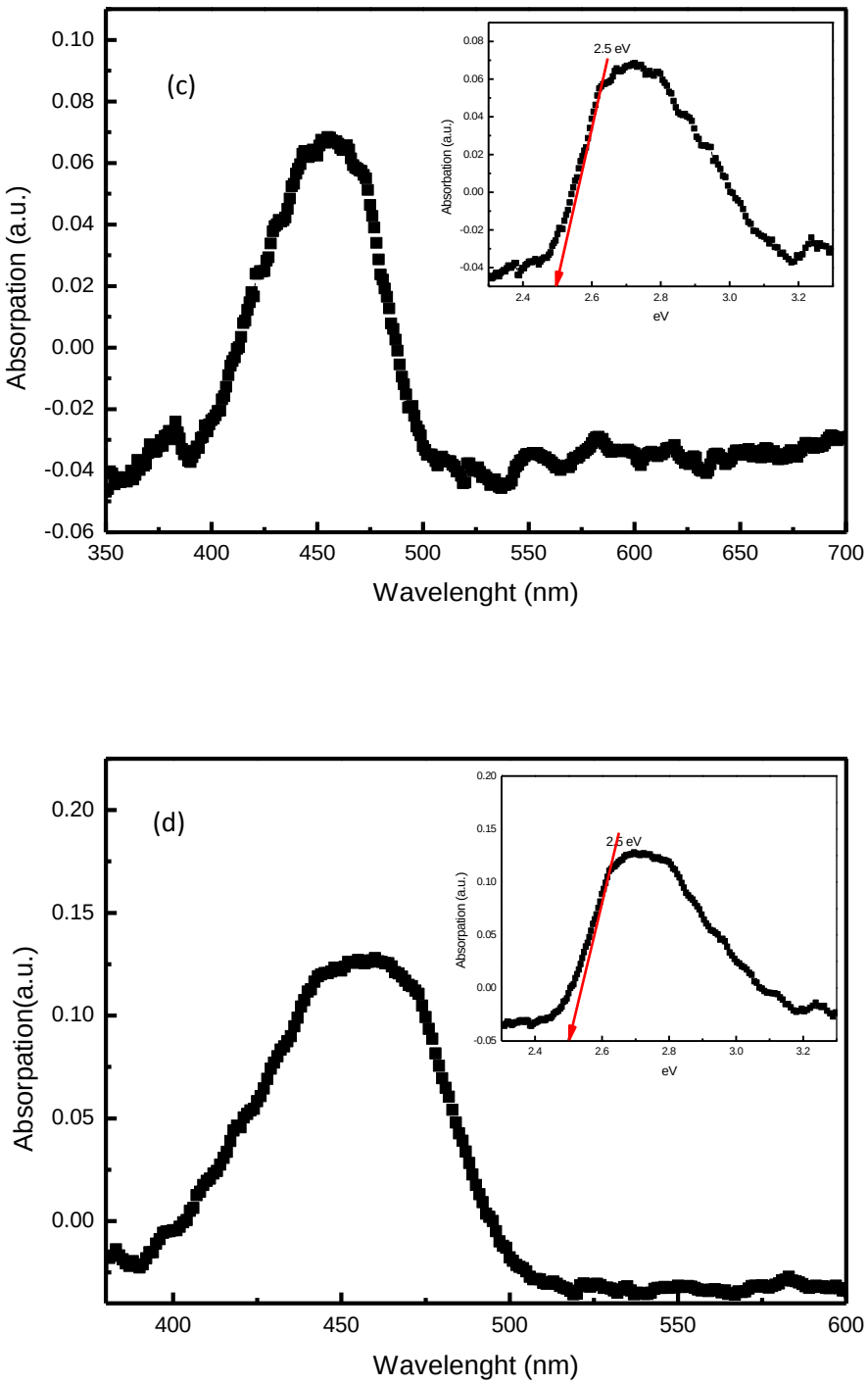

Figure 4.20: *The optical absorption of PAMAM generations a) G0, b) G0.5, c) G1 and d) G2.*

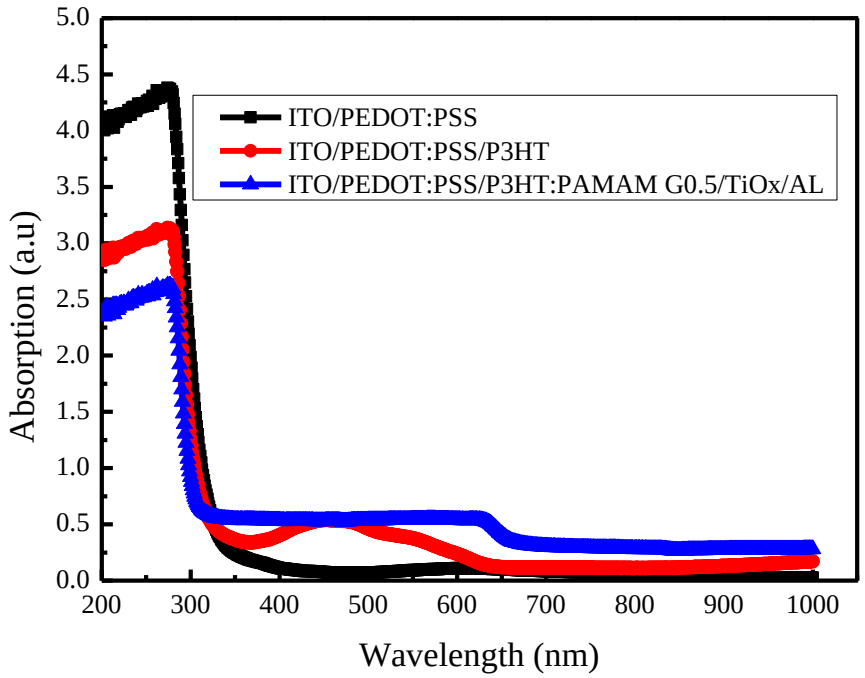

Figure 4.21: *The optical absorption of the PAMAM G0.5 ester group based OBHJ solar cells*

4.3.5 Thermal annealing of PAMAM dendritic-G0.5 bulk devices

The thermal annealing was performed for the active layer (P3HT:PAMAM G0.5) as previously mention in P3HT:PAMAM FC2 core at different temperatures for 10 min before the TiOx electron transfer layer (ETL) and vacuum deposition of the metal electrode. Figure 4.22 shows the *J–V* curves of the OBHJ solar cells with different thermal annealing temperature under the illumination of 100 mW/cm^2 white light. The same results were recorded for annealing P3HT: PAMAM FC2 blend, as P3HT: PAMAM G0.5 blend annealed at 50, 100, and 150 ^{0}C did not display any photovoltaic behaviour (no open circuit voltage was detected) under illumination with the halogen lamp (100 mW/ cm^2).

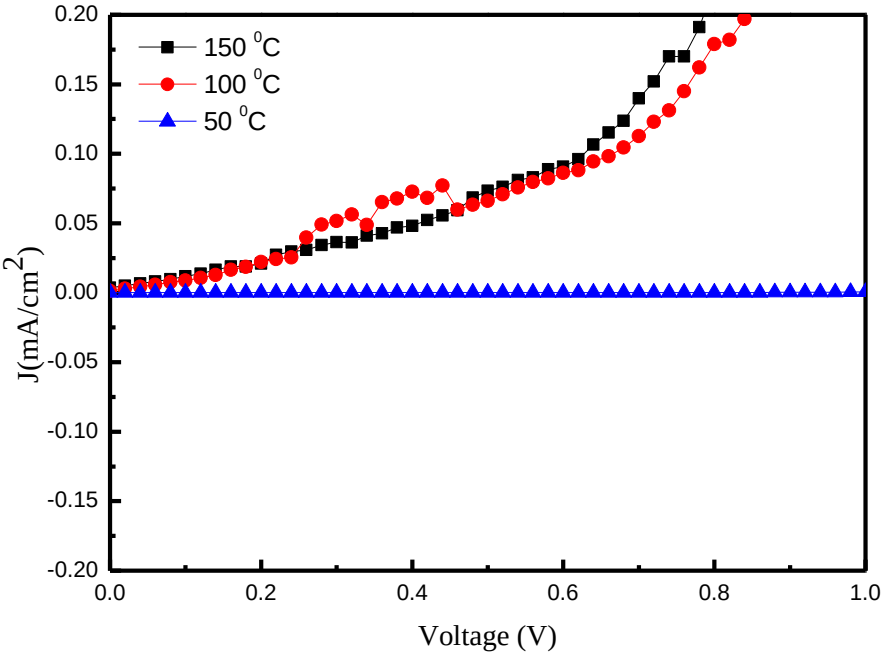

Figure 4.22: *current density–voltage (J–V) curves of the PAMAM G0.5 OBHJ solar cells with different pre-thermal annealing temperature under the illumination.*

AFM images of the active layer surface after annealing at different temperatures were studied in order to understand the morphological changes that occur in the active layer blend (P3HT:PAMAM G0.5) as a result of thermal annealing. Before annealing as seen in Fig. 4.16 PAMAM G0.5 ester group had condense branches morphology with good connections however, after annealing (as shown in Fig.4.23) grain growth and agglomeration increased as annealing temperature increased. *J-V* characterisations confirm the results as the branches disappeared and the structure of dendrimers becomes of small globular structure without any connections. Thus, energy transfers in the dendrimers become difficult.

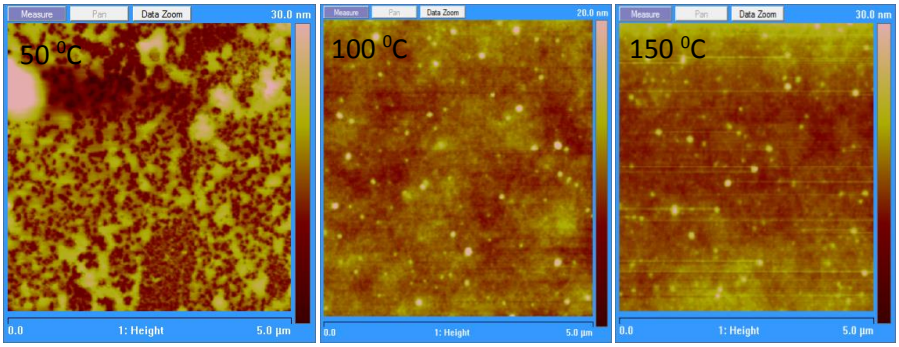

Figure 4.23: *shows the variation in active layer P3HT:IC70BM OBHJ morphology after annealing at different temperatures*

4.4 IC70BA based OBHJ solar cells

4.4.1 under different annealing conditions

4.4.1.1 Fabrication process

The structure of the IC70BA-based devices is shown in Fig.4.24. ITO-coated glass substrate were cleaned with soap, warm water and deionized water, then cleaned with ultrasonic treatments in acetone and isopropanol respectively, and were dried with nitrogen flow. Conducting PEDOT: PSS was spin-cast (5000 rpm) for 40 second with expected thickness of ~40 nm. Then, the substrates were dried for 10 minutes at 140˚C in air, and then placed in the glovebox for spin coating of the active layer. The active layer for these devices was prepared by spin coating the blend solution of P3HT: IC70BA (IC70BA in dichlorobenzene (DCB) 1:1 w/w, 34 mg/ml for P3HT:IC70BA) with a spin coating 900 rpm for 60 sec. Then, the TiOx precursor solution in methanol was spin coated with thickness ~20 nm on top of the active layer and was dried for 10 minutes at 80˚C.

Finally, the device was completed by evaporating~100 nm Al on top of TiOx. The deposited Al electrode area defines an active area of the devices as 0.12cm^2. The thermal annealing was performed at different temperatures for 10 min before the vacuum deposition of the metal electrode (pre-thermal annealing).

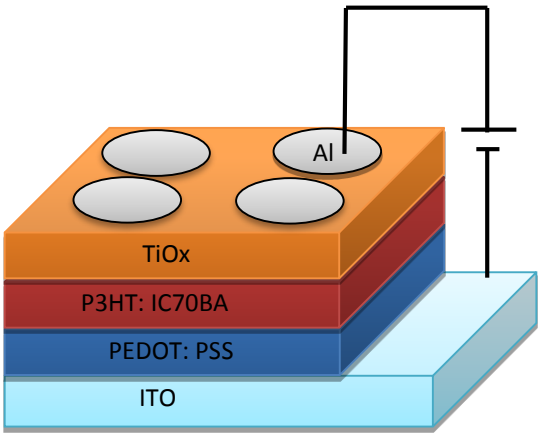

Figure 4.24: *Schematic diagram of IC70BA based OBHJ solar cells*

4.4.1.2 Surface morphology

AFM images of the active layer surface before and after annealing at different temperatures were studied to understand the morphological changes that occur in the active layer as a result of thermal annealing. The tapping-mode AFM images in fig.4.24 shows the variation in OBHJ active layer morphology before and after annealing at different temperatures. As shown in Fig.4.25, the surface of the as-cast film with no thermal treatment is amorphous and very smooth with arms roughness of 0.377 nm. This unordered structure limits the conduction and charge carrier mobility. After undergoing thermal treatment at 100 ^{0}Cand 150 °C for a period of 10 min each, the arms roughness becomes 0.662 and 0.75 nm, respectively. Further increase in temperature to 180 °C the surface becomes rough and aggregate compared to the film treated at 150 °C. The high agglomeration of the active film has negative impact on the OBHJ performance as the D:A interface area reduces the ability to separate excitons. From the AFM images the annealing at 150 °C results in good mixing structures with moderate agglomeration which gives large and connected grains. Thus the change in annealing conditions significantly modify the nature of the underlying active layer morphology, and the morphology is correlated to the cell performance [37].

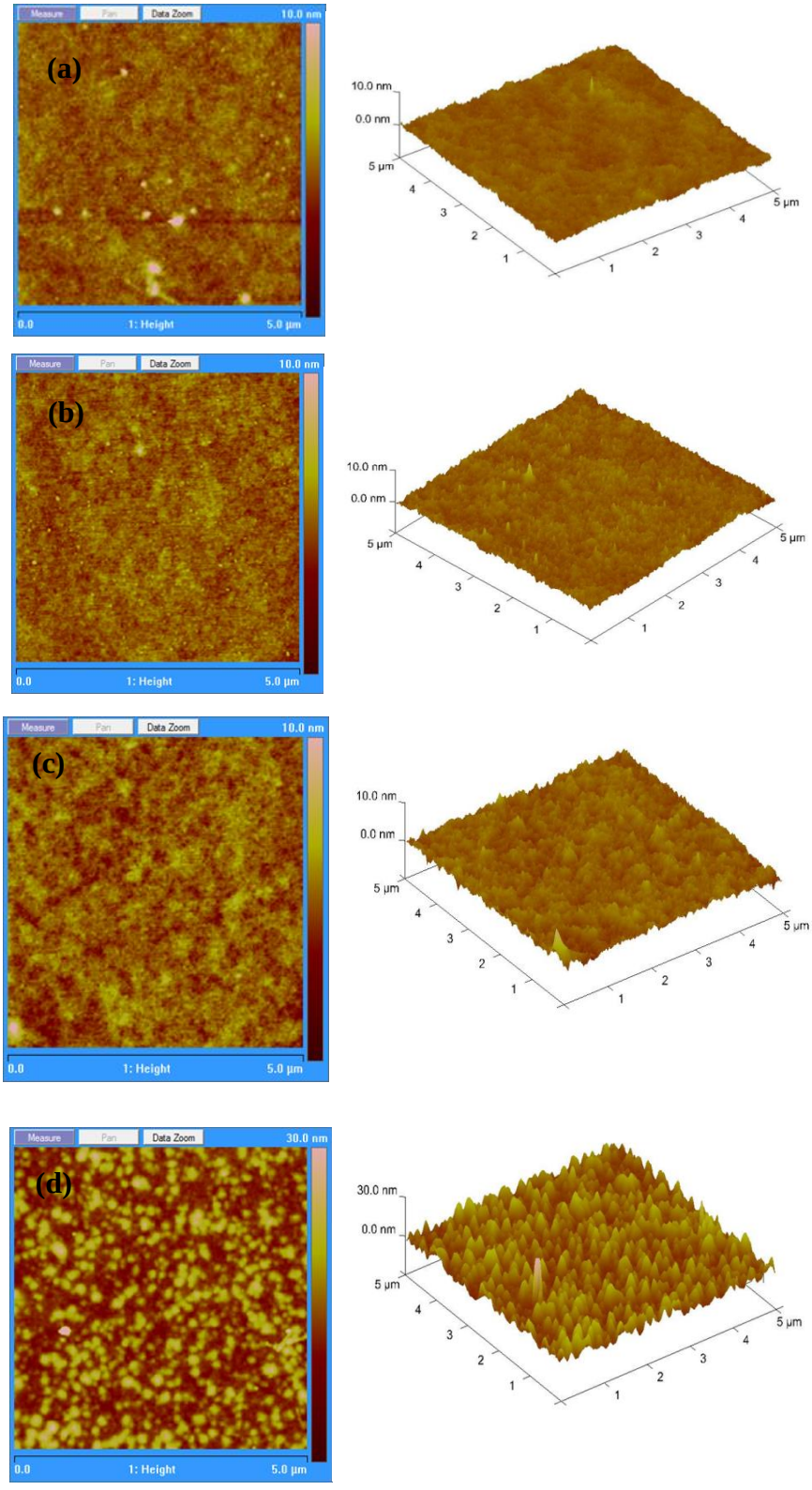

Figure 4.25: *The variation in OBHJ active layer morphology before and after annealing at different temperatures: a) before annealing, b) at 100 ^{0}C, C) at 150 ^{0}C and d) at 180 ^{0}C.*

4.4.1.3 Electrical characterisation

Figure 4.26 shows the current *J–V* curves of the OBHJ solar cells with and without thermal annealing under the illumination of 100 mW/cm^2 white light. The OBHJ solar cells performance data are summarized in Table 4.2. The performance of OBHJ solar cells improved significantly by thermal annealing. The OBHJ solar cells without thermal annealing only exhibited a *PCE* of 2.5% with *Jsc* of 20.83 mA/cm^2, V_{OC} is 0.4 V and *FF* is 27% with semi-flat curve. As the heat-treatment temperature was increased the V_{OC} and *FF* parameters were remarkably improved as the curve bended and become closer to ideal solar cells curve under illumination. As a result, the PV cell prepared with heat treatment at 150 ^{0}C showed the best device performance (*Jsc* = 23.33 mA/cm^2, V_{OC} = 0.53 V, *FF* 0.44, and *PCE* = 5.8 %) as shown in table 4.2. However, the annealing process at 180 °C for 10 min decreases the performance of the solar cell to *PCE* = 3 %. It is the variation of the optoelectrical and physical properties of the photoactive layer due to heat treatments influences the device performance significantly where the optimum annealing temperature is 150 ^{0}C for 10 min. That depends on the degree of the enhancement of the crystallinity of P3HT domains and the degree of the aggregation of IC70BA molecules in the blend film with thermal annealing to provide interpenetrating networks for charge-carrier transport [38]. The efficient OBHJ solar cells can be obtained by enhancing the P3HT crystallinity and the connectivity of IC70BA crystallites. It's believed that the process affect the photoactive layer performance with thermal annealing is the IC70BA diffusion to the P3HT order structure and IC70BA aggregation size [39]. Figure 4.27 shows the output power of the IC70BA-based OBHJ devices with respect to annealing temperature. It is clear that the output power for the device annealed at 150 C° increased more than 100% compared to the device without annealing.

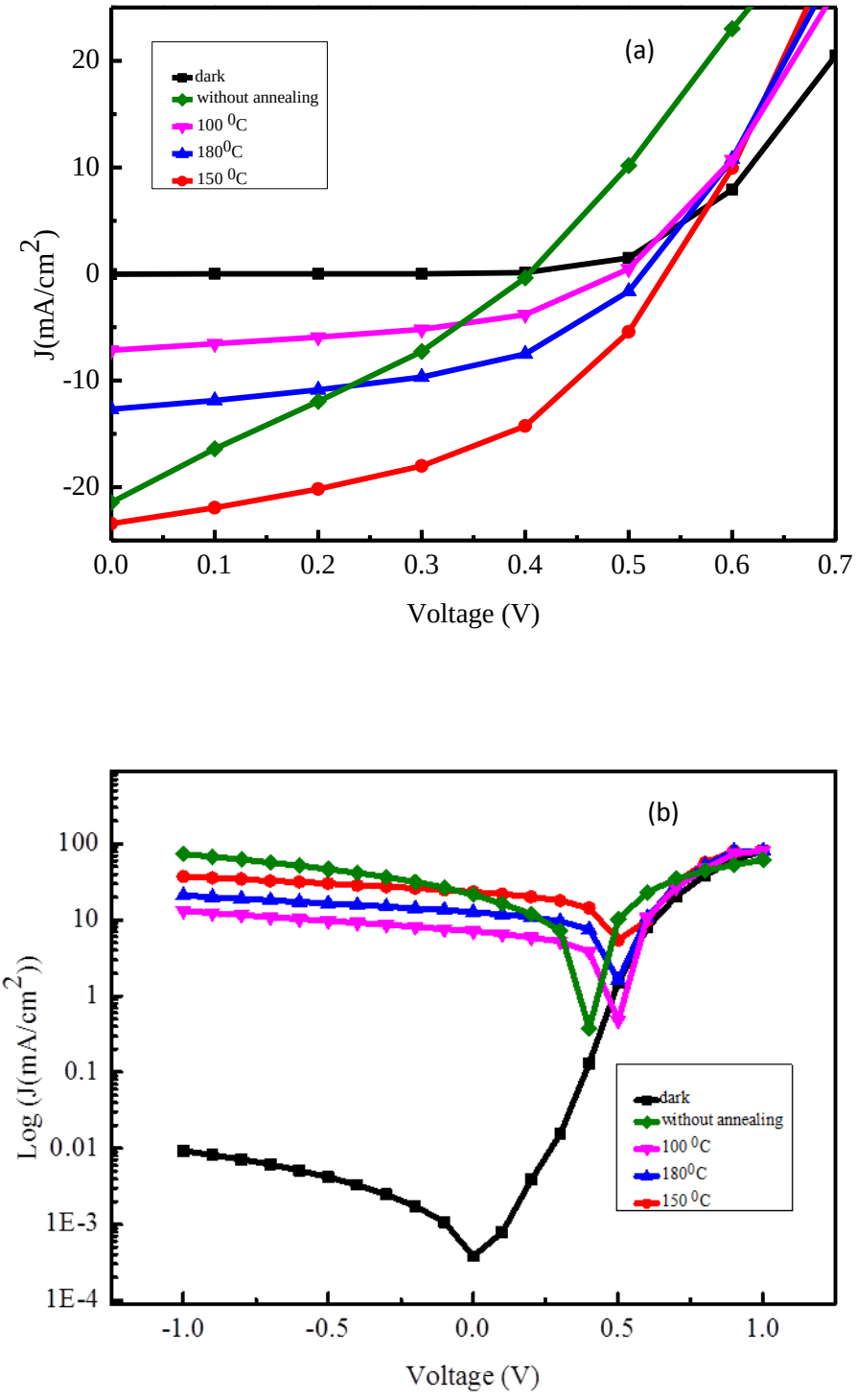

Figure 4.26: *shows J-V characteristics of the OBHJ solar cells under the illumination of 100 mW/cm^2 white light (a) linear scale and (b) logarithmic scale.*

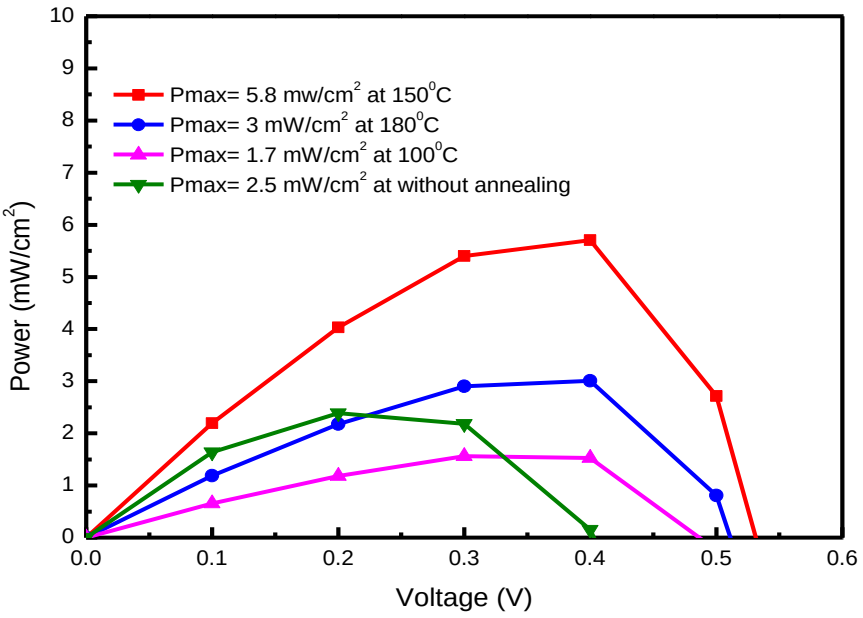

Figure 4.27: *Power curve of IC70BA bulk device at different annealing conditions*

IC70BA device	V_{OC} (V)	J_{sc}(mA/cm^2)	P_{max}(mW/cm^2)	FF (%)	PCE (%)	R_s Ω	R_{sh} Ω
Without annealing	0.4	20.83	2.5	27	2.5	66	166
100 ^{0}C	0.5	6.66	1.7	40	1.7	25	660
150 ^{0}C	0.53	23.33	5.8	44	5.8	255	416
180 ^{0}C	0.51	12.5	3	43	3	250	830

Table 4.2: *The extracted and calculated photovoltaic parameters of the fabricated devices under different annealing conditions.*

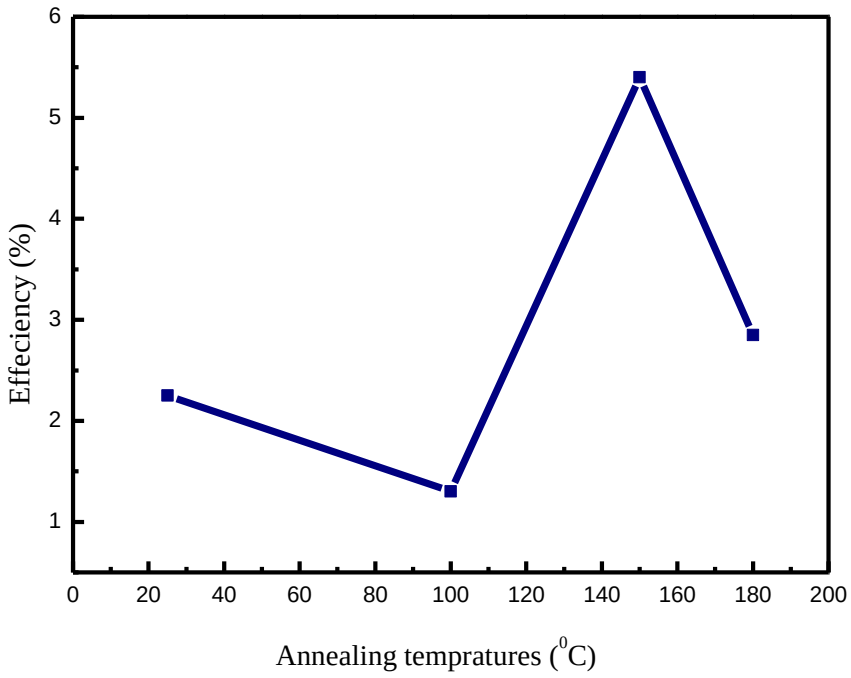

Figure 4.28: *Dependence of efficiency on annealing temperatures.*

Figure 4.29 shows the effect of thermal annealing on the UV-Vis absorption spectra for the thin films of P3HT:IC70BA. Maximum J_{SC} can be obtaining through the absorption profile of the active layer. The change in the peak and edge absorption wavelength with the different annealing temperature may be attributed to the enhancement of the crystallinity of P3HT domains and the degree of the aggregation of IC70BA molecules in the blend film as mentioned previously. For the as-deposited film the wavelength of the absorption peak (λmax) is 490 nm (2.5 eV) with edge shift to 656nm (1.89 eV). At annealing temperature lower than that required for complete reordered molecules film (at 100 ^{0}C) the λmax is shifted to 530 nm (2.3 eV) with edge shift to 670 nm (1.85 eV) but the absorption intensity lower than the absorption in the film without annealing. For thermal annealing at 150^{o}C, λmax is to 530 nm (2.3 eV) with edge shift to 688 nm (1.8 eV) and the absorption intensity increase significantly. Further increase of the annealing temperature to 180 ^{0}C results in reducing the absorption peak (λmax) to 490 nm (2.5 eV) with edge shift to 640 nm. In fact, upon thermal annealing, the absorption is red-shifted, the film structure is restored. These changes are attributed to an increase in internal order, as the polymer chains move more freely with higher temperatures. These changes indicate that thermal annealing significantly affected the molecular order of

P3HT and the connectivity of IC70BA crystallites as the thermal annealing induces a thermodynamic alteration of the photoactive layer. This causes a rearrangement of donor and acceptor phases, an increase in crystallinity of the P3HTand an improved absorption profile [40-42].

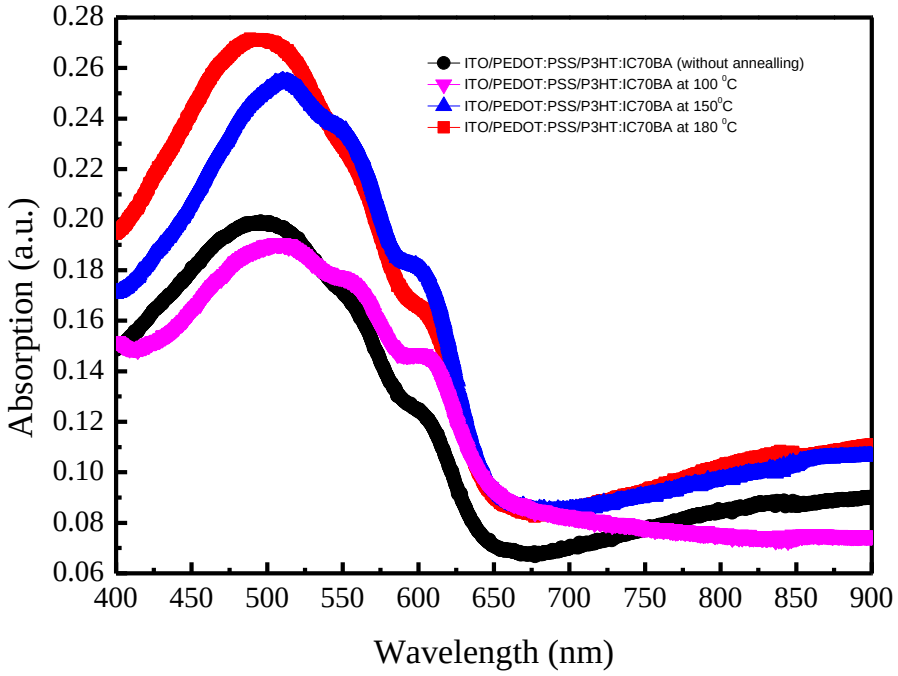

Figure 4.29: *The optical absorption of the IC70BA based OBHJ solar cells under different annealing conditions.*

Table 4.3 show that small changes in thermal annealing temperature resulted in significant changes to the bandgap and provide a direct method for tuning the bandgap in P3HT:IC70BA device structure. Before annealing the bandgap was 1.89 eV, whereas annealing at a relatively low temperature (100 ^{0}C) decrease the band gap of the blend to 1.85 eV. However, increasing annealing temperature to 150 ^{0}C cause further decrease in the bend bandgap to 1.8 eV. Annealing at higher temperatures (180 ^{0}C) results in increasing the band gap to be 1.93 eV which is more than before annealing the blend. This due to the decomposition of the blend structure. Hence, the heat treatment of the blend at optimal temperature (150 ^{0} C) causes an increase in the energy width of the

localized state thereby reducing the optical energy gap [43] and increase the number of excitons created due to light absorption.

In summary, it is clear from the optical, electrical and surface morphology results indicate that the device performance depends strongly on thermal annealing temperature. By comparing the efficiencies of the devices it can be seen that the optimum annealing temperature to enhance the performance of OBHJ solar cells based on P3HT:IC70BA is 150 C° for 10 min due to the high ordered molecules in active layer. Annealing at 150C° resulted in lower energy band gap and a moderate agglomeration grains size, which provides a favourable pathway for exciton separation and charge-carrier transport.

Annealing temperature	**Band gap (eV)**
without	1.89
100 ^0C	1.85
150 ^0C	1.8
180 ^0C	1.93

Table 4.3: *The variation of P3HT:IC70BA blend optical bandgap with different annealing temperature*

4.4.2 IC70BA-based devices under different concentration conditions

4.4.2.1 Fabrication process

The device structure is similar to the structure in Fig.4.24 with the fabrication procedure explained in the previous section (annealing effect). In order to investigate the effect of the weight ratio of the active layer on the photovoltaic properties, the active layer P3HT:IC70BA was fabricated with different weight ratios of 1:1, 1:2 , 2:1, 1:3 and 3:1, while keeping the pre-thermal annealing at 150 ℃ for 10 min.

4.4.2.2 Surface morphology

In order to understand the morphological changes that occur in the active layer as a result of changing weight ratio, AFM images of the active layer surface at different weight ratio were studied. From the surface morphology in Fig. 4.30, the 2: 1 and 3:1 weight ratios, where the percolation ratio of the P3HT phase was substantially higher than that of the PCBM phase, show many isolated PCBM domains.

However, in the case of the 1:2 and 1:3 ratios it can be seen from the morphology in Fig. 4.30 upon increase the ratio of IC70BA the IC70BA grains appeared randomly in the blends where the density and crystal grains of the P3HT decrease. In addation, from Fig.4.30 the surface of the P3HT:IC70BA film with 1:1 weight ratio shows good mixing structures with moderate agglomeration. In fact, at weight ratio of 1: 1, the percolation ratios of both the P3HT and IC70BA phases were approximately equal.

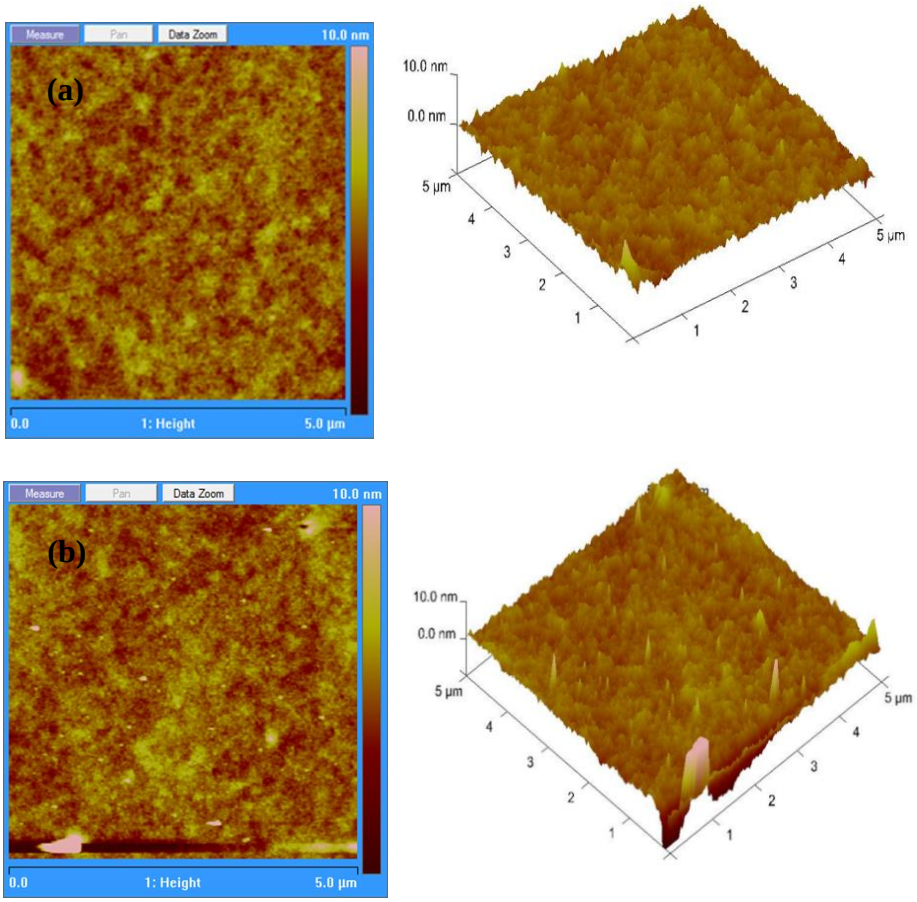

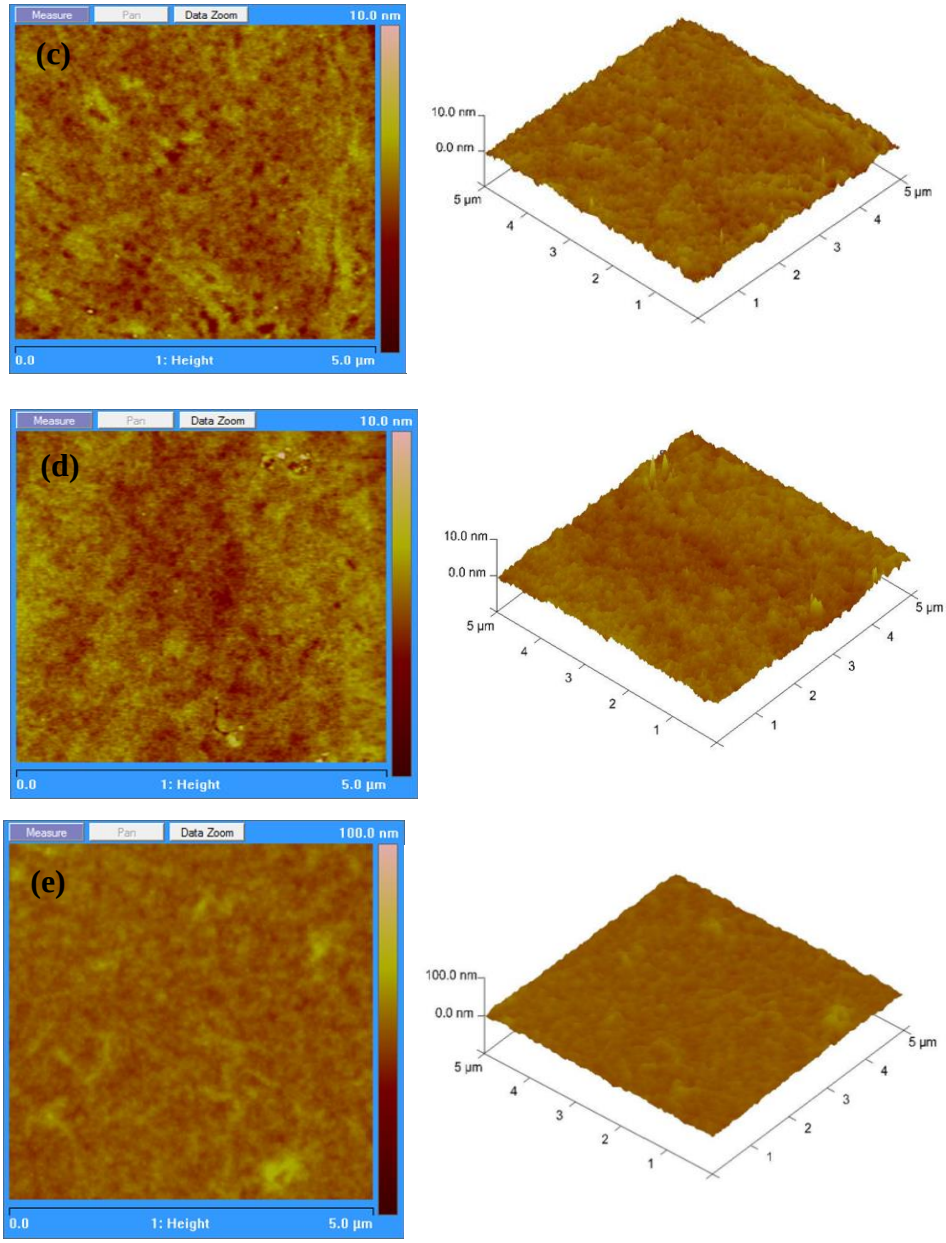

Figure 4.30: *shows the variation in ICBA based OBHJ active layer morphology at different P3HT:IC70BA weight ratios, a) 1:1, b) 2:1, c) 1:2, d)3:1, e) 1:3.*

4.4.2.3 Electrical characterisation

J–V curves of the devices tested under 100 mW cm^{-2} AM 1.5 G illumination for different P3HTto IC70BA ratios are shown in the Fig. 4.30 and device performance parameters are given in Table 4.4.

The trend of the device performance change when the P3HT:IC70BA blend weight ratio change (see Fig. 4.31 and Fig. 4.32). When the P3HT to IC70BA ratio was 1: 2, a J_{SC} of 5.83 mA/cm^2 and full factor of 68% was obtained which consequently yielded the PCE of 1.4 %. This attribute to the large difference between the mobilities of the holes and electrons, then space charge influnces due to unbalanced mobilities results in a low current density [46]. J_{SC} was greatly enhanced to 20.83 mA/cm^2 for devices with the polymer to IC70BA ratio of 1: 1, where electron and hole transport are balanced. A PCE of 5.6% for this device was achieved which is close to the parameters in last section for devices annealed at 150 ^{0}C. When the IC70BA content was further increased (1:3), the J_{SC} started to decrease again to 3.33mA/cm^2 resulted in PCE of 0.5%. In this case, lower hole mobilities compared to electron mobilities was occurred. It is quite clear that device performance weaken with increase or decrease of the concentration of IC70BA acceptor in the P3HT composite. Also, the same phenomenon occurred when the P3HT content increases (2:1), J_{SC} = 8.33 mA/cm^2 and PCE 1.7%. Despite the enhancement of hole conductivity, recombination process occurred as most of the electrons generated would be trapped within isolated IC70BA domains. Further increase in the P3HT weight ratio (3:1) decrease the J_{SC} = 4.16 mA/cm^2 due to increase recombination which reduce the device performance. This study demonstrate that at a weight ratio of 1:1 percolation ratio the phase of both P3HT and IC70BA approximately equal which prevents generated charges from becoming trapped within isolated domains .

As the P3HT ratio increase (2:1) the recombination rate increases [44]. Moreover, excessive increasing in P3HT weight ratio (3:1) result in higher recombination rate and reduce device performance. Number of percolating electron transport pathway is decreased in decreasing the concentration of fullerene in intermixed region. This creates a morphological electron trap that enhances charge carrier recombination [45]. However, increasing the IC70BA weight ratio (1:2, 1:3) reduce the photon absorption efficiency (as the polymer absorbs more light in the visible range than fullerene), resulting in an imbalance of charge transport in the device, which decrease the device performance. At a higher fullerene-to-polymer ratio, a larger domain size of fullerene

can be formed. Thus, Optimization of the composite weight ratio detects the important role played by morphology for the transport properties of P3HT:IC70BA bulk heterojunction based solar cells [47].

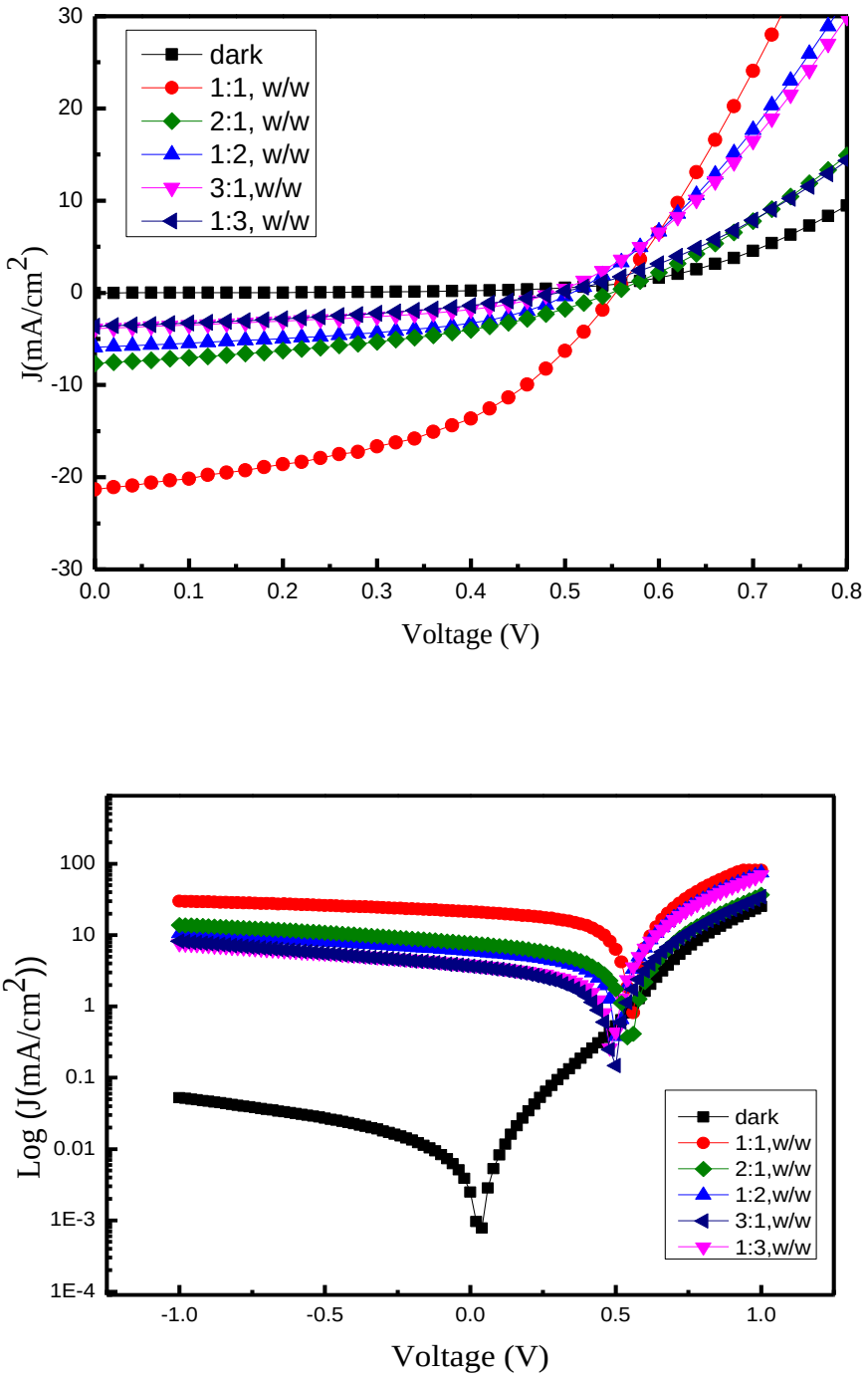

Figure 4.31: *shows J-V characteristics of the IC70BA OBHJ solar cells under the illumination of 100 mW/cm^2 white light (a) linear scale and (b) logarithmic scale.*

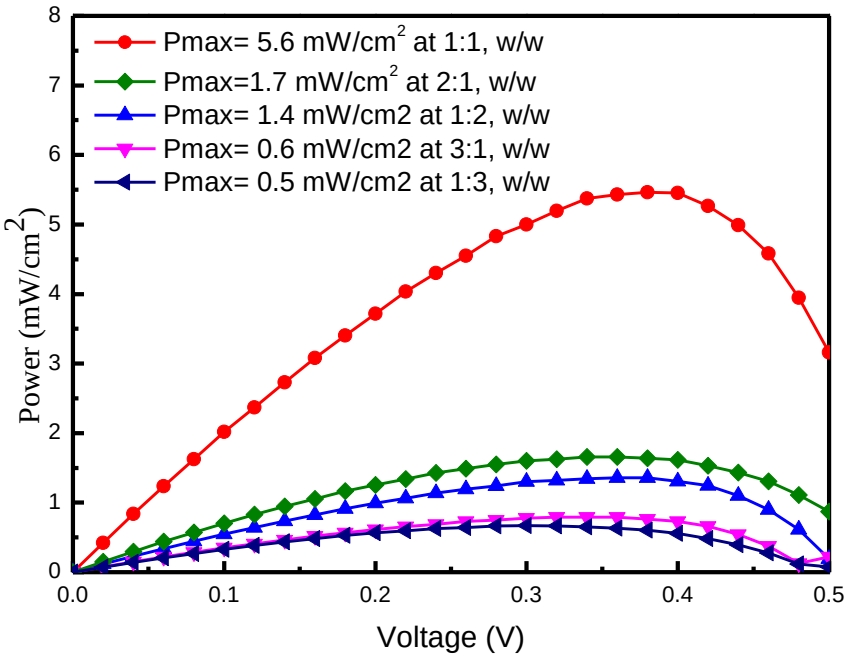

Figure 4.32: *Power curve of IC70BA bulk device at different P3HT:IC70BA at different weight ratio conditions.*

P3HT:IC70BA (weight ratio)	V_{OC} (V)	J_{sc}(mA/cm^2)	P_{max} (mW/cm^2)	FF (%)	PCE (%)
1:1	0.55	20.83	5.6	0.46	5.6
2:1	0.55	8.33	1.7	0.43	1.7
1:2	0.5	5.83	1.4	0.68	1.4
3:1	0.5	4.16	0.6	0.64	0.6
1:3	0.5	3.33	0.5	0.60	0.5

Table 4.4: *The extracted and calculated photovoltaic parameters of the fabricated P3HT:IC70BA devices under different Weight ratio conditions.*

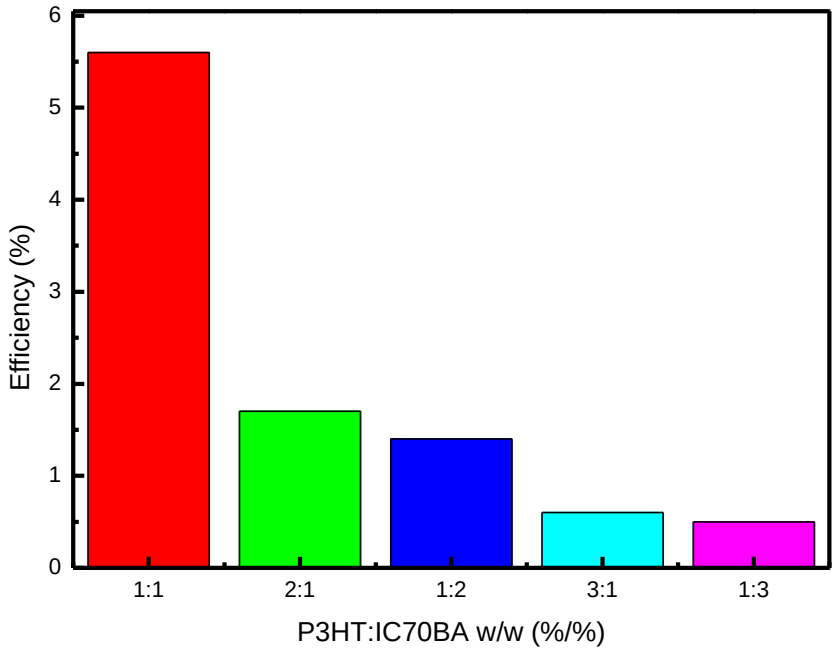

Figure 4.33: *Dependence of efficiency on P3HT:IC70BA blend concentration weight.*

4.5 Summary

Fabrications and characterisation of organic bulk-heterojunction (OBHJ) solar cells based in two new different acceptor materials, PAMAM and IC70BA, were investigated. New PAMAM cores (FC0, FC1 and FC2) as well as different PAMAM generations (G0, G0.5, G1 and G2) were used as acceptors in the fabrication of OBHJ solar cells. Optical and AFM images were used to determine the effect of the microstructure of the active layer on photovoltaic properties and how the electrical properties of the devices affected by the active layer morphology.

The electrical characterisation proved that the active layer blend of P3HT and PAMAM cores (FC0, FC1 and FC2) exhibit a composition dependent morphology. PAMAM FC2 core surface morphology which shows clear branching units similar to a tree spread on the whole surface with weak connections produced a non-zero current under illumination with the halogen lamp (100 mW/cm^2). The device produced an open circuit voltage, V_{OC}, of 0.6V, short-circuit current density, J_{SC} of 1.3 mA/ cm^2 with a fill factor of 22 % and a maximum power, $P_{max,}$ of 0.2 mW/cm^2 yielding a power conversion

efficiency of 0.2%. Optical spectroscopy shows absorption edge at 470 nm and the peak around 390 nm. However, OBHJ solar cells based in the other PAMAM cores (FC0 and FC1) did not display any photovoltaic behaviour (no open circuit voltage was detected) under illumination and this was attributed to the surface morphology of the active layers and optical absorption spectra. The morphology of the active blends containing P3HT:FC0 and P3HT:FC1 shows a clear phase separation structures with agglomeration of branching spread on the surface forming branches without connections.

Based on these results different generations (G0, G0.5, G1 and G2) were synthesis from PAMAM FC2 core to improve the efficiency. PAMAM G0, G1 and G2 are full generations where the primary amine is the surface group. The primary amine doubled with increase generation. However, PAMAM G0.5 are half generation with ester terminated group in the surface group and no primary amine in the surface group. OBHJ solar cells based on these generations also show optical absorption, morphology and surface group dependence. Cells based on PAMAM G0.5 as acceptor with condense branching units and good connections in the composition active layer film where absorption edge at 530 nm (peak 450 nm) produced a V_{OC} ~ 0.85V, J_{SC} ~ 6 mA/ cm^2 with fill factor of ~26 % and P_{max} of about 1.6 mW/cm^2 yielding a power conversion efficiency of 1.6 %. Other PAMAM generations (G0, G1 and G2) shows no open circuit voltage under illumination. This behaviour again been attributed to their surface morphology and optical absorption as well as their surface group. The full generation amine-terminate PAMAM surface group (G0, G1 and G2) are protonated at physiological pH. Thus, there is an electrostatic repulsion between the primary amine in the surface preventing the electrostatic interaction with other materials. However, ester terminated half-generation dendrimers are less susceptible to protonation compared to the full generation dendrimers and more opening structure for electrostatic interaction with other materials to occur.

Although annealing of many organic acceptor materials improved the photovoltaic behaviour of the devices, for the PAMAM-based cells, there were no photovoltaic behaviour after annealing. This behaviour was attributed to disappearance of branches with annealing and the structure of dendrimers becomes of small globular structure without any connections. Thus, energy transfers in the dendrimers become difficult.

The other material which was also investigated in this chapter is IC70BA as acceptor in organic bulk heterojunction devices. This material was studied at two different

conditions, first at different annealing temperatures, with AFM morphology show t optimum annealing temperature of 150 ^{0}C for 10 min. The annealing at 150 °C results in good mixing structures with moderate agglomeration which gives large and connected grains. As a result, the PV cells prepared with heat treatment at 150 C showed the best device performance (J_{sc} = 23. 33 mA/cm^2, V_{OC} = 0.53 V, FF 0.44, and PCE = 5.8 %). Second device condition is the fabrication of cells with P3HT-IC70BA at different weight concentrations. The result show that J_{SC} was greatly enhanced to 20.83 mA /cm^2 for devices with the polymer to IC70BA ratio of 1: 1, where electron and hole transport are balanced.

References

[1] T. Benanti and D. Venkataraman. ʻOrganic solar cells: An overview focusing on active layer morphology ', *Photosynthesis Research*, Vol. 87, pp. 73–81, **2006**.

[2] I.Botiz and N. Stingelin., ʻ Influence of Molecular Conformations and Microstructure on the Optoelectronic Properties of Conjugated Polymers ', *Materials*, Vol. 7, pp. 2273-2300, **2014**.

[3] C. Musumeci, A. Liscio, V. Palermo and P. Samori. ʻ Electronic characterization of supramolecular materials at the nanoscale by Conductive Atomic Force and Kelvin Probe Force microscopies ', *Materials Today*, Vol. 00(00), pp. 1-14, **2014**.

[4] J. Nelson, The Physics of Solar Cells. London, UK: Imperial College Press, pp 1-16, **2003.**

[5] U. Mengesha, T. Yoannes, *Solar Enery Materials and Solar Cells*, Vol. 90, pp. 3508, **2006**.

[6] J. Roncali., ʻ Molecular Engineering of the Band Gap of π-Conjugated Systems: Facing Technological Applications ', *Macromolecular Rapid Communications*, Vol. 28(17), pp.1761–1775, **2007**.

[7] B. Minnaert, and M. Burgelman., ʻ Efficiency Potential of Organic Bulk Heterojunction Solar Cells ', *Progress in Photovoltaics: Research and Applications*, Vol. 15, pp. 741-748, **2007**.

[8] J. Lu,Y. Yao, P. Shenai, L. Chen and Y. Zhao., ʻ Elucidating the enhancement in optical properties of low band gap polymers by tuning the structure of alkyl side chains ', *Physical Chemistry Chemical Physics*, Vol. 17, pp. 9541-9551, **2015**.

[9] J. Nunzi., ʻ Organic photovoltaic materials and devices ', *Comptes Rendus Physique*, Vol. 3(4), pp. 523–542, **2002**.

[10] N. Bernhard, G. H. Bauer, and W. Bloss., ʻ Bandgap engineering of amorphous semiconductors for solar cell applications ', *Progress in Photovoltaics: Research and Applications*, Vol.3 (3), pp. 149–176, **1995**.

[11] H. Bassler and A. Kohle., ʻ Charge Transport in Organic Semiconductors ', *Topics in Current Chemistry*, Vol. 312, pp. 1-6, **2012.**

[12] G. Sadashivappa and N.Sharvari., ʻ Nanoantenna–A Review ', *International Journal of Renewable Energy Technology Research*, Vol. 4(1), pp. 1-9, **2015.**

[13] S. Naza, S. Durrania, M. Mehmoodb, and M. Nadeemc. ' Hydrothermal synthesis, structural and impedance studies of nanocrystalline zinc chromite spinel oxide material ', *Journal of Saudi Chemical Society*, Vol. 2015, **2015.**

[14] S. Calnan., ' Applications of Oxide Coatings in Photovoltaic Devices ', *Coatings*, Vol. 4(1), pp.162-202, **2014**.

[15] R. Das and S. Pandey., ' Comparison of Optical Properties of Bulk and Nano Crystalline Thin Films of CdS Using Different Precursors ', *International Journal of Material Science*, Vol. 1(1), pp. 35-40, **2011.**

[16] S. Gunes, H. Neugebauer, and N. Sariciftci., 'Conjugated Polymer-Based Organic Solar Cells ', *Chemical Reviews*, Vol. 107, pp. 1324−1338, **2007.**

[17] G. Chen, J. Seo, C. Yang and P. Prasad., ' Nanochemistry and nanomaterials for photovoltaics ', *Chemical Society Reviews*, Vol. 42(1), pp. 8304-8338, **2013.**

[18] A. Ng, X. Liu, C. To, A. Djurisic, J. Zapien, and W. Chan, ' Annealing of P3HT:PCBM Blend Film - The Effect on Its Optical Properties ', *ACS Applied Materals Interfaces*, Vol.5 (10), pp. 4247-4259, **2013.**

[19] Z. Yi, W. Ni, Q. Zhang, M. Li, B. Kan, X. Wan and Y. Chen, ' Effect of thermal annealing on active layer morphology and performance for small molecule bulk heterojunction organic solar cells ', *Journal of Materials Chemistry C,* Vol.2, pp. 7247–7255, **2014.**

[20] H. Derouiche and A. Mohamed, ' Thermal Annealing Effect on Poly(3-hexylthiophene): Fullerene:Copper-Phthalocyanine Ternary Photoactive Layer , *The Scientific World Journal*, Vol. 2013, pp. 1-2, **2013.**

[21] Y. Xiao, L. Shao, T. Chung and D. Schiraldi, ' Effects of Thermal Treatments and Dendrimers Chemical Structures on the Properties of Highly Surface Cross-Linked Polyimide Films ', *Industrial and Engineering Chemistry Research*, Vol. 44(9), pp. 3059–3067, **2005.**

[22] K. Maturová , S. Bavel , M. Wienk , R. Janssen ,and M. Kemerink , ' Description of the Morphology Dependent Charge Transport and Performance of Polymer:Fullerene Bulk Heterojunction Solar Cells ', *advanced functional materials*, Vol.21, pp. 261-269, **2011.**

[23] Y. Haba , C. Kojima , A. Harada , and K. Kono. ' Control of Temperature-Sensitive Properties of Poly(amidoamine) Dendrimers Using Peripheral Modification with Various Alkylamide Groups ', *Macromolecules*, Vol. 39 (21), pp. 7451–7453, **2006.**

[24] Q. Lin, W. Jing, S. Yang, Z. Jiang, and C. Wang, ‘ Agglomeration and Dendritic Growth of Cu/Ti/Si Thin Film ’, *Journal of Nanomaterials*, Vol. 2014, pp. 1-8, **2014.**

[25] E. Verploegen, R. Monda, C. Bettinger, S. Sok, M. Toney and Z. Bao, ‘ Effects of Thermal Annealing Upon the Morphology of Polymer–Fullerene Blends ’, *Advanced Functional Materials*, Vol. 20(20),pp. 3519–3529, **2010.**

[26] A. Dualeh, N. Tétreault, T. Moehl, P. Gao, M. Nazeeruddin and M. Grätzel. ‘ Effect of Annealing Temperature on Film Morphology of Organic–Inorganic Hybrid Pervoskite Solid-State Solar Cells ’, *Advanced Functional Materials*, Vol.24 (21), pp. 3250–3258, **2014.**

[27] K. Kono, ‘ Dendrimer-based bionanomaterials produced by surface modification, assembly and hybrid formation ’, *Polymer Journal*, Vol. 44, pp. 531-540, **2012.**

[28] B. Luna, L. Godínez, F. Rodríguez, A. Rodríguez, G. Larrea, C. Ferreyra, R. Curie, J. Manríquez and E. Bustos, ‘ Applications of Dendrimers in Drug Delivery Agents,Diagnosis, Therapy, and Detection ’, *Journal of Nanomaterials*, Vol. 2014, pp. 1-19, **2014.**

[29] X. Wang , L. Guerrand , B. Wu , X. Li , L. Boldon , W. Chen and L. Liu, ‘ Characterizations of Polyamidoamine Dendrimers with Scattering Techniques ’, *Polymers*, Vol. 4, pp. 600-616, **2012.**

[30] J. Ribierrea, C. Yatesa, A. Ruseckasa, S. Statonb, P. Burnc, I. Samuela, ‘ Effects of solution processing and thermal annealing on the phosphorescence of iridium(III) complex-cored dendrimer films ’, *Organic Electronics*, Vol.11(1), pp. 62-66, **2010.**

[31] S. Duan, T. Kai, T. Saito, K. Yamazaki and K. Ikeda, ‘ Effect of Cross-Linking on the Mechanical and Thermal Properties of Poly(amidoamine) Dendrimer/Poly(vinyl alcohol) Hybrid Membranes for CO2 Separation ’, *Membranes (Basel)*, Vol. 4(2), pp. 200–209, **2014.**

[32] P. Maiti, T. Cagin, S. Lin, and W. Goddard., ‘ Effect of Solvent and pH on the Structure of PAMAM Dendrimers ’, *Macromolecules*, Vol. 38, pp. 979 -991, **2005.**

[33] I. Tanis and K. Karatasos., ‘ Molecular dynamics simulations of polyamidoamine dendrimers and their complexes with linear poly(ethylene oxide) at different pH conditions: static properties and hydrogen bonding ’, *Physical Chemistry Chemical Physics*, Vol. 11, pp. 10017–10028, **2009.**

[34] A. Nomani, I. Haririan, R. Rahimnia, S. Fouladdel, T. Gazori, R. Dinarvand, Y. Omidi, and E. Azizi., ' Physicochemical and biological properties of self-assembled antisense/poly(amidoamine) dendrimer nanoparticles: the effect of dendrimer generation and charge ratio ', *International Journal of Nanomedicine*, Vol. 5,pp. 359–369, **2010.**

[35] F. Aulenta, W. Hayesa, and S. Rannard., ' Dendrimers: a new class of nanoscopic containers and delivery devices ', *European Polymer Journal*, Vol. 39, pp. 1741–1771, **2003.**

[36] V. Gajbhiye, P. Kumar, R. Tekade and N. Jain., ' Pharmaceutical and Biomedical Potential of PEGylated Dendrimers ', *Current Pharmaceutical Design*, Vol. 13, pp. 415-429, **2007.**

[37] M. Bakshi and R. Sood., ' Favorable interactions of amine- and ester-terminated PAMAM withcationic surfactants: photophysical and transport studies ', *Journal of Colloid and Interface Science*, Vol. 277, pp. 221–229, **2004.**

[38] S. Sadekar and H. Ghandehari., ' Transepithelial transport and toxicity of PAMAM dendrimers: implication for oral drug delivery ', *Advanced Drug Delivery Reviews*, Vol. 64(6), pp. 571–588, **2012.**

[39] B. Ray, P. Nair and M. Alam., ' Annealing dependent performance of organic bulk-heterojunction solar cells: A theoretical perspective ', *Solar Energy Materials and Solar Cells*, Vol. 95, pp. 3287–3294, **2011.**

[40] M. Dang and J. Wuest., ' Using volatile additives to alter the morphology and performance of active layers in thin-film molecular photovoltaic devices incorporating bulk heterojunctions ', *Chemical Society Review*, Vol.42, pp.9105-9126, **2013.**

[41] X. Fan and S. Li, ' Understanding the phase separation evolution in efficient P3HT:IC70BA-based bulk-heterojunction polymer solar cells ', *Journal of Physics D: Applied Physics*, Vol. 46, pp. 055502-6, **2013.**

[42] V. Turkovic and S. Engmann et al., ' Multiple stress degradation analysis of the active layer in organic photovoltaics ', *Solar Energy Materials & Solar Cells*, Vol.120, pp. 654–668, **2014.**

[43] Y. Lai, Y. Cheng and C. Hsu, ' Applications of Functional Fullerene Materials in Polymer Solar Cells ', Energy and Environmental Science, Vol.7, pp. 1860-1866, **2014.**

[44] N. Abu-Zahra and M. Algazzar., ' Effect of Crystallinity on the Performance of P3HT/PC70BM/n-Dodecylthiol Polymer Solar Cells ', *Journal of Solar Energy Engineering*, Vol.136 (2), pp. 021023, **2013.**

[45] D. Ghoneim, K. Marzouk, S. EL-Sayed, N. Mohsen, A. Mahmoud., ' Effect of annealing on the electrical and optical properties of $Cu_5Ga_{33}Te_{62}$ thin film ', *Chalcogenide Letters*, Vol. 7(5), pp. 307-316, **2010.**

[46] D. Bartesaghi, I. Perez, J. Kniepert, S. Roland, M. Turbiez, D. Neher, and L. Koster, ' Competition between recombination and extraction of free charges determines the fill factor of organic solar cells ', *Nature communications*, Vol. 6, pp. 1-10, **2015.**

[47] J. Bartelt, Z. Beiley, E. Hoke, W. Mateker, J. Douglas, B. Collins, J. Tumbleston, K. Graham, A. Amassian, H. Ade, J. Fréchet, M. Toney and M. McGehee., ' The Importance of Fullerene Percolation in the Mixed Regions of Polymer–Fullerene Bulk Heterojunction Solar Cells ', *Advanced Energy Materials*, Vol. 3(3), pp. 364–374, **2012.**

[48] O. Usluer, S. Boudiba, D. Egbe, L. Hirsch and M. Abbas., ' Control of carrier mobilities for performance enhancement of anthracene-based polymer solar cells ', *RSC Advances*, Vol. 5, pp. 50668–50672, **2015.**

[49] D. Khatiwada, S. Venkatesan, J. Chen, Q. Chen, N. Adhikari, A. Dubey, A. Mitul, L. Mohammad, J. Sun, C. Zhang, L. Luo, and Q. Qiao., ' Morphological Evolution and Its Impacts on Performance of Polymer Solar Cells ', *IEEE Transactions on electron devices*, Vol. 62(4), pp. 12

Chapter 5

Organic bilayer Heterojunction solar cells

5.1 Introduction

Recently, Organic bilayer Heterojunction solar cells have attracted much interest for large scale solution processed efficient organic solar cells due to the sequential processing in the active layer formation being more straightforward. Organic electron acceptors that may not survive thermal evaporation can be used through the Sequential processing where each layer controlled and optimized independently [1, 2]. Thus, sequential solution processing of the active layers in organic solar cells would be particularly advantageous towards multiple junction cells to enhance the efficiency.

In this chapter the fabrication and characterisation of organic bilayer heterojunction solar cells (OHJ) based on different new PAMAM dendron salts acceptor materials (G 0.5, G 1.5, and G2.5) at different pH and new A-A copolymer PAMAM G0-thienopyrroledione (TPD) are investigated. The current density–voltage (*J-V*) characteristics for these devices were measured in the dark and under illumination with a halogen lamp. The experimental details, surface morphology, electrical characteristics and optical absorption measurement of each of these devices are presented and discussed in this chapter.

PAMAM G0.5, G1.5 and G2.5 salts are half generations with carboxylate- terminated group (-COONa) in the surface group. Half-generation dendrimers has anionic charges and is capable of binding with a variety of cationic guests. As the generation increase, the number of surface group double with each increasing generation see table 5.1.

PAMAM generations	Primary amine -NH2	Tertiary amine =N-	Surface group (-COONa)
G0.5	0	1	2
G1.5	0	3	4
G2.5	0	7	8

Table 5.1: *Number of surface groups, primary and tertiary amine in half generations PAMAM carboxylate- terminated group.*

5.2 PAMAM G0.5 salt based OHJ solar cells at different pH conditions

5.2.1 Fabrication process

Fabrication of OHJ solar cells with the structure of ITO/PEDOT: PSS/P3HT/ PAMAM G0.5 salt /TiO_2/Al (as shown in the Fig. 5.1) is explained in this section. The ITO-coated glass substrate were cleaned with soap, warm water and deionized water, also cleaned with ultrasonic treatments in acetone and isopropanol respectively, then were dried with nitrogen flow. The conducting poly (3, 4-ethylenedioxylenethiophene)-polystylene sulfonic acid (PEDOT: PSS) was spin-cast (5000 rpm) for 40 second with thickness ~40 nm. Then, the substrate was dried for 10 minutes at 140˚C in air, and then placed into a glove box for spin coating of the active layer. Poly (3-hexylthiophene-2, 5-diyl) (P3HT) was prepared by 1wt% in chloroform solution and then spin coated at 1000 rpm with thickness ~100 nm on top of the PEDOT layer as active layer donor. The acceptor PAMAM dendritic wedges G0.5 with different pH conditions, low, neutral, and high (1.5, 3.2, 5.7, 6.93, 9.2, 10.95, 12.44) was spin coated on top of the P3HT at 700 rpm with ≈ 70 nm thickness. Then, titanium dioxide (TiOx) precursor solution in methanol was spin coated with thickness ~20 nm in air on top of PAMAM wedges G0.5 pH as electron transport layer and was dried for 10 minutes in air at 80˚C. Finally, the device was completed by evaporating~100 nm Al on top of TiOx. The deposited Al electrode area defines an active area of the devices as 0.12cm^2.All films preparation and materials evaporation technique were discussed in chapter 3.

The acidity or basicity of a substance is defined by the pH of the material. Acids in aqueous solution produce hydrogen H^+ ions. The greater the concentration of hydrogen ions the more acid the solution and the lower the pH.

Hydrochloric acid: $HCl\ (g) + aq \Longrightarrow H^+(aq) + Cl^-(aq)$

Alkalis in aqueous solution produce $OH^-(aq)$ hydroxide ions. The greater the concentration of hydroxide ions the more alkaline the solution and the higher the pH.

Sodium hydroxide: $NaOH(s) + aq \Longrightarrow Na^+(aq) + OH^-(aq)$

If the concentration of the hydrogen ion (H^+) is equal to the concentration of hydroxide ion (OH^-), the solution is called neutral solution.

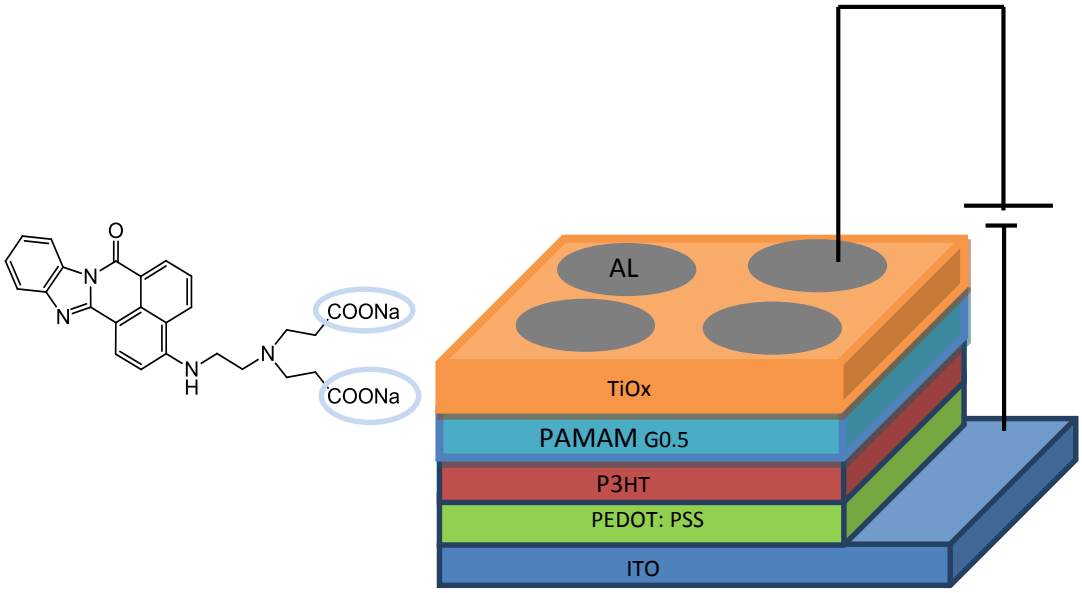

Figure 5.1: *PAMAM G0.5 salt chemical structure and Schematic diagram of PAMAM G0.5 salt based OHJ solar cells*

5.2.2 Surface morphology

One of the critical factors in determining the performance of solar cells is the morphology of the active layer. Thus, optimise the donor/acceptor nanoscale morphology is essential for dissociating the photogenerated excitons within their diffusion length and facilitating an efficient charge collection [3-5]. Active layer morphology of OHJ solar cells is our main interest as it was mentioned previously that the surface morphology of PAMAM dendrimers can be adjusted as function of pH. It was reported that the surface morphology of the electron acceptor layer affected the current and voltage outputs of the photovoltaic cells [6].

Atomic Force Microscopy (AFM) used to study donor/ acceptor surface structure and the differences in performance characteristics depend on the different morphology structure of the devices [7-9].

Optical image was taken to the PAMAM G0.5 salt at different pH (low, neutral, high) condition on the top of and P3HT layer to examine the distribution of PAMAM G0.5 salt layer at different pH. Figure 5.2 show that PAMAM G0.5 distribution is highly dependent on its pH concentrations. At low pH (pH < 5) the optical image showed high density small grains in the film. At neutral the optical image shows very clear branches and tree structure distributed almost uniformly and grown in the same direction. However, at high pH (pH > 10) the optical image showed that, no branches can be seen; branches fade and dissolve in the film structure.

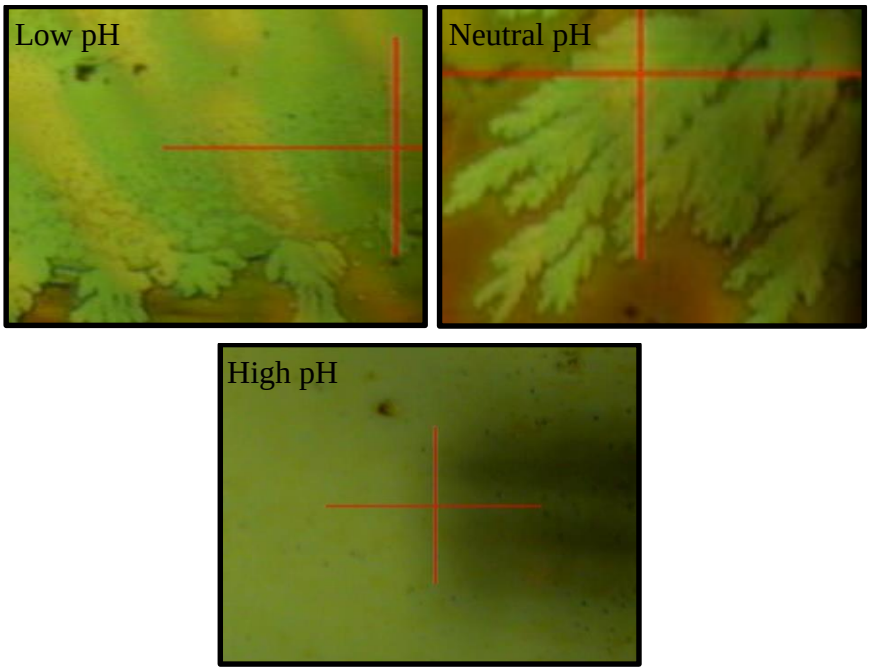

Figure 5.2: *Optical image of PAMAM G0.5 salt on top of the P3HTlayer at different pH conditions.*

The morphology characterization of the P3HT/PAMAM G0.5 based bilayer devices was limited to the characterization of the acceptor active layer. Figure 5.3 shows the AFM images of the deposited PAMAM-G0.5 acceptor layer at different pH concentrations, starting from very acidic solution increasing to reach neutral concentrations and afterwards reaching a more alkaline solution.

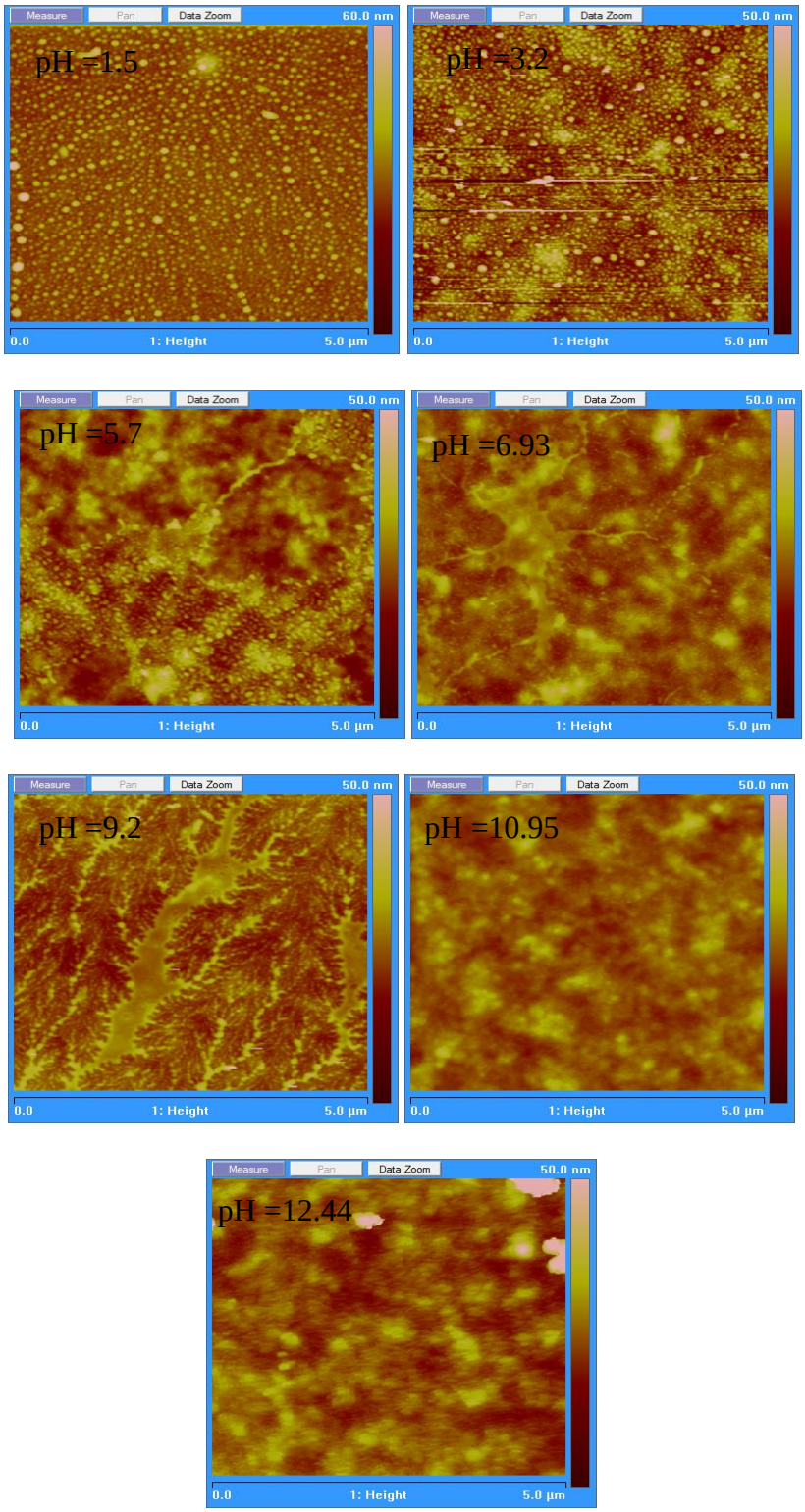

Figure 5.3: *AFM morphology images of PAMAM G0.5 acceptor layer on top of the P3HTlayer at different pH concentrations.*

It was reported that PAMAM structure, size and rigidity rely on their pH [10-12]. The tapping-mode AFM images in Fig. 5.3 show significant differences in the topographies of PAMAM G0.5 at different pH condition. The effect of pH on PAMAM G0.5 size and shape can be explained by electrostatic attraction between the PAMAM G0.5 and P3HT. It can be seen from PAMAM G0.5 AFM at different pH in Fig 5.3 that high pH results in a compact structure with dense PAMAM G0.5 core where the periphery found to be largest at neutral pH and shrink at low pH. At low pH PAMAM G0.5 tertiary amine and interior tertiary amine are positively charged, which make it less flexible due to the intermolecular electrostatic interactions and hence more water can penetrate in the interior of the dendritic. At neutral pH, only the tertiary amines in PAMAM G0.5 are positively charged. This makes it more flexible and a more homogeneous distribution result in larger dendritic size. At higher pH none of tertiary amine or interior tertiary amine in PAMAM G0.5 are charged which make it to be highly flexible where there is no connection between the PAMAM G0.5 end branches [13-16].

5.2.3 Electrical characterisation

The electrical characterization of the P3HT/PAMAM G0.5 salt based bilayer solar cells was carried on in a similar way to the characterization of the bulk heterojunction solar cells in chapter 4. The *J-V* characteristics were recorded under dark then recorded under incident light illumination with intensity equals to 1.5 AM radiation. Both bias scans started from -1V and ended at +1V. Figure 5.4 shows the electrical characteristics of the P3HT/PAMAM G0.5-based bilayer devices at different pH conditions of the PAMAM-G0.5. Figure 5.4 consist of 7 graphs each graph presents the electrical characterization of a device fabricated with a pH concentration of the PAMAM-G0.5. Figure 5.4 show that all the devices exhibit the photovoltaic behaviour. In dark the current remains at Zero until the threshold voltage of rectification behaviour was reached then the current increases suddenly. On the other hand, under 1 sun light illumination intensity, in all seven devices the current start from a non-zero current value showing the existence of the generated carriers due to the absorption of incident photons. However, the photovoltaic behaviour of these devices showed that it is highly relying on the morphology of the PAMAM-G0.5 pH layer. Thus the difference in the morphology of the deposited PAMAM-G0.5 at different pH was reflected as well on the photovoltaic device parameters. Table 5.1 summarizes the extracted photovoltaic

parameters such as V_{OC}, J_{SC} and P_{max} from the recorded characteristics of each device, also, the calculated fill factor and the solar cell efficiency for each device. It is clear from Table 5.2 that the V_{OC} increased with the increase of pH, increased from 0.3 V at pH = 1.5 to reach 0.85 V at pH = 9.2. Further increase of pH to higher values decrease the V_{OC} to a value of 0.7 V. Table 5.2 also shows the dependence of the J_{SC} of the fabricated devices on the morphology of the PAMAM-G0.5, it increased from 0.5 mA/cm^2 at pH = 1.5 to reach 8 mA/cm^2 at pH = 9.2. Further increase of pH to higher values decrease the J_{SC} to a value of 0.4 mA/cm^2. This can be explained by the complete existence of the branches and tree-like structure in the deposited acceptor layer at this pH=9.2. This may be confirmed by the abrupt decrease in the I_{SC} at higher pH where the branches disappear and thus the collection of electrons by the electrodes is not facilitated by the existence of the branches. This can be explained by the changes in the degree of protonation of the PAMAM G0.5 at different pH. Changes in pH alter the protonation of both the internal and the end amine groups of the molecules, leading to variations of their charge density, hydrophobicity and solubility [17, 18]. It was discovered that PAMAM dendritic become positively charged at the natural pH 6-9 as all the primary amines (tertiary amine in the half generation PAMAM) protonated result of attractive Coulomb interactions between the negatively charged surface carboxy-groups and the positively charged tertiary amines in the inner shells of the dendrimer leading to create electric current at the interface with opposite material P3HT, then the electric current will flow through the solar cell device in order to encourage more electrons to transfer from the donor (P3HT) to acceptor (PAMAM G0.5) and reduce the recombination of charge. From a morphology point of view, significant branch back-folding occurred at neutral pH (pH 6-9) in addition to major peripheral distribution of the terminal groups. Thus, the mobility and diffusion length of the electrons injected in the acceptor layer may enhanced by a complete existence of the branches and tree-like structure in the deposited acceptor layer at neutral pH (pH=9.2) thus facilitates its collection by the electrode.

However, at high pH (pH $\geq$10) none of the tertiary amines protonated (neutral PAMAM) which means there are no positive charges that can bend the negative charges from the P3HT. At this pH, the morphology as it was mentioned before become globular and compact as the charge of the molecule becomes neutral. This explained the abrupt decrease in the J_{SC} at higher pH. On the other hand, at low pH (pH $\leq$ 5) all the tertiary amine and interior tertiary amine groups of the PAMAM G0.5 dendrimer are

protonated. Thus, electrostatic repulsion between tertiary amine and interior tertiary amine positively charged amines is larger than the electrostatic attractive interaction between P3HT and PAMAM G0.5, resulting in a low J_{SC} at this pH. Furthermore, at low pH of PAMAM G0.5 the branches tend to shrink due to electrostatic repulsion between tertiary amine and interior tertiary amine. It was found that the size of the PAMAM G0.5 dendritic increases from high to low pH reflecting swelling due to the electrostatic phenomenon [19, 20].

The abrupt increase in the J_{SC} at pH = 9.2 was reflected in P_{MAX} as shown in Table 5.1, where the P_{MAX} had its highest value of 1.8 mW/cm^2 while it had much lower values at other pH values. The abrupt increase in the J_{SC} and P_{MAX} was reflected in the calculated efficiency also.

Table 5.2: *The extracted and calculated photovoltaic parameters of the fabricated PAMAM G0.5 based devices under different pH conditions.*

PAMAM G0.5 pH	V_{OC} (V)	J_{SC}(mA/cm^2)	P_{MAX} (mW/cm^2)	*FF* (%)	PCE (%)	R_S (Ω)	R_{SH} (Ω)
1.5	**0.3**	**0.5**	**0.055**	**36**	**0.055**	**550**	**25000**
3.2	**0.6**	**0.4**	**0.055**	**22**	**0.055**	**930**	**8300**
5.7	**0.68**	**0.6**	**0.085**	**21**	**0.085**	**400**	**4200**
6.93	**0.79**	**2.2**	**0.45**	**26**	**0.45**	**210**	**4200**
9.2	**0.85**	**8**	**1.8**	**26**	**1.8**	**70**	**600**
10.95	**0.7**	**0.65**	**0.11**	**24**	**0.11**	**400**	**5500**
12.44	**0.7**	**0.4**	**0.065**	**23**	**0.065**	**1040**	**11110**

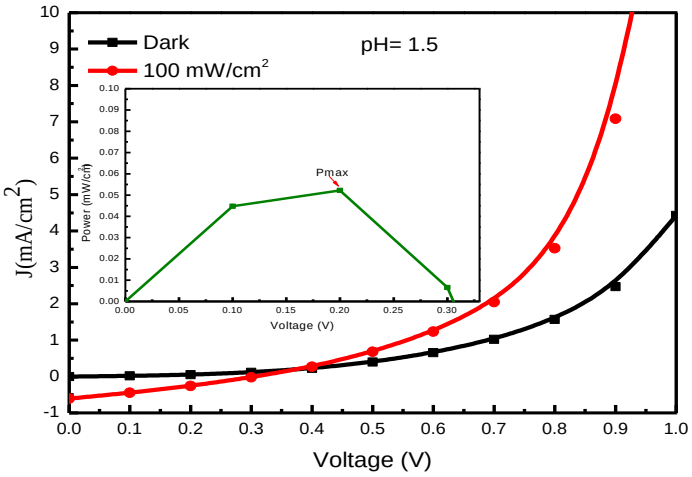
Dark
100 mW/cm2
pH= 1.5
J(mA/cm2)
Voltage (V)
Pmax
Power (mW/cm2)
Voltage (V)

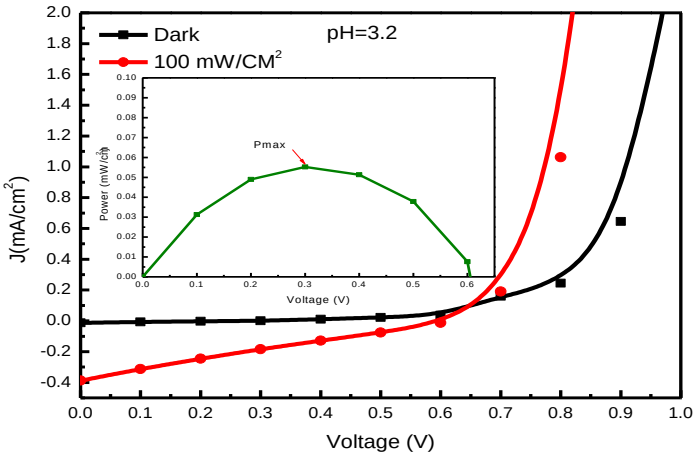
Dark
100 mW/CM2
pH=3.2
J(mA/cm2)
Voltage (V)
Pmax
Power (mW/cm2)
Voltage (V)

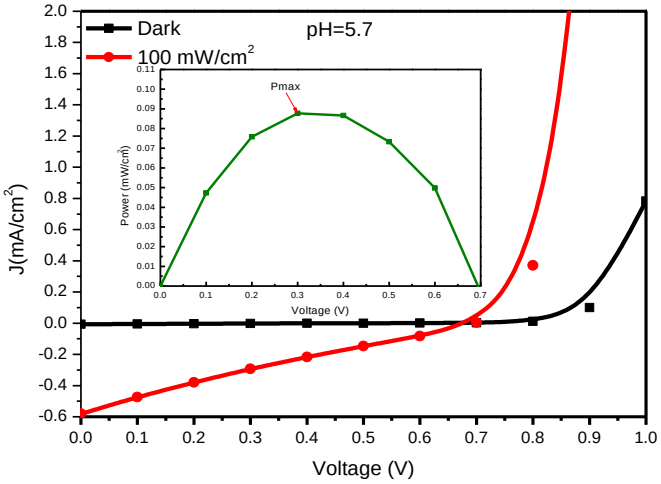
Dark
100 mW/cm2
pH=5.7
J(mA/cm2)
Voltage (V)
Pmax
Power (mW/cm2)
Voltage (V)

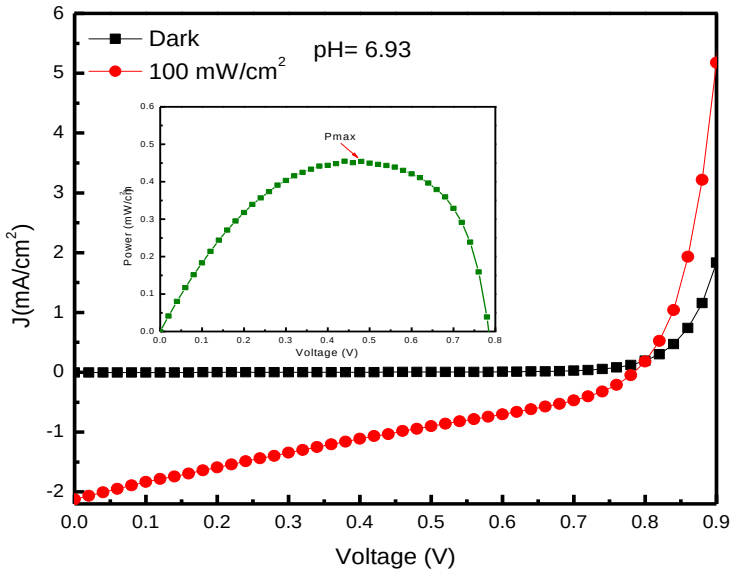
Dark
100 mW/cm2
pH= 6.93
Pmax
Power (mW/cm2)
Voltage (V)
J(mA/cm2)
Voltage (V)

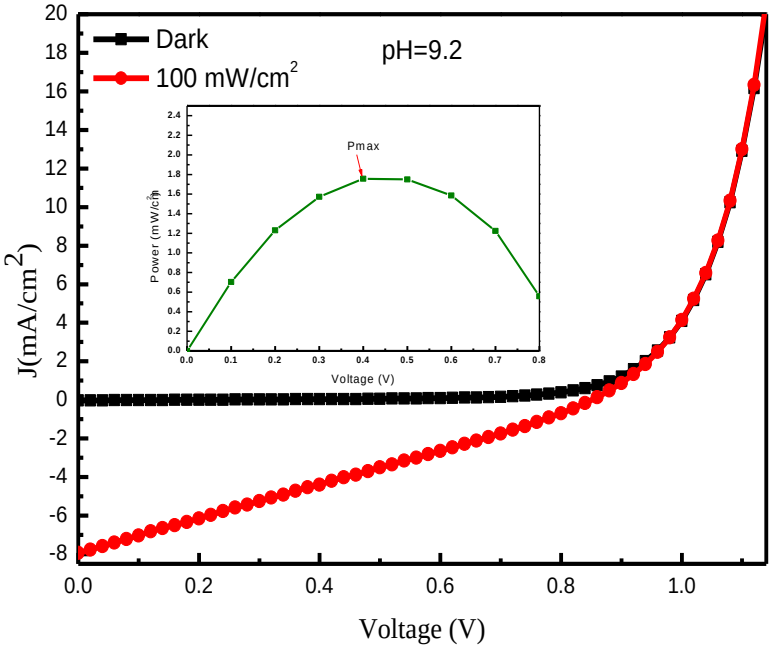
Dark
100 mW/cm2
pH=9.2
Pmax
Power (mW/cm2)
Voltage (V)
J(mA/cm2)
Voltage (V)

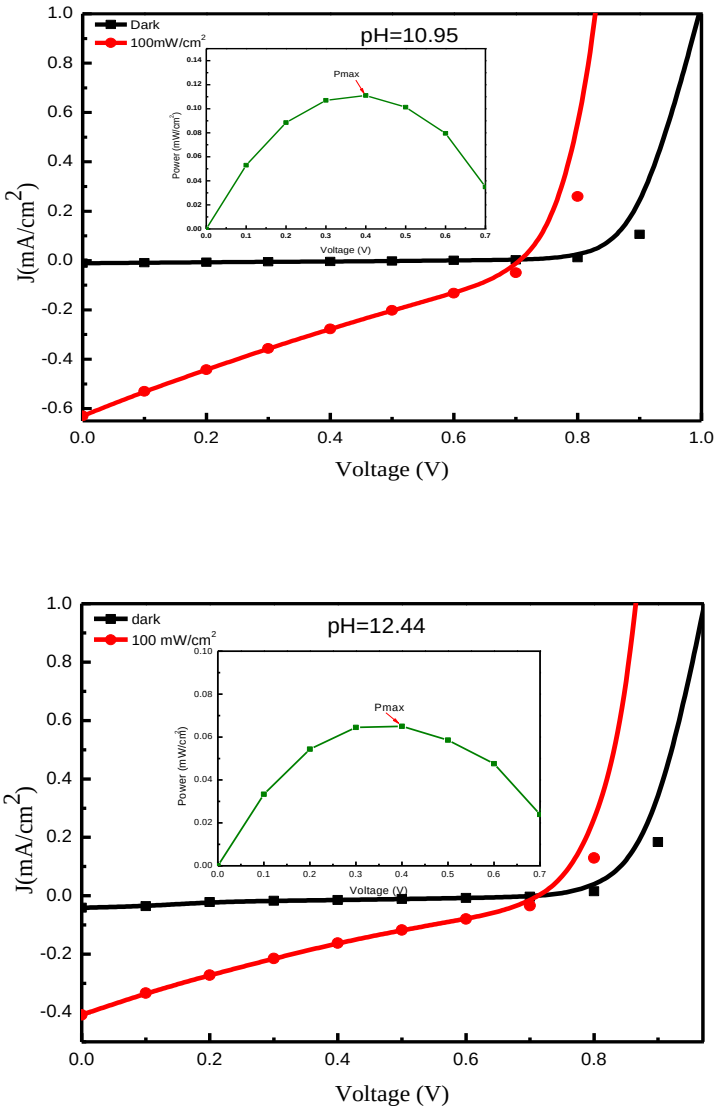

Figure 5.4: *Electrical characterisation of the PAMAM-G0.5/P3HT Based Organic Bilayer Devices at different pH concentrations of the PAMAM-G0.5 acceptor layer*

The plot of the calculated efficiency of the fabricated P3HT/ PAMAM GO.5-based bilayer devices versus the pH of the PAMAM-G0.5 acceptor layer is shown in Fig 5.5. It shows the abrupt increase in the efficiency at pH = 9.2 where the tertiary amine was positively charges branches and tree-like structure of the PAMAM-G0.5 acceptor layer was formed which enhanced diffusion length and the efficient collection of the electrons by the electrodes. While at low and high PAMAM G0.5 pH there were no branches exist and the efficiency decreases at least an order of magnitude accordingly. As mentioned earlier, this is directly related to the repulsion force at low pH as the tertiary

and interior tertiary amine was positively charges where as at high pH, PAMAM G0.5 becomes neutral without charges. Also, it is clear from Table 5.2 that when the current density is high (8 mA/cm^2) at pH= 9.2 the series resistance (R_S) decreases to 70 Ω.

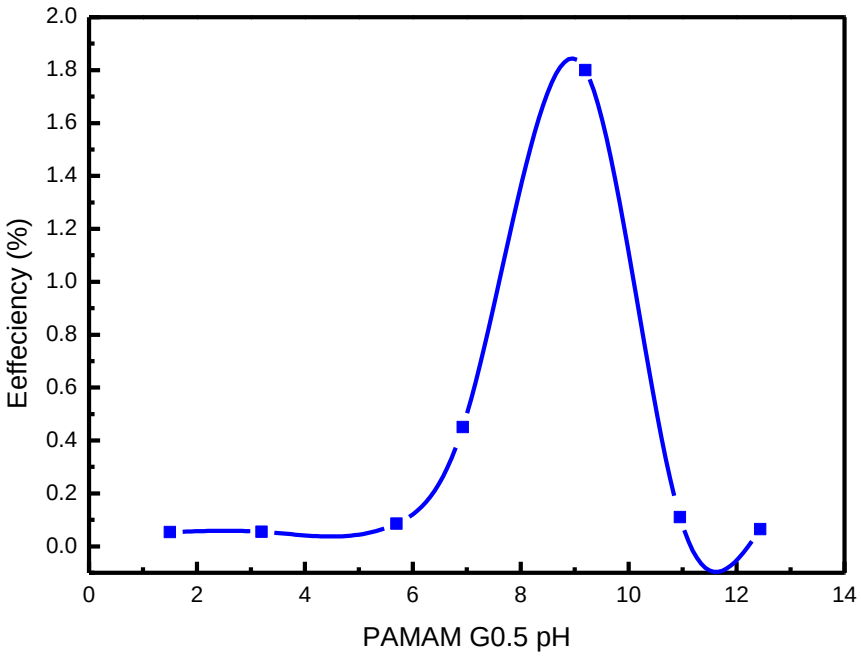

Figure 5.5: *The plot of the efficiency of the fabricated PAMAM-G0.5/P3HT-based bilayer devices versus the pH of PAMAM-G0.5.*

Figure 5.6 shows the dependence of open circuit voltage (V_{OC}) and current density (J_{SC}) on the pH level of the PAMAM G0.5 material. It is clear from Fig. 5.6 (a) that V_{OC} increased at low pH values and reaches maximum at about pH = 9.2, then become steady at 0.7 V at high pH values. Whereas, J_{SC} is very low at all pH values except for pH = 9.2 where the short circuit current increased sharply.

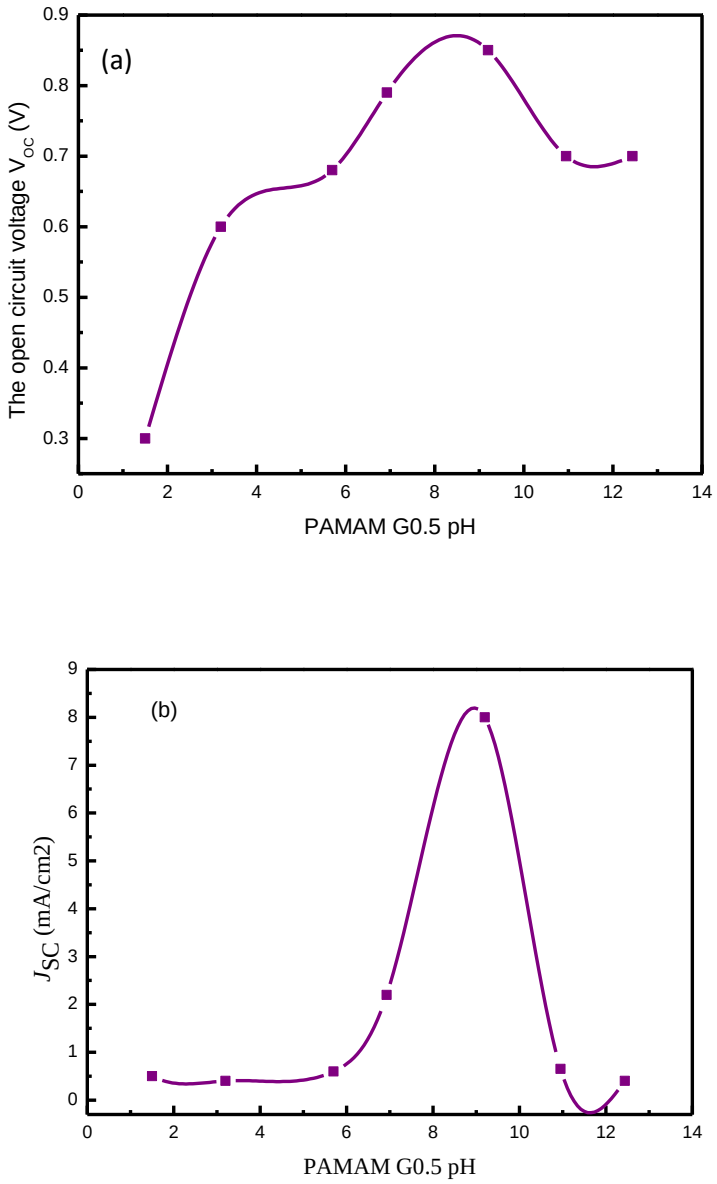

Figure 5.6: *The plot of (a) the open circuit voltage (b) the current density of the fabricated P3HT/PAMAM G0.5-based bilayer devices versus the pH of the PAMAM-G0.5.*

5.2.4 Optical Absorption measurement

UV-Vis spectrum (absorbance Vs wavelength) of PAMAM G0.5 at different pH conditions is shown in Fig. 5.7. At acidic PAMAM-G0.5 solution (low pH values), the absorption is very low. At low pH, the absorption edge around 510 nm where the bandgap at this point is 2.4 eV and peak absorption at 450 nm (2.7 eV). On the other hand, around pH = 5-9 where the solution tends to be neutral, the absorption intensity increased, reaching the maximum at pH= 9.2. At this pH the absorption edge around 550 (2.2 eV) with a peak absorption at 470 nm (2.6 eV).

However, at basic solutions (high pH values), the absorption edge decreases to around 530 (2.3 eV) with a peak absorption at 450 nm (2.7 eV). This decrease in absorption edge is due to protonation/deprotonation processes high and low pH. At low pH, the tertiary and interior tertiary amine are protonated resulting in repulsion force between them blocking electron transfer reactions between the P3HT and PAMAM-G0.5. As pH increased (neutral pH) the interior tertiary amine became deprotonated where tertiary amine protonated, allowing electron transfer reactions between the P3HT and PAMAM-G0.5. However, at high pH, the tertiary and interior tertiary amine become deprotonation reducing electron transfer reactions between the P3HT and PAMAM-G0.5

The neutral solution tends to have not only strong morphological changes, but also the optical properties tend to be totally different than acidic or basic solutions. The better absorption can be attributed to the crystallization of the material at such pH value.

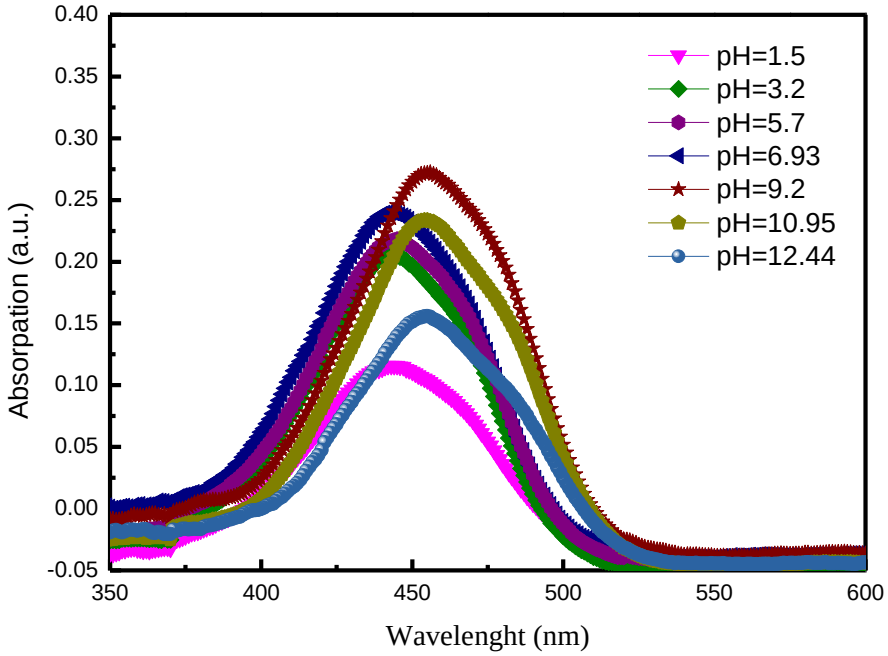

Figure 5.7: *Influence of pH on the absorption of PAMAM-G0.5.*

Table 5.3 show that changes in the PAMAM-G0.5 pH result in significant changes to the bandgap and provide a straightforward method for tuning the bandgap of PAMAM-G0.5 in the application of organic bilayer solar cells. At low pH, (pH $\leq$5) the bandgap was 2.4 eV. Increasing the pH to neutral level (pH 6-9) decrease the band gap to 2.2 eV. However, increasing the pH at high Values (pH$\geq$ 10) results in increasing the band gap to be 2.3 eV. Thus, optimized the pH level of PAMAM-G0.5 is crucial point in the organic bilayer device performance based on PAMAM-G0.5 pH as acceptor.

PAMAM-G0.5 pH	***Band gap (eV)***
1.5	2.4
3.2	2.4
5.7	2.3
6.93	2.3
9.2	2.2
10.95	2.3
12.44	2.3

Table 5.3: *The variation of PAMAM-G0.5 optical bandgap with different pH conditions.*

5.2.5 PAMAM-G0.5 pH bilayer devices thermal annealing

Thermal annealing is one way to overcome the lower efficiency in bilayer hetrojunction device by increase the donor acceptor interfacial area through introducing of nanostructures in either donor (D) or acceptor (A) layers. Thus, the distance between the acceptor and donor will be reduce and allow for better charge transfer. Introducing nanostructure in the active layer (D/A lead to more ordered bulk heterojunction structure. This gives large donor-acceptor interface area for exciton dissociation and good carrier transport [21, 22]. However, it was reported that PAMAM dendrimers show stronger cross-linking ability at room temperature. Prior to thermal treatment, the dendrimer film is quite pH-dependent. Heating dramatically changes the dendrimer film properties, leading to a monolithic nanocomposite that is pH independent. The nature of the thermally induced changes in these films depends on the incorporated dendrimer [23-25].

The thermal annealing was performed for the PAMAM G0.5 pH (low, neutral, high) layer at different temperatures for 10 min before the TiOx electron transfer layer (ETL) and vacuum deposition of the metal negative electrode (pre-thermal annealing). Figure 5.8 shows the *J–V* curves of the OHJ solar cells with different pre-thermal annealing temperature under the illumination of 100 mW/cm^2 white light.

At low pH and after annealing for 50 0C the J-V characteristics did not display any photovoltaic behaviour (no open circuit voltage was detected under illumination). Also, when annealing temperature increased to 100 0C and 150 0C the same behaviour was observed. The same results were achieved with neutral pH PAMAM G0.5 under thermal annealing at different temperatures. However, at high pH there is a small photovoltaic behaviour which was improved with increasing annealing temperature from 50 0C to 150 0C.

In order to understand the morphological changes that occur in the polymer layer as a result of thermal annealing, the AFM images of the PAMAM G0.5 pH layer surface after annealing at different temperatures was studied. The AFM images in Fig. 5.9 show the variation in PAMAM G0.5 pH layer morphology after annealing.

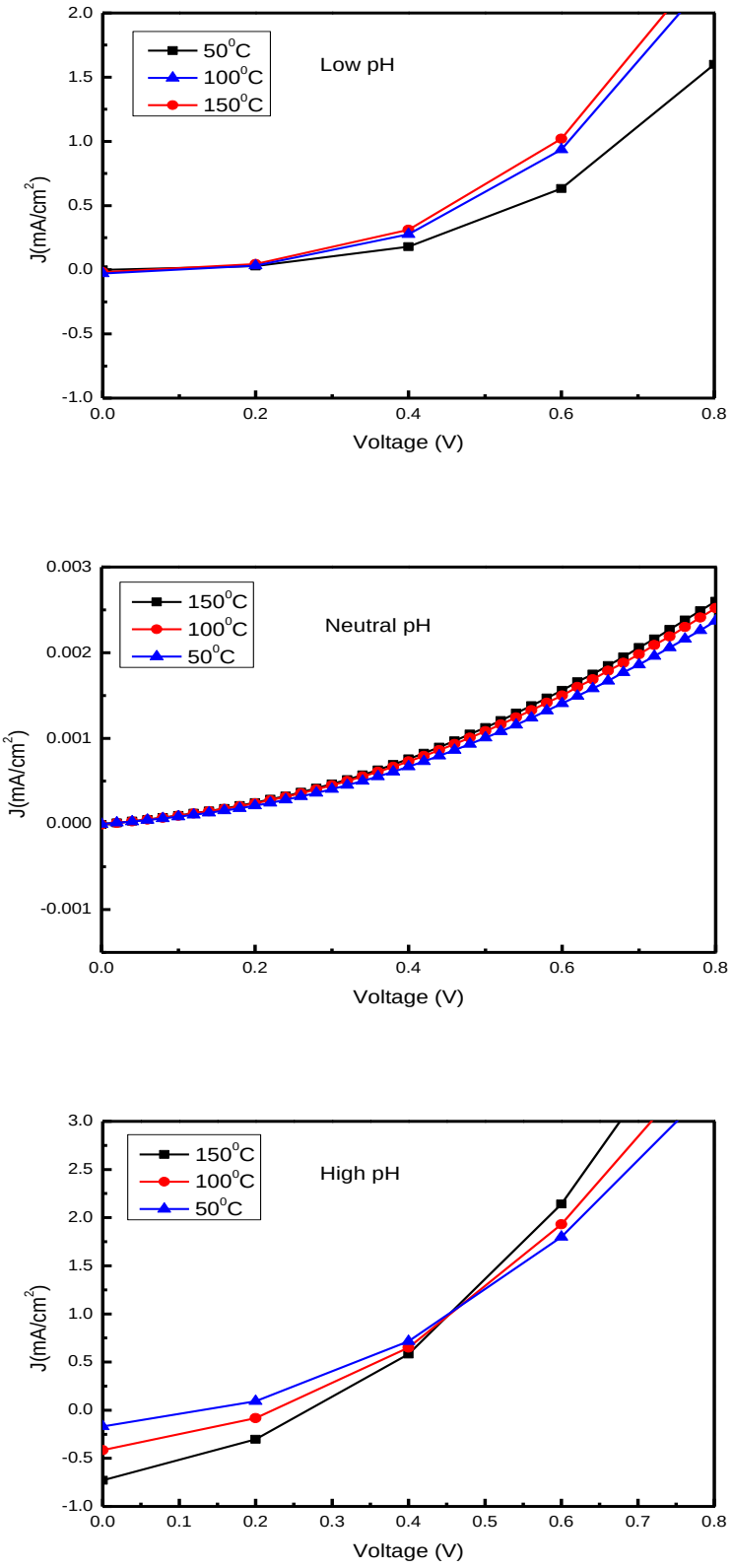

Figure 5.8: *current density–voltage (J–V) curves of the PAMAM G0.5 pH (low, neutral, high) OHJ solar cells with different pre-thermal annealing temperature.*

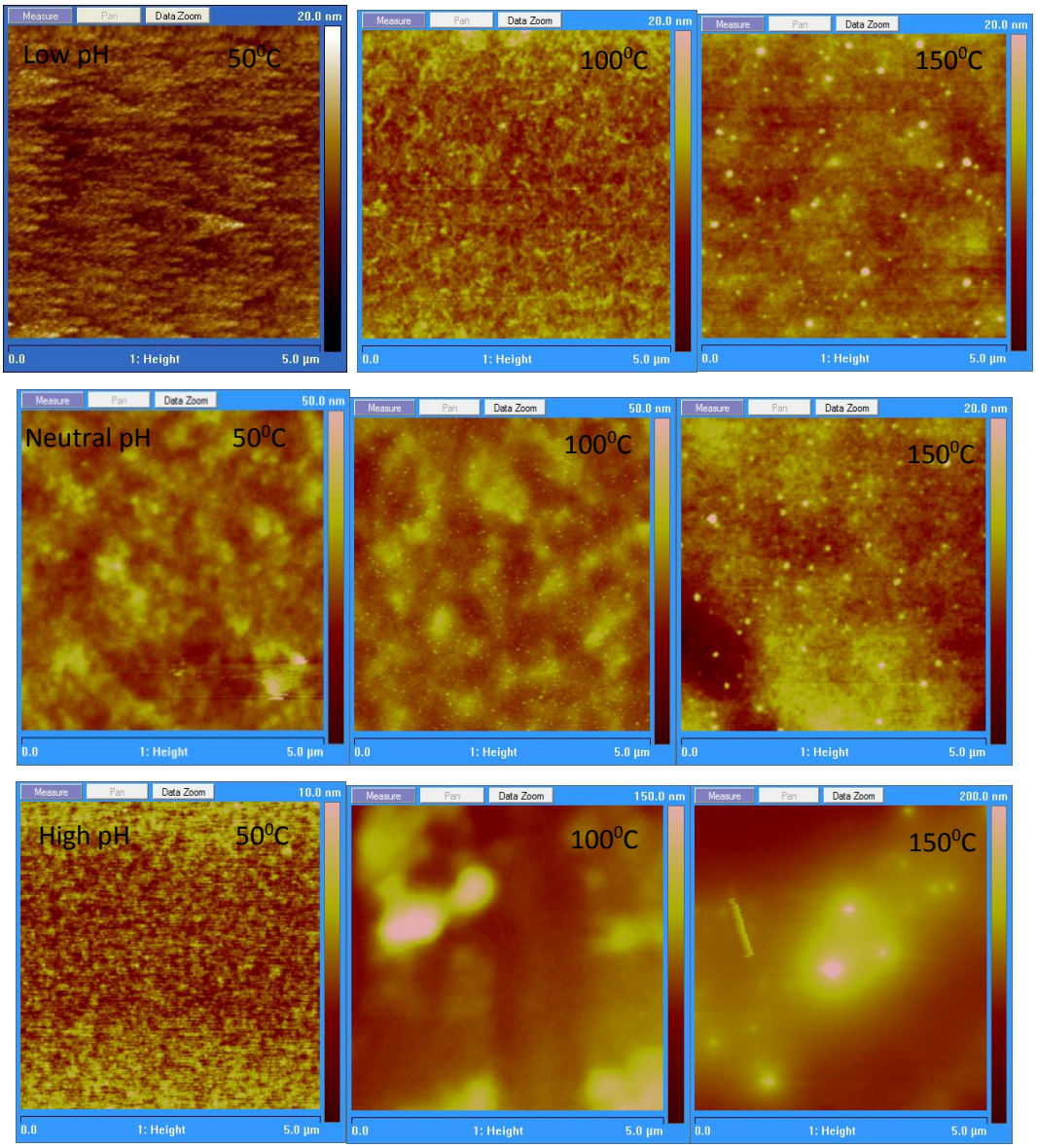

Figure 5.9: *shows the variation in PAMAM G0.5 pH layer morphology after annealing at different annealing temperature.*

At low pH, before annealing as seen in figure 5.3 PAMAM G0.5 had dense shell with maximum density at the dendrimer periphery, after annealing (Fig.5.9) grain growth and agglomeration increased upon annealing increased. It was reported that PAMAM dendrimers undergo some folding, shape and size changes in response to changes in their environment, such as altered solvent type, pH and temperature [26]. It can be seen that, the film morphology was changed from dense shell morphology to globular

structures upon temperature increase. This result in good correlation with which other reported that dendrimers with temperature retain their globular structure and uniformity at the molecular level [27-29]. It was observed that PAMAM G0.5 was minimized upon increasing annealing temperature. That demonstrate the dendrimer minimized after each annealing cycle [30, 31]. On other hand, other reported that thermal annealing enhanced phase separation at a micrometre scale and that results in incomplete energy transfer in the dendrimer [32]. These confirming the *J-V* characterisation results as the branches morphology with annealing disappear and the structure of denderimers become globular structure without any connections. Thus, energy transfers in the dendrimers become difficult. The same things occur at neutral and high pH. At neutral pH, before annealing complete existence of the branches and tree-like structure, after annealing the branches fades and grain growth increased upon annealing increased. However, at high pH before annealing PAMAM G0.5 had a compact structure with dense core, after annealing PAMAM G0.5 was minimized upon increasing annealing temperature taking grain structures. Theses grains become dense and smaller upon increasing annealing temperature without any connections between them. This can disturb energy transfer in dendrimers.

5.3 PAMAM G1.5 salt based OHJ solar cells at different pH conditions

5.3.1 Fabrication process

The structure of the ITO/PEDOT: PSS/P3HT/PAMAM G1.5 /TiO2/Al is shown in Figure 5.10. All fabrication conditions and experimental steps were the same as the previous PAMAM G0.5 based OHJ devices (shown in Section 5.2.1). The difference between the two structures is that PAMAM G1.5 with different pH conditions low, neutral, and high (1.43, 3.80, 5.27,7.03, 9.38, 10.73, 12.42) was used as the acceptor layer instead of PAMAM G0.5 pH. PAMAM-GO.5 has one teriatery amine and two –COONa surface group where PAMAM-G1.5 has three tertiary amine and four –COONa surface group.

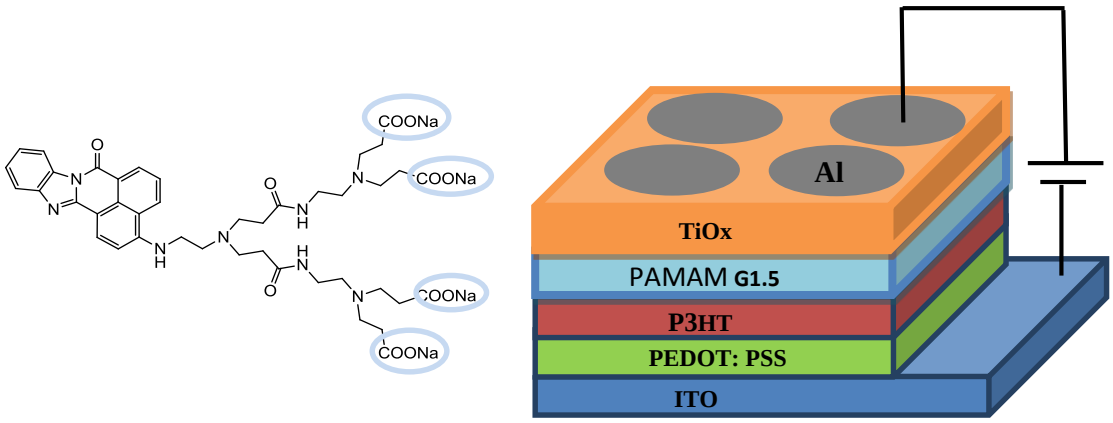

Figure 5.10: *PAMAM G1.5 salt chemical structure and Schematic diagram of PAMAM G1.5 salt based OHJ solar cells.*

5.3.2 Surface morphology

Optical images of the PAMAM G1.5 salt at different pH (low, neutral, high) condition on the top of and P3HT layer is shown in Fig. 5.11. Figure 5.11 shows that PAMAM G1.5 distributions are again highly dependent on its pH concentrations. The effect of different pH conditions on the morphology of PAMAM G1.5 is somewhat similar to that observed on PAMAM G0.5 morphology at different pH conditions. At low pH (pH < 5) the optical image showed high density small agglomeration in the film. At Neutral the optical image shows very clear branches and tree structure distributed almost uniformly and grown in the same direction. However, at high pH (pH > 10) the optical image showed that, no branches can be seen; branches fade and dissolve in the film structure.

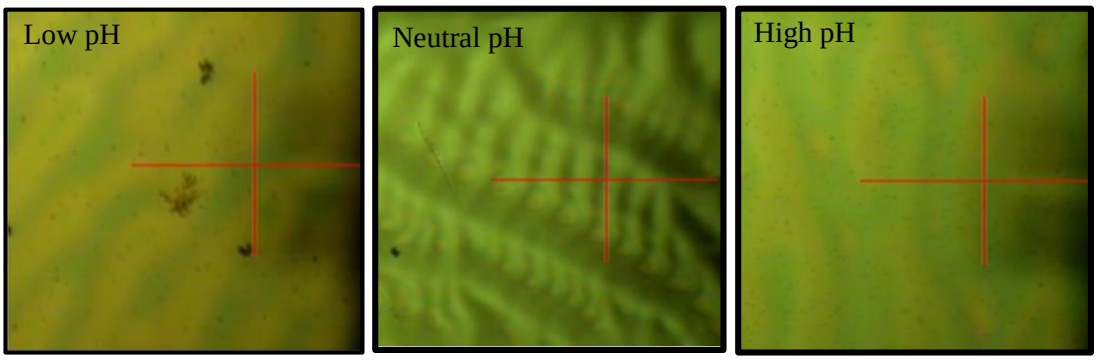

Figure 5.11: *Optical image of PAMAM G1.5 salt on top of the P3HTlayer at different pH conditions.*

Figure 5.12 shows the AFM images of the deposited PAMAM-G1.5 acceptor layer at different pH concentrations, starting from very acidic solution then increasing the pH to reach neutral concentrations and afterwards reaching very basic solution. As it was found previously in the PAMAM G0.5 pH the AFM images in Fig. 5.12 show significant differences in the topographies of PAMAM G1.5 at different pH conditions. The effect of pH on PAMAM G1.5 size and shape can be explained by repulsive forces between the tertiary and interior tertiary amine in PAMAM G1.5with changing pH. As it can be seen from PAMAM G1.5 AFM at different pH in Fig 5.12 the high pH results in a dense PAMAM G1.5 core where the periphery found to be largest at neutral pH and shrink at low pH. The low pH PAMAM G1.5 are positively charged, which make it less flexible due to the intermolecular electrostatic interactions and hence more water can penetrate in the interior of the dendritic. Therefore, low pH leads to a "dense shell", rigid structure and nonuniform void spacing [12]. At neutral pH, only the tertiary amines in PAMAM G1.5 are positively charged. These make it more flexible and a more homogeneous distribution result in larger dendritic size. At higher pH none of PAMAM G1.5 atoms are charged which make it to be highly flexible where there is no connection between the PAMAM G1.5 end branches. Thus, at high pH it has a rather dense core. In rigid dendritic materials electron transfer was found to be slower than flexible dendritic materials. This is because the rigid dendritic materials keep a large cage around the centre, forcing electrons to travel along a larger distance than in their flexible counterparts (P3HT) [33]. However, at natural pH the end branches (periphery) expanded on the surface and flatten with good connections to each other's. Despite the similarity in architecture and size, there are significant changes in the conformations of PAMAM G1.5 at different pH conditions. The size of the PAMAM G1.5 dendritic was found to increase from high to low pH reflecting swelling due to the electrostatic phenomenon.

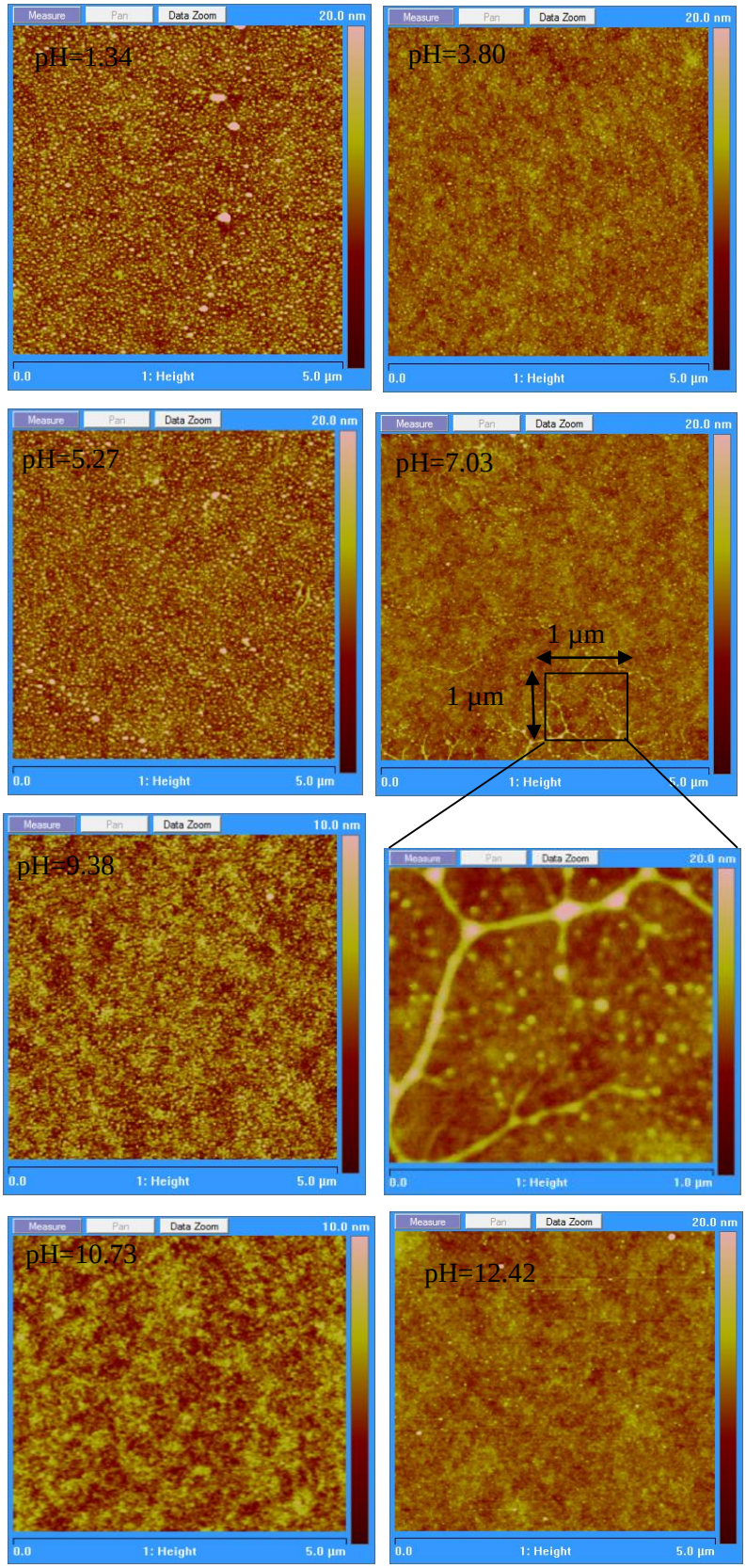

Figure 5.12: *AFM morphology images of PAMAM G1.5 acceptor layer on top of the P3HTlayer at different pH concentrations.*

5.3.3 Electrical characterisation

J-V characteristics of the P3HT/PAMAM G1.5 -based bilayer devices at different pH concentrations of the PAMAM-G1.5 are shown in Fig. 5.13. It consists of 7 graphs each graph presents the electrical characterization of a device fabricated with a pH concentration of the PAMAM-G1.5. All devices exhibit photovoltaic behaviour under dark and under incident light illumination with intensity equals to 1.5 AM radiation. The photovoltaic behaviour of these devices showed that it is highly dependent on the morphology of the PAMAM-G1.5 pH layer. Thus the difference in the morphology of the deposited PAMAM-G1.5 at different pH was reflected as well on the photovoltaic device parameters. Table 5.3 summarizes the extracted photovoltaic parameters such as V_{OC}, J_{SC} and P_{MAX} from the recorded characteristics of each device, also, the calculated fill factor and the solar cell efficiency for each device. It can be observed from table 5.4 that the V_{OC} exhibits a fluctuating behaviour. V_{OC} fluctuate with pH increase, it increase from 0.6 V at pH = 1.43 to reach 0.7 V at pH = 3.80. Further increase of pH to higher values decrease the V_{OC} to a value of 0.2 V at pH= 9.38 then increase to 0.36 V at pH= 10.73 and decrease again to 0.23 V when the pH increase to 12.42. This fluctuation may occur as result of PAMAM G1.5 band gap variation through increasing its pH values. Table 5.3 also shows the dependence of the J_{SC} of the fabricated devices on the pH of the PAMAM-G1.5, it increased from 0.4 mA/cm^2 at pH = 1.43 to reach 66 mA/cm^2 at pH = 7.03. Further increase of pH to higher values decrease the J_{SC} to a value of 2 mA/cm^2. This can be explained by the large and highly branches units in acceptor layer at this pH=7.03.

On the other hand, PAMAM G1.5 pH OHJ based devices behaved in the same trend with increasing pH as PAMAM G0.5 pH OHJ based devices. At high pH (pH >10) none of the tertiary or interior tertiary amines protonated (neutral PAMAM) which means there are no positive charges can bend the negative charges from the P3HT.Also, at this pH the morphology as it was mentioned before become globular and compact. This explained the abrupt decrease in the J_{SC} at higher pH. On the other hand, at low pH (pH < 5) all the tertiary and interior tertiary amine groups of the PAMAM G1.5 dendrimer are protonated. Thus, electrostatic repulsion between tertiary and interior tertiary amine positively charged amines larger than the electrostatic attractive interaction between P3HT and PAMAM G1.5 result in low J_{SC} at this pH. Furthermore, at low pH of PAMAM G1.5 the branches tend to shrink due to electrostatic repulsion

between primary and tertiary amine. It was found that the size of the PAMAM G1.5 dendritic was found to increase from high to low pH reflecting swelling due to the electrostatic phenomenon. However, at neutral pH (pH =6-9) all the tertiary amines protonated leading to create electric current at the interface with opposite material P3HT, then the electric current will flow through the solar cell device in order to encourage more electrons to transfer from the donor (P3HT) to acceptor (PAMAM G1.5) and reduce the recombination of charge. From a morphology point of view, significant branch back-folding occurred at neutral pH (pH 6-9) in addition to major peripheral distribution of the terminal groups. Thus, complete existence of the branches and tree-like structure in the deposited acceptor layer at neutral pH (pH=7.03) may enhance the mobility and diffusion length of the electrons injected in the acceptor layer and thus facilitates its collection by the electrode.

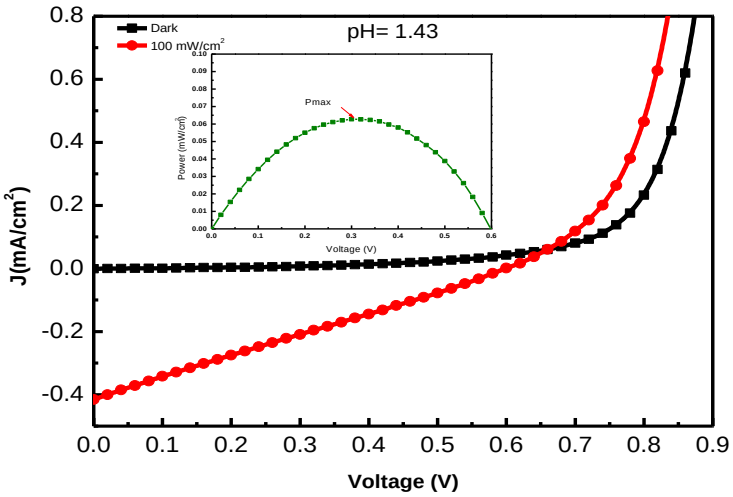
pH= 1.43
Dark
100 mW/cm2
Pmax
Power (mW/cm2)
Voltage (V)
J(mA/cm2)
Voltage (V)

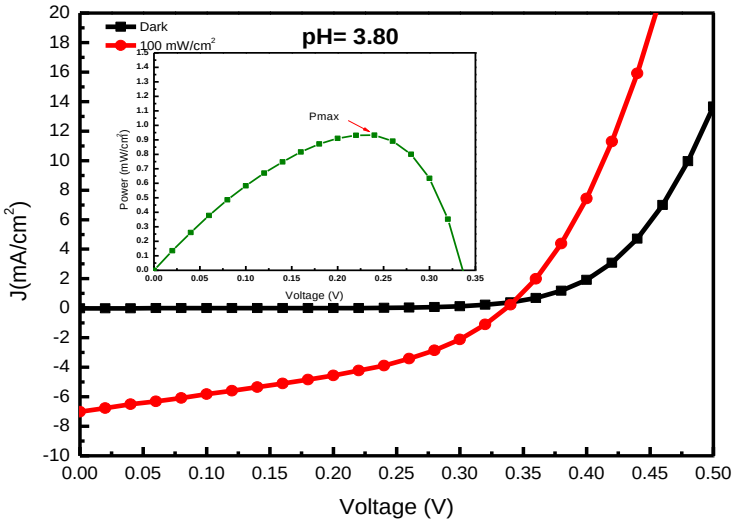
pH= 3.80
Dark
100 mW/cm2
Pmax
Power (mW/cm2)
Voltage (V)
J(mA/cm2)
Voltage (V)

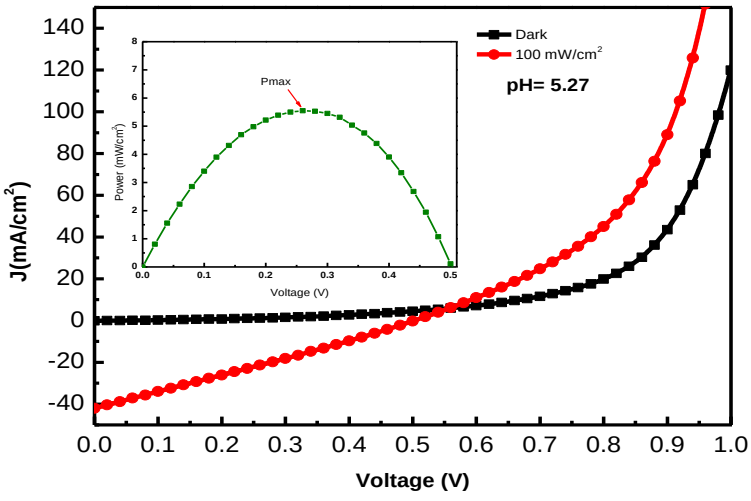
pH= 5.27
Dark
100 mW/cm2
Pmax
Power (mW/cm2)
Voltage (V)
J(mA/cm2)
Voltage (V)

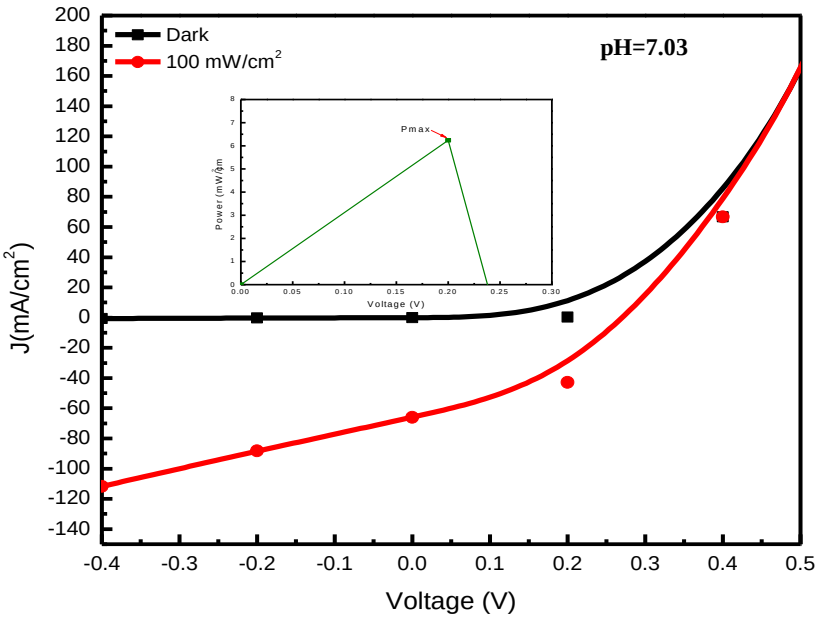
Dark
100 mW/cm2
pH=7.03
Pmax
Power (mW/cm2)
Voltage (V)
J(mA/cm2)
Voltage (V)

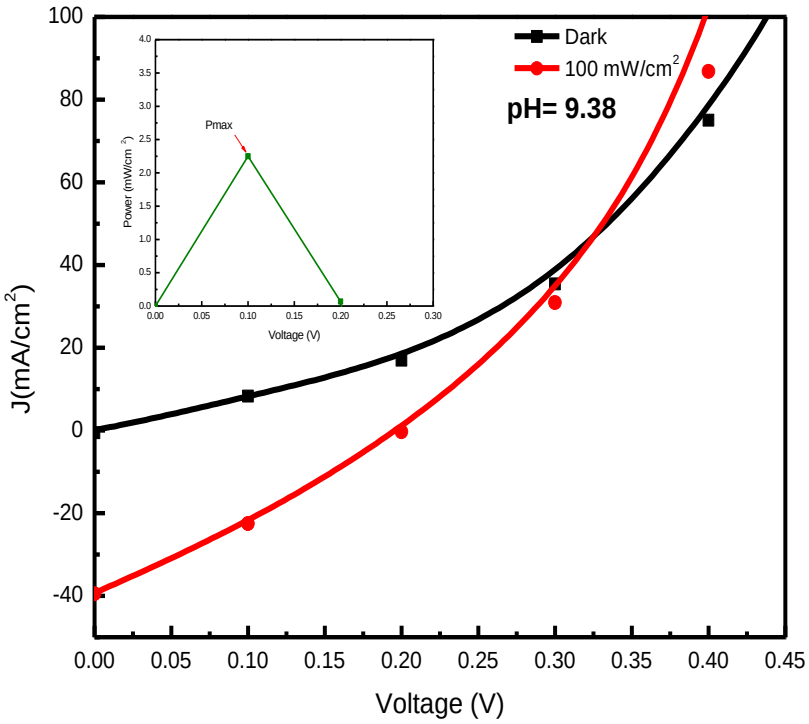
Dark
100 mW/cm2
pH= 9.38
Pmax
Power (mW/cm2)
Voltage (V)
J(mA/cm2)
Voltage (V)

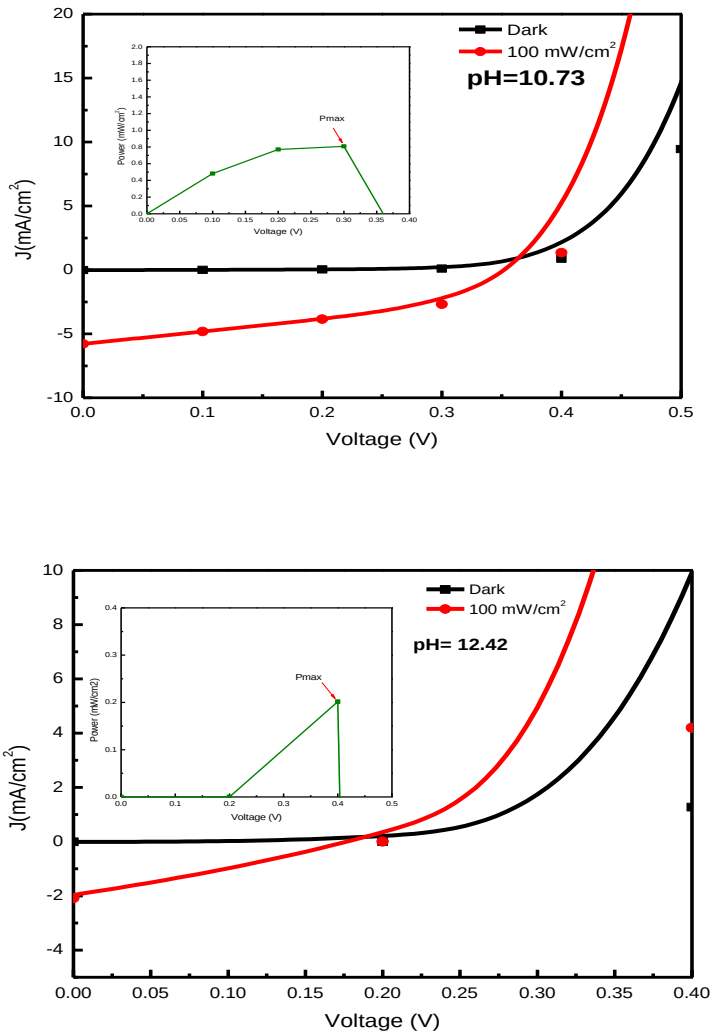

Figure 5.13: *Electrical characterisation of the PAMAM-G1.5/P3HT Based Organic Bilayer Devices at different pH concentrations of the PAMAM-G1.5*

The abrupt increase in the J_{SC} at pH=7.03 was reflected in P_{MAX} as shown in table 5.4, where the P_{max} had its highest value of 6.24 mW/cm^2 while it had much lower values at other pH values. The abrupt increase in the J_{SC} and P_{max} was reflected in the calculated efficiency also. Furthermore, a lower serial resistance value was found to be at neutral pH=7.03 when the current density J_{SC}= 66 mA/cm^2. It is clear that the PAMAM-G1.5 based organic heterojunction bilayer solar cell exhibit efficiency higher than the PAMAM-G0.5 based device. This due to the increase in the tertiary amine and surface group number as PAMAM-G0.5 has one tertiary amine and two –COONa surface group, while PAMAM-G1.5 has three tertiary amine and four –COONa surface group. This change increases the number of electrons generated through the device and then increase the efficiency.

PAMAM G1.5 pH	V_{OC} (v)	J_{SC}(mA/cm^2)	P_{MAX} (mW/cm^2)	*FF* (%)	*PCE* (%)	R_S (Ω)	R_{SH} (Ω)
1.43	**0.6**	**0.4**	**0.065**	**27**	**0.065**	**1190**	**8300**
3.80	**0.7**	**7**	**0.95**	**19.4**	**0.95**	**50**	**830**
5.27	**0.5**	**41**	**5.5**	**27**	**5.5**	**14**	**83**
7.03	**0.26**	**66**	**6.24**	**36.4**	**6.24**	**2**	**200**
9.38	**0.2**	**40**	**2.3**	**29**	**2.3**	**5**	**42**
10.73	**0.36**	**5.8**	**0.8**	**38**	**0.8**	**7**	**170**
12.42	**0.23**	**2**	**0.2**	**43.5**	**0.2**	**41**	**1700**

Table 5.4: *The extracted and calculated photovoltaic parameters of the fabricated PAMAM G1.5 based devices under different pH conditions*

The plot of the calculated efficiency of the fabricated P3HT/ PAMAM G1.5-based bilayer devices versus the pH of the PAMAM-G1.5 acceptor layer is shown in Fig 5.14 It shows the abrupt increase in the efficiency at pH = 7.03 where the tertiary amine was positively charges and branches and tree-like structure of the PAMAM-G1.5 acceptor layer was formed which enhanced diffusion length and the efficient collection of the electrons by the electrodes. While at low and high PAMAM G1.5 pH where no branches exist the efficiency decreases one order of magnitude.

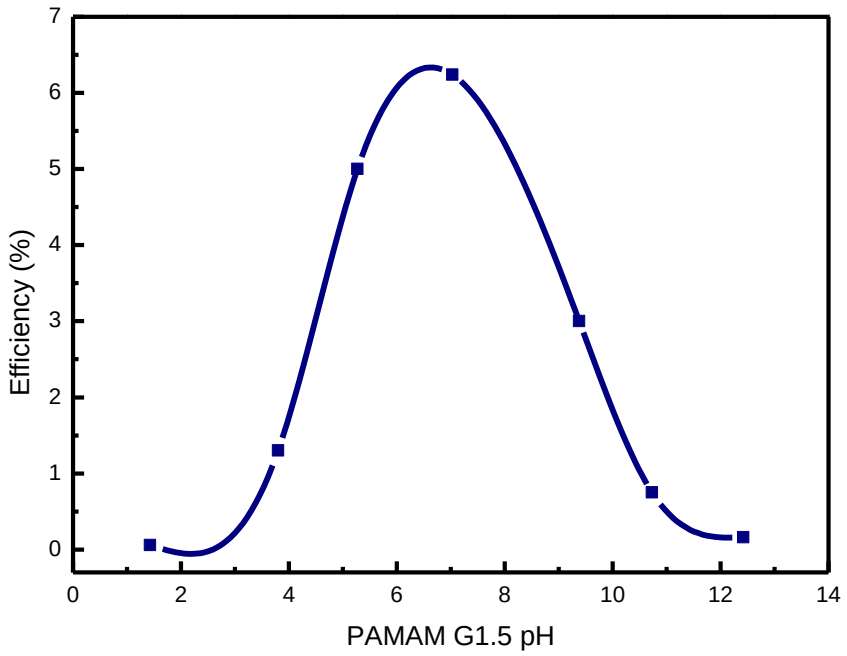

Figure 5.14: *The plot of the efficiency of the fabricated PAMAM-G1.5/P3HT-based bilayer devices versus the pH of PAMAM-G1.5.*

Figure 5.15 shows the open circuit voltage (V_{OC}) and current density (J_{SC}) behaviour with changing pH level of the PAMAM G1.5 material. It is clear from Fig. 5.15 (a) that V_{OC} fluctuate with pH increase, it increase from 0.6 V at pH = 1.43 to reach 0.7 V at pH = 3.80. Further increase of pH to higher values decrease the V_{OC} to a value of 0.2 V at pH= 9.38 then increase to 0.36 V at pH= 10.73 and decrease again to 0.23 V when the pH increase to 12.42.Whereas, J_{SC} is low at all pH values except for pH = 7.03 where the short circuit current increased sharply.

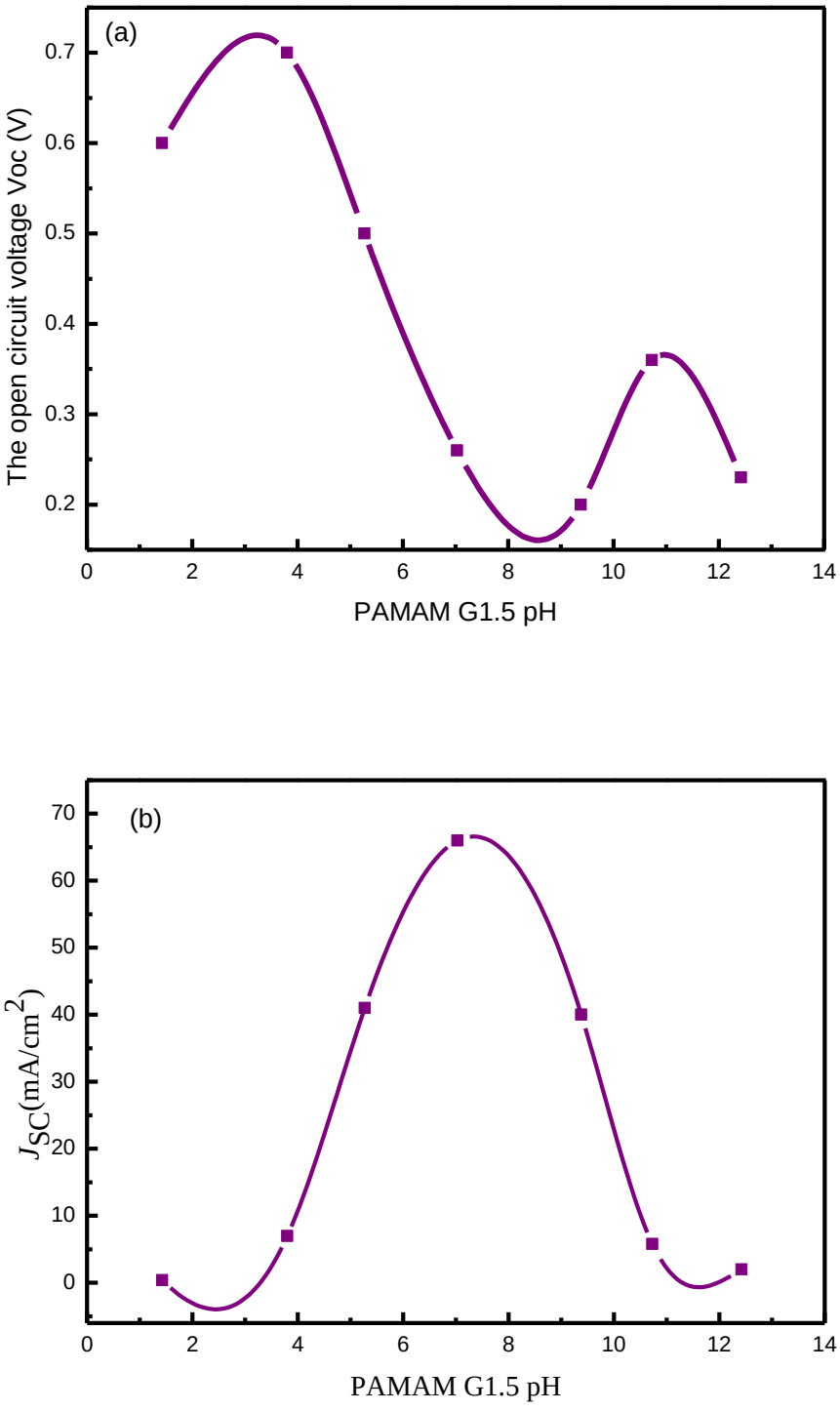

Figure 5.15: *The plot of (a) the open circuit voltage (b) the current density of the fabricated P3HT/PAMAM G1.5-based bilayer devices versus the pH of the PAMAM-G1.5.*

5.3.4 Optical Absorption measurement

Figure 5.16 present the UV-Vis spectrum (absorbance Vs wavelength) of PAMAM G1.5 at different pH conditions. At low pH, the absorption edge around 500 nm where the bandgap at this point 2.48 eV. The peak absorption at 440 nm (2.8 eV). On the other hand, around pH = 6-9 where the solution tends to be neutral, the absorption intensity increased reach the maximum at pH= 7.03. At this pH the absorption edge around 530 (2.3 eV) with a peak absorption at 460 nm (2.7 eV).

However, at basic solutions (high pH values), the absorption decrease the absorption edge around 520 (2.38 eV) with a peak absorption at 450 nm (2.8 eV). This due to protonation/deprotonation processes at different pH. It was mentioned previously that at low pH, when the tertiary and interior tertiary are protonated the repulsion force between them blocking or enabling electron transfer reactions between the P3HT and PAMAM-G0.5. As pH increased (neutral pH) the interior tertiary amine became deprotonated where tertiary amine protonated allowing electron transfer reactions between the P3HT and PAMAM-G0.5.

However, at high pH, the tertiary and interior tertiary amine became deprotonation which reduce electron transfer reactions between the P3HT and PAMAM-G0.5

This high efficiency OHJ solar cell based on PAMAM G1.5 at neutral pH attributed to the strong morphological changes with strong absorption at this pH.

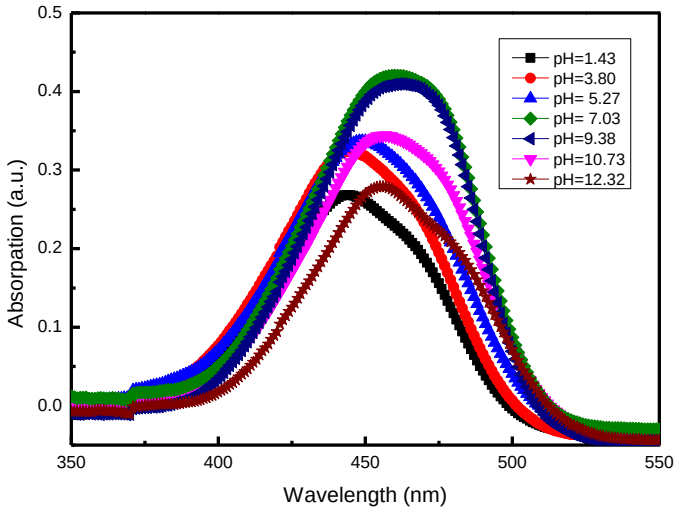

Figure 5.16: *Influence of pH on the absorption of PAMAM-G1.5.*

Table 5.5 shows that changes in the PAMAM-G1.5 pH result in significant changes to the bandgap and morphology and provide a straightforward method for tuning the bandgap and morphology of PAMAM-G1.5 in the application of organic bilayer solar cells. At low pH, (pH <5) the bandgap was 2.48 eV. Increasing the pH to neutral level (pH 6-9) decrease the band gap to 2.3 eV. However, increasing the pH at high Values (pH> 10) results in increasing the band gap to be 2.38 eV. Thus, optimized the pH level of PAMAM-G1.5 is critical point in the organic bilayer device performance based on PAMAM-G1.5 pH as acceptor.

PAMAM-G1.5 pH	***Band gap (eV)***
1.43	*2.48*
3.80	*2.43*
5.27	*2.38*
7.03	*2.3*
9.38	*2.38*
10.73	*2.38*
12.42	*2.38*

Table 5.5: *The variation of PAMAM-G1.5 optical bandgap with different pH conditions.*

5.3.5 PAMAM-G1.5 pH bilayer devices thermal annealing

The thermal annealing was performed for the acceptor layer PAMAM G1.5 pH (low, neutral, high) at different temperatures for 10 min before the TiOx electron transfer layer (ETL) and vacuum deposition of the metal negative electrode (pre-thermal annealing). Fig. 5.17 shows the current density–voltage *(J–V)* curves of the OHJ solar cells with different pre-thermal annealing temperature under the illumination of 100 mW/cm^2 white light. The same result was recorded as annealing of PAMAM G0.5 pH

devices. At low pH PAMAM G1.5, after annealing acceptor layer for 50 ^{0}C the *J-V* characteristics did not display any photovoltaic behaviour (no open circuit voltage was detected) under illumination with the halogen lamp (100 mW/cm^{2}). Also, when annealing temperature increased to 100 ^{0}C and 150 ^{0}C the same behaviour was observed. The same results was achieved with neutral and high pH PAMAM G1.5 under thermal annealing at different temperatures.

The effects of annealing temperature on the PAMAM G1.5 pH (low, neutral, high) layer at different annealing temperatures was studied. The tapping-mode atomic force microscope (AFM) images in Fig.5.18 shows the variation in PAMAM G1.5 pH layer morphology after annealing at low pH. Similar annealing effects were observed in PAMAM G1.5 pH layer as PAMAM G0.5 pH under different thermal annealing temperatures.

At low pH, before annealing, as seen in Fig. 5.12, PAMAM G1.5 had dense shell with maximum density at the dendrimer periphery, after annealing (Fig.5.18) grain growth and agglomeration increased upon annealing increased. The same thing occurs at neutral and high pH. At neutral pH, before annealing complete existence of the branches and tree-like structure, after annealing the branches fade and grain growth increased upon annealing increased. However, at high pH before annealing PAMAM G1.5 had compact structure with dense core, after annealing PAMAM G1.5 was minimized upon increasing annealing temperature taking grain structures. Theses grains become dens and smaller upon increasing annealing temperature without any connections between them. This can disturb energy transfer in dendrimers.

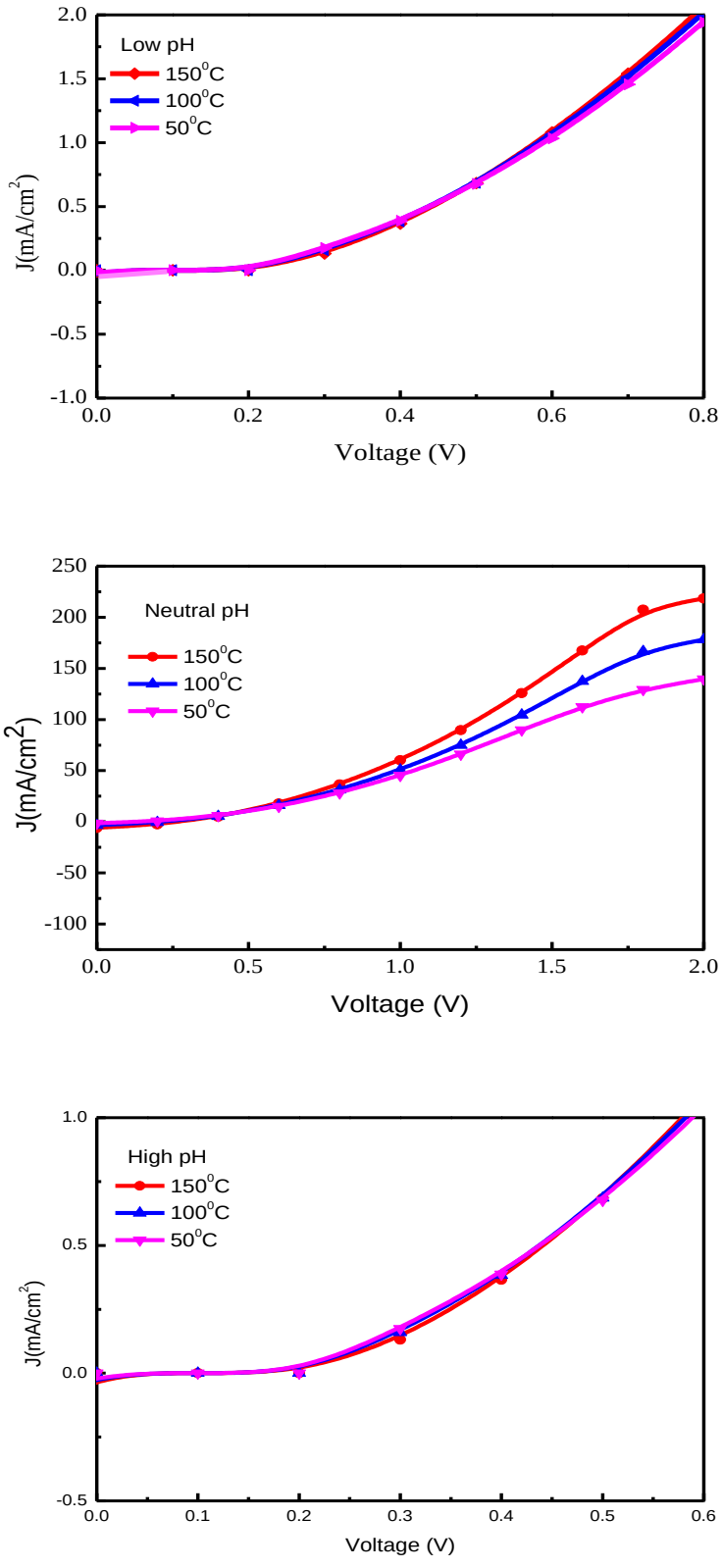

Figure 4.21: *current density–voltage (J–V) curves of the PAMAM G1.5 OHJ solar cells with different pre-thermal annealing temperature under the illumination of 100 mW/cm^2 white light.*

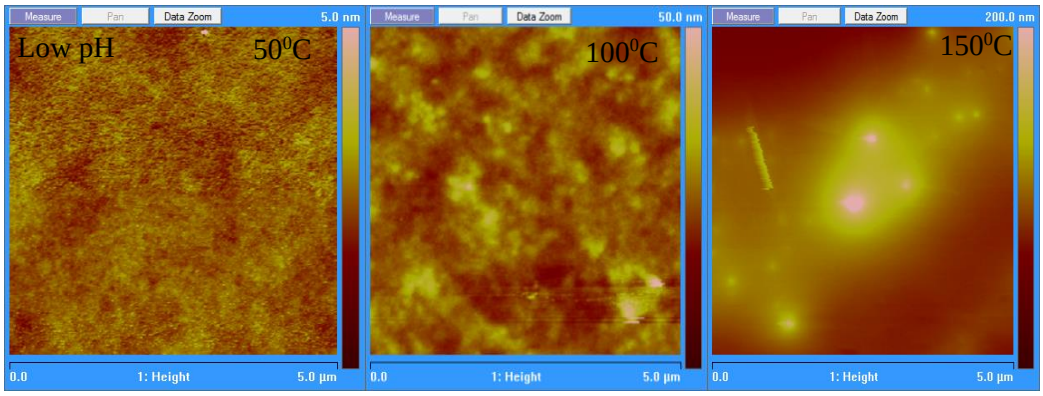

Figure 5.18: *shows the variation in PAMAM G1.5 pH layer morphology after annealing at low pH.*

5.4 PAMAM G2.5 salt based OHJ solar cells at different pH conditions

5.4.1 Fabrication process

The structure of the ITO/PEDOT: PSS/P3HT/PAMAM G2.5 /TiO2/Al is shown in Figure 5.19. All fabrication conditions and experimental steps were the same as the previous PAMAM G0.5 based OHJ devices (shown in Section 5.2.). The difference is in the generation size. PAMAM G2.5 with different pH conditions low, neutral, and high (1.25, 2.52, 5.43, 6.85, 8.05, 10.71, 12.52) was used as the acceptor layer instead of PAMAM G0.5 pH. PAMAM-G0.5 has one tertiary amine and two –COONa surface group where PAMAM-G2.5 has seven tertiary amine and eight –COONa surface group.

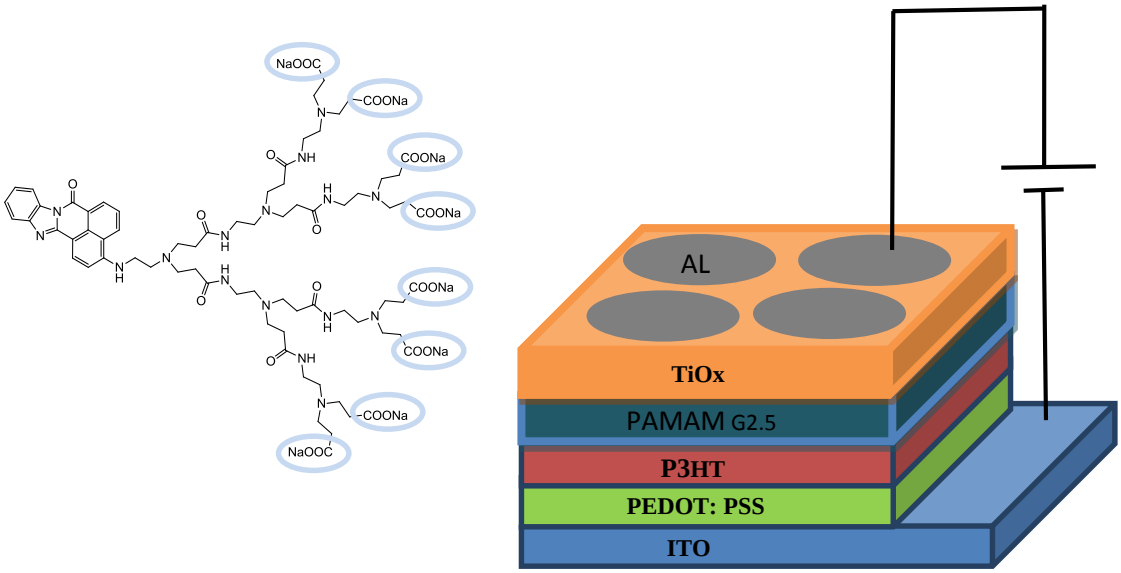

Figure 5.19: *PAMAM G2.5 salt chemical structure and Schematic diagram of PAMAM G2.5 salt based OHJ solar cells.*

5.4.2 Surface morphology

Figure 5.20 show optical images of the PAMAM G2.5 salt at different pH (low, neutral, high) condition on the top of and P3HT layer. It show that PAMAM G2.5 distribution are highly dependent on its pH concentrations. The effect of different pH conditions on the morphology of PAMAM G2.5 is somewhat similar to that observed on PAMAM G0.5 and G1.5 morphologies at different pH conditions. At low pH (pH < 5) the optical image showed high density small agglomeration in the film. At Neutral the optical image shows very clear branches and tree structure distributed almost uniformly and grown in the same direction. However, at high pH (pH > 10) the optical image showed that, no branches can be seen, branches fade and dissolve in the film structure.

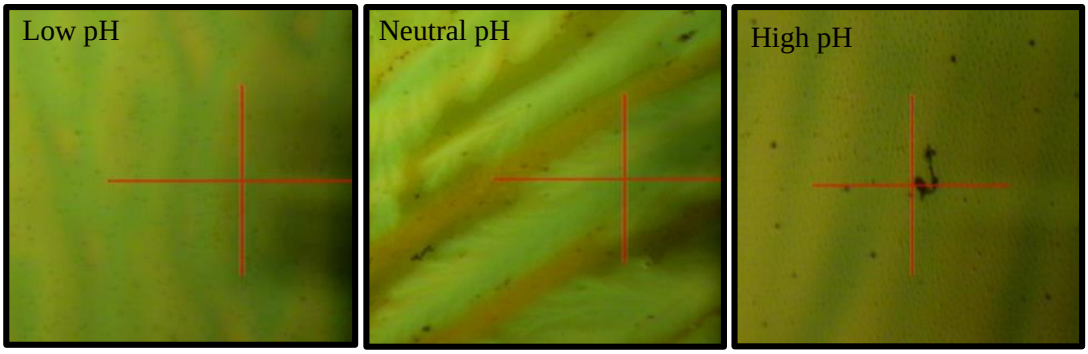

Figure 5.20: *Optical image of PAMAM G2.5 salt on top of the P3HTlayer at different pH conditions.*

AFM images in the Fig.5.21 shows the deposited PAMAM-G2.5 acceptor layer at different pH concentrations, starting from very acidic solution then increasing the pH to reach neutral concentrations and afterwards reaching very basic solution. As it was found previously in the PAMAM G0.5 and G1.5 pH, AFM images in Fig.5.21 show significant differences in the topographies of PAMAM G2.5 at different pH conditions. The effect of pH on PAMAM G2.5 size and shape can be explained by repulsive forces between the primary and tertiary amine in PAMAM G2.5with changing pH. As it can be seen from PAMAMG2.5 AFM at different pH in Fig.5.21 the high pH results in a dense PAMAM G2.5 core where the periphery found to be largest at neutral pH and shrink at low pH. At low pH, PAMAM is known to adopt more rigid conformation due to electrostatic repulsions among the protonated amine groups along the branches [34]. Thus, at low pH PAMAM G2.5 is positively charged, which make it less flexible due to the intermolecular electrostatic interactions and hence more water can penetrate in the interior of the dendritic. Therefore, low pH leads to a "dense shell", rigid structure and nonuniform void spacing. In rigid dendritic materials electron transfer was found to be slower than flexible dendritic materials. This is because the rigid dendritic materials keep a large cage around the centre, forcing electrons to travel along a larger distance than in their flexible counterparts (P3HT). However, at natural pH the end branches (periphery) expanded on the surface and flatten with good connections to each other's. At neutral pH, only the tertiary amines in PAMAM G2.5 are positively charged. These make it more flexible and a more homogeneous distribution result in larger dendritic size. At high pH PAMAM G2.5 has a compact conformation because the amine groups are no longer protonated and the branches are more flexible. Thus,

none of PAMAM G2.5 atoms are charged which make it to be highly flexible where there is no connection between the PAMAM G2.5 end branches, and has a rather dense core. In a similar fashion as G0.5-based device, the size of the PAMAM G2.5 dendritic was found to increase from high to low pH reflecting swelling due to the electrostatic phenomenon.

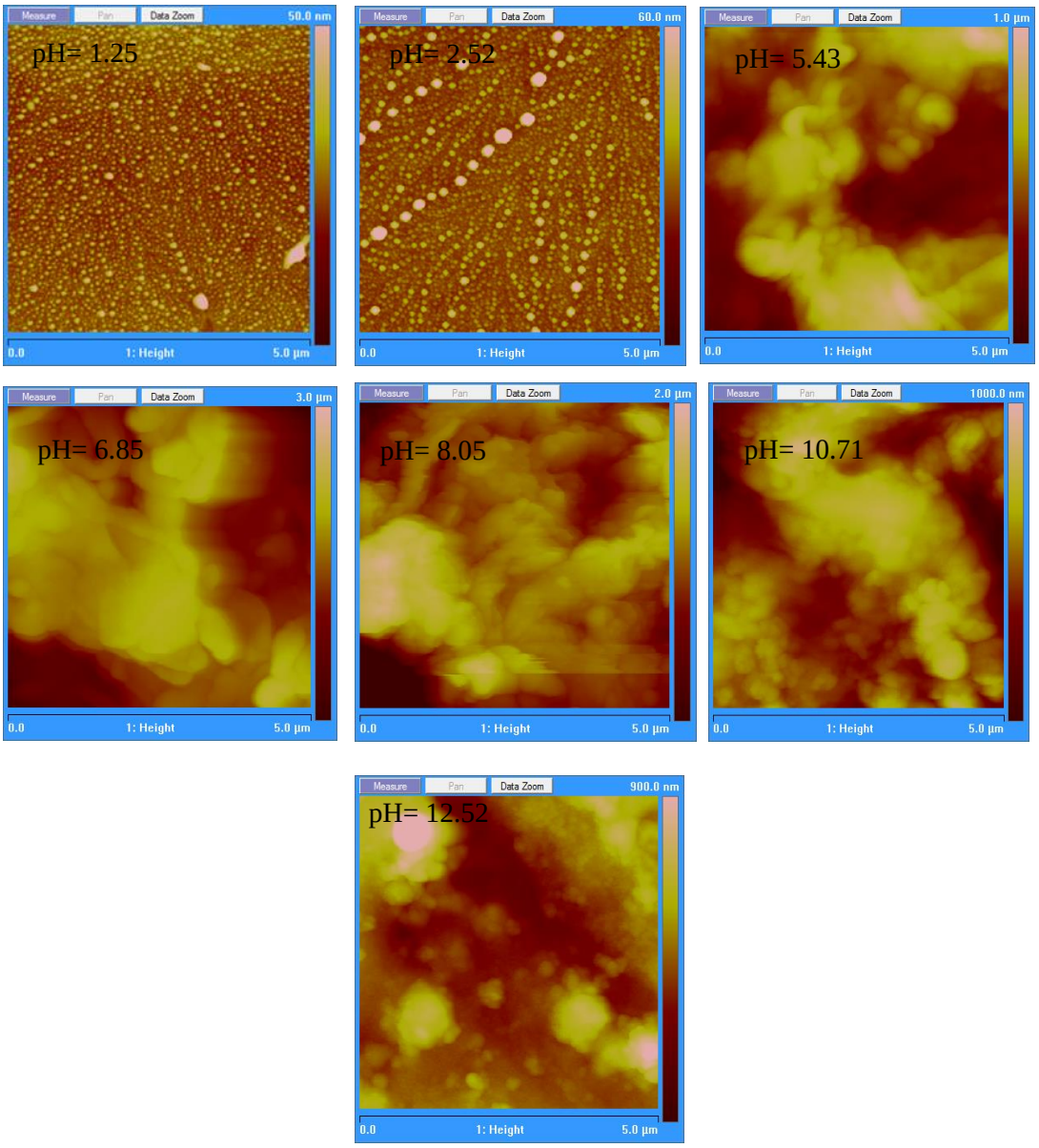

Figure 5.21: *AFM morphology images of PAMAM G2.5 acceptor layer on top of the P3HTlayer at different pH concentrations.*

5.4.3 Electrical characterisation

Figure 5.22 shows the J-V characteristics of the P3HT/PAMAM G2.5 -based Organic bilayer devices at different pH concentrations of the PAMAM-G2.5. It contains 7 graphs each graph presents the electrical characterization of a device fabricated with a pH concentration of the PAMAM-G2.5. All devices at different PAMAM G2.5 pH concentrations exhibit photovoltaic behaviour under light and under incident light illumination with intensity equals to 1.5 AM radiation. The photovoltaic behaviour of these devices showed that it is highly dependent on the morphology of the PAMAM-G2.5 pH layer. Thus the difference in the morphology of the deposited PAMAM-G2.5 at different pH was reflected as well on the photovoltaic device parameters. Table 5.6 optimize the extracted photovoltaic parameters such as V_{OC}, J_{SC} and $P_{\max}$ from the recorded characteristics of each device, also, the calculated fill factor and the solar cell efficiency for each device. It is clear from Table 5.6 that the V_{OC} increased with the increase of pH, it increased from 0.35 V at pH = 1.25 to reach 0.8 V at pH = 6.85. Further increase of pH to higher values increase and steady the V_{OC} to a value of 0.85 V. Table 5.6 also shows the dependence of the J_{SC} of the fabricated devices on the morphology of the PAMAM-G2.5, it increased from 0.6 mA/cm^2 at pH = 1.25 to reach 35 mA/cm^2 at pH = 6.85. Further increase of pH to higher values decrease the J_{SC} to a value of 3.5 mA/cm^2. This can be explained by the large and highly branches units in acceptor layer at this pH=6.85. On the other hand, PAMAM G2.5 pH OHJ based devices behaved in the same trend with increasing pH as PAMAM G0.5 and PAMAM G1.5 pH OHJ based devices. At high pH (pH >10) none of the tertiary or interior tertiary amines protonated (neutral PAMAM-G2.5) which means there are no positive charges can bend the negative charges from the P3HT.Also, at this pH the morphology as it was mentioned before become globular and compact as the charge of the molecule becomes neutral. This explained the abrupt decrease in the J_{SC} at higher pH. On the other hand, at low pH (pH < 5) all the tertiary and interior tertiary amine groups of the PAMAM G2.5 dendrimer are protonated. Thus, electrostatic repulsion between tertiary and interior tertiary amine positively charged amines larger than the electrostatic attractive interaction between P3HT and PAMAM G1.5 result in low J_{SC} at this pH. Furthermore, at low pH of PAMAM G2.5 the branches tend to shrink due to electrostatic repulsion between tertiary and interior tertiary amine. It was found that the size of the PAMAM G2.5 dendritic increase from high to low pH reflecting swelling

due to the electrostatic phenomenon. However, at neutral pH (pH =6-9) all the tertiary amines protonated leading to create electric current at the interface with opposite material P3HT, then the electric current will flow through the solar cell device in order to encourage more electron to transfer from the donor (P3HT) to acceptor (PAMAM G2.5) and reduce the recombination of charge. From a morphology point of view, significant branch back-folding occurred at neutral pH (pH 6-9) in addition to major peripheral distribution of the terminal groups. Thus, complete existence of the branches and tree-like structure in the deposited acceptor layer at neutral pH (pH=6.85) may enhance the mobility and diffusion length of the electrons injected in the acceptor layer and thus facilitates its collection by the electrode.

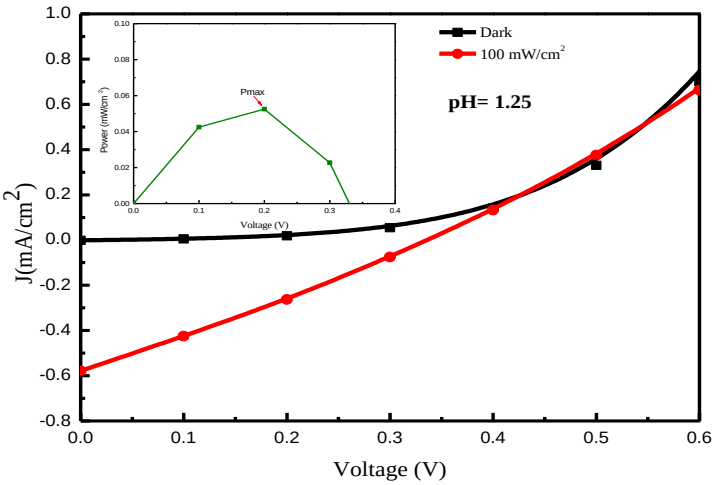

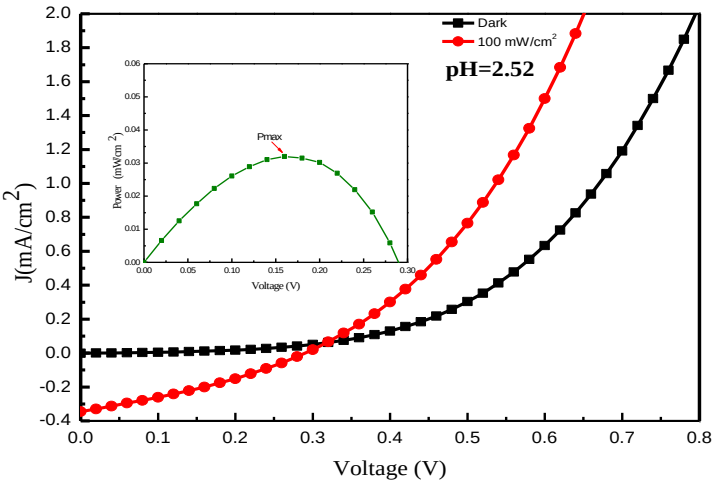
Dark
100 mW/cm2
pH=2.52
Pmax
Power (mW/cm 2)
Voltage (V)
J(mA/cm2)
Voltage (V)

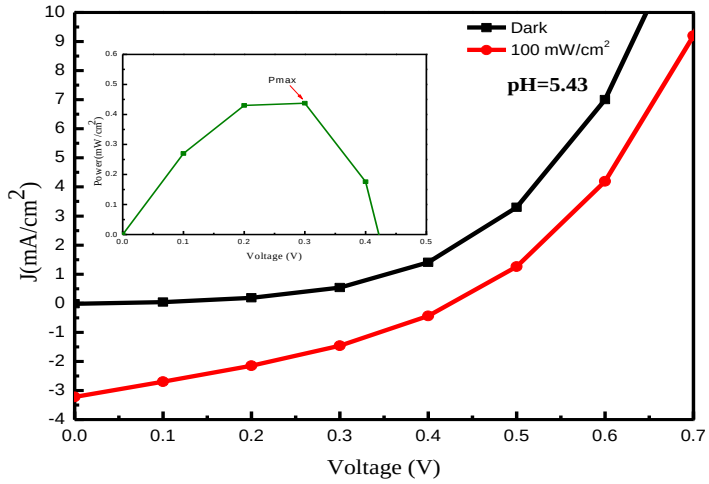
Dark
100 mW/cm2
pH=5.43
Pmax
Power(mW/cm2)
Voltage (V)
J(mA/cm2)
Voltage (V)

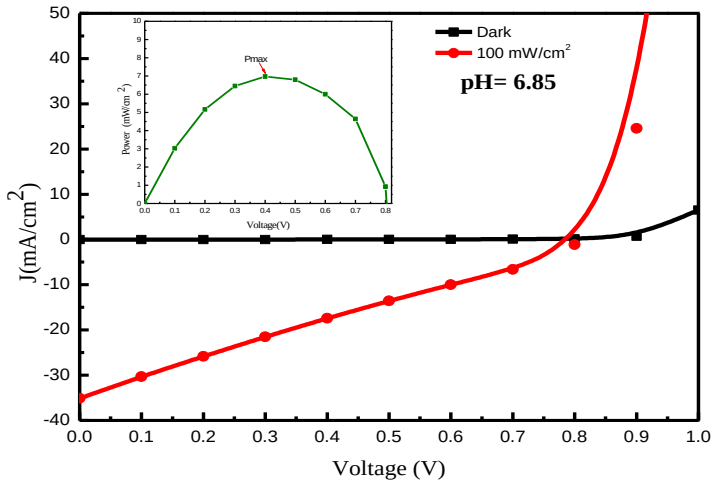
Dark
100 mW/cm2
pH= 6.85
Pmax
Power (mW/cm 2)
Voltage(V)
J(mA/cm2)
Voltage (V)

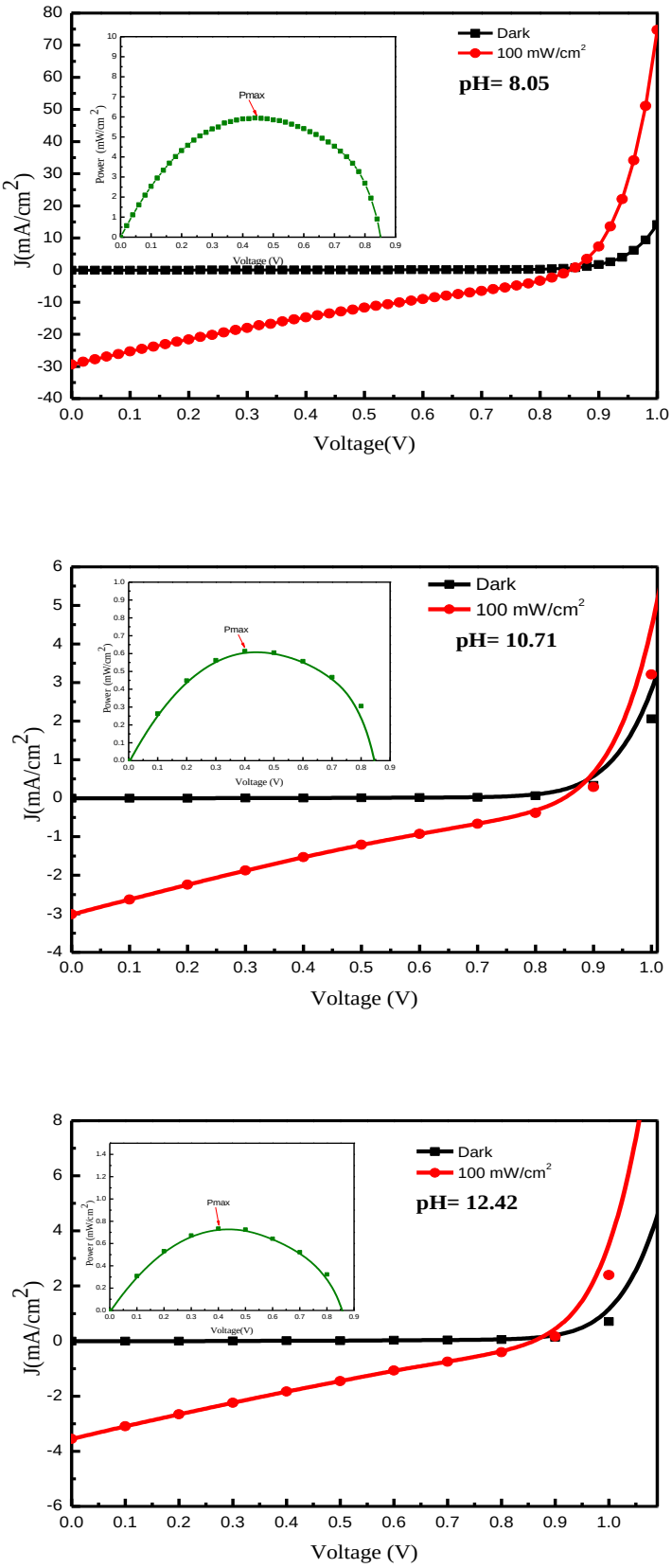

Figure 5.22: *Electrical characterisation of the PAMAM-G2.5/P3HT Based Organic Bilayer Devices at different pH concentrations of the PAMAM-G2.5 acceptor layer.*

The abrupt increase in the J_{SC} at pH=6.85 was reflected in P_{MAX} as shown in table 5.6, where the P_{MAX} had its highest value of 7 mW/cm^2 while it had much lower values at other pH values. The abrupt increase in the J_{SC} and P_{max} was reflected in the calculated efficiency also. The current density also increases when the series resistance reduced reaching 8.33 Ω (J_{SC}= 35 mA/cm^2) at pH= 6.85 (see Table 5.6).

The efficiency of PAMAM-G2.5 based device at neutral pH (PCE=7%) is higher than the efficiency of PAMAM-G0.5 (PCE=1.8%) and PAMAM-G1.5 (PCE=6.24%) at the same pH. As it was mentioned before this due to the increase in the number of tertiary amine and –COONa surface group when the generation increase from G0.5 to G2.5. This leads to generate more electrons through the device and increase the device efficiency.

PAMAM G2.5 pH	***V*OC (V)**	***J*SC(mA/cm^2)**	***P*MAX (mW/cm^2)**	***FF* (%)**	***PCE* (%)**	***R*S (Ω)**	***R*SH (Ω)**
1.25	**0.35**	**0.6**	**0.055**	**26**	**0.055**	**2000**	**4200**
2.52	**0.3**	**0.33**	**0.033**	**33**	**0.033**	**1190**	**1000**
5.43	**0.43**	**3.3**	**0.45**	**32**	**0.45**	**28**	**1250**
6.85	**0.8**	**35**	**7**	**25**	**7**	**8.33**	**167**
8.05	**0.85**	**30**	**6**	**24**	**6**	**11.90**	**185**
10.71	**0.85**	**3**	**0.6**	**23.5**	**0.6**	**83.3**	**1666**
12.52	**0.85**	**3.5**	**0.7**	**33.5**	**0.7**	**92**	**833**

Table 5.6: *The extracted and calculated photovoltaic parameters of the fabricated PAMAM G2.5 based devices under different pH conditions*

The plot of the calculated efficiency of the fabricated P3HT/ PAMAM G2.5-based bilayer devices versus the pH of the PAMAM-G2.5 acceptor layer is shown in Fig 5.23 It shows the abrupt increase in the efficiency at pH = 6.85 where the tertiary amine was positively charges and branches and tree-like structure of the PAMAM-G2.5 acceptor layer was formed which enhanced diffusion length and the efficient collection of the electrons by the electrodes. While at low and high PAMAM G2.5 pH when no branches exist the efficiency decreases one order of magnitude. As mentioned earlier this is directly related to repulsion force at low pH as the tertiary and interior tertiary amine was positively charges where at high pH PAMAM G2.5 become neutral uncharged.

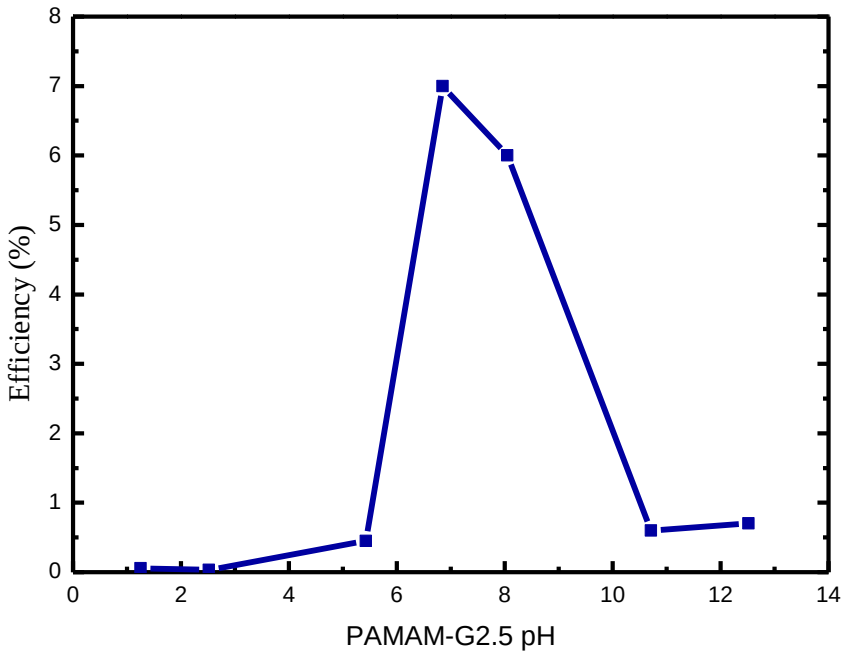

Figure 5.23: *The plot of the efficiency of the fabricated PAMAM-G2.5/P3HT-based bilayer devices versus the pH of PAMAM-G2.5.*

Figure 5.24 shows the dependence of open circuit voltage (V_{OC}) and current density (J_{SC}) on pH level of the PAMAM G2.5 material. It is clear from Fig. 5.24 (a) that V_{OC} increased linearly at low pH values and reaches maximum at about pH =8.05 then steady at 0.85 V at high pH values. Whereas, J_{SC} is very low at all pH values except for pH = 6.85 where the current density increased sharply.

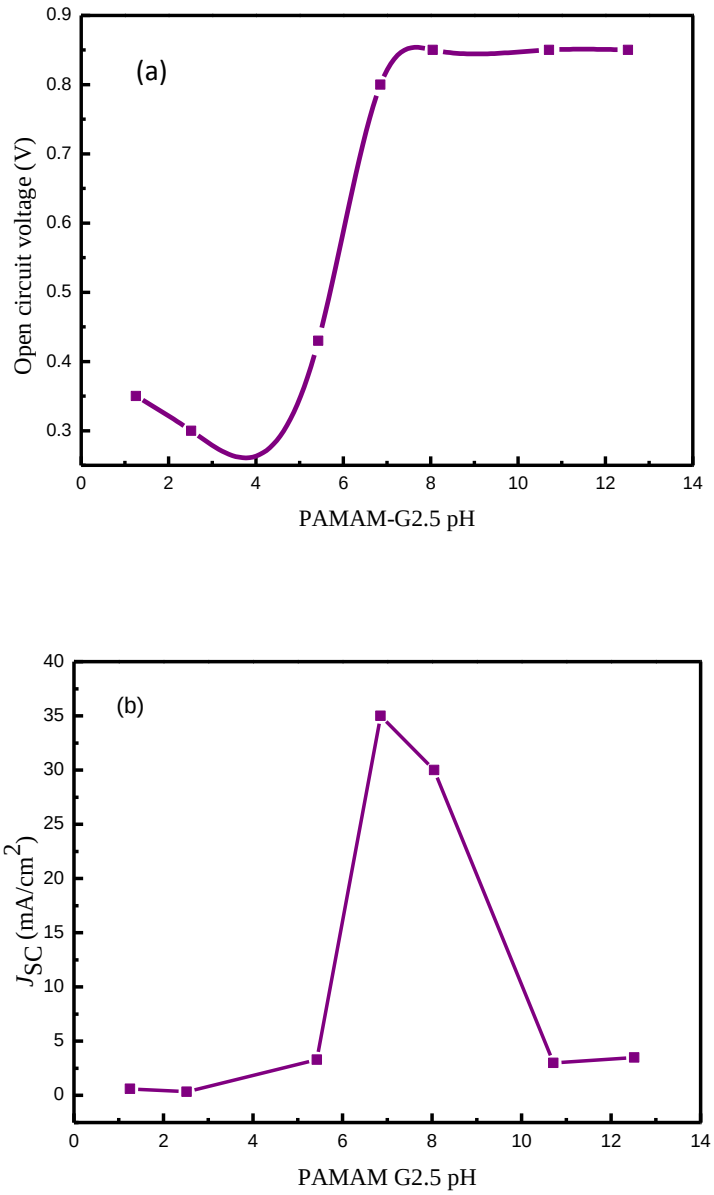

Figure 5.24: *The plot of (a) the open circuit voltage (b) the current density of the fabricated P3HT/PAMAM G2.5-based bilayer devices versus the pH of the PAMAM-G2.5.*

5.4.4 Optical Absorption measurement

Figure 5.25 present the UV-Vis spectrum (absorbance Vs wavelength) of PAMAM G2.5 at different pH conditions. At low pH, the absorption edge around 500 nm where the bandgap at this point 2.48 eV. The peak absorption at 440 nm (2.8 eV). On the other hand, around pH = 6-9 where the solution tends to be neutral, the absorption intensity increased reach the maximum at pH= 6.85-8.05. At this pH the absorption edge around 520 (2.38 eV) with a peak absorption at 460 nm (2.7 eV).

However, at basic solutions (high pH values), the absorption decrease the absorption edge around 510 (2.43 eV) with a peak absorption at 460 nm (2.7 eV). This due to protonation/deprotonation processes at different pH. It was mentioned previously that at low pH, when the tertiary and interior tertiary are protonated the repulsion force between them blocking or enabling electron transfer reactions between the P3HT and PAMAM-G2.5. As pH increased (neutral pH) the interior tertiary amine became deprotonated where tertiary amine protonated allowing electron transfer reactions between the P3HT and PAMAM-G2.5.

However, at high pH, the tertiary and interior tertiary amine became deprotonation which reduce electron transfer reactions between the P3HT and PAMAM-G2.5

This high efficiency OHJ solar cell based on PAMAM G2.5 at neutral pH attributed to the strong morphological changes with strong absorption at this pH.

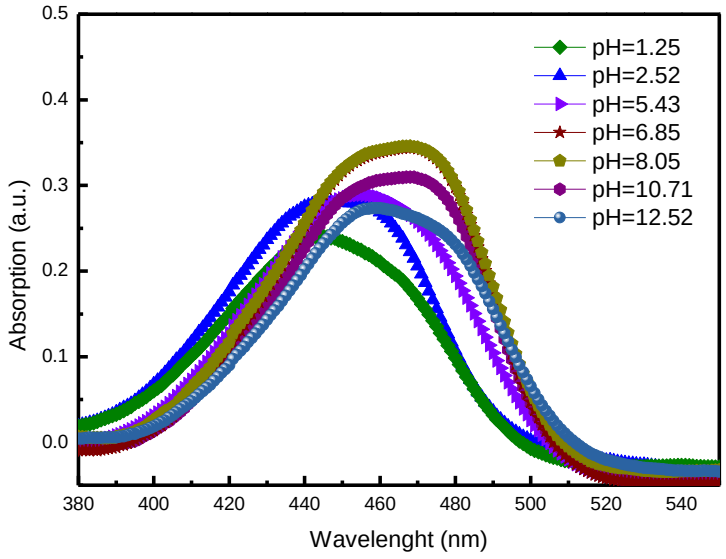

Figure 5.25: *Influence of pH on the absorption of PAMAM-G2.5.*

Table 5.7 show that changes in the PAMAM-G2.5 pH result in significant changes to the bandgap and morphology and provide a straightforward method for tuning the bandgap and morphology of PAMAM-G2.5 in the application of organic bilayer solar cells. At low pH, (pH <5) the bandgap was 2.48 eV. Increasing the pH to neutral level (pH 6-9) decrease the band gap to 2.38 eV. However, increasing the pH at high Values (pH> 10) results in increasing the band gap to be 2.43 eV. Thus, optimized the pH level of PAMAM-G2.5 is critical point in the organic bilayer device performance based on PAMAM-G2.5 pH as acceptor.

PAMAM-G2.5 pH	**Band gap (eV)**
1.25	2.48
2.52	2.48
5.43	2.43
6.85	2.38
8.05	2.38
10.71	2.43
12.52	2.43

Table 5.7: *The variation of PAMAM-G2.5 optical bandgap with different pH conditions.*

5.5 Acceptor–Acceptor Conjugated Copolymers Based OHJ solar cells

5.5.1 PAMAM G0- thienopyrroledione (TPD) based OHJ solar cells

The development of block copolymers for photovoltic applications has a long history, focuing on control donor-acceptor interfaces [35]. Alternative copolymers that comprise two different types of electronic moieties have become one of important classes in conjugated polymers. In the most cases, the backbone adopted one electron-rich and one electron-deficient unit due to their strong properties and ease of synthesis. In general Intramolecular charge transfer (ICT) interactions occur between electron-rich and electron-deficient units, where electron transfers from the electron-rich unit to electron-deficient unit. Thus, the electron-rich unit behaves as an electron donor (D), while the electron-deficient unit as an electron acceptor (A), and the copolymer is called a donor–acceptor (D–A) conjugated copolymer. One of the most successful strategies to develop low bandgap polymers is by combining electron-rich and electron-deficient units to form donor-acceptor (D-A) copolymer. The advantage of copolymer structures is that the photoelectronic properties including absorption spectra and energy levels can be easily tuned by combining different electron-rich and electron-deficient units as well as by introducing different side groups. As a result, D–A copolymers were used in a variety of applications including organic photovoltaics. Organic photovoltaics have achieved a huge progress in the past decade. The power conversion efficiency (PCE) has been enhanched from 3 to 5% before 2005 to reach nowadays over 9% [36].

However, alternative conjugated copolymers could combine two different electron-deficient units acceptor-acceptor copolymers (A–A copolymers). The advantages of this structure is to tune the frontier orbital energy levels effectively and enhance intermolecular charge-carrier hopping. Ober and coworkers reported an A–A copolymer based on 2-alkylbenzotriazole and 2,1,3-benzothiadiazole (BT) and demonstrated an electron mobility of 0.02 $cm^2 V^{-1} s^{-1}$ for its OFET devices [37].

On the other hand, conjugated polymers containing thienopyrroledione (TPD) as the electron acceptor unit are expected to enhance the charge transport properties compared with polymers without a TPD moiety [38]. Ma et al. reported a TPD-based polymer that achieved PCE of 6.17%. Posteriorly, Beaujuge et al. reported that through the optmazation of alkyl side-chain lengths on the same polymer backbone PCE of OPVs can be reach 8.5% [39]. TPD is very attractive due to its properites. It’s simple,

symmetric, compact, and planar structure, which is beneficial for electron delocalization when incorporated into conjugated polymers. Thus, conjugated polymers containing TPD units are expected to enhance charge transport properties compared with polymers without a TPD moiety. Therefore, TPD has recently obtained significant attention in the OPV applications and is being integrated into a number of different polymer systems [40-44].

As it was observed in chapter 4 that organic solar cells based on PAMAM full generations (G0,G1,G2) as acceptors exhibit non-photovoltaic behaviour under illumination of 100 mW/cm^2 white light. Thus, in this section the PAMAM G0 copolymerised with a thienopyrrolodione (TPD) accepting moiety as A-A copolymer structures in order to enhance their charge transport properties. PAMAMG0-TPD was used as electron acceptor component coupled with P3HT as donor in OHJ solar cells structure.

5.5.2 Fabrication process

The structure of the ITO/PEDOT: PSS/P3HT/PAMAM G0-TPD /TiO2/Al is shown in Figure 5.27. All fabrication conditions and experimental steps were the same as the previous PAMAM G0.5 based OHJ devices (shown in Section 5.2). The difference is in the acceptor layer. A–A copolymer (PAMAMG0-TPD) used as an acceptor layer instead of PAMAMG0.5.

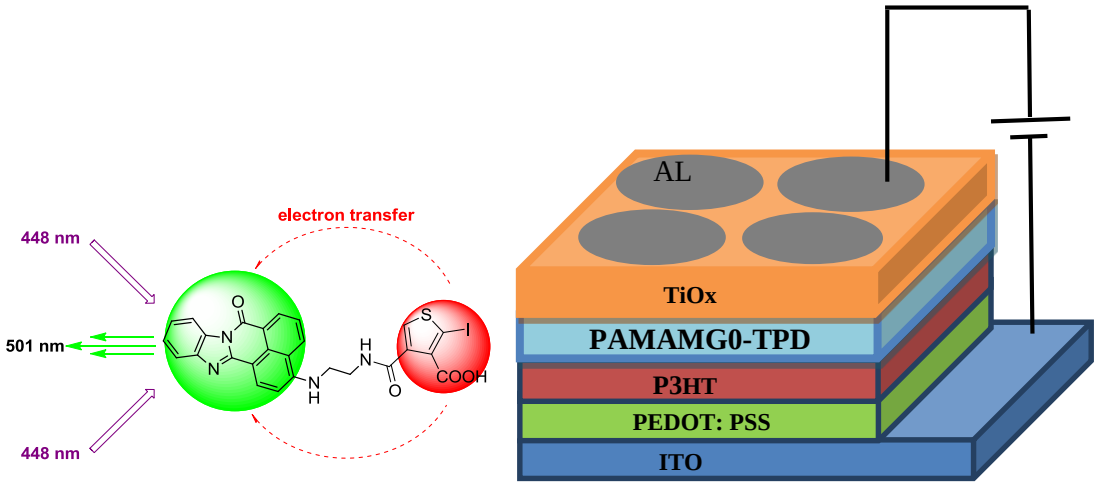

Figure 5.27: *PAMAM G0-TPD chemical structure and Schematic diagram of PAMAM G0-TPDbased OHJ solar cells*

5.5.3 Surface morphology

Copolymers can yield diverse ordered structures of morphologies, including spheres, cylinders, bicontinuous structures, lamellae, vesicles, and many other complex or hierarchical assemblies. These aggregates provide potential applications in many fields including solar cells [45]. Figure 5.28 show optical image of the PAMAMG0-TPD on top of P3HT layer. The optical image shows high density of interpenetrating network structure spread on the whole surface.

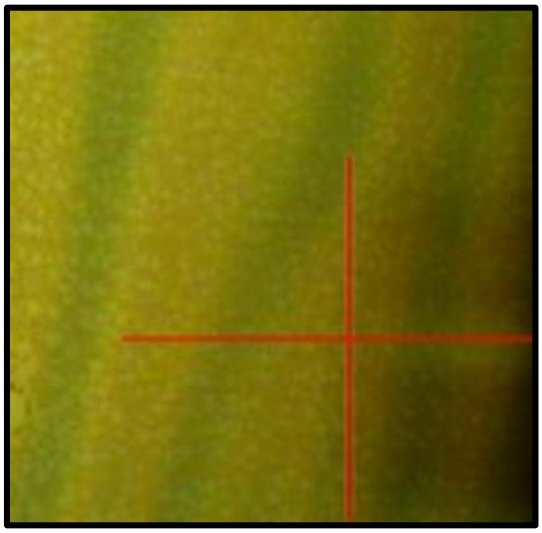

Figure 5.28: *Optical image of PAMAM G0-TPD on top of the P3HT layer.*

However, the Morphology of PAMAMG0-TPD (fig.5.29) show structure between grains-like with different sizes and interpenetrating network structure. It is clear that the copolymers incorporating two acceptors (PAMAMG0-TPD) showed self-assembly characteristics similar to those of diblock copolymers (D-A copolymer). It was reported that interpenetrating networks can ensure the efficient charge separation and transport required in polymer solar cells devices [46, 47].

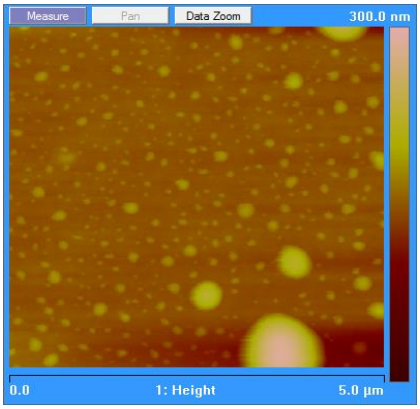

Figure 5.29: *AFM morphology images of PAMAM G0-TPD acceptor layer on top of P3HT layer.*

5.5.4 Electrical characterisation

J-V characteristics of the PAMAMG0-TPD based devices are shown in Fig. 5.30. First, the device was tested with ITO/PEDOT:PSS/PAMAMG0-TPD/TiOx/Al structure without adding P3HT (Fig.5.30 (a)) and then it was tested again when P3HT was added as donor layer with the structure ITO/PEDOT:PSS/P3HT/PAMAMG0-TPD/TiOx/Al (fig.5.30.(b)). The device parameters are summarized in Table 5.8. The device based on PAMAMG0-TPD without P3HT as active layer exhibit clear photovoltaic behaviour with a PCE of 0.0034%, J_{SC} of 0.0133 mA, V_{OC} is 0.7 V and *FF* is 36%.

However, the device performance was remarkably improved when the P3HT was added as donor layer and PAMAMG0-TPD serve as acceptor. The device produced an open circuit voltage, V_{OC}, ~ 0.79V, short-circuit current density, J_{SC},~20 mA/ cm^2 with fill factor of ~27 % and P_{MAX} 4.5 mW/cm^2 yielding a power conversion efficiency of 4.5 %.

In chapter 4, it was observed that PAMAM G0 based device exhibit non-photovoltaic behaviour, however when the PAMAMG0 copolymerise with TPD as A-A copolymer, electron transfer enhanced due to the present of TPD moity in PAMAMG0-TPD structure. However, the device performance based on PAMAMG0-TPD only as active layer achieved very low efficiency. On the other hand, when P3HT as donor combined with PAMAMG0-TPD as acceptor in OHJ solar cells the PCE performance was remarkably improved to reach 4.5%. This confirm that PAMAMG0-TPD serve as A-A

copolymer structures. Moreover, these results demonstrated the potential to use PAMAM-TPD based conjugated copolymers as acceptor component for organic solar cells.

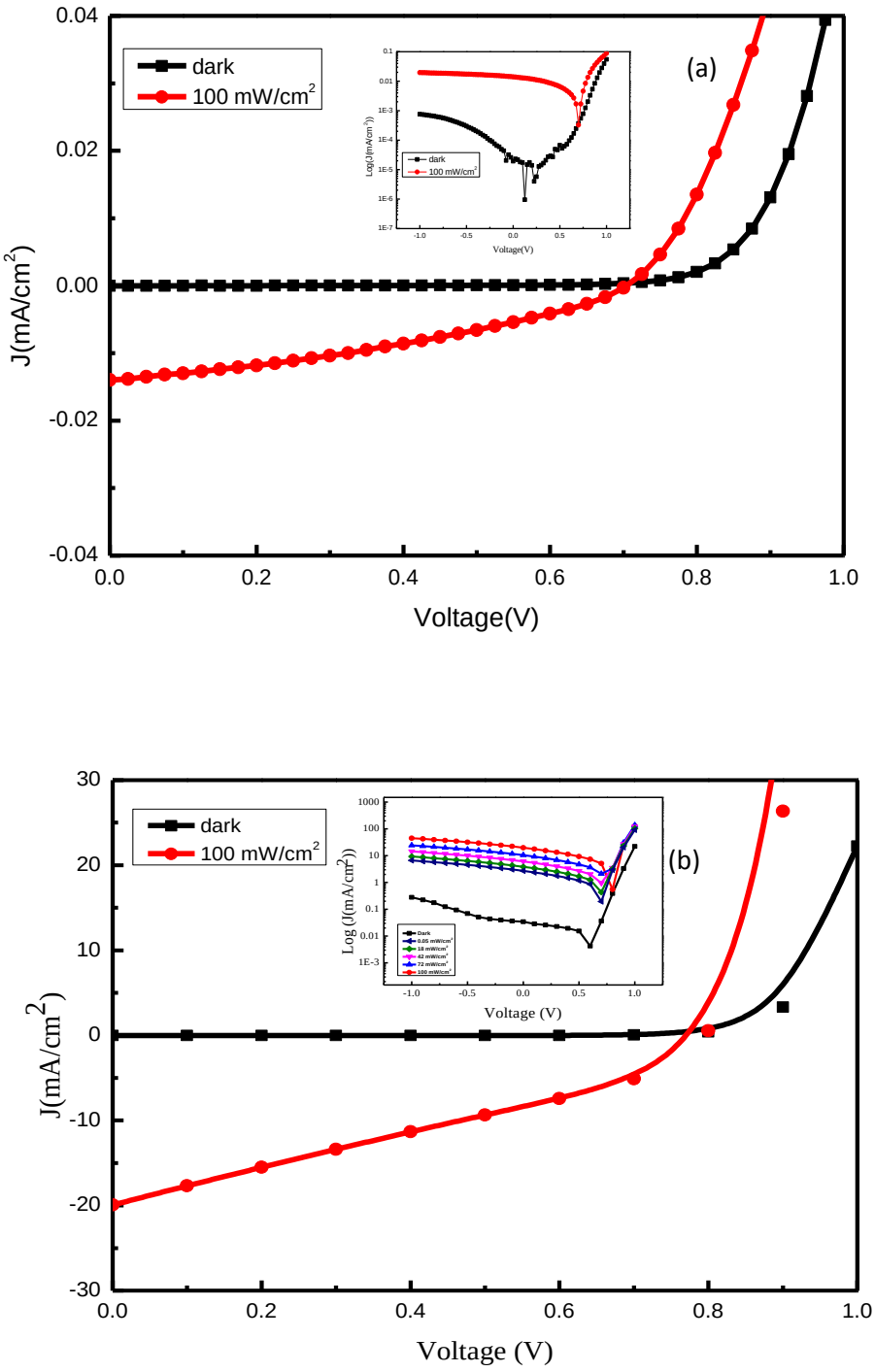

Figure 5.30: *Electrical characterisation of the PAMAMG0-TPD Based Organic solar cells Devices a) before adding the P3HT,b) after adding P3HT as donor.*

Device	V_{OC} (V)	J_{SC}(mA/cm^2)	P_{MAX} (mW/cm^2)	FF (%)	*PCE* (%)	R_S Ω	R_{SH} Ω
PAMAMG0-TPD	**0.7**	**0.0133**	**0.0034**	**36**	**0.0034**	**28571**	**1M**
P3HT/ PAMAMG0-TPD	**0.79**	**20**	**4.5**	**27**	**4.5**	**9**	**400**

Table 5.8: *The extracted and calculated photovoltaic parameters of the fabricated PAMAM 0-TPD based devices*

5.5.5 Optical Absorption measurement

UV-Vis spectrum (absorbance Vs wavelength) of PAMAMG0-TPD shown in Fig. 5.31. As it was mentioned in chapter 4 PAMAM G0 absorption edge at 500 nm where the bandgap at this point 2.5 eV. A peak absorption at 440 nm (2.8 eV). However, PAMAM G0-TPD has the same bandgap and absorption edge. However, PAMAMG0-TPD peak absorption at 450 nm (2.7 eV). Also, PAMAMG0-TPD has higher absorption intensity than PAMAMG0. Fig5.31 shows the UV–visible absorption spectra of the materials used for OHJ solar cells based on P3HT/PAMAM G0-TPD as an acceptor. For OHJ device with the structure of ITO/PEDOT: PSS/P3HT: PAMAM G0-TPD /TiOx/Al the absorption edge shifts to ~650nm (1.9 eV) as a result of absorption in the P3HT.

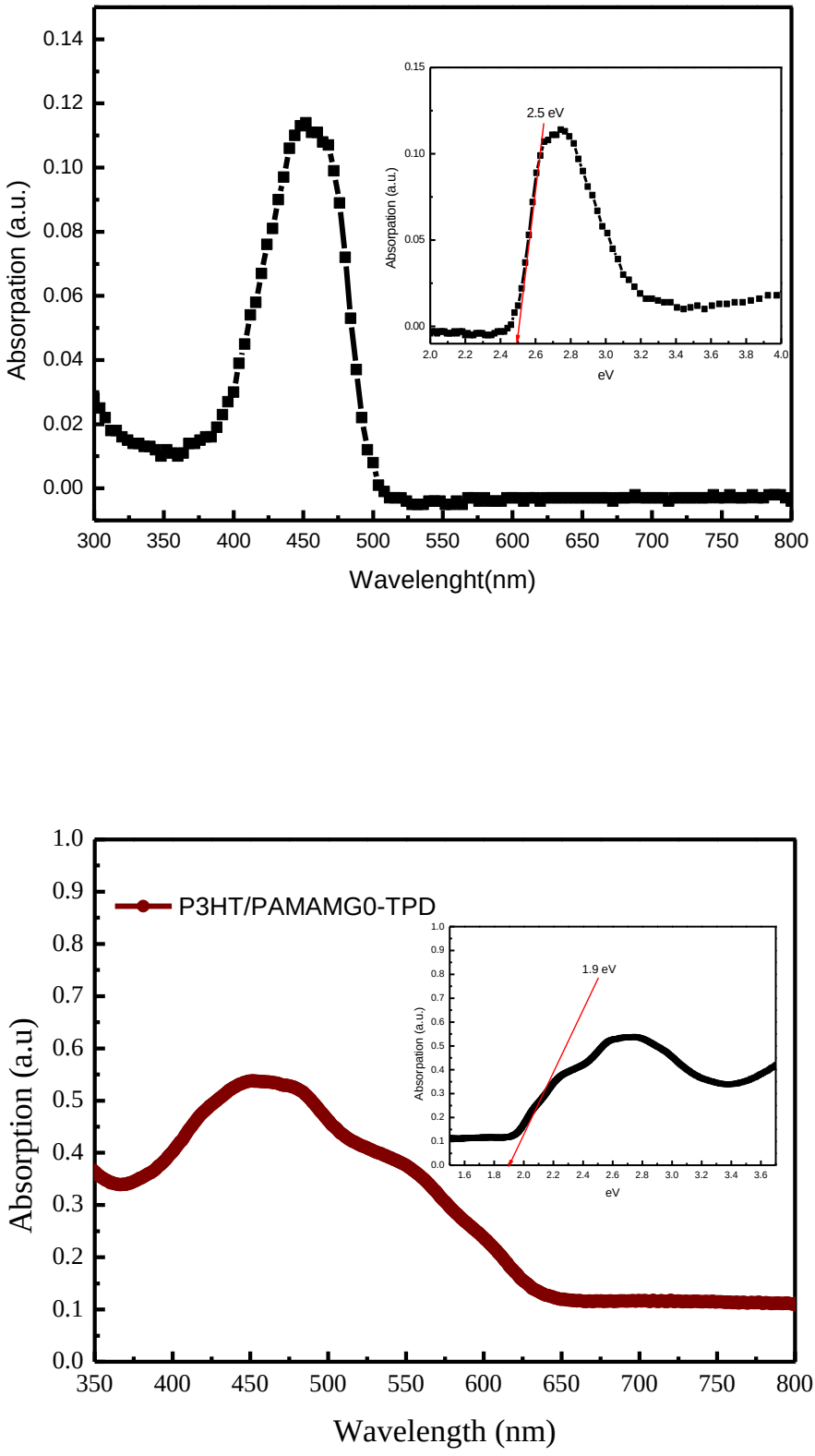

Figure 5.31: *The optical absorption of the PAMAMG0-TPD based solar cells*

5.6 Summary

This chapter aimed to investigate the effect of generation size of new PAMAM dendritic acceptor materials (G 0.5, G 1.5, and G2.5) at different pH on the performance of organic bilayer heterojunction solar cells. It was observed that increasing PAMAM dendritic generation from G0.5 to G2.5 influence significantly the bilayer OHJ solar cells efficiency as the surface group doubled with every increase in generation. Power-conversion efficiencies (PCE) of 7 % were achieved at the natural PAMAM G2.5 pH 6.85. This is attributed to the fact that all tertiary amines in PAMAM G2.5 dendritic are positively charged at the natural pH, while in the low pH < 5 all tertiary and interior tertiary molecules positively charged leading to a strong electrostatic repulsion between them. Atomic force microscopy shows that PAMAM morphology changes with changing the generation and pH values. The effective charges which interact with an external electric field or other charges were found to increase with increasing generation of the dendrimers at neutral pH. Thin films of PAMAM at neutral pH exhibits a major peripheral distribution. At low pH <5, it was found to be shrank to smaller sizes. The organic bilayer solar cell performance change dramatically with changing PAMAM generation size and their pH conditions. The improved performance seen with PAMAM G2.5 at natural pH is due to the number of surface group and tertiary amines in the dendrimer increases with generation size. At neutral pH dendrimers afford a more elongated dendrimer morphology able to interact more with other molecules while at high and low pH, the "contracted" dendrimer morphology decreases the possibility of reaction with other molecules.

Also, in this chapter the PAMAM G0 copolymerised with a thienopyrrolodione (TPD) accepting moiety as A-A copolymer structures was investigated in order to enhance charge transport properties. PAMAMG0-TPD was used as electron acceptor component coupled with P3HT as donor in OHJ solar cells structure. The device produced an open circuit voltage, V_{OC}, ~ 0.79V, short-circuit current density, J_{SC}, ~ 20.83 mA/ cm^2 with fill factor of ~27 % and P_{max} of 4.5 mW/cm^2 yielding a power conversion efficiency of 4.5 %. This result demonstrated the potential to use PAMAM-TPD based conjugated copolymers as acceptor component for organic solar cells.

References

[1] A. Ayzner, C. Tassone, S. Tolbert, and B. Schwartz, ' Reappraising the Need for Bulk Heterojunctions in Polymer-Fullerene Photovoltaics: The Role of Carrier Transport in All-Solution-Processed P3HT/PCBM Bilayer Solar Cells ', *The Journal of Physical Chemistry C*, Vol. 113, PP. 20050–20060, **2009.**

[2] K. Lee, P. Schwenn, A. Smith, H. Cavaye , P. Shaw , M. James , K. Krueger , I. Gentle , P. Meredith , and P. Burn., ' Morphology of All-Solution-Processed "Bilayer" Organic Solar Cells ', *Advanced materials*, Vol. 23, pp. 766–770, **2011.**

[3] D. Stevens, Y. Qin, M. Hillmyer, and C. Frisbie, ' Enhancement of the Morphology and Open Circuit Voltage in Bilayer Polymer/Fullerene Solar Cells ', *The Journal of Physical Chemistry C*, Vol. 133, pp. 11408–11415, **2009.**

[4] S. Veenstra, J. Loos, and J. Kroon, ' Nanoscale Structure of Solar Cells Based on Pure Conjugated Polymer Blends ', *progress in photovoltaics: research and applications*, Vol.15, pp. 727–740, **2007.**

[5] J. Amonoo, A. Li, G. Purdum, M.Sykes, B. Huang, E. Palermo, A. McNeil, M. Shtein, Y. Loo and P. Green., ' An all-conjugated gradient copolymer approach formorphological control of polymer solar cells ', *Journal of Materials Chemistry A*, Vol.3,pp. 20174– 20184, **2015.**

[6] T. Benanti and D. Venkataraman., ' Organic solar cells: An overview focusing on active layer morphology ', *Photosynthesis Research*, Vol. 87, pp. 73-81, **2006.**

[7] J. Kim, J. Jung, S. Williams, F. Liu, T. Russell and A. Jen., ' Enhanced crystalline morphology of a ladder-type polymer bulk-heterojunction device by blade-coating ', *Nanoscale*, Vol. 7,pp. 10936–1093,**2015.**

[8] F. Liu, C. Wang, J. Baral, L. Zhang, J. Watkins, A. Briseno, and T. Russell, ' Relating Chemical Structure to Device Performance via Morphology Control in Diketopyrrolopyrrole-Based Low Band Gap Polymers ', *Journal of the American Chemical Society*, Vol. 135,pp. 19248−19259, **2013.**

[9] S. Park, S. Kim, K. Kim, H. Joe, B. Jung, E. Kim, W. Kim, B. Min and J. Hwang., 'Fabrication of ordered bulk heterojunction organic photovoltaic cells using nanopatterning and electrohydrodynamic spray deposition methods ', *Nanoscale*, Vol. 4, pp. 7773–7779, **2012.**

[10] P. Maiti, T. Cagin, S. Lin, and W.Goddard., 'Effect of Solvent and pH on the Structure of PAMAM Dendrimers ', *Macromolecules*, Vol. 38, pp. 979-991,**2005.**

[11] M. Kleinman, J. Flory, D. Tomalia, and N. Turro., ‘Effect of Protonation and PAMAM Dendrimer Size on the Complexation and Dynamic Mobility of 2-Naphthol ’, *American Chemical Society B,* Vol. 104(48), pp. 11472–11479, **2000.**

[12] Y. Liu, V. Bryantsev, M. Diallo and W. Goddard., ‘PAMAM Dendrimers Undergo pH Responsive Conformational Changes without Swelling’, *American Chemical Society,* Vol. 131(8), pp. 2798–2799, **2009.**

[13] N. Geitner, B. Wang, R. Andorfer, D. Ladner and P.Ke., ‘The structure-function relationship of PAMAM dandrimers as robust oil dispersants’. *Environmental Science & Technology (ACS Publications),* Vol. 48 (21), pp.12868–12875, **2014.**

[14] S. Lin, P. Maiti, and W. Goddard, ‘Dynamics and Thermodynamics of Water in PAMAM Dendrimers at Subnanosecond Time Scales’, *The Journal of Physical Chemistry B,* Vol. 109, pp.8663-8672, **2005.**

[15] E. Fernandez, P. Paulo and S. Costa., ‘Evaluation of electrostatic binding of PAMAM dendrimers and charged phthalocyanines by fluorescence correlation spectroscopy’, *Physical Chemistry Chemical Physics,* Vol. 17, pp. 4319-4327, **2015.**

[16] D. Lombardo., ‘Modeling Dendrimers Charge Interaction in Solution: Relevance in Biosystems’, *Biochemistry Research International,* Vol. 2014, pp 1-10, **2014.**

[17] Q. Liu, J. Tian, C. Zhang, H. Yang, Y. Liu, W. Qin, Z. Liu., ‘Cationic poly(amidoamine) dendrimers as additives for capillary electroseparation and detection of proteins’, *Electrophoresis,* Vol. 32, pp. 1302–1308, **2011.**

[18] W. Chen, D. Tomalia, and J. Thomas., ‘Unusual pH-Dependent Polarity Changes in PAMAM Dendrimers: Evidence for pH-Responsive Conformational Changes’, *Macromolecules,* Vol. 33, pp. 9169-9172, **2000.**

[19] K. Karatasos, P. Posocco, E. Laurini, S. Pricl., ‘Poly(amidoamine)-based Dendrimer/siRNA Complexation Studied by Computer Simulations: Effects of pH and Generation on Dendrimer Structure and siRNA Binding’, *macromolecular bioscience,* Vol. 12, pp. 225-240, **2012.**

[20] S. Kim and M. Lamm., ‘Multiscale Modeling for Host-Guest Chemistry of Dendrimers in Solution’, *Polymers,* Vol. 4, pp. 463-485, **2014.**

[21] D. Lee, Y. Yang, J. You, E. Richard and G. Li., ‘Immiscible solvents enabled nanostructure formation for efficient polymer photovoltaic cells’, *Nanotechnology,* Vol.25, pp. 1-7, **2014.**

[22] B. Yang, Y. Yuan, and J. Huang., ʻReduced Bimolecular Charge Recombination Loss in Thermally Annealed Bilayer Heterojunction Photovoltaic Devices with Large External Quantum Efficiency and Fill Factor', *Journal of Physical Chemistry C*, Vol.118, pp. 5196−5202, **2014.**

[23] Y. Xiao, L. Shao, T. Chung, and D. Schiraldi., ʻEffects of Thermal Treatments and Dendrimers Chemical Structures on the Properties of Highly Surface Cross-Linked Polyimide Films', *Industrial and Engineering Chemistry Research*, Vol. 44., pp. 3059-3067, **2005.**

[24] M. Zhao, Y. Liu, R. Crooks, and D. Bergbreiter., ʻPreparation of Highly Impermeable Hyperbranched Polymer Thin-Film Coatings Using Dendrimers First as Building Blocks and Then as in Situ Thermosetting Agents', *Journal of the American Chemical Society*, Vol. 121, pp. 923-930, **1999.**

[25] D. Astruc, E. Boisselier, and C. Ornelas., ʻDendrimers Designed for Functions: From Physical, Photophysical, and Supramolecular Properties to Applications in Sensing, Catalysis, Molecular Electronics, Photonics, and Nanomedicine', *Chemical Reviews*, Vol. 110, pp. 1857–1959, **2010.**

[26] A. Sharma, D. Mohanty, A. Desai, and Riaz Ali., ʻA simple polyacrylamide gel electrophoresis procedure for separation of polyamidoamine dendrimers' *Electrophoresis*, Vol. 24, pp. 2733–2739, **2003.**

[27] K. Kono., ʻDendrimer-based bionanomaterials produced by surface modification, assembly and hybrid formation', Polymer *Journal*, Vol. 44, pp. 531-540, **2012.**

[28] T. Garg, O. Singh, S. Arora, and R. Murthy., ʻDendrimer-a novel scaffold for drug delivery', Vol.7(2), pp. 211-220, **2011.**

[29] L. Zhao, and Z. Lin., ʻSelf-assembly of non-linear polymers at the air/water interface: the effect of molecular architecture', *Soft Matter*, Vol.7, pp. 10520–1053, **2011.**

[30] S. Lalwani, A. Chouai, L. Perez, V. Santiago, S. Shaunak, and E. Simanek., ʻMimicking PAMAM Dendrimers with Ampholytic, Hybrid Triazine Dendrimers: A Comparison of Dispersity and Stability', *Macromolecules*, Vol. 42(17), pp. 6723–3732, **2009.**

[31] H. Crampton, E. Hollink, L. Perez, and E. Simanek., ʻA divergent route towards single-chemical entity triazine dendrimers with opportunities for structural diversity', *New Journal of Chemistry*, Vol. 31(7), pp. 1283–1290, **2007.**

[32] J. Ribierre, C. Yates, A. Ruseckas, S. Staton, P. Burn, and I. Samuel., ʻEffects of solution processing and thermal annealing on the phosphorescence of iridium (III) complex-cored dendrimer films', *Organic Electronics,* Vol. 11(1), pp. 26-66, **2010.**

[33] D. Astruc., ʻElectron-transfer processes in dendrimers and their implication in biology, catalysis, sensing and nanotechnology', *Nature Chemistry*, Vol. 4, pp. 255–267, **2012.**

[34] N. Suek and M. Lamm., ʻComputer Simulation of Architectural and Molecular Weight Effects on the Assembly of Amphiphilic Linear−Dendritic Block Copolymers in Solution', *Langmuir,* Vol. 24, pp. 3030-3036, **2008.**

[35] Y. Lee, and E. Gomez., ʻChallenges and Opportunities in the Development of Conjugated Block Copolymers for Photovoltaics', *Macromolecules,* Vol. 2015, pp. 1-11, **2015.**

[36] C. Ge, C. Mei, J. Ling, J. Wang, F. Zhao, L. Liang, H. Li, Y. Xie, and W. Li., ʻAcceptor–Acceptor Conjugated Copolymers Based on Perylenediimide and Benzothiadiazole for All-Polymer Solar Cells', *Journal of polymer science, part A: polymer chemistry,*Vol.52(8), pp. 1200- 1215, **2014.**

[37] H. Bronstein, Z. Chen, R. Ashraf, W. Zhang, J. Du, J. Durrant, P. Tuladhar, K. Song, S. Watkins, Y. Geerts, M. Wienk, R. Janssen, T. Anthopoulos, H. Sirringhaus, M. Heeney and I. McCulloch., ʻThieno 3,2-b thiophene-Diketopyrrolopyrrole-Containing Polymers for High-Performance Organic Field-Effect Transistors and Organic Photovoltaic Devices', Vol. 133(10), pp. 3272-3275, **2011.**

[38] Y. Cheon, Y. Kim, J. Ha, M. Kim, C. Park, and Y. Kim., ʻTPD-Based Copolymers with Strong Interchain Aggregation and High Hole Mobility for Efficient Bulk Heterojunction Solar Cells', *Macromolecules,* Vol. 47, pp. 8570−8577, 2014.

[39] J. Kim, J. Park, F. Xu, D. Kim, J. Kwak, A. Grimsdale, and D. Hwang., ʻEffect of π-conjugated bridges of TPD-based medium bandgap conjugated copolymers for efficient tandem organic photovoltaic cells', *Energy & Environmental Science,* Vol. 7, pp. 4118– 4131, **2014.**

[40] J. Jiang, M. Yuan, K. Dinakaran, A. Hariharan and K. Wei., ʻCrystalline donor-acceptor conjugated polymers for bulk heterojunction photovoltaics', *Journal of Materials Chemistry A,* Vol. 1, pp. 4415–4422, **2013.**

[41] X. Hu, M. Shi, , L. Zuo, Y. Nan, Y. Liu, L. Fu, and H. Chen., ʻSynthesis, characterization, and photovoltaic property of a low band gap polymer alternating dithienopyrrole and thienopyrroledione unitsʼ, *Polymer*, Vol. 52(12), pp. 2559–2564, **2011.**

[42] Y. Zou, A. Najari, P. Berrouard, S. Beaupré, B. Aïch, Y. Tao, and M. Leclerc., ʻA Thieno[3,4-c]pyrrole-4,6-dione-Based Copolymer for Efficient Solar Cellsʼ, *Journal of the American Chemical Society*, Vol. 132(15), pp. 5330–5331, **2010.**

[43] Y. Hwang,T. Earmme, S. Subramaniyan and S. Jenekhe., ʻSide chain engineering of n-type conjugated polymer enhances photocurrent and efficiency of all-polymer solar cellsʼ, *Chemical Communications*, Vol. 50, pp. 10801-10804, **2014.**

[44] C. Small, S. Chen, J. Subbiah, C. Amb, S. Tsang, T. Lai, J. Reynolds, and F. So., ʻHigh-efficiency inverted dithienogermole–thienopyrrolodione-based polymer solar cellsʼ, *Nature Photonics*, Vol. 6, pp. 115-120, **2012.**

[45] Y. Maia and A. Eisenberg., ʻSelf-assembly of block copolymersʼ, *Chemical Society Reviews*, Vol. 41, pp. 5969-5985, **2012.**

[46] R. Singh, and O. Kushwaha., ʻ Polymer Solar Cells: An Overviewʼ, *Macromolecular Symposia*, Vol. 327, pp. 128–149, **2013.**

[47] J. Amonoo, A. Li, G. Purdum, M. Sykes, B. Huang, E. Palermo, A. McNeil, M. Shtein, Y. Looc and P. Green., ʻ An all-conjugated gradient copolymer approach for morphological control of polymer solar cellsʼ, *Journal of Materials Chemistry*, Vol. 3, pp. 20174-20184, **2015.**

Chapter 6

Organic Tandem Solar Cells

6.1 Introduction

The major losses occurring in single junction solar cells are the sub-band gap transmission and the thermalization of hot charge carriers. However, the multi-junction solar cell structures, where two or further sub-cells with complementary absorption are connected in series or parallel, provide an excellent approach to overcome the single junction limitations of organic solar cells and improve their power conversion efficiency [1-4]. Nowadays, PCE of 10% are reached for organic tandem cells [5-7]. This efficiency is about the same as the efficiency of a single-junction organic cell which indicate that development in the field of multi-junction organic solar cells is still possible.

In this chapter the fabrication and characterisation of three different organic tandem solar cells (OSCs) based on titanium oxide intermediate layer are investigated. The bottom cell active layer is P3HT:IC70BA as bulk-heterojunction layer for all three tandem devices. However, the top cell consists of P3HT as the donor layer in bilayer heterojunction for all three tandem devices with different acceptor layer. The three acceptors used in the top layer are PAMAM-G1.5 at neutral pH (7.03), PAMAM-G2.5at neutral pH (6.39), PAMAM-G0-TPD. These three acceptors exhibit the highest efficiency in the previous chapters.

The current density–voltage *(J-V)* characteristics for these devices were measured in the dark and under illumination with a halogen lamp. The experimental details, surface morphology, electrical characteristics and optical absorption measurement of each of these devices are presented and discussed in this chapter.

6.2 PAMAM G1.5 based organic tandem solar cells

6.2.1 Fabrication process

Fabrication of organic tandem solar cells with the structure of ITO/PEDOT: PSS/P3HT:IC70BA/TiOx/PEDOT (pH500)/P3HT/PAMAMG1.5 (pH= 7.03)/TiOx/Al is explained in this section. Organic tandem solar cell with same donor (P3HT) in sub cells but with different acceptor (IC70BA in bottom cell and PAMAM G1.5 (PH=7.03) on top cells) is shown in the Fig. 6.1. A P3HT:IC70BA cell showing high open-circuit voltage (V_{OC}) (chapter 4) was employed as the bottom cell and a P3HT: PAMAM G1.5 cell showing high short-circuit current (J_{SC}) (chapter 5) is employed as the top cell.
The bottom cell was processed on an ITO substrate covered by a 40 nm thick layer of PEDOT: PSS (Baytron P). The active layer of the bottom cell was prepared by spin coating the blend solution of P3HT/IC70BA (1:1 w/w) in dichlorobenzene (DCB) with a spin coating of 900 rpm for 60 sec. The active layer was thermally annealed at 150 ℃ for 10 min. Then, for the separation layer, TiOx precursor solution in methanol was spin-cast at 5000 rpm for 20 second with thickness ~20 nm in air. After 10 minutes in air at 80°C, the precursor is converted to TiOx by hydrolysis. For the second charge separation layer of the tandem cell, highly conductive PEDOT: PSS (Baytron PH500) was spin-cast (5000 rpm) for 40 second with thickness ~40 nm and moved into a glove box to dry for 10 minutes at 120°C. For the top cell active layer the P3HT was spin-cast with thickness of 100 nm on top of the PEDOT layer then, the acceptor G1.5 (7.03 pH) was spin-cast on the top of the P3HT spin-cast at 700 rpm for 60 second with the thickness of 70 nm. Then, for the electron transport layer of second charge separation layer, TiOx precursor solution in methanol was spin-cast with thickness ~20 nm in air. During 10 minutes in air at 80°C, the precursor converts to TiOx by hydrolysis. Finally, the device was pumped down in vacuum (~10^{-7} torr), and a ~100 nm Al electrode was deposited on top. The deposited Al electrode area defines an active area of the devices as 0.12cm^2.All films preparation and materials evaporation technique were discussed in chapter 3.

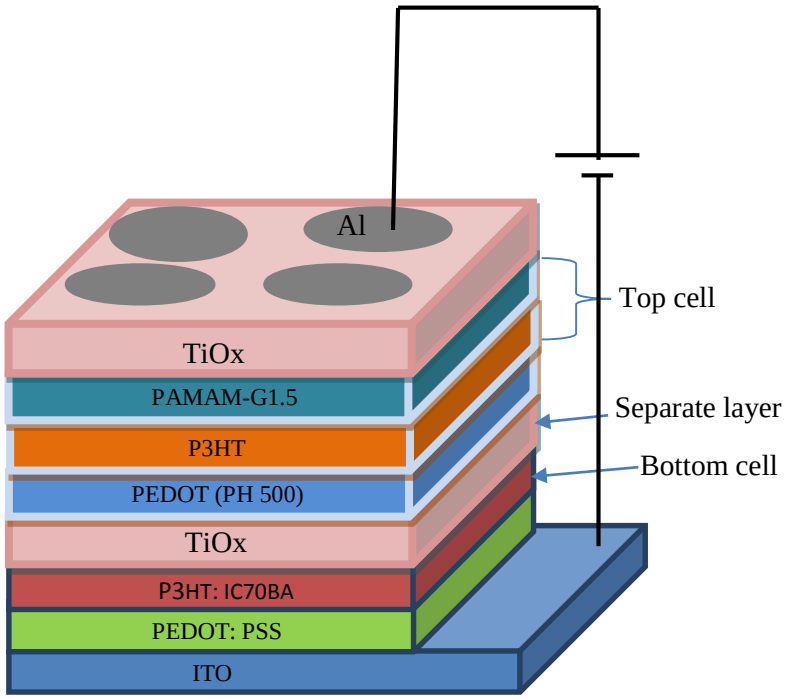

Figure 6.1: *The structure of organic tandem solar cell based on PAMAM-G1.5 (pH= 7.03) as acceptor layer in the top cell: the structure of the tandem cell is:*

6.2.2 Surface morphology

In tandem OSCs, the intermediate layer is crucial and should have low electrical resistance, high optical transparency in the visible and infra-red range, low barriers for both electron and hole extractions, easy-fabrication process, and the protection for the prior-deposited active layer in solution-processed tandem OSCs [8].

In 2007, Kim et al. reported a highly efficient tandem solar cell with titanium oxide (TiOx) /PEDOT:PSS as intermediate layers [9,10]. It is considered advancement in solution processed tandem solar cell research with a PCE of 6.5% being recorded. The inorganic TiOx layer can block physical or chemical damage during the subsequent solution processing, and it is robust to postponement the penetration of oxygen and moisture. TiOx layer is insensitive to the acidity of the PEDOT:PSS. It offer large freedom in the design and fabrication of solution processed multijunction devices. The TiOx layer was fabricated by a low temperature sol-gel process (a temperature of 150^0C was required for annealing), which is compatible with the annealing of the polymer: PCBM blends [10].

Figure 6.2 shows the surface morphology (tapping mode AFM images) of the active layer of the bottom cell (P3HT:IC70BA) before depositing the intermediate layer, TiOx on top of the bottom cells, PEDOT:PSS on the top of TiOx, P3HT the donor layer of the top cell active layer, and PAMAM-G1.5 (PH=7.03) the acceptor layer of the top cell on top of the P3HT layer. TiOx film display a rather smooth surface with a root-mean-square (RMS) surface roughness of 0.703 nm. Obviously, the deposited TiOx layer (20 nm) does not cause an increase in surface roughness (0.740 nm) which means there is no interlayer mixing. It is clear from Fig. 6.2 that Multilayer morphologies demonstrated sharp interfaces with no evidence of interlayer mix. Thus, the TiOx layer work as an electron transport and collecting layer for the first cell and as a stable foundation that allows the fabrication of the second cell to complete the tandem cell fabrication.

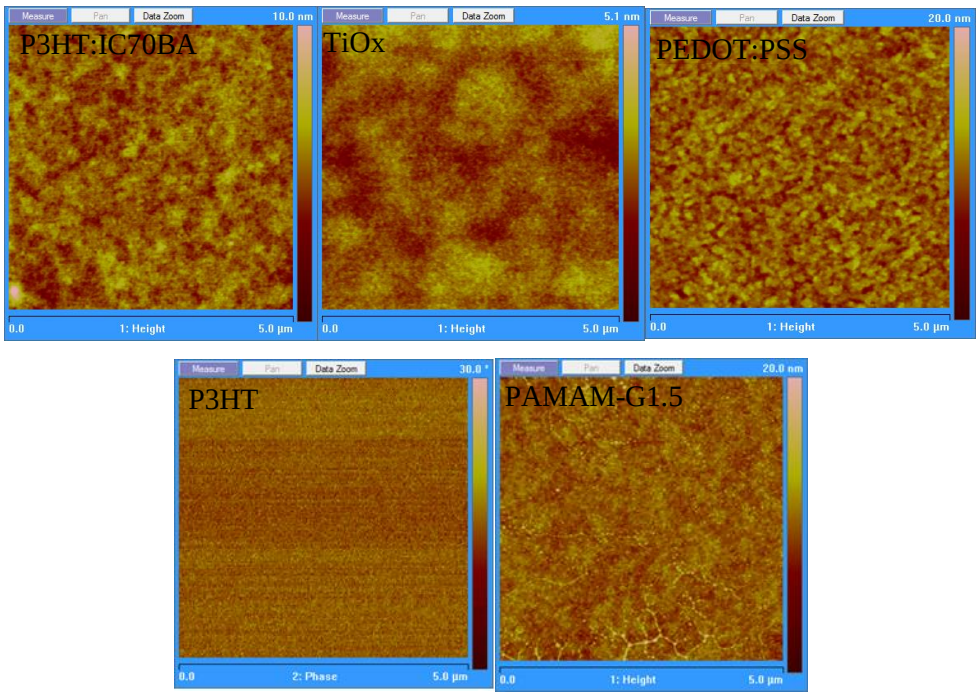

Figure 6.2: *AFM images of the deposited tandem multilayer interfaces structure.*

6.2. 3 Electrical characterisation

Figure 6.3 shows the current density–voltage *(J–V)* curves of single solar cells and the tandem solar cell with P3HT: IC70BA and P3HT: PAMAM G1.5 polymer systems under AM1.5G illumination with an intensity of 100 mW/cm^2. The photovoltaic performance of the single cells and tandem cells are summarized in table 6.1.

The single devices show a typical photovoltaic response with device performance comparable to that in previous chapters (4 and 5); the P3HT:IC70BA single cell yields J_{SC} = 23 mA/cm^2, V_{OC} = 0.54 V, *FF* = 0.45, and PCE = 5.5%, and the P3HT/ PAMAM-G1.5 single cell yields *J*sc = 49 mA/cm^2, V_{OC} = 0.28 V, *FF* = 0.43, and *PCE* = 6%.

Tandem organic solar cells show V_{OC} of 0.82 V, a J_{SC} of 32 mA/cm^2, *FF* of 0.25 and a PCE of 6.6 %. This result shows that the V_{OC} of tandem organic solar cells is the sum of the V_{OC} of the bottom and top cells; with no loss observed. This due to a well-matched energy level of the intermediate layer as it provides a recombinant region for electrons and holes between the top and bottom component cells. Current-limiting sub-cell in tandem solar cells influences the FF. The lower fill factor of the top cell strongly decreases the fill factor of the series tandem device. Furthermore, the fill factors of the series tandem devices are higher than the fill factors of the top cells [11]. The fill factor of 0.25, which is much lower than those of the two sub cells, can be seen as the bottleneck in the overall efficiency.

Moreover, the final J_{SC} of the tandem cells in series is dependent on the smaller J_{SC} in the bottom and top cells; the J_{SC} of tandem cell is slightly higher than half the *J*sc of the top cell [11]. The *J*sc of the tandem device using the same polymer is limited by the current of the less absorbing rear cell. This prevents our tandem structure from achieving even higher efficiency. Overall, the tandem cell has the PCE of 6.6 %, which is comparable with the bottom and top cells'. However, it is worth mentioning that the V_{OC} is increased largely by stacking these two cells with the same polymer as the active layer, which can be applied to drive some optoelectronic devices with low driving voltages although the PCE is not increase as high as expected. Furthermore, the light absorbed by the top cell in tandem structure is believed to be smaller than that in the single cell since the same polymer blend as the active layer was used in our tandem cell.

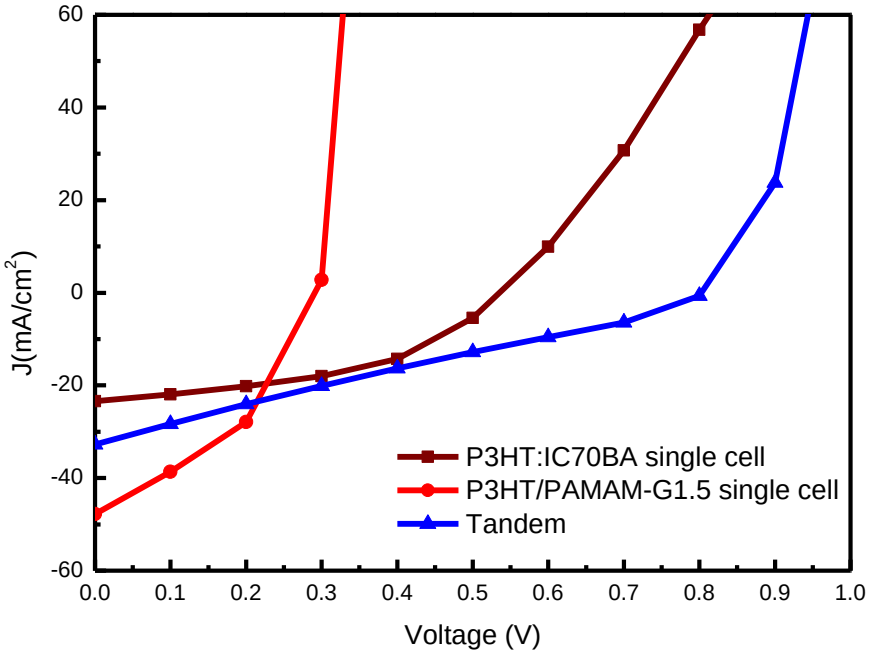

Figure 6.3: *The current density-voltage (J-V) characteristics of single reference cells using P3HT:IC70BA and P3HT: PAMAM G1.5 and tandem cell fabricated using the same polymer system under illumination.*

Device	V_{OC} (V)	J_{SC} (mA/cm^2)	P_{max} (mW/cm^2)	*FF* (%)	*PCE* (%)
P3HT:IC70BA	**0.54**	**23**	**5.5**	**45**	**5.5**
P3HT/PAMAM G1.5	**0.28**	**49**	**6**	**43**	**6**
Tandem	**0.82**	**32**	**6.6**	**25**	**6.6**

Table 6.1: *Photovoltaic performance of the single reference cells and the corresponding tandem cell.*

The absorption of tandem cells is shown in Fig. 6.4; for comparison, the absorption of corresponding sub-cells are also included. Compared to the absorption of single

junction devices, the absorption of the tandem in the infrared region is similar to single junction. While the absorption in the visible region significantly increases from 40% and 60%, suggesting that the tandem structure of identical sub cells certainly improves light harvesting.

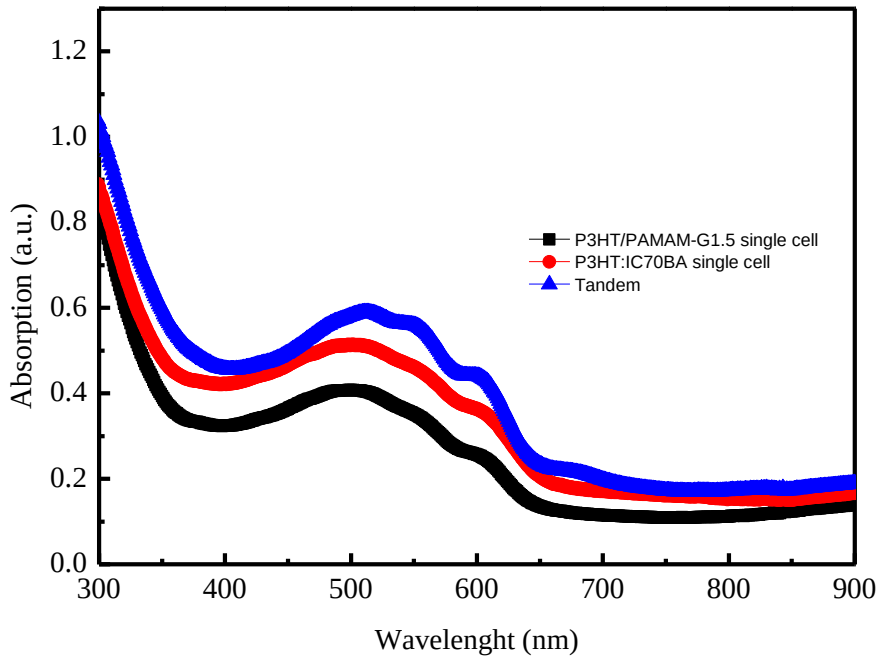

Figure 6.4: *Absorption spectra of a P3HT:IC70BA bulk heterojunction composite film, a P3HT/PAMAM G1.5 heterojunction composite film, and the tandem device structure.*

6.3 PAMAM G2.5 based organic tandem solar cells

6.3.1 Fabrication process

The structure of this device is ITO/PEDOT:PSS/P3HT:IC70BA/TiOx/PEDOT(pH 500)/P3HT/PAMAMG2.5(pH= 6.85)/TiOx/Al as shown in Fig. 6.5. All fabrication conditions and experimental steps were the same as the previous device of PAMAM G1.5 based organic tandem solar cell. The difference between the two structures is that PAMAM G2.5 with pH= 6.85 was used as acceptor in the top cell instead of PAMAM G1.5.

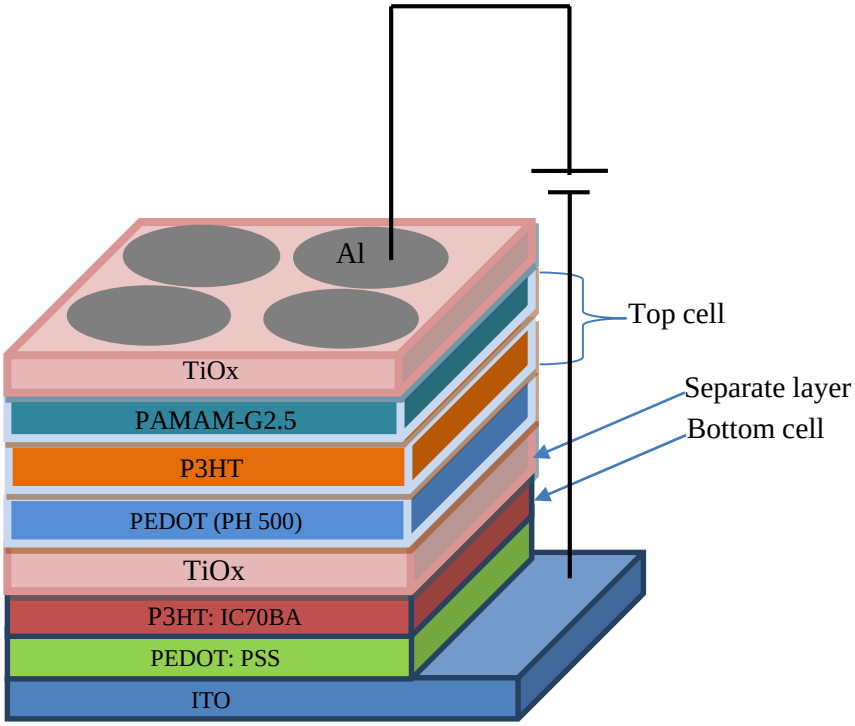

Figure 6.5: *Schematic diagram of organic tandem solar cell based on the PAMAM-G2.5 (pH= 6.85) as acceptor layer in the top cell.*

6.3.2 Surface morphology of intermediate layer

Figure 6.6 shows the surface morphology of deposited top cell acceptor layer PAMAM-G2.5 at pH =6.85 on top of the P3HT layer. As it was mentioned in chapter 5, at neutral pH the PAMAM end branches (periphery) expanded on the surface with good connections to each other. These properties make the material more flexible and more homogeneously distribution in larger dendritic size. Also, the surface morphology of the PAMAM-G2.5 show no interlayer mixed with donor layer (P3HT) and the branches are clear and connected to each other.

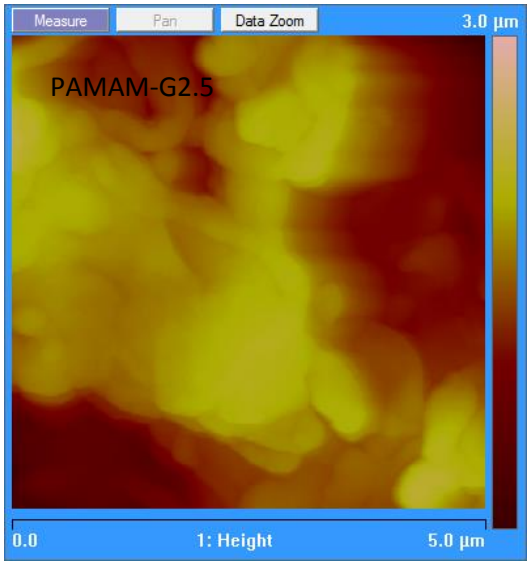

Figure 6.6: *AFM images of the deposited top cell acceptor layer on the top of the P3HT.*

6.3.3 Electrical characterisation

Figure 6.7 shows the current density–voltage (*J–V*) curves of single solar cells and the tandem solar cell with P3HT: IC70BA and P3HT: PAMAM G2.5 polymer systems under AM1.5G illumination with an intensity of 100 mW/cm^2. The photovoltaic performance of the single cells and tandem cells are summarized in table 6.2.

Again the single devices show a typical photovoltaic response with device performance comparable to that in previous chapters (4 and 5); the P3HT:IC70BA single cell yields J_{SC} = 23 mA/cm2, V_{OC} = 0.54 V, FF = 0.45, and *PCE* = 5.5%, and the P3HT/ PAMAM-G2.5 single cell yields J_{SC} = 35 mA/cm2, V_{OC} = 0.8 V, FF = 0.23, and ηe = 6.6%.

Tandem organic solar cells show V_{OC} of 1.3 V, a J_{SC} of 20 mA/cm^2, a *FF* of 0.27 and a PCE of 7 %. This result shows that the V_{OC} of tandem organic solar cells is the sum of the V_{OC} of the bottom and top cells. This demonstrates that the two sub cells have been successfully connected in series. The lower fill factor of the top cell strongly decreases the fill factor of the series tandem device. Furthermore, the fill factors of the series tandem devices are higher than the fill factors of the top cells.

The J_{SC} of the tandem cell is limited by the lowest J_{SC} of the top and the bottom unit cells because the two unit cells are electrically connected in series. Therefore, the photocurrents of the top and the bottom cells must be the same in order to improve the

efficiency of the tandem cell. Overall, the tandem cell has the PCE of 7 %, which is higher than either of the individual single cells due to the increase of the V_{OC}.

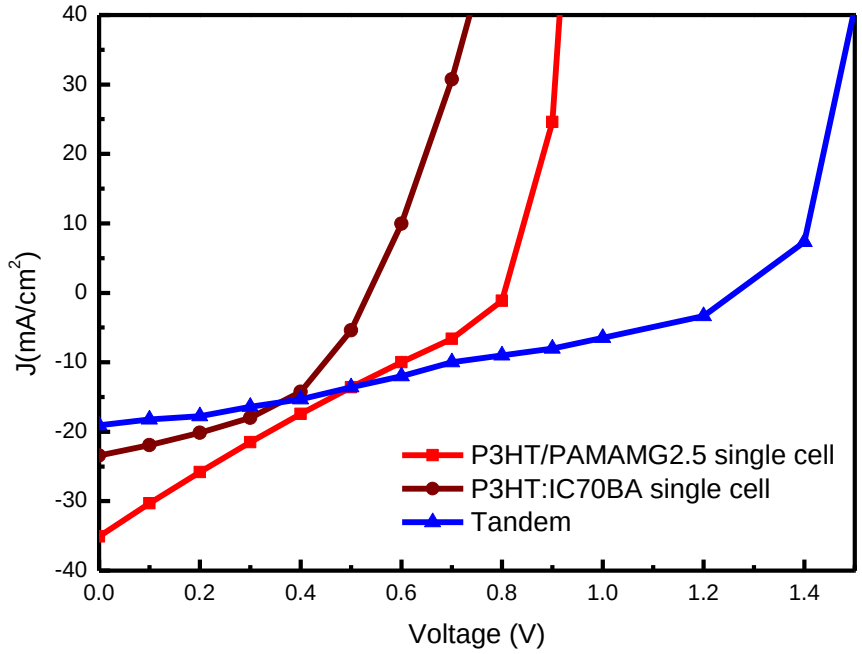

Figure 6.7: *The current density-voltage (J-V) characteristics of single reference cells using P3HT:IC70BA and P3HT: PAMAM G2.5 and tandem cell fabricated using the same polymer system under illumination.*

Device	V_{OC} (V)	J_{SC} (mA/cm^2)	P_{max} (mW/cm^2)	FF (%)	PCE (%)
P3HT:IC70BA	0.54	23	5.5	45	5.5
P3HT/PAMAM G2.5	0.8	35	6.6	23	6.6
Tandem	1.3	20	7	27	7

Table 6.2: *Photovoltaic performance of the single reference cells and the corresponding tandem cell.*

The absorption of tandem cells is shown in Fig. 6.8; for comparison, the absorption of corresponding sub-cells are also included. In a similar fashion as previous device, the absorption of the tandem in the infrared region is similar to single junction. While the absorption in visible significantly increases from 45% and 65%, suggesting that the tandem structure of identical sub cells surely improves light harvesting.

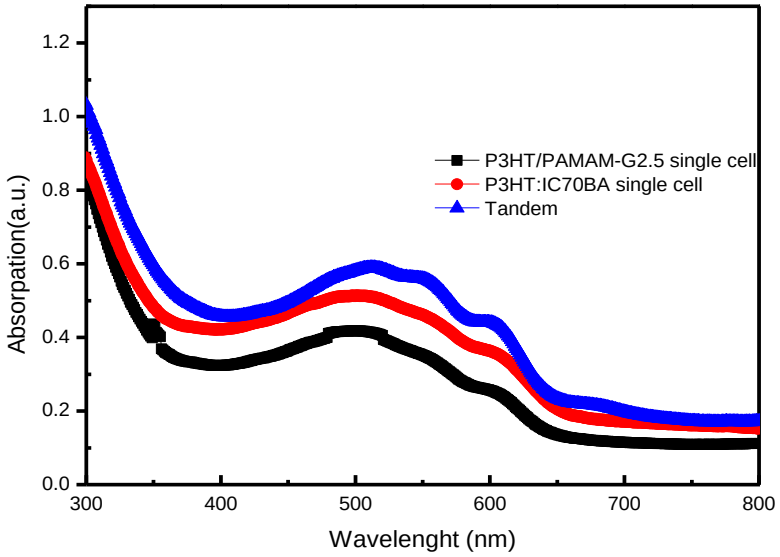

Figure 6.8: *Absorption spectra of a P3HT:IC70BA bulk heterojunction composite film, a P3HT/PAMAM G2.5 heterojunction composite film, and the tandem device structure.*

6.4 PAMAMG0-TPD based organic tandem solar cells

6.4.1 Fabrication process

The tandem structure is ITO/PEDOT:PSS/P3HT:IC70BA/TiOx/PEDOT(pH 500)/P3HT/PAMAMG0-TPD/TiOx/Al as shown in Figure 6.9. All fabrication conditions and experimental steps were the same as the previous PAMAM G1.5 based organic tandem solar cells. The difference between the two structures is that PAMAMG0-TPD was used as acceptor in the top cell instead of PAMAM G1.5.

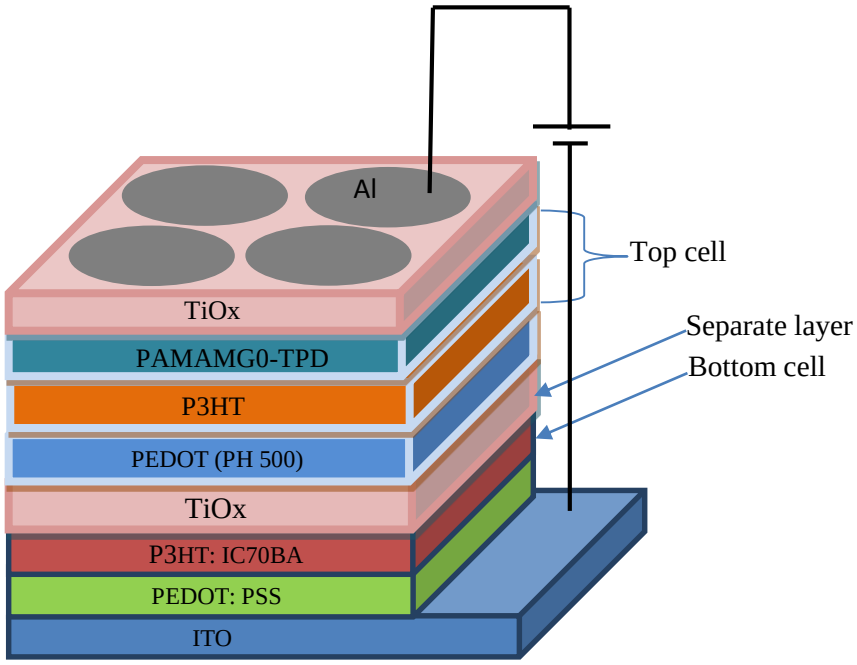

Figure 6.9: *The structure of organic tandem solar cells based on the PAMAMG0-TPD as acceptor layer in the top cell.*

6.4.2 Surface morphology

Figure 6.10 shows the surface morphology of the deposited top cell acceptor layer PAMAM-G0-TPD on top of the P3HT layer. The surface morphology of the PAMAM-G2.5 show no interlayer mix with donor layer (P3HT). It also show self-assembly characteristics similar to those of diblock copolymers (D-A copolymer) spared on the whole surface.

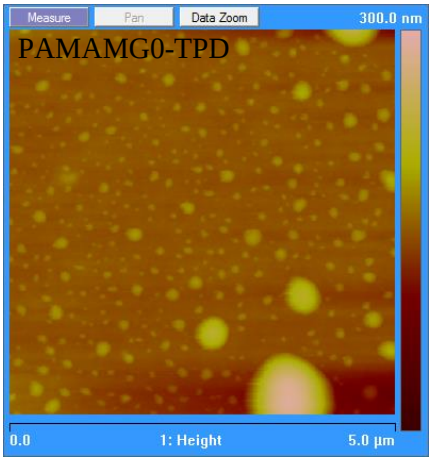

Figure 6.10: *AFM images of the deposited* of the deposited top cell acceptor layer PAMAM-G0-TPD on top of P3HT

6.4.3 Electrical characterisation

Figure 6.11 shows the current density–voltage (*J*–*V*) curves of single solar cells and the tandem solar cell with P3HT: IC70BA and P3HT: PAMAMG0-TPD polymer systems under AM1.5G illumination with an intensity of 100 mW/cm^2. The photovoltaic performance of the single cells and tandem cells are summarized in table 6.3.

The single devices show a typical photovoltaic response with device performance comparable to that in previous chapters (4 and 5); the P3HT:IC70BA single cell yields J_{SC}= 23 mA/cm2, V_{OC} = 0.54 V, FF = 0.45, and PCE = 5.5%, and the P3HT/ PAMAM-G2.5 single cell yields J_{SC} = 20 mA/cm2, V_{OC} = 0.79 V, FF = 0.27, and PCE = 4.5%.

Tandem organic solar cells show V_{OC} of 1.19 V, a J_{SC} of 16 mA/cm2, a *FF* of 0.34 and a PCE of 6.6 %. This result shows that the V_{OC} of tandem organic solar cells is 0.14V less than that of the top and bottom cell V_{OC} combination. The difference may come from (a) the small resistance of the interconnecting layer, and/or (b) the slight V_{OC} drop of the rear cell since the light intensity on the rear cell in the tandem structures is lower compared with one sun illumination. Therefore, the V_{OC} of the tandem solar cell are almost equal to the sum of the single junction cells' V_{OC}, which prove the effectiveness of the interlayer connection. Furthermore, the fill factors of the series tandem devices are higher than the fill factors of the top cells.

In addition, the J_{SC} decrease to (16 mA/cm^2) compared to that of the bottom cell (23 mA/cm^2) and that of the top cell (20 mA/cm^2). Finally, the tandem cell has the PCE of

6.6 %, which is higher than either of the individual single cells due to the enhanced of the V_{OC}.

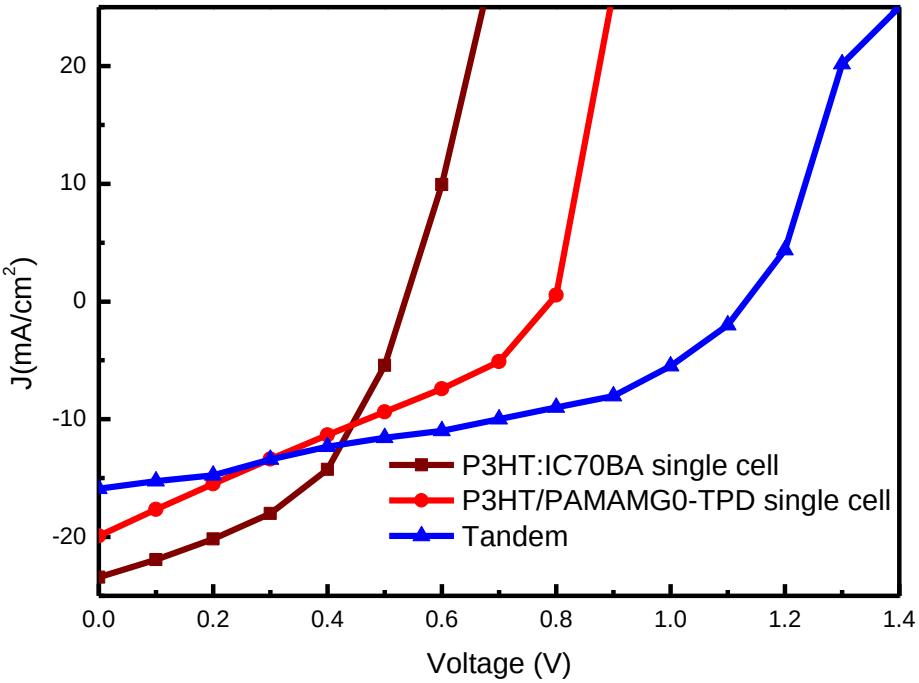

Figure 6.11: *The current density-voltage (J-V) characteristics of single reference cells using P3HT:IC70BA and P3HT: PAMAMG0-TPD and tandem cell fabricated using the same polymer system under illumination.*

Device	V_{OC} (V)	J_{SC} (mA/cm^2)	P_{MAX} (mW/cm^2)	*FF* (%)	PCE (%)
P3HT:IC70BA	0.54	23	5.5	45	5.5
P3HT/ PAMAM G0-TPD	0.79	20	4.5	27	4.5
Tandem	1.19	16	6.6	34	6.6

Table 6.3: *Photovoltaic performance of the single reference cells and the corresponding tandem cell.*

The absorption of tandem cells is shown in Fig. 6.12; for comparison, the absorption of corresponding sub-cells are also included. Once again the absorption of the tandem in

the infrared region is similar to single junction. While the absorption in visible significantly increases from 40% and 65%, suggesting that the tandem structure of identical sub cells surely improves light harvesting.

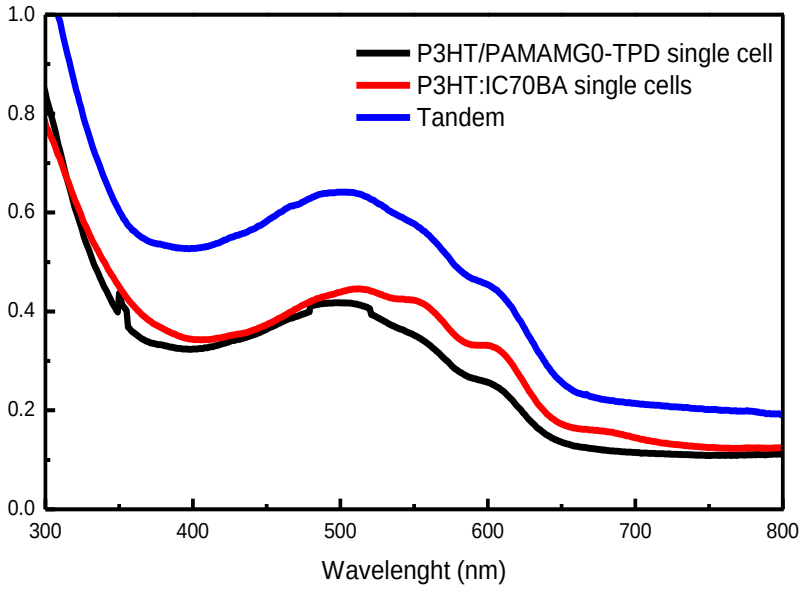

Figure 6.12: *Absorption spectra of a P3HT:IC70BA bulk heterojunction composite film, a P3HT/PAMAMG0-TPD heterojunction composite film, and the tandem device structure.*

6.5 Summary

In summary three different organic tandem solar cells were fabricated and characterised. They have the same active layer (P3HT:IC70BA) as bulk-heterojunction structure in the bottom cells where the top cell is a bilayer heterojunction structure. The differences between the three devices is the acceptor layer of the top cells. From the results in Chapter 5 PAMAM-G1.5 (pH= 7.03), PAMAM-G2.5 (pH= 6.85) and PAMAM-G0-TPD acceptor layers were chose to as they have the highest efficiency to be applied as the top cells of organic tandem structures. Surface morphology of the fabricated layers was observed by AFM. The multilayer morphologies demonstrated sharp interfaces with no evidence of interlayer mix. The absorption in the visible region for all three tandem structures significantly improved.

The fabricated organic tandem devices and their extracted electronic parameters from the *I-V* characteristics are summarized in Table 6.4.

Tandem devices	V_{OC} **(V)**	J_{SC} **(mA/cm^2)**	P_{max} **(mW/cm^2)**	***FF*** **(%)**	**PCE (%)**
PAMAM-G1.5 based	0.83	32	6.6	25	6.6
PAMAM-G2.5 based	1.3	20	7	27	7
PAMAM-G0-TPD based	1.19	16	6.6	34	6.6

Table 6.4: *A summary of the electronic properties of the tandem devices.*

On all three devices the V_{OC} are almost equal to the sum of the single junction cells' V_{OC}, indicating the effectiveness of the interconnection layer. Therefore, the TiOx/PEDOT middle contact serves as a stable foundation that enables the fabrication of the second cell to complete the tandem cell architecture without damaging or dissolving the underlying layers. The PCE of all three tandem structures are significantly improved in comparison to their corresponding sub cells due to the enhanced in V_{OC}. These results establish the use of the PAMAM dendrimers as acceptor in the application of organic tandem solar cells.

References

1. T. Ameri, G. Dennler, C. Lungenschmied, and C. Brabec., ' Organic tandem solar cells: A review ', *Energy & Environmental Science*, Vol. 2(4), pp. 347-363, **2009.**
2. T. Ameri, N. Lia, and C. Brabeca., ' Highly efficient organic tandem solar cells: a follow up review ', *Energy & Environmental Science*, Vol. 6(8), pp. 2390-2413, **2013.**
3. S. Sista, Z. Hong, L. Chen and Y. Yang., ' Tandem polymer photovoltaic cells—current status, challenges and future outlook ', *Energy &Environmental Science*, Vol. 4, pp. 1606–1620, **2011.**
4. *F. Guo, N. Li, F. Fecher, N. Gasparini, C. Quiroz, C. Bronnbauer, Y. Hou, V. Radmilovic, V. Radmilovic, E. Spiecker, K. Forberich & C.Brabec., '* A generic concept to overcome bandgap limitations for designing highly efficient multi-junction photovoltaic cells ', *Nature Communications*, Vol.6, pp. 1-9, **2015.**
5. B. Minnaert, and P. Veelaert., ' Guidelines for the Bandgap Combinations and Absorption Windows for Organic Tandem and Triple-Junction Solar Cells ', *Materials*, Vol. 5, pp. 1933-1953, **2012.**
6. J. You, L. Dou, K. Yoshimura, T. Kato, K. Ohya, T. Moriarty, K. Emery, C. Chen, J. Gao, G. Li, and Y. Yang., ' A polymer tandem solar cell with 10.6% power conversion efficiency ', *Nature communications*, Vol. 4(1446), pp. 1-10, **2012.**
7. Z. Zheng, S. Zhang, M. Zhang, K. Zhao, L. Ye, Y. Chen, B. Yang, and J. Hou., ' Highly Efficient Tandem Polymer Solar Cells with a Photovoltaic Response in the Visible Light Range ', *Advanced Materials*, Vol. 27, pp. 1189–1194, **2015.**
8. D. Zhao, X. Sun, C. Jiang, A. Kyaw, G. Lo, and D. Kwong., ' Efficient tandem organic solar cells with an Al / MoO_3 intermediate layer ', *Applied physics letters*, Vol. 93, pp. 083305-3, **2008.**
9. J. Kim, K. Lee, N. Coates, D. Moses, T. Nguyen, M. Dante, A. Heeger., 'Efficient Tandem Polymer Solar Cells Fabricated by All-Solution Processing', *Science*, Vol. 13, pp. 222-225, **2007.**
10. Y. Yuan, J. Huang and G. Li., 'Intermediate Layers in Tandem Organic Solar Cells', *Green*, Vol. 1, pp. 65–80, **2011.**

11. A. Hadipour, B. Boer, P. Blom, ‘Device operation of organic tandem solar cells’, *Organic electronics*, Vol. 9(5), pp. 617-624,2008.

Chapter 7

Conclusions and Further Work

7.1 Conclusions

This thesis has investigated the use of new advanced materials as acceptor in the application of organic solar cells to improve power conversion efficiency (PCE). Conjugated dendrimers have been successfully employed in organic light emitting diodes, and in this work they have been applied to organic solar cells. This work demonstrated that polyamidoamine (PAMAM) dendrimers is a potential candidate to be used as acceptor in high efficient organic solar cells applications. The material was used in different structures and different generations. It was used in the bulk heterojunction, bilayer heterojunction and multijunction structures. Indene-C70 bisadduct (IC70BA) was also utilized as a new material for potential use as acceptor in organic solar cells. Thin films of IC70BA were used in bulk heterojunction and multijunction structures in single cells where the other cells contained the new PAMAM acceptors. Poly(3-hexylthiophene-2,5-diyl) (P3HT) was used as the donor layer in all fabricated structures.

Organic Bulk-Heterojunction (OBHJ) solar cells: Blends of PAMAM cores (FC0, FC1, FC2) and P3HT as the active layers were used to fabricate OBHJ solar cells. The *J-V* characteristics for the fabricated devices in the dark and under illumination with the halogen lamp (100 mW/cm^2), did not display any photovoltaic behaviour (no open circuit voltage was detected) for the devices based on P3HT: PAMAM core FC0 and FC1 as active layers due to low conductivity. This means that, PAMAM cores FC0 and FC1 cannot be used as acceptor materials in organic solar cells. However, for the device based on P3HT: PAMAM core FC2 a non-zero current is recorded which reflects the existence of the generated carriers due to light absorption and good conducting behaviour of the structure. The device produced an open circuit voltage, V_{oc}, ~ 0.6V, short-circuit current density, J_{sc}, ~1.3 mA/ cm^2 with fill factor of ~22 % and a maximum

power (P_{max}) of 0.2 mW/cm^2 yielding a PCE of 0.2%. PAMAM FC2 core surface morphology presented clear splitting units similar to tree spread on throughout the surface with some connections resulting in good conduction behaviour. As for FC0 and FC1-based blended films, clear separation structures with agglomeration of branching spread on the surface forming branches without connections. Also, blends of PAMAM with different generation size (G0, G0.5, G1 and G2) with P3HT were used as the active layer in other OBHJ structures. The *J-V* characteristics under illumination showed no open circuit voltage for the PAMAM dendritic G0, G1 and G2 due to low conductivity in such films. However, the device based on P3HT: PAMAM G0.5 show a non-zero current which reflects the existence of the generated carriers due to light absorption. These devices produced V_{OC}, ~ 0.85V, J_{sc}, ~ 6 mA/cm^2 with FF of ~26 % and P_{max} of 1.6 mW/cm^2 yielding a PCE of 1.6%. This kind of behaviour was attributed to that full generation amine-termnate PAMAM surface group (G0, G1 and G2) are protonated at physiological pH. Thus there is electrostatic repulsion between the primary amine in the surface preventing electrostatic interaction with other materials. Whereas ester terminated half-generation dendrimers are less susceptible to protonation compared to the full generation dendrimers and more opening structure for electrostatic interaction with other materials can occur.

The effect of thermal annealing to improve the efficiency of devices based on PAMAM core FC2 and PAMAM G0.5 was investigated. The devices after annealing did not display any photovoltaic behaviour. This due to the effect of thermal annealing on the morphology of the active layer blend. After annealing the film morphology was changed from branched morphology to globular structures upon temperature increase. These confirming the *J-V* characterisation results as the branches morphology disappeared, thus, energy transfers in the dendrimers become difficult. Optical spectroscopy also supported the electronic and morphology findings. Optical absorption measurements showed a band gap of 2.6 eV for FC2-based films and 3.54 for FC0 and FC1-based cells.

On the other hand the other acceptor material (IC70BA) was also investigated through the fabrication of OBHJ solar cells which uses a blend of IC70BA and P3HT as the active layer in two cases: under different annealing temperature and under different concentration conditions.

In the case of different annealing temperatures the OBHJ solar cells performance improved significantly due to the thermal annealing. The OBHJ solar cells without

thermal annealing exhibited only a PCE of 2.5% with J_{SC} of 20.83 mA/Cm^2, $V_{OC} \approx 0.4$ V and *FF* of 27% with semi-flat curve. As the heat-treatment temperature was increased the V_{OC} and *FF* parameters were remarkably improved as the curve bended and becomes closer to typical solar cells curve under illumination. As a result, the PV cell prepared with heat treatment at 150 ^{0}C displayed the best device performance as J_{sc} = 23. 33 mA/cm^2, V_{OC} = 0.53 V, FF 0.44, and PCE = 5.6 %. However, in case of under different concentration ratios J_{SC} was greatly enhanced to 20.83 mA /cm^2 for devices with the polymer to IC70BA ratio of 1:1, where electron and hole transport are balanced. A PCE of 5.8% for this device was achieved which is the highest efficiency achieved with this material. This study demonstrate that at a weight ratio of 1:1 percolation ratio at the phase of both P3HT and IC70BA approximately equal which preventing generated charges from becoming trapped within isolated domains.

Organic Bilayer Heterojunction solar cells: two different new PAMAM dendrimers salts acceptor materials (G0.5, G1.5, and G2.5) at different pH and a new accepter – accepter (A-A) copolymer of PAMAM G0-TPD are investigated. The pH was varied between very acidic solution and alkaline solution. This study aimed to investigate the effect of generation size of the PAMAM dendritic materials (G 0.5, G1.5, and G2.5) at different pH on the performance of organic bilayer heterojunction solar cells. It was observed that increasing PAMAM dendritic generation from G0.5 to G2.5 influence significantly the bilayer OHJ solar cells efficiency performance. PCE of 7 % were achieved at the natural PAMAM G2.5 at pH 6.85. The results were explained as all tertiary amines in PAMAM G2.5 dendritic are positively charged at the natural pH, where in the low pH < 5 all tertiary and interior tertiary molecules positively charged leading to a strong electrostatic repulsion between them. At high pH >10 PAMAM G2.5 is uncharged. Atomic force microscopy (AFM) shows that PAMAM morphology change with PAMAM generation and pH values. The effective charges which interact with the external electric field or other charges were found to increase with increasing generation of the dendrimers at neutral pH. AFM study shows that neutral pH exhibit a major peripheral distribution where in the low pH <5 the film found to shrink. For the A-A copolymer PAMAM G0-TPD based organic bilayer heterojunction solar cells, electrons transfer were enhanced due to the present of TPD moiety in PAMAMG0-TPD structure. However, the device performance based on PAMAMG0-TPD only as active layer achieved very low efficiency of about 0.0034% with J_{SC} of 0.0133 mA/Cm^2, V_{OC}

is 0.7 V and FF of 36%. On the other hand, when P3HT was used as the donor combined with PAMAMG0-TPD as acceptor the PCE performance was remarkably improved. The device produced V_{OC}, ~ 0.79V, J_{SC},~20 mA/ cm^2 with FF of ~27 % and $P_{max} \approx 4.5$ mW/cm^2 yielding a power conversion efficiency of 4.5 %. This confirm that PAMAMG0-TPD serve as A-A copolymer structures. Moreover, these results demonstrated the potential to use PAMAM G0-TPD based conjugated copolymers as acceptor component for organic solar cells.

Organic Tandem Solar Cells: IC70BA and the best performance PAMAM acceptor materials were combined with P3HT to form the active layers of the tandem solar cells. Three different organic tandem solar cells based on titanium oxide as intermediate layer were fabricated and characterized. The bottom cell contained the P3HT:IC70BA as the active layer for all three tandem devices. The change occur in the top cell as the best performance PAMAM acceptor materials in the previous studied devices was selected, PAMAM G1.5 and G2.5 at neutral pH and PAMAM G0-TPD.

PAMAM G1.5 (PH=7.03) based organic tandem solar cells with same donor (P3HT) in sub cells was first fabricated and characterised. The P3HT:IC70BA single cell yields J_{SC} = 23 mA/cm^2, V_{OC} = 0.54 V, FF = 0.45, and PCE = 5.5%, while the P3HT/ PAMAM-G1.5 single cell yields J_{SC} = 49 mA/cm^2, V_{OC} = 0.28 V, FF = 0.43, and PCE = 6%. The overall tandem cell shows V_{OC} of 0.82 V, a J_{SC} of 32 mA/cm^2, a FF of 0.25 and a PCE of 6.6 %. This result shows that the V_{OC} of tandem organic solar cell is the sum of the V_{OC} of the bottom and top cells; with no loss observed. This due to a well-matched energy level of the intermediate layer as it provides a recombinant region for electrons and holes between the top and bottom component cells. In tandem solar cells, the FF is mostly affected by the current-limiting sub-cell. The lower fill factor of the top cell strongly decreases the fill factor of the series tandem device. Furthermore, the fill factors of the series tandem devices are higher than the fill factors of the top cells. The fill factor of 0.25, which is much lower than those of the two sub cells, can be seen as the bottleneck in the overall efficiency. Moreover, as the final J_{SC} of the tandem cell in series relies on the smaller J_{SC} in the bottom and top cells. In fact the J_{SC} of the tandem cell is slightly higher than half the J_{SC} of the top cell. The J_{SC} of the tandem device using the same polymer is limited by the current of the less absorbing rear cell. This prevents our tandem structure from achieving higher efficiency. Overall, the tandem cell has the PCE of 6.6 %, which is comparable with the bottom and top cells.

However, it is worth mentioning that the V_{OC} is increased largely by stacking these two cells with the same polymer as the active layer, which can be applied to fabricate some optoelectronic devices with low driving voltages although the PCE is not increase as high as expected.

Furthermore, PAMAM G2.5 organic tandem structures show the same behaviour of the previous tandem structure (PAMAM G1.5) with slightly higher efficiency (V_{OC} of 1.3 V, a J_{SC} of 20 mA/cm^2, a FF of 0.27 and a PCE of 7 %.). However, the organic tandem solar cell based on PAMAMG0-TPD as acceptor in the top cell shows much more enhancement in the power conversion efficiency compare with sub cells, with V_{OC} of 1.19 (which is approximately the sum of the V_{OC} of the individual cells), a J_{SC} of 16 mA/cm2, a FF of 0.34 and a PCE of 6.6 %. This result confirm that using conjugated polymers containing TPD units are expected to have enhanced charge transport properties compared with polymers without a TPD moiety.

7.2 Further work

There are many avenues available for pursuit as a result of this work in order to improve the efficiency of organic solar cells based on these new materials:

1- Determine the HOMO and LUMO energy levels of these new acceptor materials (PAMAM dendrimers) as the molecular energy level control are of great importance in improving photovoltaic properties of conjugated polymers.
2- As it was reported that PAMAM dendrimers at room temperature exhibit strong cross linking structures, the study of thermal annealing effect on these material at temperatures between 25^0C and 50^0C to determine the optimal temperature to enhance the branches and improve their efficiency.
3- Instead of drying the electron transfer layer (TiOx) at high temperature 150^0C above these acceptors the slow drying process can be used to improve the efficiency as high temperature $\geq 50^0$C has negative effect on the morphology and performance of these materials.
4- Also, in order to improve the efficiency of the organic tandem solar cells based on these materials the donor material in the top cell, P3HT, which consider to

be wide band gap semiconductor could be replaced with other lower band gap polymer to absorb complementary wavelengths. Thus, thermalisation losses can be reduced by absorbing high energy photons in a wide bandgap cell, while transmission losses can be reduced by absorbing low energy photons in a small bandgap cell.